MIMO-OFDM for LTE, WIFI and WIMAX
Coherent versus Non-Coherent and Cooperative Turbo-Transceivers

by

L. Hanzo, J. Akhtman, M. Jiang, L. Wang

UNIVERSITY OF SOUTHAMPTON

We dedicate this monograph to the numerous contributors of this field, many of whom are listed in the Author Index

The MIMO capacity theoretically increases linearly with the number of transmit antennas, provided that the number of receive antennas is equal to the number of transmit antennas. With the further proviso that the total transmit power is increased proportionately to the number of transmit antennas, a linear capacity increase is achieved upon increasing the transmit power. However, under realistic conditions the theoretical MIMO-OFDM performance erodes and hence to circumvent this degradation, our monograph is dedicated to the design of practical coherent, non-coherent and cooperative MIMO-OFDM turbo-transceivers...

Contents

About the Authors

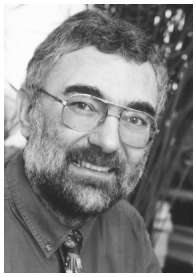

Lajos Hanzo (http://www-mobile.ecs.soton.ac.uk) FREng, FIEEE, FIET, DSc received his degree in electronics in 1976 and his doctorate in 1983. During his career he has held various research and academic posts in Hungary, Germany and the UK. Since 1986 he has been with the School of Electronics and Computer Science, University of Southampton, UK, where he holds the chair in telecommunications. He has co-authored 19 books on mobile radio communications totalling in excess of 10 000, published 844 research entries at IEEE Xplore, acted as TPC Chair of IEEE conferences, presented keynote lectures and been awarded a number of distinctions. Currently he is directing an academic research team, working on a range of research projects in the field of wireless multimedia communications sponsored by industry, the Engineering and Physical Sciences Research Council (EPSRC) UK, the European IST Programme and the Mobile Virtual Centre of Excellence (VCE), UK. He is an enthusiastic supporter of industrial and academic liaison and he offers a range of industrial courses. He is also an IEEE Distinguished Lecturer as well as a Governor of both the IEEE ComSoc and the VTS. He is the acting Editor-in-Chief of the IEEE Press. For further information on research in progress and associated publications please refer to http://www-mobile.ecs.soton.ac.uk

Dr Yosef (Jos) Akhtman received a B.Sc. degree in Physics and Mathematics from the Hebrew University of Jerusalem, Israel in June 2000 and the Ph.D. degree in Electronics Engineering from the University of Southampton in July 2007. He was awarded a full Ph.D. studentship in the University of Southampton as well as an Outstanding Contribution Award for his work as part of the Core 3 research programme of the Mobile Virtual Centre of Excellence in Mobile Communications (MobileVCE). He has also received a BAE Prize for Innovation in Autonomy for his contribution to the Southampton Autonomous Underwater Vehicle (SotonAUV) project. Between January 2007 and Dec. 2009 he conducted research as a senior research fellow in the 5* School of Electronics and Computer Science at Southampton University.

Dr. Ming Jiang (S'04-M'09) received B.Eng. and M.Eng. degrees in Electronics Engineering in 1999 and 2002 from South China University of Technology (SCUT), China, and Ph.D. degree in Telecommunications in 2006 from University of Southampton, UK, respectively. From 2002 to 2005, he was involved in the Core 3 research project of Mobile Virtual Centre of Excellence (VCE), UK on air-interface algorithms for MIMO OFDM systems. Since April 2006, Dr. Jiang has been with Advanced Technology, Standards and Regulation (ATSR) of Samsung Electronics Research Institute (SERI), UK, working on the European FP6 WINNER project as well as internal projects on advanced wireless communication systems. His research interests fall in the general area of wireless communications, including multi-user detection, channel estimation, space-time processing, heuristic and adaptive optimization, frequency-hopping, MIMO OFDM and OFDMA systems, etc. Dr. Jiang has co-authored one IEEE Press book chapter, 6 IEE/IEEE journal papers, and 8 IEE/IEEE conference papers. Recently he returned to his native country China and had been working for Nortel.

Li Wang received his BEng degree with distinction in information engineering from Chengdu University of Technology (CDUT), Chengdu, P. R. China, in 2005 and his MSc degree (with distinction) in radio frequency communication systems from University of Southampton, Southampton, UK, in 2006. Between October 2006 and January 2010 he was a PhD student in the Communication Group, School of Electronics and Computer Science, University of Southampton, UK, and participated in the Delivery Efficiency Core Research Program of the Virtual Centre of Excellence in Mobile and Personal Communications (Mobile VCE). His research interests include space-time coding, channel coding, multi-user detection for future wireless networks. Upon the completion of his PhD in January 2010 he joined the Communications Group as a postdoctoral researcher.

Other Wiley and IEEE Press Books on Related Topics [1]

- R. Steele, L. Hanzo (Ed): *Mobile Radio Communications: Second and Third Generation Cellular and WATM Systems*, John Wiley and IEEE Press, 2nd edition, 1999, ISBN 07 273-1406-8, 1064 pages
- L. Hanzo, T.H. Liew, B.L. Yeap: *Turbo Coding, Turbo Equalisation and Space-Time Coding*, John Wiley and IEEE Press, 2002, 751 pages
- L. Hanzo, C.H. Wong, M.S. Yee: *Adaptive Wireless Transceivers: Turbo-Coded, Turbo-Equalised and Space-Time Coded TDMA, CDMA and OFDM Systems*, John Wiley and IEEE Press, 2002, 737 pages
- L. Hanzo, L-L. Yang, E-L. Kuan, K. Yen: *Single- and Multi-Carrier CDMA: Multi-User Detection, Space-Time Spreading, Synchronisation, Networking and Standards*, John Wiley and IEEE Press, June 2003, 1060 pages
- L. Hanzo, M. Münster, T. Keller, B-J. Choi, *OFDM and MC-CDMA for Broadband Multi-User Communications, WLANs and Broadcasting*, John-Wiley and IEEE Press, 2003, 978 pages
- L. Hanzo, S-X. Ng, T. Keller and W.T. Webb, *Quadrature Amplitude Modulation: From Basics to Adaptive Trellis-Coded, Turbo-Equalised and Space-Time Coded OFDM, CDMA and MC-CDMA Systems*, John Wiley and IEEE Press, 2004, 1105 pages
- L. Hanzo, T. Keller: *An OFDM and MC-CDMA Primer*, John Wiley and IEEE Press, 2006, 430 pages
- L. Hanzo, F.C.A. Somerville, J.P. Woodard: *Voice and Audio Compression for Wireless Communications*, John Wiley and IEEE Press, 2007, 858 pages
- L. Hanzo, P.J. Cherriman, J. Streit: *Video Compression and Communications: H.261, H.263, H.264, MPEG4 and HSDPA-Style Adaptive Turbo-Transceivers* John Wiley and IEEE Press, 2007, 680 pages
- L. Hanzo, J.S. Blogh, S. Ni: *3G, HSDPA, HSUPA and FDD Versus TDD Networking: Smart Antennas and Adaptive Modulation* John Wiley and IEEE Press, 2008, 564 pages
- L. Hanzo, O. Alamri, M. El-Hajjar, N. Wu: *Near-Capacity Multi-Functional MIMO Systems: Sphere-Packing, Iterative Detection and Cooperation,* IEEE Press - John Wiley, 2009
- L. Hanzo, R.G. Maunder, J. Wang and L-L. Yang: *Near-Capacity Variable-Length Coding: Regular and EXIT-Chart Aided Irregular Designs*, IEEE Press - John Wiley, 2010

[1] For detailed contents and sample chapters please refer to http://www-mobile.ecs.soton.ac.uk

Acknowledgements

We are indebted to our many colleagues who have enhanced our understanding of the subject. These colleagues and valued friends, too numerous to be mentioned individually, have influenced our views concerning the subject of the book. We thank them for the enlightenment gained from our collaborations on various projects, papers, and books. We are particularly grateful to our academic colleagues Prof. Sheng Chen, Dr. Soon-Xin Ng, Dr. Rob Maunder and Dr. Lie-Liang Yang. We would also like to express our appreciation to Osamah Alamri, Sohail Ahmed, Andreas Ahrens, Jos Akhtman, Jan Brecht, Jon Blogh, Nicholas Bonello, Marco Breiling, Marco del Buono, Sheng Chen, Peter Cherriman, Stanley Chia, Byoung Jo Choi, Joseph Cheung, Jin-Yi Chung, Peter Fortune, Thanh Nguyen Dang, Sheyam Lal Dhomeja, Lim Dongmin, Dirk Didascalou, Mohammed El-Hajjar, Stephan Ernst, Eddie Green, David Greenwood, Chen Hong, Hee Thong How, Bin Hu, Ming Jiang, Thomas Keller, Lingkun Kong, Choo Leng Koh, Ee Lin Kuan, W. H. Lam, Wei Liu, Kyungchun Lee, Xiang Liu, Fasih Muhammad Butt, Matthias Münster, Song Ni, C. C. Lee, M. A. Nofal, Xiao Lin, Chee Siong Lee, Tong-Hooi Liew, Noor Shamsiah Othman,Raja Ali Raja Riaz, Vincent Roger-Marchart, Redwan Salami, Prof. Raymond Steele, Shinya Sugiura, David Stewart, Clare Sommerville, Tim Stevens, Shuang Tan, Ronal Tee, Jeff Torrance, Spyros Vlahoyiannatos, Jin Wang, Li Wang, William Webb, Chun-Yi Wei, Hua Wei, Stefan Weiss, John Williams, Seung-Hwang Won, Jason Woodard, Choong Hin Wong, Henry Wong, James Wong, Andy Wolfgang, Nan Wu, Lei Xu, Chong Xu, Du Yang, Wang Yao, Bee-Leong Yeap, Mong-Suan Yee, Kai Yen, Andy Yuen, Jiayi Zhang, Rong Zhang, and many others with whom we enjoyed an association.

We also acknowledge our valuable associations with the Virtual Centre of Excellence in Mobile Communications, in particular with its chief executive, Dr. Walter Tuttlebee, and other members of its Executive Committee, namely Dr. Keith Baughan, Prof. Hamid Aghvami, Prof. Mark Beach, Prof. John Dunlop, Prof. Barry Evans, Prof. Peter Grant, Dr. Dean Kitchener, Prof. Steve MacLaughlin, Prof. Joseph McGeehan, Dr. Tim Moulsley, Prof. Rahim Tafazolli, Prof. Mike Walker and many other valued colleagues. Our sincere thanks are also due to John Hand and Andrew Lawrence EPSRC, UK for supporting our research. We would also like to thank Dr. Joao Da Silva, Dr Jorge Pereira, Bartholome Arroyo, Bernard Barani, Demosthenes Ikonomou, and other valued colleagues from the Commission of the European Communities, Brussels, Belgium.

Similarly, our sincere thanks are due to Mark Hammond, Sarah Tilly and their colleagues at Wiley in Chichester, UK. Finally, our sincere gratitude is due to the numerous authors listed in the Author Index — as well as to those, whose work was not cited owing to space limitations — for their contributions to the state-of-the-art, without whom this book would not have materialised.

Lajos Hanzo, Jos Akhtman, Ming Jiang and Li Wang
School of Electronics and Computer Science
University of Southampton, UK

Preface

The rationale and structure of this volume is centred around the following 'story-line'. The conception of *parallel transmission of data* over dispersive channels dates back to the seminal paper of Doelz *et al.* published in 1957, leading to the OFDM philosophy, which has found its way into virtually all recent wireless systems, such as the WiFi, WiMax, LTE and DVB as well as DAB broadcast standards. Although *MIMO techniques* are significantly 'younger' than OFDM, they *also reached a state of maturity* and hence the family of recent wireless standards includes the optional employment of MIMO techniques, which motivates the joint study of OFDM and MIMO techniques in this volume.

The research of MIMO arrangements was motivated by the observation that the MIMO capacity increases linearly with the number of transmit antennas, provided that the number of receive antennas is equal to the number of transmit antennas. With the further proviso that the total transmit power is increased proportionately to the number of transmit antennas, a linear capacity increase is achieved upon increasing the transmit power. This is beneficial, since according to the classic Shannon-Hartley law the achievable channel capacity increases only logarithmically with the transmit power. Hence *MIMO-OFDM may be considered a 'green' transceiver solution.*

Therefore this volume sets out to explore the recent research advances in MIMO-OFDM techniques as well as their limitations. The basic types of multiple antenna-aided OFDM systems are classified and their benefits are characterised. Spatial Division Multiple Access (SDMA), Spatial Division Multiplexing (SDM) and space-time coding MIMOs are addressed. We also argue that *under realistic propagation conditions*, when for example the signals associated with the MIMO elements become correlated owing to shadow fading, *the predicted performance gains may substantially erode.* Furthermore, owing to the limited dimensions of shirt-pocket-sized handsets, the employment of multiple antenna elements at the mobile station is impractical.

Hence in practical terms only the family of distributed MIMO elements, which relies on the cooperation of potentially single-element mobile stations is capable of eliminating the correlation of the signals impinging on the MIMO elements, as it will be discussed in the book. The topic of *cooperative wireless communications* cast in the context of distributed MIMOs has recently attracted substantial research interests, but nonetheless, it *has numerous open problems, before all the idealized simplifying assumptions currently invoked in the literatue are eliminated.*

On a more technical note, *we aim for achieving a near-capacity MIMO-OFDM performance*, which requires sophisticated designs, as detailed below:

- A high throughput may be achieved with the aid of a high number of MIMO elements, but this is attained at a *potentially high complexity, which exponentially increases as a function of both the number of MIMO elements as well as that of the number of bits per symbol*, when using a full-search based Maximum Likelihood (ML) multi-stream/multi-user detector.

- In order to approach the above-mentioned near-capacity performance, whilst circumventing the problem of an exponentially increasing complexity, *we design radical multi-stream/multi-user detectors, which 'capture' the ML solution with a high probability at a fraction of the ML-complexity.*

- This ambitious design goal is achieved with the aid of sophisticated *soft-decision-based Genetic Algorithm (GA) assisted MUDs or new sphere detectors, which are capable of operating in the high-importance rank-deficient scenarios*, when the number of transmit antennas may be as high as twice the number of receiver antennas.

- The achievable gain of space-time codes is further improved with the aid of *sphere-packing modulation, which allows us to design the space-time symbols of multiple transmit antennas jointly*, whilst previous designs made no effort to do so. Naturally, this joint design no longer facilitates low-complexity single-stream detection, but our sphere-decoders allow us to circumvent this increased detection complexity.

- Sophisticated *joint coding and modulation schemes* are used, which accommodate the parity bits of the channel codec without bandwidth extension, simply by extending the modulation alphabet.

- Estimating the MIMO channel for a high number of transmit and receive antennas becomes extremely challenging, since we have to estimate $N_t \cdot N_r$ channels, although in reality we are only interested in the data symbols, but not the channel. *This problem becomes even more grave in the context of the above-mentioned rank-deficient scenarios, since we have to estimate more channels, than the number of received streams.* Finally, the pilot overhead imposed by estimating $N_t \cdot N_r$ channels might become prohibitive, which erodes the attainable throughput gains.

- In order to tackle the above-mentioned challenging channel estimation problem, we designed *new iterative joint channel estimation and data detection techniques.* More explicitly, provided that a powerful MIMO MUD, such as the above-mentioned GA-aided or sphere-decoding based MUD is available for delivering a sufficiently reliable first data estimate, the power of decision-directed channel estimation may be invoked, which exploits that after a first tentative data decision - in the absence of decision errors - the receiver effectively knows the transmitted signal and hence may now exploit the presence of 100% pilot information for generating a more accurate channel estimate. Again, this design philosophy is detailed in the book in great depth in the context of joint iterative channel estimation and data detection.

- Although the number of studies/papers on cooperative communications increased exponentially over the past few years, most *investigations stipulate the simplifying assumption of having access to perfect channel information* - despite the fact that as detailed under the previous bullet-point, this is an extremely challenging task even for co-located MIMO elements.

- Hence it is necessary to design new non-coherently detected cooperative systems, which can dispense with the requirement of channel estimation, despite the typical 3 dB performance loss of differential detection. It is demonstrated in the book that *the low-complexity non-coherent detector's potential performance penalty can in fact be recovered with the aid of jointly detecting a number of consecutive symbols with the aid of the so-called multiple-symbol differential detector*, although this is achieved at the cost of an increased complexity.

- *Hence the proposed sphere-detector may be invoked again, but now as a reduced-complexity multiple-symbol differential detector*.

- The above-mentioned cooperative systems require *specifically designed resource allocation*, including the choice of the relaying protocols, the selection of the cooperating partners and the power-control techniques.

- It is demosntrated that when the available relaying partners are roaming close to the source, decode-and-forward (DF) is the best cooperating protocol, which avoids potential error-precipitation. By contrast, in case the cooperating partners roam closer to the destination, then the amplify-and-forward (AF) protocol is preferred for the same reasons. *These complementary features suggest the emergence of a hybrid DF/AF protocol*, which is controlled with the aid of our novel resource-allocation techniques.

- The book is concluded by outlining a variety of promising *future research directions.*

Our intention with the book is:

1. First, to pay tribute to all researchers, colleagues and valued friends, who contributed to the field. Hence this book is dedicated to them, since without their quest for better MIMO-OFDM solutions this monograph could not have been conceived. They are too numerous to name here, hence they appear in the author index of the book. Our hope is that the conception of this monograph on the topic will provide an adequate portrayal of the community's research and will further fuel this innovation process.

2. We expect to stimulate further research by exposing open research problems and by collating a range of practical problems and design issues for the practitioners. The coherent further efforts of the wireless research community is expected to lead to the solution of the range of outstanding problems, ultimately providing us with flexible coherent- and non-coherent detection aided as well as cooperative MIMO-OFDM wireless transceivers exhibiting a performance close to information theoretical limits.

List of Symbols

$(\cdot)[n,k]$	The indices indicating the k^{th} subcarrier of the n^{th} OFDM symbol
$(\cdot)^T$	The transposition operation
$(\cdot)^{\boldsymbol{H}}$	Hermitian transpose
$(\cdot)^*$	Complex conjugate
$\Im$	The imaginary component of a complex number
$\Re$	The real component of a complex number
$\mathcal{I}\{\cdot\}$	Imaginary part of a complex value
$\mathcal{I}$	Mutual information,sort
π	The ratio of the circumference of a circle to the diameter
$\mathcal{R}\{\cdot\}$	Real part of a complex value
$\exp(\cdot)$	The exponential operation
$\mathbf{A}^{(l)}$	The remaining user set for the l^{th} iteration of the subcarrier-to-user assignment process
$\boldsymbol{A}^{\mathrm{T}}$	Matrix/vector transpose
$\boldsymbol{A}^{\mathrm{H}}$	Matrix/vector hermitian adjoint, *i.e.* complex conjugate transpose
$\boldsymbol{A}^*$	Matrix/vector/scalar complex conjugate
$\boldsymbol{A}^{-1}$	Matrix inverse
$\boldsymbol{A}^+$	Moore-Penrose pseudoinverse
$\mathtt{tr}\,(\boldsymbol{A})$	Trace of matrix, *i.e.* the sum of its diagonal elements
α_p	The user load of an L-user and P-receiver conventional SDMA system
B_{r}	The overall system throughput in bits per OFDM symbol
$(i_{\mathrm{ce}}, i_{\mathrm{det}}, i_{\mathrm{dec}})$	Number of (channel estimation,detection,decoding) iterations
E_b	Energy per transmitted bit
E_s	Energy per transmitted M-QAM symbol
L_f	Number of data-frames per transmission burst
N_d	Number of data SDM-OFDM symbols per data-frame
N_p	Number of pilot SDM-OFDM symbols in burst preamble
T	OFDM symbol duration
T_s	OFDM FFT frame duration
f_{D}	Maximum Doppler frequency
K	Number of OFDM subcarriers
B	Signal bandwidth
β	RLS CIR tap prediction filter forgetting factor
$\mathcal{C}$	Uncostrained capacity
f_{c}	Carrier frequency
η	PASTD aided CIR tap tracking filter forgetting factor
γ	OHRSA search resolution parameter
m_{t}	Number of receive antennas
n_{r}	Number of transmit antennas
ν_τ	OFDM-symbol-normalized PDP tap drift rate
ρ	OHRSA search radius factor parameter
σ_w^2	Gaussian noise variance

τ_{rms}	RMS delay spread
ε	Pilot overhead
ζ	MIMO-CTF RLS tracking filter forgetting factor
b_{l,m_B}	The $(m_B)^{th}$ bit of the l^{th} user's transmitted symbol
r	Size of the transmitted bit-wise signal vector $\mathbf{t}$
$\hat{b}_s^{(l)}[n,k]$	The l^{th} user's detected soft bit
$\hat{\mathbf{b}}_s^{(l)}$	The detected soft bit block of the l^{th} user
$\mathbf{b}^{(l)}$	The information bit block of the l^{th} user
$\mathbf{b}_s^{(l)}$	The coded bit block of the l^{th} user
$\mathbb{C}$	The complex space
$\mathbb{C}^{(x\times y)}$	The $(x \times y)$-dimensional complex space
$\mathbf{CC}(n,k,K)$	Convolutional codes with the number of input bits k, the number of coded bits n and the constraint length K
$\boldsymbol{I}$	Identity matrix
$\mathcal{H}$	Hadamard matrix
$\mathcal{L}$	Log Likelihood Ratio value
$\mathcal{M}$	Set of M-PSK/M-QAM constellation phasors
$c_{g_l}(t)$	The DSS signature sequence assigned to the l^{th} user and associated with the g^{th} DSS group
$\bar{\mathbf{c}}_{G_q}$	The $(1 \times L_q)$-dimensional DSS code vector
$\check{\mathbf{c}}_{G_q}$	The $(G_q \times 1)$-dimensional DSS code vector
$\mathbf{c}_g$	The spreading code sequence associated with the g^{th} DSS group
$\mathbf{c}$	The user signature vector
$\mathbf{c}^{(l)}$	the l^{th} user's code sequence
$\mathbf{c}_{g_l}$	The DSS code vector for the l^{th} user in the g^{th} DSS group
$\check{\mathbf{s}}$	*A priori* signal vector estimate
$\hat{\mathbf{s}}$	*A posteriori* signal vector estimate
$\hat{\mathbf{x}}$	Unconstrained *a posteriori* signal vector estimate
$\mathbf{H}$	Subcarrier-related MIMO CTF matrix
$\mathbf{d}$	Transmitted bit-wise signal
$\mathbf{s}$	Transmitted subcarrier-related SDM signal
$\mathbf{t}$	Transmitted subcarrier-related bit-wise SDM signal
$\mathbf{y}$	Received subcarrier-related SDM signal
$\mathbf{w}$	Gaussian noise sample vector
$\tilde{\mathbf{s}}$	Soft-information aided signal vector estimate
$\Delta_{p,(y,x)}^{(l)}[n,k]$	The random step size for the $(p,l)^{th}$ channel gene during step mutation associated with the x^{th} individual of the y^{th} generation
ϵ	The pilot overhead
F_D	The OFDM-symbol-normalized Doppler frequency
$\texttt{Cov}\{\cdot,\cdot\}$	Covariance of two random variables
$\texttt{Var}\{\cdot\}$	Variance of a random variable
$\texttt{E}\{\cdot\}$	Expectation of a random variable
$\texttt{Ei}\{\cdot\}$	Exponential integral
$\texttt{JacLog}(\cdot)$	Jacobian logorithm
κ	Channel estimation efficiency criteria
$\|\cdot\|_2$	Second order norm
$\texttt{P}\{\cdot\}$	Probability density function
$\text{rms}\{\cdot\}$	Root mean square value
f_d'	Normalized Doppler frequency
f_c	Carrier frequency
f_d	Maximum Doppler frequency
f_q	Carrier frequency associated with the q^{th} sub-band

$f_{(y,x)}$	The fitness value associated with the x^{th} individual of the y^{th} generation
G	The number of DSS user groups in a DSS/SSCH system
G_q	The total number of different DSS codes used by the users activating the q^{th} subcarrier
$\Gamma_\tau(t)$	The rectangular pulse within the duration of $[0, \tau)$
$H_p^{(l)}$	The FD-CHTF associated with the l^{th} user and the p^{th} receiver antenna element
$H_{p,q}^{(l)}$	The FD-CHTF associated with the specific link between the l^{th} user and the p^{th} receiver at the q^{th} subcarrier
$H_p^{(l)}[n,k]$	The true FD-CHTF associated with the channel link between the l^{th} user and the p^{th} receiver
$\hat{H}_p^{(l)}[n,k]$	The improved *a posteriori* FD-CHTF estimate associated with the channel link between the l^{th} user and the p^{th} receiver
$\mathbf{H}$	The FD-CHTF matrix
$\mathbf{H}^{(l)}$	The FD-CHTF vector associated with the l^{th} user
$\mathbf{H}_{g,q}^{(l)}$	The $(P \times 1)$-dimensional FD-CHTF vector associated with the transmission paths between the l^{th} user's transmitter antenna and each element of the P-element receiver antenna array, corresponding to the g^{th} DSS group at the q^{th} subcarrier
$\mathbf{H}_p$	The p^{th} row of the FD-CHTF matrix $\mathbf{H}$
$\mathbf{H}_{g,q}$	The $(P \times l_g)$-dimensional FD-CHTF matrix associated with the g^{th} DSS group at the q^{th} subcarrier
$\mathbf{H}_{p,g,q}$	The p^{th} row of the FD-CHTF matrix $\mathbf{H}_{g,q}$ associated with the g^{th} DSS group at the q^{th} subcarrier
$\mathbf{H}_p[n,k]$	The initial FD-CHTF estimate matrix associated with all the channel links between each user and the p^{th} receiver
$\tilde{\mathbf{H}}_{p,q}$	The L_q users' $(L_q \times L_q)$-dimensional diagonal FD-CHTF matrix associated with the q^{th} subcarrier at the p^{th} receiver
$\tilde{\mathbf{H}}_p[n,k]$	The diagonal FD-CHTF matrix associated with all the channel links between each user and the p^{th} receiver
$\tilde{\mathbf{H}}[n,k]$	The trial FD-CHTF matrix of the GA-JCEMUD
$\tilde{\mathbf{H}}_{(y,x)}[n,k]$	The FD-CHTF chromosome of the GA-JCEMUD individual associated with the x^{th} individual of the y^{th} generation
$\tilde{H}_{p,(y,x)}^{(l)}[n,k]$	The $(p,l)^{th}$ channel gene of the GA-JCEMUD FD-CHTF chromosome associated with the x^{th} individual of the y^{th} generation
$\tilde{H}_p^{(l)}[0,k]$	The initial FD-CHTF estimate associated with the channel link between the l^{th} user and the p^{th} receiver at the k^{th} subcarrier in the first OFDM symbol duration
$\tilde{h}_p^{(l)}[n,k]$	The initial estimate of the CIR-related taps associated with the channel link between the l^{th} user and the p^{th} receiver
$\mathbf{I}$	Identity matrix
K_0	The range of CIR-related taps to be retained
L	Number of simultaneous mobile users supported in a SDMA system
L_q	The number of users that activate the q^{th} subcarrier
$\mathcal{L}_{l,m_B}$	The LLR associated with the $(m_B)^{th}$ bit position of the l^{th} user's transmitted symbol
$\Lambda_q^{(l)}(t)$	The subcarrier activation function
l_g	The number of users in the g^{th} DSS group
λ_{max}	The maximum mutation step size of the step mutation
$M_{\mathbf{WHT}}$	The WHT block size
$\mathcal{M}^L$	The set consisting of 2^{mL} number of $(L \times 1)$-dimensional trial vectors
$\mathcal{M}_{l,m_B,b}^L$	The specific subset associated with the l^{th} user, which is constituted by those specific trial vectors, whose l^{th} element's $(m_B)^{th}$ bit has a value of b

$\mathcal{M}_c$	The set containing the 2^m number of legitimate complex constellation points associated with the specific modulation scheme employed
m_B	The bit position of a constellation symbol
$\overline{\text{MSE}}$	The average FD-CHTF estimation MSE
$\overline{\text{MSE}}[n]$	The average FD-CHTF estimation MSE associated with the n^{th} OFDM symbol
N_T	The total number of OFDM symbols transmitted
$n_p(t)$	The AWGN at the p^{th} receiver
$n_{p,q}$	The noise signal associated with the q^{th} subcarrier at the p^{th} receiver
$\bar{\mathbf{n}}_{p,q}$	The $(G_q \times 1)$-dimensional effective noise vector associated with the q^{th} subcarrier at the p^{th} receiver
$\mathbf{n}$	Noise signal vector
ω_{ij}	The cross-correlation coefficient of the i^{th} DSS group's and the j^{th} DSS group's signature sequence
$\Omega(\cdot)$	The GA's joint objective function for all antennas
$\Omega_{g,q}(\cdot)$	The GA's joint objective function for all antennas associated with the g^{th} DSS group at the q^{th} subcarrier
$\Omega_{p,g,q}(\cdot)$	The GA's objective function associated with the g^{th} DSS group of the p^{th} antenna at the q^{th} subcarrier
$\Omega_p(\cdot)$	The GA's objective function associated with the p^{th} antenna
$\Omega_{y,T}$	The maximum GA objective score generated by evaluating the T individuals in the mating pool
P	Number of receiver antenna elements employed by the BS in SDMA systems
P_T	Transmitted signal power
$\tilde{p}_{mt}^{(ij)}$	The normalized mutation-induced transition probability
$p_{mt}^{(ij)}$	The 1D transition probability of mutating from a 1D symbol s_{Ri} to another 1D symbol s_{Rj}
$p_{mt}^{(ii)}$	The original legitimate constellation symbol's probability of remaining unchanged
$p_{mt}^{(ij)}$	The mutation-induced transition probability, which quantifies the probability of the i^{th} legitimate symbol becoming the j^{th}
p_m	The mutation probability, which denotes the probability of how likely it is that a gene will mutate
$\Phi(\cdot)$	The cost function of the OHRSA MUD
$\Phi_i(\cdot)$	The cumulative sub-cost function of the OHRSA MUD at the i^{th} recursive step
$\varphi^{(l)}$	The l^{th} user's phase angle introduced by carrier modulation
$\phi(\cdot)$	The sub-cost function of the OHRSA MUD
$Q(x)$	The Q-function
$\mathbf{Q}_L$	The L-order full permutation set
Q_c	The number of available subcarriers in conventional or SSCH systems
Q_f	The number of available sub-bands in SFH systems
Q_g	The number of subcarriers in a USSCH subcarrier group
$\mathbf{q}_k$	The subcarrier vector generated for the k^{th} subcarrier group
$\mathfrak{q}^{(l)}$	The USSCH pattern set of the l^{th} user
R	Code rate
$\mathbf{R}_\mathbf{n}$	The $(P \times P)$-dimensional covariance matrix
$\bar{\mathbf{R}}_{G_q}$	The $(G_q \times L_q)$-dimensional cross-correlation matrix of the L_q users' DSS code sequences
$r_p(t)$	The received signal at the p^{th} receiver
$r_{p,q}$	The discrete signal received at the q^{th} subcarrier of the p^{th} receiver during an OFDM symbol duration
$x_{p,g}(t)$	The despread signal of the g^{th} DSS group at the p^{th} receiver

$\hat{s}_i^{(l)}$	The i^{th} constellation point of $\mathcal{M}_c$ as well as a possible gene symbol for the l^{th} user
$s'^{(l)}_{g_l,q}(t)$	The transmitted signal at the q^{th} subcarrier associated with the l^{th} user in the g^{th} DSS group
$s^{(l)}$	The transmitted signal of the l^{th} user at a subcarrier
$s^{(l)}_{g_l,q}(t)$	The information signal at the q^{th} subcarrier associated with the l^{th} user in the g^{th} DSS group
s_{Ri}	The i^{th} 1D constellation symbol in the context of real axis
$\bar{\mathbf{s}}_q$	The L_q users' $(L_q \times 1)$-dimensional information signal vector
$\check{\mathbf{s}}$	The candidate trial vector
$\check{\mathbf{s}}_i$	The sub-vector of $\check{\mathbf{s}}$ at the i^{th} OHRSA recursive step
$\hat{\mathbf{s}}^{(l)}$	The l^{th} user's estimated information symbol block of the FFT length
$\hat{\mathbf{s}}^{(l)}_{\mathbf{w}}$	The estimated l^{th} user's WHT-despreading signal block
$\hat{\mathbf{s}}^{(l)}_{\mathbf{w},0}$	The estimated l^{th} user's WHT-despread signal block
$\hat{\mathbf{s}}_{\mathbf{GA}}$	The estimated transmitted symbol vector detected by the GA MUD
$\hat{\mathbf{s}}_{\mathbf{GA}_{g,q}}$	The GA-based estimated $(l_g \times 1)$-dimensional signal vector associated with the g^{th} DSS group at the q^{th} subcarrier
$\hat{\mathbf{s}}_{\mathbf{MMSE}_{g,q}}$	The MMSE-based estimated $(l_g \times 1)$-dimensional signal vector associated with the g^{th} DSS group at the q^{th} subcarrier
$\tilde{\mathbf{s}}[n,k]$	The trial data vector of the GA-JCEMUD
$\tilde{\mathbf{s}}_{(y,x)}$	The x^{th} individual of the y^{th} generation
$\tilde{\mathbf{s}}_{(y,x)}[n,k]$	The symbol chromosome of the GA-JCEMUD individual associated with the x^{th} individual of the y^{th} generation
$\mathbf{s}$	Transmitted signal vector
$\mathbf{s}^{(l)}$	The l^{th} user's information symbol block of the FFT length
$\mathbf{s}^{(l)}_{\mathbf{w}}$	The l^{th} user's WHT-spread signal block
$\mathbf{s}^{(l)}_{\mathbf{w},0}$	The l^{th} user's WHT-spreading signal block
$\mathbf{s}_g$	The $(l_g \times 1)$-dimensional trial symbol vector for the GA's objective function associated with the g^{th} DSS group
$\tilde{s}^{(l)}_{(y,x)}[n,k]$	The l^{th} symbol gene of the GA-JCEMUD symbol chromosome associated with the x^{th} individual of the y^{th} generation
σ_l^2	Signal variance associated with the l^{th} user
σ_n^2	Noise variance
T_h	The FH dwell time
$\mathbf{TC}(n,k,K)$	Turbo convolutional codes with the number of input bits k, the number of coded bits n and the constraint length K
T_r	The reuse time interval of hopping patterns
T_c	The DSS chip duration
$\mathbf{U}_{\mathbf{WHT}_K}$	The K-order WHT matrix
$u_{g_l}[c]$	The c^{th} element of the g^{th} row in the $(G \times G)$-dimensional WHT matrix, which is associated with the l^{th} user
$\mathbf{V}$	The upper-triangular matrix having positive real-valued elements on the main diagonal
ν	CM code memory
W	System bandwidth
W_{sc}	Subcarrier bandwidth
$\mathbf{W}_{\mathbf{MMSE}}$	The MMSE-based weight matrix
$\mathbf{W}_{\mathbf{MMSE}_{g,q}}$	The MMSE-based $(P \times l_g)$-dimensional weight matrix associated with the g^{th} DSS group at the q^{th} subcarrier
X	GA population size
x_p	The received signal at the p^{th} receiver at a subcarrier

$\bar{\mathbf{x}}_{p,q}$	The despread signal associated with the q^{th} subcarrier at the p^{th} receiver
$\mathbf{x}$	Received signal vector
$\mathbf{x}_p$	The received symbol block of the FFT length at the p^{th} receiver
$\mathbf{x}_{g,q}$	The $(P \times 1)$-dimensional despread signal vector associated with the g^{th} DSS group at the q^{th} subcarrier
Y	Number of GA generations

Chapter 1

Introduction to OFDM and MIMO-OFDM

1.1 OFDM History

In recent years Orthogonal Frequency Division Multiplexing (OFDM) [3–6] has emerged as a successful air-interface technique. In the context of wired environments, OFDM techniques are also known as Discrete MultiTone (DMT) [7] transmissions and are employed in the American National Standards Institute's (ANSI) Asymmetric Digital Subscriber Line (ADSL) [8], High-bit-rate Digital Subscriber Line (HDSL) [9], and Very-high-speed Digital Subscriber Line (VDSL) [10] standards as well as in the European Telecommunication Standard Institute's (ETSI) [11] VDSL applications. In wireless scenarios, OFDM has been advocated by many European standards, such as Digital Audio Broadcasting (DAB) [12], Digital Video Broadcasting for Terrestrial television (DVB-T) [13], Digital Video Broadcasting for Handheld terminals (DVB-H) [14], Wireless Local Area Networks (WLANs) [15] and Broadband Radio Access Networks (BRANs) [16]. Furthermore, OFDM has been ratified as a standard or has been considered as a candidate standard by a number of standardization groups of the Institute of Electrical and Electronics Engineers (IEEE), such as the IEEE 802.11 [17] and the IEEE 802.16 [18] standard families.

The concept of parallel transmission of data over dispersive channels was first mentioned as early as 1957 in the pioneering contribution of Doelz *et al.* [19], while the first OFDM schemes date back in 1960s, which were proposed by Chang [20] and Saltzberg [21]. In the classic parallel data transmission systems [20, 21], the Frequency-Domain (FD) bandwidth is divided into a number of non-overlapping subchannels, each of which hosts a specific carrier widely referred to as a subcarrier. While each subcarrier is separately modulated by a data symbol, the overall modulation operation across all the subchannels results in a frequency-multiplexed signal. All of the sinc-shaped subchannel spectra exhibit zero-crossings at all of the remaining subcarrier frequencies and the individual subchannel spectra are orthogonal to each other. This ensures that the subcarrier signals do not interfere with each other, when communicating over perfectly distortionless channels, as a consequence of their orthogonality [5].

The early OFDM schemes [20–23] required banks of sinusoidal subcarrier generators and demodulators, which imposed a high implementation complexity. This drawback limited the application of OFDM to military systems until 1971, when Weinstein and Ebert [24] suggested that the Discrete Fourier Transform (DFT) can be used for the OFDM modulation and demodulation processes, which significantly reduces the implementation complexity of OFDM. Since then, more practical OFDM research has been carried out. For example, in the early 1980s Peled and Ruiz [25] proposed a simplified FD data transmission method using a cyclic prefix aided technique and exploited reduced-complexity algorithms for achieving a significantly lower computational complexity than that of classic single-carrier time-domain Quadrature Amplitude Modulation (QAM) [26] modems. Around the same era, Keasler *et al.* [27] invented a high-speed OFDM modem for employment in switched networks, such as the telephone network. Hirosaki designed a subchannel-based equalizer for an orthogonally multiplexed QAM system in 1980 [28] and later introduced the DFT-based implementation of OFDM systems [29], based on which a so-called groupband data modem was developed [30]. Cimini [31] and Kalet [32] investigated the performance of OFDM modems in mobile communication channels. Furthermore, Alard and Lassalle [33] applied OFDM in digital broadcasting systems, which was the pioneering work of the European DAB standard [12] established in the mid-1990s. More recent advances in OFDM transmission were summarized in the state-of-the-art collection of works edited by Fazel and Fettweis [34]. Other important recent OFDM references include the books by Hanzo *et al.* [5] and Van Nee *et al.* [6] as well as a number of overview papers [35–37].

OFDM has some key advantages over other widely-used wireless access techniques, such as Time Division Multiple Access (TDMA) [38], Frequency Division Multiple Access (FDMA) [38] and Code Division Multiple Access (CDMA) [39–43]. The main merit of OFDM is the fact that the radio channel is divided into many narrow-band, low-rate, frequency-nonselective subchannels or subcarriers, so that multiple symbols can be transmitted in parallel, while maintaining a high spectral efficiency. Each subcarrier may deliver information for a different user, resulting in a simple multiple access scheme known as Orthogonal Frequency Division Multiple Access (OFDMA) [44–47]. This enables different media such as video, graphics, speech, text, or other data to be transmitted within the same radio link, depending on the specific types of services and their Quality-of-Service (QoS) requirements. Furthermore, in OFDM systems different modulation schemes can be employed for different subcarriers or even for different users. For example, the users close to the Base Station (BS) may have a relatively good channel quality, thus they can use high-order modulation schemes to increase their data rates. By contrast, for those users that are far from the BS or are serviced in highly-loaded urban areas, where the subcarriers' quality is expected to be poor, low-order modulation schemes can be invoked [48].

Besides its implementational flexibility, the low complexity required in transmission and reception as well as the attainable high performance render OFDM a highly attractive candidate for high data rate communications over time-varying frequency-selective radio channels. For example, in classic single-carrier systems, complex equalizers have to be employed at the receiver for the sake of mitigating the Inter-Symbol Interference (ISI) introduced by multi-path propagation. By contrast, when using a cyclic prefix [25], OFDM exhibits a high resilience against the ISI. Incorporating channel coding techniques into OFDM systems, which results in Coded OFDM (COFDM) [49, 50], allows us to maintain robustness against frequency-selective fading channels, where busty errors are encountered at specific subcarriers in the FD.

However, besides its significant advantages, OFDM also has a few disadvantages. One problem is the associated increased Peak-to-Average Power Ratio (PAPR) in comparison to single-carrier systems [5], requiring a large linear range for the OFDM transmitter's output amplifier. In addition, OFDM is sensitive to carrier frequency offset, resulting in Inter-Carrier Interference (ICI) [51].

As a summary of this section, we outline the milestones and the main contributions found in the OFDM literature in Tables 1.1 and 1.2.

1.1.1 Multiple-Input Multiple-Output Assisted OFDM

1.1.1.1 The Benefits of MIMOs

High data-rate wireless communications have attracted significant interest and constitute a substantial research challenge in the context of the emerging WLANs and other indoor multimedia networks. Specifically, the employment of multiple antennas at both the transmitter and the receiver, which is widely referred to as the Multiple-Input Multiple-Output (MIMO) technique, constitutes a cost-effective approach to high-throughput wireless communications.

The concepts of MIMOs have been under development for many years for both wired and wireless systems. One of the earliest MIMO applications for wireless communications dates back to 1984, when Winters [93] published a breakthrough contribution, where he introduced a technique of transmitting data from multiple users over the same frequency/time channel using multiple antennas at both the transmitter and receiver ends. Based on this work, a patent was filed and approved [94]. Sparked off by Winters' pioneering work [93], Salz [95] investigated joint transmitter/receiver optimization using the MMSE criterion. Since then, Winters and others [96–104] have made further significant advances in the field of MIMOs. In 1996, Raleigh [105] and Foschini [106] proposed new approaches for improving the efficiency of MIMO systems, which inspired numerous further contributions [107–115].

As a key building block of next-generation wireless communication systems, MIMOs are capable of supporting significantly higher data rates than the Universal Mobile Telecommunications System (UMTS) and the High Speed Downlink Packet Access (HSDPA) based 3G networks [116]. As indicated by the terminology, a MIMO system employs multiple transmitter and receiver antennas for delivering parallel data streams, as illustrated in Figure 1.1. Since the information is transmitted through different paths, a MIMO system is capable of exploiting both transmitter and receiver diversity, hence maintaining reliable communications. Furthermore, with the advent of multiple antennas, it becomes possible to jointly process/combine the multi-antenna signals and thus improves the system's integrity and/or throughput. Briefly, compared to Single-Input Single-Output (SISO) systems, the two most significant advantages of MIMO systems are:

- A significant increase of both the system's capacity and spectral efficiency. The capacity of a wireless link increases linearly with the minimum of the number of transmitter or the receiver antennas [105, 107]. The

Year	Milestone
1957	The concept of parallel data transmission by Doelz *et al.* [19].
1966	First OFDM scheme proposed by Chang [20] for dispersive fading channels.
1967	Saltzberg [21] studied a multi-carrier system employing Orthogonal QAM (O-QAM) of the carriers.
1970	U.S. patent on OFDM issued [23].
1971	Weinstein and Ebert [24] applied DFT to OFDM modems.
1980	Hirosaki designed a subchannel-based equalizer for an orthogonally multiplexed QAM system [28].
	Keasler *et al.* [27] described an OFDM modem for telephone networks.
1985	Cimini [31] investigated the feasibility of OFDM in mobile communications.
1987	Alard and Lasalle [33] employed OFDM for digital broadcasting.
1991	ANSI ADSL standard [8].
1994	ANSI HDSL standard [9].
1995	ETSI DAB standard [12]: the first OFDM-based standard for digital broadcasting systems.
1996	ETSI WLAN standard [15].
1997	ETSI DVB-T standard [13].
1998	ANSI VDSL and ETSI VDSL standards [10, 11].
	ETSI BRAN standard [16].
1999	IEEE 802.11a WLAN standard [52].
2002	IEEE 802.11g WLAN standard [53].
2003	Commercial deployment of FLASH-OFDM [54, 55] commenced.
2004	ETSI DVB-H standard [14].
	IEEE 802.16-2004 WMAN standard [56].
	IEEE 802.11n draft standard for next generation WLAN [57].
2005	Mobile cellular standard 3GPP Long-Term Evolution (LTE) [58] downlink.
2007	Multi-User MIMO-OFDM for Next-Generation Wireless [59]
	Adaptive HSDPA-Style OFDM and MC-CDMA Transceivers [60].

Table 1.1: Milestones in the history of OFDM.

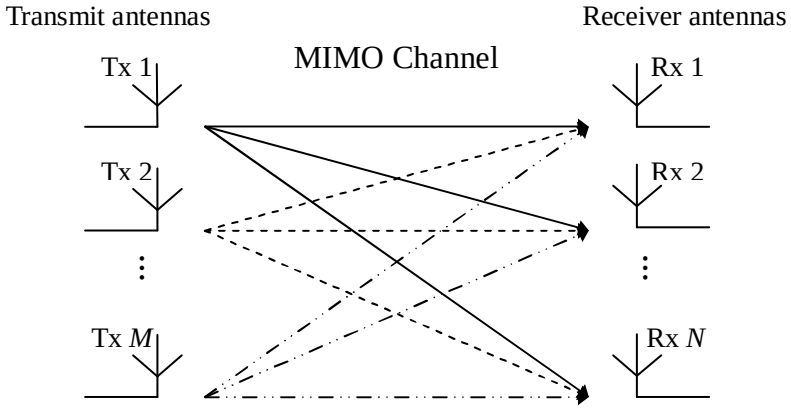

Figure 1.1: Schematic of the generic MIMO system employing M transmitter antennas and N receiver antennas.

Year	Author(s)	Contribution
1966	Chang [20]	Proposed the first OFDM scheme.
1967	Saltzberg [21]	Studied a multi-carrier system employing O-QAM.
1968	Chang and Gibby [22]	Presented a theoretical analysis of the performance of an orthogonal multiplexing data transmission scheme.
1970	Chang [23]	U.S. patent on OFDM issued.
1971	Weinstein and Ebert [24]	Applied DFT to OFDM modems.
1980	Hirosaki [28]	Designed a subchannel-based equalizer for an orthogonally multiplexed QAM system.
	Peled and Ruiz [25]	Described a reduced-complexity FD data transmission method together with a cyclic prefix technique.
	Keasler *et al.* [27]	Invented an OFDM modem for telephone networks.
1981	Hirosaki [29]	Suggested a DFT-based implementation of OFDM systems.
1985	Cimini [31]	Investigated the feasibility of OFDM in mobile communications.
1986	Hirosaki, Hasegawa and Sabato [30]	Developed a groupband data modem using an orthogonally multiplexed QAM technique.
1987	Alard and Lasalle [33]	Employed OFDM for digital broadcasting.
1989	Kalet [32]	Analyzed multitone QAM modems in linear channels.
1990	Bingham [3]	Discussed various aspects of early OFDM techniques in depth.
1991	Cioffi [8]	Introduced the ANSI ADSL standard.
1993-1995	Warner [61], Moose [51] and Pollet [62]	Conducted studies on time and frequency synchronization in OFDM systems.
1994-1996	Jones [63], Shepherd [64] and Wulich [65, 66]	Explored various coding and post-processing techniques designed for minimizing the peak power of the OFDM signal.
1997	Li and Cimini [67, 68]	Revealed how clipping and filtering affect OFDM systems.
	Hara and Prasad [69]	Compared various methods of combining CDMA and OFDM.
1998	Li, Cimini and Sollenberger [70]	Designed a robust Minimum Mean Square Error (MMSE) based channel estimator for OFDM systems.
	May, Rohling and Engels [49]	Carried out a performance analysis of Viterbi decoding in the context of 64-Differential Amplitude and Phase-Shift Keying (64-DAPSK) and 64QAM modulated OFDM signals.
1999	Li and Sollenberger [71]	Focused on parameter estimation invoked by a MMSE diversity combiner designed for adaptive antenna array aided OFDM.
	Armour, Nix and Bull [72–74]	Illustrated the combined OFDM-equalization aided receiver and the design of pre-Fast Fourier Transform (FFT) equalizers.
	Prasetyo and Aghvami [75, 76]	Simplified the transmission frame structure for achieving fast burst synchronization in OFDM systems.
	Wong *et al.* [77]	Advocated a subcarrier, bit and power allocation algorithm to minimize the total transmit power of multi-user OFDM.
2000	Fazel and Fettweis [34]	A collection of state-of-the-art works on OFDM.
	Van Nee and Prasad [6]	OFDM for wireless multimedia communications.
	Lin, Cimini and Chuang [50]	Invoked turbo coding in an OFDM system using diversity.
2001-2002	Lu and Wang [78–81]	Considered channel coded STC-assisted OFDM systems.
2003	Hanzo, Münster, Choi and Keller [5]	OFDM for broadband multi-user communications, WLANs and broadcasting.
2004	Simeone, Bar-Ness and Spagnolini [82]	Demonstrated a subspace tracking algorithm used for channel estimation in OFDM systems.
	J. Zhang, Rohling and P. Zhang [83]	Adopted an Inter-Carrier Interference (ICI) cancellation scheme to combat the ICI in OFDM systems.
	Necker and Stüber [84]	Exploited a blind channel estimation scheme based on the Maximum Likelihood (ML) principle in OFDM systems.
	Doufexi *et al.* [85]	Reflected the benefits of using sectorized antennas in WLANs.
	Alsusa, Lee and McLaughlin [86]	Proposed packet based multi-user OFDM systems using adaptive subcarrier-user allocation.
2005	Williams *et al.* [87]	Evaluated a pre-FFT synchronisation method for OFDM.
2007	Jiang and Hanzo [59]	Multi-user MIMO-OFDM for next-generation wireless.
	Hanzo and Choi [60]	Adaptive HSDPA-style OFDM and MC-CDMA transceivers.
2009	Fischer and Siegl [88]	Peak-to-average power ratio reduction in single- and multi-antenna OFDM.
	Mileounis *et al.* [89]	Blind identification of Hammerstein channels using QAM, PSK, and OFDM inputs.
	Huang and Hwang [90]	Improvement of active interference cancellation: avoidance technique for OFDM cognitive radio.
	Chen *et al.* [91]	Spectrum sensing for OFDM systems employing pilot tones.
	Talbot and Farhang-Boroujeny [92]	Time-varying carrier offsets in mobile OFDM

Table 1.2: Main contributions on OFDM.

data rate can be increased by spatial multiplexing without consuming more frequency resources and without increasing the total transmit power.

- Dramatic reduction of the effects of fading due to the increased diversity. This is particularly beneficial, when the different channels fade independently.

An overview of MIMO techniques covering channel models, performance limits, coding and transceiver designs can be found in [117].

1.1.1.2 MIMO OFDM

The quality of a wireless link can be described by three basic parameters, namely the transmission rate, the transmission range and the transmission reliability. Conventionally, the transmission rate may be increased by reducing the transmission range and reliability. By contrast, the transmission range may be extended at the cost of a lower transmission rate and reliability, while the transmission reliability may be improved by reducing the transmission rate and range [118]. However, with the advent of MIMO assisted OFDM systems, the above-mentioned three parameters may be simultaneously improved [118]. Initial field tests of broadband wireless MIMO-OFDM communication systems have shown that an increased capacity, coverage and reliability is achievable with the aid of MIMO techniques [119]. Furthermore, although MIMOs can potentially be combined with any modulation or multiple access technique, recent research suggests that the implementation of MIMO aided OFDM is more efficient, as a benefit of the straightforward matrix algebra invoked for processing the MIMO OFDM signals [118].

MIMO OFDM, which is claimed to be invented by Airgo Networks [120], has formed the foundation of all candidate standards proposed for IEEE 802.11n [121]. In recent years, this topic has attracted substantial research efforts, addressing numerous aspects, such as system capacity [122, 123], space/time/frequency coding [124–128], Peak-to-Average Power Ratio (PAPR) control [129–131], channel estimation [132–134], receiver design [135–138], etc. Recently, Paulraj *et al.* [117] and Stüber *et al.* [139] provided compelling overviews of MIMO OFDM communications. Furthermore, Nortel Networks has developed a MIMO OFDM prototype [140] during late 2004, which demonstrates the superiority of MIMO OFDM over today's networks in terms of the achievable data rate. For the reader's convenience, we have summarized the major contributions on MIMO OFDM in Tables 1.3, 1.4 and 1.5 at a glance.

1.1.1.3 SDMA-based MIMO OFDM Systems

As a subclass of MIMO arrangements, recently the Space Division Multiple Access (SDMA) [5, 194–196] based techniques have attracted substantial interest. As one of the most promising techniques aiming at solving the capacity problem of wireless communication systems, SDMA enables multiple users to simultaneously share the same bandwidth in different geographical locations. More specifically, the exploitation of the spatial dimension, namely the so-called spatial signature, makes it possible to identify the individual users, even when they are in the same time/frequency/code domains, thus increasing the system's capacity.

In Figure 1.2 we illustrate the concept of SDMA systems. As shown in Figure 1.2, each user exploiting a single transmitter antenna aided Mobile Station (MS) simultaneously communicates with the BS equipped with an array of receiver antennas. Explicitly, SDMA can be considered as a specific branch of the family of MIMO systems, where the transmissions of the multiple transmitter antennas cannot be coordinated, simply because they belong to different users. Briefly speaking, the major advantages of SDMA techniques are [197]:

- *Range extension*: With the aid of antenna array, the coverage area of high-integrity reception can be significantly larger than that of any single-antenna aided systems. In a SDMA system, the number of cells required for covering a given geographic area can be substantially reduced. For example, a ten-element array offers a gain of ten, which typically doubles the radius of the cell and hence quadruples the coverage area.

- *Multi-path mitigation*: Benefitting from the MIMO architecture, in SDMA systems the detrimental effects of multi-path propagations are effectively mitigated. Furthermore, in specific scenarios the multi-path phenomenon can even be exploited for enhancing the desired users' signals by employing efficient receiver diversity schemes.

- *Capacity increase*: Theoretically, SDMA can be incorporated into any existing multiple access standard at the cost of a limited increase in system complexity, while attaining a substantial increase in capacity. For instance, by applying SDMA to a conventional TDMA system, two or more users can share the same time slots, resulting in a doubled or higher overall system capacity.

Year	Author(s)	Contribution
	Piechocki *et al.* [141]	Reported on the performance benefits of spatial multiplexing using ML decoding for a Vertical Bell Labs Layered Space-Time (V-BLAST) OFDM system.
2001	Blum, Li, Winters and Yan [124]	Studied improved space-time coding techniques for MIMO OFDM systems.
	Li [132]	Exploited optimum training sequence design and simplified channel estimation for improving the performance and for reducing the complexity of channel parameter estimation in MIMO OFDM systems.
	Bolckei, Gesbert and Paulraj [122]	Analyzed the influence of physical parameters such as the amount of delay spread, cluster angle spread and total angle spread, as well as system parameters such as the number of antennas and the antenna spacing on both the ergodic capacity and outage capacity.
	Catreux *et al.* [142]	Offered an overview of the challenges and promises of link adaptation in future broadband wireless networks.
2002	Piechocki *et al.* [143]	Presented a performance evaluation of spatial multiplexing and space-frequency coded modulation schemes designed for WLANs.
	Molisch, Win and Winters [144]	Proposed a reduced-complexity method for grouping multiple antennas and space-time codes.
	Li, Winters and Sollenberger [135]	Invoked space-time coding and Successive Interference Cancellation (SIC) in MIMO OFDM systems.
	Stamoulis *et al.* [145]	Revealed the effects of ICI on MIMO-OFDM.
	Doufexi *et al.* [146]	Characterized the outdoor physical layer performance of a coded MIMO OFDM system using space-time processing.
	Giangaspero *et al.* [136]	Compared two Co-Channel Interference (CCI) cancellation schemes in the context of MIMO OFDM.
	Li, Letaief and Cao [137]	Advocated a CCI cancellation method using angle diversity based on null-steering or minimum variance distortion response beamforming.
	Bölcskei, Borgmann and Paulraj [147]	Measured the impact of the propagation environment on the performance of space-frequency coded MIMO OFDM.
	Barhumi, Leus and Moonen [133]	Described a Least-Squares (LS) channel estimation scheme designed for MIMO OFDM systems based on pilot tones.
	Ganesan and Sayeed [123]	Derived a virtual MIMO framework for single-transmitter, single-receiver multipath fading channels that enables maximal exploitation of channel diversity at both the transmitter and the receiver.
2003	Gamal *et al.* [125]	Utilized an OFDM technique to transform the MIMO multi-path channel into a MIMO flat block fading channel, where the associated diversity is exploited by employing space-frequency codes.
	Moon *et al.* [129]	Evaluated the PAPR performance in a MIMO OFDM-based WLAN system using a Space-Time Block Code (STBC).
	Cai, Song and Li [148]	Developed a technique based on the auto-correlation function for estimating the Doppler spread in Rayleigh fading channels for mobile OFDM systems using multiple antennas.
	Leus and Moonen [149]	Employed tone-by-tone based equalization techniques in MIMO OFDM systems.
	Lee *et al.* [130]	Investigated the PAPR characteristics in a MIMO OFDM system using the selective mapping approach.
	Piechocki *et al.* [150]	Devised a blind method for joint detection of space-time coded MIMO OFDM.

Table 1.3: Main contributions on MIMO OFDM (Part 1).

Year	Author(s)	Contribution
2004	Shin, H. Lee and C. Lee [134]	Suggested a cyclic comb-type training structure for reducing the Mean-Square Errors (MSEs) at the edge subcarriers of MIMO OFDM signals.
	Xia, Zhou and Giannakis [151]	Created an adaptive MIMO OFDM transmitter by applying an adaptive two-dimensional coder-beamformer with the aid of partial channel knowledge.
	Huang and Letaief [152]	Portrayed an OFDM symbol based space diversity technique.
	Butler and Collings [153]	Employed an approximate log-likelihood decoding approach based on a Zero-Forcing (ZF) receiver for bit-interleaved coded modulation assisted MIMO OFDM systems.
	Stüber *et al.* [139]	Summarized various physical layer research challenges in MIMO-OFDM system design.
	Paulraj *et al.* [117]	Provided an overview of MIMO and/or MIMO OFDM systems.
	Lu, Yue and Wang [154]	Identified the performance of an optimized MIMO OFDM scheme using Low Density Parity Check (LDPC) codes.
	Van Zelst and Schenk [155]	Implemented MIMO OFDM processing and evaluated its performance by both simulations and experimental test results.
	Pascual-Iserte, Pérez-Neira and Lagunas [156]	Conducted studies on maximizing the Signal to Noise and Interference Ratio (SNIR) over the subcarriers subject to a total transmit power constraint.
	Zeng and Ng [157]	Contrived a subspace-based semi-blind method for estimating the channel responses of a multi-user and multi-antenna OFDM uplink system.
	Alien *et al.* [158]	Assessed the performance of spatial diversity in an OFDM WLAN for various antenna topologies.
	Dayal, Brehler and Varanasi [126]	Introduced space-time channel-sounding training codes designed for multiple-antenna, noncoherent, multiple block Rayleigh fading channel.
	Park and Kang [138]	Adopted a reduced-complexity iterative algorithm for joint Maximum-A-Posteriori (MAP) detection and CCI suppression in MIMO OFDM systems.
	Tan and Stüber [159]	Combined cyclic delay diversity and MIMO OFDM for achieving full spatial diversity in flat-fading channels.
	Wang, Shayan and Zeng [160]	Illustrated the diversity and coding advantages in terms of the minimum Hamming distance and the minimum squared product distance of the code as well as the relative frequencies.
	Pan, Letaief and Cao [161]	Discussed dynamic spatial subchannel allocation in conjunction with adaptive beamforming in broadband OFDM wireless systems.
	Tepedelenlioğlu and Challagulla [162]	Demonstrated how to achieve high diversity gains in MIMO OFDM systems with the aid of fractional sampling.
	Baek *et al.* [163]	Addressed a time-domain semi-blind channel estimation approach and a PAPR Reduction scheme for MIMO OFDM.
	Dubuc *et al.* [140]	Outlined Nortel Networks' MIMO OFDM concept prototype and provided measured performance results.
	Barriac and Madhow [164]	Offered guidelines for optimizing the antenna spacing in MIMO OFDM systems using feedback of the covariance matrix of the downlink channel.

Table 1.4: Main contributions on MIMO OFDM (Part 2).

- *Interference suppression*: The interference imposed by other systems and by users in other cells can be significantly reduced by exploiting the desired user's unique, user-specific Channel Impulse Responses (CIRs).
- *Compatibility*: SDMA is compatible with most of the existing modulation schemes, carrier frequencies and other specifications. Furthermore, it can be readily implemented using various array geometries and antenna types.

The combination of SDMA and OFDM results in SDMA-OFDM systems [5, 194, 198, 199], which exploit the merits of both SDMA and OFDM, having attracted more and more interest [199–204]. Tables 1.6 and 1.7 summarize the main contributions on SDMA and SDMA-OFDM found in the open literature.

1.2 OFDM Schematic

In this section we briefly introduce Orthogonal Frequency Division Multiplexing (OFDM) as a means of dealing with the problems of frequency selective fading encountered, when transmitting over a high-rate wideband radio channel.

In the OFDM scheme of Figure 1.3 the serial data stream of a traffic channel is passed through a serial-to-parallel convertor, which splits the data into a number of parallel sub-channels. The data in each sub-channel are applied

Year	Author(s)	Contribution
	Su, Safar and Liu [127, 128]	Designed a general space-frequency block code structure capable of providing full-rate, full-diversity MIMO OFDM transmission.
	Zhang, Kavcic and Wong [165]	Researched an optimal QR decomposition technique designed for a precoded MIMO OFDM system using successive-cancellation detection.
	Yao and Giannakis [166]	Proposed a low-complexity blind Carrier Frequency Offset (CFO) estimator for OFDM systems.
	Zheng *et al.* [167]	Extended Time-Division Synchronous CDMA (TD-SCDMA) to Time-Division Code-Division Multiplexing OFDM (TD-CDM-OFDM) for future 4G systems.
	Yang [168]	Reviewed the state-of-the-art approaches in MIMO OFDM air-interface.
	Zhang and Letaief [169]	Aimed at developing an adaptive resource-allocation approach which jointly allocates subcarriers, power and bits for multi-user MIMO OFDM systems.
	Ma [170]	Established a pilot-assisted modulation scheme for CFO and channel estimation in OFDM transmissions over frequency-selective MIMO fading channels.
	Fozunbal, McLaughlin and Schafer [171]	Calculated a sphere packing lower bound and a pairwise error upper bound of the error probability of space-time-frequency coded OFDM systems using multiple antennas for transmission over block-fading channels.
	Nanda *et al.* [172]	Built a MIMO WLAN prototype that provides data rates over 200Mb/s.
	Kim *et al.* [173]	Invoked a QR-Decomposition combined with the M-algorithm (QRD-M) for joint data detection and channel estimation in MIMO OFDM.
	Qiao *et al.* [174]	Contrived an iterative LS channel estimation algorithm for MIMO OFDM.
	Sampath, Erceg and Paulraj [175]	Validated the properties of the transmit correlation matrix through field trial results obtained from a MIMO OFDM wireless system operated in a macro-cellular environment.
	Rey, Lamarca and Vazquez [176]	Used a Bayesian approach to design transmit prefiltering matrices for closed-loop schemes, which is robust to channel estimation errors.
2005	Sun, Xiong and Wang [177]	Targeted at designing CFO estimator aided Expectation Maximization (EM) based iterative receivers for MIMO OFDM systems.
	Han and Lee [131]	Provided an overview of PAPR reduction techniques for multicarrier transmission.
	Lodhi *et al.* [178]	Evaluated the complexity and performance of a Multi-Carrier Code-Division Multiple-Access (MC-CDMA) system exploiting STBCs and Cyclic Delay Diversity (CDD).
	Wang, Han and Liu [179]	Advanced MIMO OFDM channel estimation using a scheme based on estimating the Time-of-Arrivals (TOAs).
	Wen, Wang and Chen [180]	Reported on a low-complexity multi-user angle-frequency coding scheme based on the Fourier basis structure for downlink wireless systems.
	Su, Safar and Liu [181]	Performance analysis of MIMO OFDM systems invoking coding in spatial, temporal and frequency domains.
	Tan, Latinović and Bar-Ness [182]	Advocated a scheme of cross-antenna rotation and inversion utilizing additional degrees of freedom by employing multiple antennas in OFDM systems.
	Park and Cho [183]	Characterized a MIMO OFDM technique based on the weighting factor optimization for reducing the ICI caused by time-varying channels.
	Shao and Roy [184]	Maximized the diversity gain achieved over frequency-selective channels by employing a full-rate space-frequency block code for MIMO OFDM systems.
	Schenk *et al.* [185]	Quantified how the transmitter/receiver phase noise affects the performance of a MIMO OFDM system.
	Borgmann and Bölcskei [186]	Contributed to the code designs for noncoherent frequency-selective MIMO OFDM fading links.
	Tarighat and Sayed [187]	Examined the effect of IQ imbalances on MIMO OFDM systems and developed a digital signal processing framework for combating these distortions.
	Jiang, Li and Hager [188]	Formulated a joint transceiver design combining the Geometric Mean Decomposition (GMD) with ZF-type decoders.
	Choi and Heath [189]	Constructed a limited feedback architecture that combines beamforming vector quantization and smart vector interpolation.
	Baek *et al.* [190]	Incorporated multiple antennas into high-rate DAB systems.
2007	Jiang and Hanzo [59]	Reduced-complexity Near-ML SDMA-MUDs and joint iterative channel estimation.
	Hanzo and Choi [60]	Near-instantaneously adaptive HSPA-style OFDM and MC-CDMA transceivers.
	Fischer and Siegl [88]	Peak-to-average power ratio reduction in single- and multi-antenna OFDM.
	Fakhereddin *et al.* [191]	Reduced feedback and random beamforming for OFDM MIMO.
2009	De *et al.* [192]	Linear prediction based semiblind channel estimation for multiuser OFDM.
	Haring *et al.* [193]	Fine frequency synchronization in the uplink of multiuser OFDM systems.

Table 1.5: Main contributions on MIMO OFDM (Part 3).

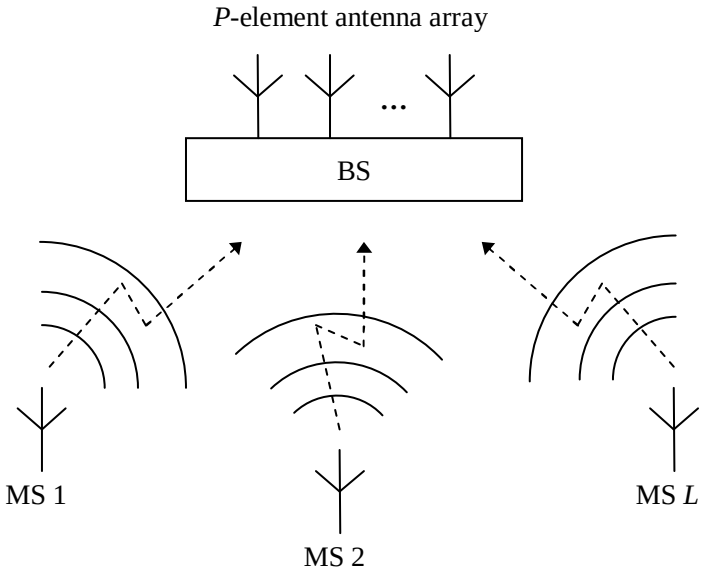

Figure 1.2: Illustration of the generic SDMA system employing a P-element receiver antenna array for supporting L number of mobile users.

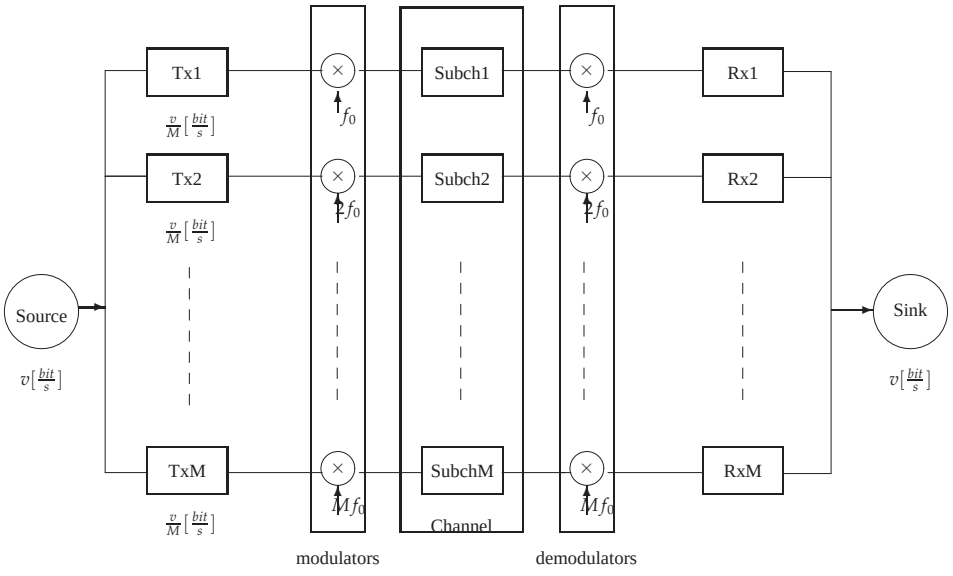

Figure 1.3: Simplified blockdiagram of the orthogonal parallel modem

Year	Author(s)	Contribution
1982	Yeh and Reudink [205]	Illustrated that high spectrum efficiencies can be achieved in mobile radio systems using a modest number of space diversity branches.
1983	Ko and Davis [206]	Early studies on SDMA in the context of satellite communication networks.
1989	Swales, Beach and Edwards [207, 208]	Devised a multi-beam adaptive BS antenna in an attempt to mitigate the problem of limited radio resources.
1990	Agee, Schell and Gardner [209]	Invoked narrowband antenna arrays for blind adaptive signal extraction.
1991	Anderson *et al.* [210]	Adopted adaptive antenna techniques to increase the channel capacity.
1992	Balaban and Salz [211, 212]	Provided a comprehensive characterization of space diversity reception combined with various equalization techniques.
1994	Xu *et al.* [213]	Offered preliminary results of experimental studies on SDMA systems.
	Talwar, Viberg and Paulraj [214]	Described an approach for separating and estimating multiple co-channel signals with the aid of an antenna array.
1995	Van Der Veen *et al.* [215]	Blindly identified Finite Impulse Response (FIR) channels using oversampling and the finite-alphabet property of digital signals.
	Khalaj, Paulraj and Kailath [216]	Estimated the spatio-temporal characteristics of the radio channel in coherent direct-sequence spread-spectrum systems.
	Anand, Mathew and Reddy [217]	Established a method of blind separation of co-channel Binary Phase-Shift Keying (BPSK) signals arriving at an antenna array.
1997	Liu and Xu [218]	Addressed the SDMA uplink blind channel and sequence estimation problem.
	Tsoulos, Beach and McGeehan [219]	Reported the research of the TSUNAMI project that demonstrated the benefits of SDMA in wireless communications.
1998	Deneire and Slock [220]	Derived a subspace fitting and linear prediction method using cyclic statistics of fractionally sampled channels for channel identification in multi-user and multi-antenna systems.
	Tsoulos, McGeehan and Beach [221, 222]	Provided an experimental demonstration of both transmit and receive beamforming supporting SDMA user access.
	Barroso *et al.* [223]	Introduced a blind algorithm referred to as Array Channel Division Multiple Access (AChDMA) for advanced SDMA in mobile communications systems.
	Demmerle and Wiesbeck [224]	Designed a biconical multi-beam antenna structure for SDMA communications.
	Lindmark [225]	Built a dual-polarized antenna array for a SDMA system working in the 1850-1990MHz band.
	Suard *et al.* [226]	Investigated the channel capacity enhancement of a SDMA system.
	Jeng *et al.* [227]	Presented extensive experimental results of spatial signature variation using a smart antenna testbed.
	Petrus, Ertel and Reed [228]	Proved that capacity improvement can be achieved using adaptive arrays at the BS of an Advanced Mobile Phone Service (AMPS) system.
	Xavier, Barroso and Moura [229]	Targeted at designing a closed-form estimator for the SDMA MIMO channel based on second-order statistics.
	Farsakh and Nossek [230]	Developed an approach for jointly calculating array weights in such a way that all users receive their signal at a given SINR level.
1999	Tsoulos [231]	Provided an overview of smart antennas in the context of current and future personal communication systems.
	Piolini and Rolando [232]	Analyzed a channel-assignment algorithm for SDMA mobile systems.
	Vandenameele *et al.* [194, 198, 199]	Advocated a combined SDMA-OFDM approach that couples the capabilities of the two techniques.
	Galvan-Tejada and Gardiner [233, 234]	Calculated the theoretical blocking probability resulting from SDMA technology in two different channel allocation schemes.
	Tsoulos [235]	Focused on TDMA air interface techniques combined with SDMA schemes.
	Vornefeld, C. Walke and B. Walke [236]	Applied SDMA techniques to WATM systems.

Table 1.6: Main contributions on SDMA (Part 1).

Year	Author(s)	Contribution
2000	Djahani and Kahn [237]	Discussed the employment of multi-beam transmitters and imaging receivers in SDMA implementations.
2001	Shad *et al.* [238]	Invoked dynamic slot allocation in packet-switched SDMA systems.
	Kuehner *et al.* [239]	Considered a BS that communicates with smart-antenna aided mobiles operating in multi-beam, packet-switched and SDMA modes.
2002	Jeon *et al.* [240]	Contrived a smart antenna assisted system using adaptive beamforming for broadband wireless communications.
	Bellofiore *et al.* [241,242]	Emphasized the interaction and integration of several critical components of a mobile communication network using smart-antenna techniques.
	Fang [243]	Carried out a realistic performance analysis of resource allocation schemes for SDMA systems and obtained analytical results for blocking probability.
	Arredondo, Dandekar and Xu [244]	Employed a novel synthesis and prediction filter at the smart-antenna aided BS for predicting vector channels in time-division duplex systems.
	Walke and Oechtering [245]	Conducted investigations on the Cumulative Dstribution Function (CDF) of the uplink carrier-to-interference ratio in a cellular radio network.
	Zwick, Fischer and Wiesbeck [246]	Proposed a stochastic channel model for indoor propagations in future communication systems equipped with multiple antennas.
	Zekavat, Nassar and Shattil [247]	Combined smart antenna arrays and MC-CDMA systems.
	Pan and Djurić [248]	Suggested sectorized multi-beam cellular mobile communications combined with dynamic channel assignment to beams.
	Cavalcante, Cavalcanti and Mota [249]	Exploited a blind adaptive optimisation criterion for SDMA detection.
	Yin and Liu [250]	Developed a Medium Access Control (MAC) protocol for multimedia SDMA/TDMA packet networks.
	Thoen *et al.* [200]	Showed that the performance of OFDM/SDMA processors can be significantly enhanced by adapting the constellation size applied on the individual subcarriers to the channel conditions.
	Rim [251]	Examined the performance of a high-throughput downlink MIMO SDMA technique.
2003	Thoen *et al.* [201]	Utilized a Constrained Least-Squares (CLS) receiver in multi-user SDMA systems.
	Alastalo and Kahola [202]	Reported link-level results of an adaptive antenna array assisted system compatible with IEEE 802.11a WLANs.
	Bradaric, Pertropulu and Diamantaras [252]	Characterized a blind nonlinear method for identifying MIMO FIR CDMA and SDMA systems.
	Alias *et al.* [203]	Constructed a Minimum Bit Error Rate (MBER) Multi-User Detector (MUD) for SDMA-OFDM systems.
	Hanzo, Münster, Choi and Keller [5]	Elaborated on channel estimation and multi-user detection techniques designed for SDMA-OFDM systems.
2004	Spencer, Swindlehurst and Haardt [253]	Delivered two constrained solutions referred to as the block-diagonalization and the successive optimization schemes contrived for downlink SDMA systems.
	Li, Letaief and Cao [254]	Explored a low-complexity ML-based detection scheme using a so-called 'sensitive-bits' algorithm.
	Choi and Murch [255]	Formulated a pre-Bell Labs Layered Space-Time (BLAST) decision-feedback equalization technique for downlink MIMO channels.
2005	Ajib and Haccoun [256]	Overviewed the scheduling algorithms proposed for 4G multi-user wireless networks based on MIMO technology.
	Dai [204]	Performed an analysis of CFO estimation in SDMA-OFDM systems.
	Nasr, Costen and Barton [257]	Researched the estimation of the local average signal level in an indoor environment based on a 'wall-imperfection' model.

Table 1.7: Main contributions on SDMA (Part 2).

Table 1.8: Major contributions addressing channel estimation in multi-carrier systems.

[258, 259] Höher *et. al.*, 1997	Cascaded 1D-FIR Wiener filter based channel interpolation.
[260] Edfors *et al.*, 1998	Detailed analysis of SVD-aided CIR-related domain noise reduction for DDCE.
[261] Li, 1998	DDCE using DFT-based 2D interpolation and robust prediction.
[262] Li, 2000	2D pilot pattern aided channel estimation using 2D robust frequency domain Wiener filtering.
[263] Yang *et al.*, 2001	Detailed discussion of parametric, ESPRIT-assisted channel estimation.
[264] Münster and Hanzo, 2003	RLS-adaptive PIC assisted DDCE for OFDM.
[265] Otnes and Tüchler, 2004	Iterative channel estimation for turbo equalization.

to a modulator, such that for M channels there are M modulators whose carrier frequencies are f_0, f_1, ...f_M. The difference between adjacent channels is Δf and the overall bandwidth W of the N modulated carriers is $M\Delta f$.

These M modulated carriers are then combined to give an OFDM signal. We may view the serial-to-parallel convertor, as applying every Mth symbol to a modulator. This has the effect of interleaving the symbols into each modulator, hence symbols S_0, S_M, S_{2M},.... are applied to the modulator whose carrier frequency is f_1. At the receiver the received OFDM signal is demultiplexed into M frequency bands, and the M modulated signals are demodulated. The baseband signals are then recombined using a parallel-to-serial convertor.

The main advantage of the above OFDM concept is that because the symbol period has been increased, the channel delay spread is a significantly shorter fraction of a symbol period than in the serial system, potentially rendering the system less sensitive to ISI than the conventional serial system. In other words, in the low-rate subchannels the signal is no longer subject to frequency-selective fading, hence no channel equalisation is necessary.

A disadvantage of the OFDM approach shown in Figure 1.3 is the increased complexity over the conventional system caused by employing M modulators and filters at the transmitter and M demodulators and filters at the receiver. It can be shown that this complexity can be reduced by the use of the discrete Fourier transform (DFT), typically implemented as a Fast Fourier Transform (FFT) [5]. The subchannel modems can use almost any modulation scheme, and 4- or 16-level QAM is an attractive choice in many situations.

The FFT-based QAM/FDM modem's schematic is portrayed in Figure 1.4. The bits provided by the source are serial/parallel converted in order to form the n-level Gray coded symbols, M of which are collected in TX buffer 1, while the contents of TX buffer 2 are being transformed by the IFFT in order to form the time-domain modulated signal. The digital-to-analogue (D-A) converted, low-pass filtered modulated signal is then transmitted via the channel and its received samples are collected in RX buffer 1, while the contents of RX buffer 2 are being transformed to derive the demodulated signal. The twin buffers are alternately filled with data to allow for the finite FFT demodulation time. Before the data is Gray coded and passed to the data sink, it can be equalised by a low complexity method, if there some dispersion within the narrow subbands. For a deeper tutorial exposure the interested reader is referred to [5].

1.3 Channel Estimation for Multicarrier Systems

The ever-increasing demand for high data-rates in wireless networks requires the efficient utilisation of the limited bandwidth available, while supporting a high grade of mobility in diverse propagation environments. Orthogonal Frequency Division Multiplexing (OFDM) and Multi-Carrier Code Division Multiple Access (MC-CDMA) techniques [266] are capable of satisfying these requirements. This is a benefit of their ability to cope with highly time-variant wireless channel characteristics. However, as pointed out in [267], the capacity and the achievable integrity of communication systems is highly dependent on the system's knowledge concerning the channel conditions encountered. Thus, the provision of an accurate and robust channel estimation strategy is a crucial factor in achieving a high performance.

Well-documented approaches to the problem of channel estimation are constituted by *pilot assisted*, *decision directed* and *blind* channel estimation methods [266, 268].

The family of *pilot assisted* channel estimation methods was investigated for example by Li [262], Morelli and Mengali [269], Yang *et al.* [263] as well as Chang and Su [270], where the channel parameters are typically estimated by exploiting the channel-sounding signal. For example, in OFDM and MC-CDMA often a set of frequency-domain pilots are transmitted for estimating the Frequency-Domain Channel Transfer Function (FD-CTF), which are known at the receiver [266]. The main drawback of this method is that the pilot symbols do not carry any useful information

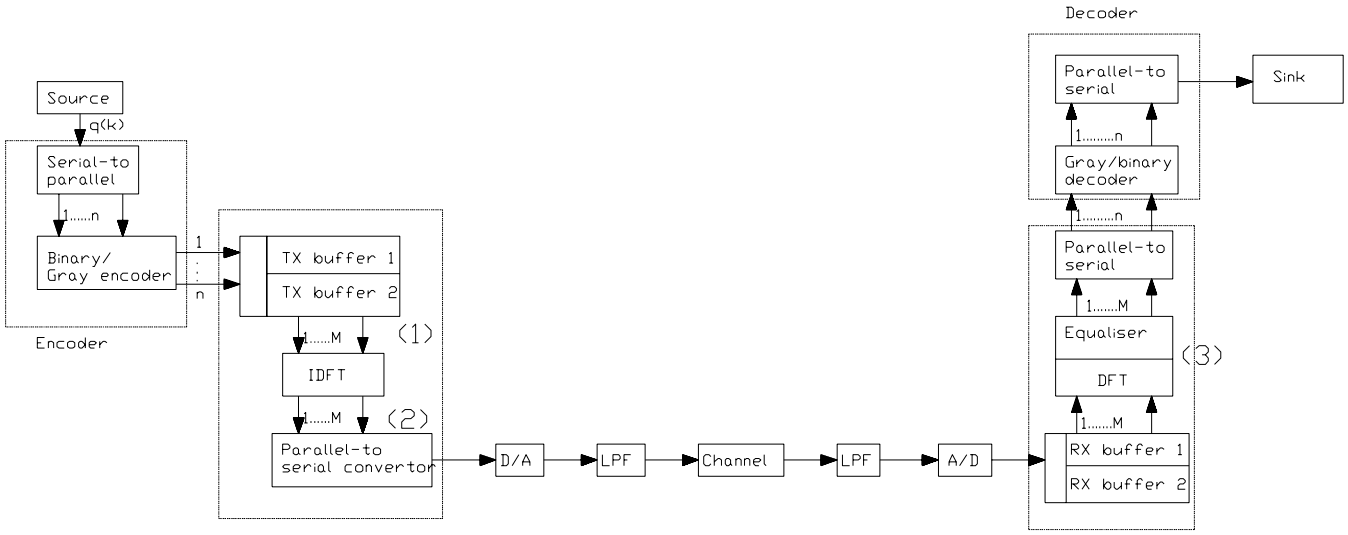

Figure 1.4: FFT-based OFDM modem schematic ©Hanzo *et al.* 2003 [5]

and thus they reduce the system's effective throughput.

By contrast, in Decision Directed Channel Estimation (DDCE) methods both the pilot symbols as well as all the information symbols are utilised for channel estimation [266]. The simple philosophy of this method is that in the absence of transmission errors we can benefit from the availability of 100% pilot information by using the detected subcarrier symbols as an *a posteriori* reference signal. The employment of this method allows us to reduce the number of pilot symbols required. This technique is particularly efficient under benign channel conditions, where the probability of a decision error is low, but naturally, this approach is also prone to error propagation effects. The family of DDCE techniques was investigated for example by van de Beek *et al.* [271], Mignone and Morello [272], Edfors *et al.* [260], Li *et al.* [261], Li and Sollenberg [273] as well as Münster and Hanzo [268, 274–276].

The class of iterative DDCE scemes, where the channel estimation is carried out through a series of iterations utilizing the increasingly-refined soft-decision-based feedback, was explored by Sandell *et. al.* [277], Valenti [278], Yeap *et. al.* [279], Song *et. al.* [280, 281], as well as by Otnes and Tüchler [265, 282].

The closely related class of joint receivers, where the channel parameters and the transmitted information-carrying symbols are estimated jointly was explored for example by Seshadri [283], developed further by Knickenberg *et. al.* [284] recently revisited by Cozzo and Hughes [285] as well as Cui and Tellambura [286, 287].

Finally, the class of *blind* estimation methods eliminates all redundant pilot symbols. Most of these methods rely on the employment of decision feedback and on the exploitation of the redundancy often found in the structure of the modulated signal, as exemplified by the techniques described for example by Antón-Haro *et. al.* [288], Boss *et. al.* [289], Endres *et. al.* [290], Giannakis and Halford [291], Zhou and Giannakis [292] as well as by Necker and Stüber [293].

Additional major subject, closely related to channel estimation, namely the prediction of fast fading channels was extensive studied by Haykin [294]. A so-called robust predictor was proposed by Li [261] and revised by Münster and Hanzo [275]. An adaptive RLS channel predictor was proposed by Schafhuber and Matz [295].

Subsequently, in this treatise we propose a DDCE scheme, which is suitable for employment in both OFDM and MC-CDMA systems. We analyse the achievable performance of the estimation scheme considered in conjunction with a realistic dispersive Rayleigh fading channel model having a Fractionally-Spaced (FS) rather than Symbol-Spaced (SS) Power Delay Profile (PDP).

A basic component of the DDCE schemes proposed in the literature is an *a posteriori* Least Squares (LS) temporal estimator of the OFDM-subcarrier-related Frequency-Domain Channel Transfer Function (FD-CTF) coefficients [261, 266]. The accuracy of the resultant temporal FD-CTF estimates is typically enhanced using one- or two-dimensional interpolation exploiting both the time- and the frequency-domain correlation between the desired FD-CTF coefficients. The LS-based temporal FD-CTF estimator was shown to be suitable for QPSK-modulated OFDM systems [261, 266], where the energy of the transmitted subcarrier-related information symbols is constant. However, as it will be pointed out in Section 7.3.1 of this treatise, the LS method cannot be readily employed in MC-CDMA systems, where – in contrast to OFDM systems – the energy of the transmitted subcarrier-related information symbols fluctuates as a function of both the modulated sequence and that of the choice of the potentially non-constant-modulus modulation

Table 1.9: Major contributions addressing the problem of channel estimation in MIMO systems.

[296] Li *et. al.*, 2002	MIMO-OFDM for wireless communications: signal detection with enhanced channel estimation.
[297] Stüber *et. al.*, 2004	An important overview encompassing most of the major aspects of the broadband MIMO-OFDM wireless communications including channel estimation, signal detection as well as time and frequency syncronization.
[298] Deng *et. al.*, 2003	Decision directed iterative channel estimation for MIMO systems.
[285] Cozzo and Hughes, 2003	Joint channel estimation and data detection in space-time communications.
[299] Münster and Hanzo,2005	Parallel-interference-cancellation-assisted decision-directed channel estimation for OFDM systems using multiple transmit antennas.
[300] Yatawatta and Petropulu, 2006	Blind channel estimation in MIMO-OFDM systems with multiuser interference.

scheme itself. Thus we propose a Minimum Mean Square Error (MMSE) estimation based DDCE method, which is an appropriate solution for employment in both OFDM and MC-CDMA systems.

The system model and the channel model considered are described in Section 1.7 of this treatise. The difficulty of employing the LS approach to the problem of estimating the OFDM-subcarrier-related FD-CTF coefficients is described in Section 7.3.1. The alternative MMSE FD-CTF estimator circumventing the problem outlined in Section 7.3.1 is analyzed in Section 7.3.2. Our discourse evolves further by proposing a MMSE CIR estimator exploiting the frequency-domain correlation of the FD-CTF coefficients in Section 7.4.1 and a reduced-complexity version of the CTF MMSE estimator considered is proposed in Section 7.4.2. The computational complexity of both methods is compared in Section 7.4.3.

In Section 7.4 we continue our discourse with the derivation of both sample-spaced as well as fractionally-spaced Channel Impulse Response (CIR) estimator. In Section 7.4.5 we then perform a comparison between the two methods considered and demonstrate the advantages of the later, *i. e.* fractionally-spaced scheme. Subsequently, in Section 7.5 we develope a method of parametric tracking of the fractionally-spaced channel impulse response (CIR) taps, which facilitates low-complexity channel etimation in realistic channel conditions characterized by time-variant fractionally-spaced power delay profile. More specifically we employ the Projection Approximation Subspace Tracking (PAST) method for the sake of recursive tracking of the channel transfer function's (CTF) covariance matrix and subsequent tracking of the corresponding CIR taps. We demonstrate that the PAST-aided decision directed channel estimation scheme proposed exhibits good performance over the entire range of practical conditions.

In Section 7.6 we discuss two major CIR tap prediction strategies. Specifically, In Section 7.6.2 the so-called *robust* implementation of the stationary Minimum Mean Square Error (MMSE) CIR predictor is considered. The *robust* CIR predictor [261] assumes a constant-valued, limited-support channel scattering function [266] during the design of the CIR tap prediction filter and hence relies on the assumption of encountering the worst possible channel conditions. On the other hand, in Section 7.6.4 we discuss the adaptive Recursive Least Squares (RLS) method of CIR prediction [295]. As opposed to the robust CIR predictor of [261], the RLS CIR predictor does not require any explicit information concerning the channel conditions encountered. Consequently, in Section 7.6.5 we characterize and compare the achievable performance of both methods considered and draw conclusions concerning their relative merits. Specifically, we demonstrate that the RLS prediction technique outperforms its robust counterpart over the entire range of the relevant channel conditions.

In Section 7.7 we characterize the achievable performance of the resultant PAST-aided DDCE scheme. We report an estimation efficiency of $\kappa = -18dB$ exhibited by a system employing 10% of pilots and communicating over a dispersive Rayleigh fading channel having a Doppler frequency of $f_D = 0.003$. Furthermore, we report a BER performance, which is only 3 dB from the corresponding BER performance exhibited by a similar system assuming perfect channel knowledge.

1.4 Channel Estimation for MIMO-OFDM

In spite of an immense interest from both the academic and the industrial communities, a practical multiple-input multiple-output (MIMO) transceiver architecture, capable of approaching channel capacity boundaries in realistic channel conditions remains largely an open problem. In particular, a robust and accurate channel estimation in MIMO systems constitutes a major issue, preventing us from achieving the high capacities predicted by the relevant theoretical analysis.

Some of the major contributions addressing the problem of channel estimation in MIMO systems are summarized in Table 1.9. More specifically, a combined OFDM/SDMA approach was discussed by Vandenameele *et. al.* [301]. A pilot-based approach to the problem of MIMO channel estimation has been explored by Jungnickel *et. al.* in [302], by Bolcskei *et. al.* [303] as well as by Zhu *et. al.* [304]. On the other hand, decision directed iterative channel estimation for MIMO systems was addressed by Li *et al* [296, 305, 306] as well as Deng *et al* [298]. Furthermore, parallel interference cancellation-assisted decision-directed channel estimation scheme for MIMO-OFDM systems was proposed by Münster and Hanzo [299, 307]. Joint decoding and channel estimation for MIMO channels was considered by Grant [308] and further investigated by Cozzo and Hughes [285]. Iterative channel estimation for space-time block coded systems was addressed by Mai *et al* [309], while joint iterative DDCE for turbo coded MIMO-OFDM systems was investigated by Qiao [310]. Blind channel estimation in MIMO-OFDM systems with multiuser interference was explored by Yatawatta and Petropulu [300].

Other closely related issues, namely the iterative tracking of the channel-related parameters using soft decision feedback was studied by Sandell *et. al* [277], while the iterative channel estimation in the context of turbo equalization was considered by Song *et. al.* [281], Mai *et. al.* [311], as well as Otnes and Tüchler [265].

Finally, an important overview publication encompassing most major aspects of broadband MIMO-OFDM wireless communications including channel estimation and signal detection, as well as time and frequency syncronization was contributed by Stüber *et. al.* [297].

Agains this background, in this treatise we propose a decision-directed channel estimation (DDCE) scheme, which is suitable for employment in a wide range of multi-antenna multi-carrier systems as well as over the entire range of practical channel conditions. In particular, we consider mobile wireless multipath channels, which exhibit fast Rayleigh frequency-selective fading and are typically characterized by time-variant power delay profile (PDP).

We consider a generic MIMO-OFDM system employing K orthogonal frequency-domain subcarriers and having $m_{\rm t}$ and $n_{\rm r}$ transmit and receive antennas, respectively. Consequently, our MIMO channel estimation scheme comprises an array of K per-subcarrier MIMO-CTF estimators, followed by a $(n_{\rm r} \times m_{\rm t})$-dimensional array of parametric CIR estimators and a corresponding array of $(n_{\rm r} \times m_{\rm t} \times L)$ CIR tap predictors, where L is the number of tracked CIR taps per link for the MIMO channel.

In Section 7.8.1 we explore a family of recursive MIMO-CTF tracking methods, which in conjunction with the aforementioned PAST-aided CIR-tracking method of Section 7.5 as well as the RLS CIR tap prediction method of Section 7.6.4, facilitate an effective channel estimation scheme in the context of a MIMO-OFDM system. More specifically, in Section 7.8.1 we consider both hard- and soft-feedback assisted least mean squares (LMS) and recursive least squares (RLS) tracking algorithms as well as the modified RLS algorithm, which is capable of improved utilization of the soft information associated with the decision-based estimates.

Finally, in Section 7.8.1.5 we document the achievable performance of resultant MIMO-DDCE scheme employing the recursive CTF tracking followed by the parametric CIR tap tracking and CIR tap prediction. We demonstrate that the MIMO-DDCE scheme proposed exhibits good performance over the entire range of practical conditions.

Both the bit error rate (BER) as well as the corresponding mean square error (MSE) performance of the channel estimation scheme considered is characterized in the context of a turbo-coded MIMO-OFDM system. We demostrate that the MIMO-DDCE scheme proposed remains effective in channel conditions associated with high terminal speeds of up to 130 km/h, which corresponds to the OFDM-symbol normalized Doppler frequency of 0.006. Additionally, we report a virtually error-free performance of a rate $1/2$ turbo-coded 8x8-QPSK-OFDM system, exhibiting a total bit rate of 8 bits/s/Hz and having a pilot overhead of only 10%, at SNR of 10dB and normalized Doppler frequency of 0.003, which corresponds to the mobile terminal speed of roughly 65 km/h[1].

1.5 Signal Detection in MIMO-OFDM Systems

The demand for both high data-rates, as well as for improved transmission integrity requires an efficient utilisation of the limited system resources, while supporting a high grade of mobility in diverse propagation environments. Consequently, the employment of an appropriate modulation format, as well as an efficient exploitation of the available bandwidth constitute crucial factors in achieving a high performance.

The OFDM modulation scheme employed in conjunction with a Multiple-Input Multiple-Output (MIMO) architecture [266], where multiple antennas are employed at both the transmitter and the receiver of the communication system, constitutes an attractive solution in terms of satisfying these requirements. Firstly, the OFDM modulation

[1]Additional system parameters are characterized in Table 1.11.

technique is capable of coping with the highly frequency selective, time-variant channel characteristics associated with mobile wireless communication channels, while possessing a high grade of structural flexibility for exploiting the beneficial properties of MIMO architectures.

It is highly beneficial that OFDM and MIMOs may be conveniently combined, since the information-theoretical analysis predicts [312] that substantial capacity gains are achievable in communication systems employing MIMO architectures. Specifically, if the fading processes corresponding to different transmit-receive antenna pairs may be assumed to be independently Rayleigh distributed[2], the attainable capacity was shown to increase linearly with the smaller of the numbers of the transmit and receive antennas [312]. Additionally, the employment of MIMO architectures allows for the efficient exploitation of the spatial diversity available in wireless MIMO environments, thus improving the system's BER, as well as further increasing the system's capacity.

The family of space-time signal processing methods, which allow for the efficient implementation of communication systems employing MIMO architectures are commonly referred to in parlance as *smart antennas*. In recent years, the concept of smart antennas has attracted intensive research interest in both the academic and the industrial communities. As a result, a multiplicity of smart antenna-related methods has been proposed. These include methods implemented at the transmitter, the receiver or both.

The classification of the smart-antenna techniques is illustrated in Figure 1.5. It should be noted, however, that the classification presented here is somewhat informal and its sole purpose is to appropriately position the content of this treatise in the context of the extensive material available on the subject.

Figure 1.5: Classification of space-time processing techniques.

Two distinctive system scenarios employing smart antennas can be identified. The first is the so-called Space Devision Multiplexing (SDM)-type scenario [313], where two *peer* terminals each employing multiple antennas, communicate with each other over a MIMO channel and the multiple antennas are primarily used for achieving a multiplexing gain, *i.e.* a higher throughput [314]. The second scenario corresponds to the Space Devision Multiple Access (SDMA) configuration [266], where a single *base-station*, employing multiple antennas communicates simultaneously using a single carrier frequency with multiple *user* terminals, each employing one or several antennas.

The various *point-to-multipoint* smart antenna applications can be further subdivided into *uplink*- and *downlink*-related applications. The *uplink*-related methods constitute a set of techniques, which can be employed in the *base station* in order to detect the signals simultaneously transmitted by multiple *user* terminals. More specifically, provided that the Channel Impulse Response (CIR) of all users is accurately estimated, it may be used as their unique, user-specific spatial signature for differentiating them, despite communicating within the same frequency

[2] This assumption is typically regarded as valid, if the appropriate antenna spacing is larger than of $\lambda/2$, where λ is the corresponding wavelength.

band [266]. Hence, the corresponding space-time signal processing problem is commonly referred to as Multi-User Detection (MUD) [266], while the multi-antenna multi-user systems employing *uplink* space-time MUD are commonly referred to as SDMA systems [266]. In contrast to the SDM-type systems designed for achieving the highest possible multiplexing gain, the design objective of the SDMA techniques is the maximization of the number of users supported. By contrast, the class of beamformers [315] creates angularly selective beams for both the up-link and down-link in the direction of the desired user, while forming nulls towards the interfering users. Finally, the family of Space-Time Codes (STC) [316] was optimized for achieving the highest possible transmit diversity gain, rather than for multiplexing gain or for increasing the number of users supported. At the time of writing new research is aiming for achieving both the maximum attainable diversity and multiplexing gain with the aid of eigen-value decomposition [317].

As stated above, two benefits of employing smart antennas are the system's improved integrity, as well as the increased aggregate throughput. Hence an adequate performance criterion of the particular smart antenna implementation is a combination of the system's attainable aggregate data-throughput, as well as the corresponding data integrity, which can be quantified in terms of the average Bit Error Rate (BER). Consequently, in the context of point-to-multipoint-related smart antenna applications the achievable capacity associated with the particular space-time processing method considered may be assessed as a product of the simultaneously supported number of individual users and the attainable data-rate associated with each supported user. The measure of data-integrity may be the average BER of all the users supported. Thus, the typical objective of the multi-user-related smart antenna implementations, such as that of an SDMA scheme is that of increasing the number of the simultaneously supported users, while sustaining the highest possible integrity of all the data communicated.

In this treatise, however, we would like to focus our attention on the family of space-time processing methods associated with the *point-to-point* system scenario. The main objective of point-to-point space-time processing is to increase the overall throughput of the system considered, as opposed to increasing the number of individual users simultaneously supported by the system, which was the case in the multi-user SDMA scenario described above. As illustrated in Figure 1.5, the family of time-space processing methods associated with the *point-to-point*-related smart antenna applications entail two different approaches, namely that of Space-Time Codes (STC) [316] as well as various layered space-time architectures, best known from Bell Labs Layered Space-Time (BLAST) scheme [314].

The STC methods may be classified in two major categories, namely the Space-Time Block Codes (STBC) and the Space-Time Trellis Codes (STTC). A simple method of STBC was first presented by Alamouti in [318]. Various STBC techniques were then extensively studied in a series of major publications by Tarokh *et al.* in [319–325] as well as by Ariyavistakul *et al.* in [326,327]. On the other hand, the original variant of BLAST, known as the Diagonal BLAST (D-BLAST) scheme, was first introduced by Foschini in [314]. A more generic version of the BLAST architecture, the so-called Vertical BLAST (V-BLAST) arrangement was proposed by Golden *et al.* in [328]. Furthermore, the comparative study of the D-BLAST, as well as the V-BLAST systems employing various detection techniques such as Least Squares (LS) and Minimum Mean Square Error (MMSE)-aided Parallel Interference Cancellation (PIC), as well as the LS- and MMSE-aided Successive Interference Cancellation (SIC) was carried out by Sweatman *et al.* in [329]. Typically, however, the term BLAST refers to the point-to-point single-carrier MIMO architecture employing the SIC detection method, as it was originally proposed in [314].

For the sake of accuracy, in this work we employ the alternative terminology of Space Division Multiplexing (SDM) in order to refer to a generic MIMO architecture. The corresponding detection methods are referred to as SDM Detection (SDMD) techniques, as opposed to the MUD techniques employed in the context of SDMA systems [266]. Naturally, however, the SDMD and MUD schemes share the same signal detection methods, regardless, whether the signal arrived from multiple antennas of the same or different users. The classification of the most popular SDMD/MUD schemes is depicted in Figure 1.6. The methods considered include the linear LS and MMSE techniques, as well as non-linear techniques, such as Maximum Likelihood (ML), Successive Interference Cancellation (SIC), Genetic Algorithm-aided MMSE (GA-MMSE) [330, 331] as well as the novel Optimized Hierarchy Reduced Search Algorithm (OHRSA)-aided methods proposed in this treatise.

In the course of this treatise both the MIMO channel model considered as well as the SDM-OFDM system model are described in Section 1.8. The various SDM detection methods considered are outlined in Chapter 15. Specifically, in Section 15.2.1 we demonstrate that the linear increase in capacity, predicted by the information-theoretic analysis [267], may indeed be achieved by employing a relatively low-complexity linear SDM detection method, such as the MMSE SDM detection technique [332]. Secondly, in Section 15.3.1 we show that a substantially better performance can be achieved by employing a non-linear Maximum Likelihood (ML) SDM detector [313, 333, 334], which constitutes the optimal detection method from a probabilistic sequence-estimation point of view. To elaborate a little further, the ML SDM detector is capable of attaining transmit diversity in *fully-loaded* systems, where the number of transmit and receive antennas is equal. Moreover, as opposed to the linear detection schemes considered, the ML SDM detector is capable of operating in the *rank-deficient* system configuration, when the number of transmit anten-

Figure 1.6: SDM detection methods classification.

Table 1.10: Major Contributions Addressing the Sphere Decoder-Aided Space-Time Processing.

[335] Fincke *et. al.*, 1985	Sphere decoder technique introduced.
[336] Damen *et. al.*, 2000	Sphere decoder was first proposed for employment in the context of space-time processing, where it is utilized for computing the ML estimates of the modulated symbols transmitted simultaneously from multiple transmit antennas.
[337] Hochwald and Brink, 2003	The *complex* version of the sphere decoder.
[338] Damen *et. al.*, 2003	Further results on SD.
[339] Pham *et al.*, 2004	Improved version of the complex sphere decoder.
[340] Tellambura *et al.*, 2005	Multistage sphere decoding was introduced.

nas exceeds that of the receive antennas. Unfortunately, however, the excessive computational complexity associated with the exhaustive search employed by the ML detection method renders it inapplicable to practical implementation in systems having a large number of transmit antennas. Subsequently, in Sections 15.3.2 and 15.3.3 we explore a range of advanced non-linear SDM detection methods, namely the SIC and Genetic Algorithm-aided MMSE detection, respectively, where the latter may potentially constitute an attractive compromise between the low complexity of the linear SDM detection and the high performance of the ML SDM detection schemes. Indeed, we will demonstrate in Section 15.3.3 that the SDM detection method based on the SIC as well as on the GA-MMSE detector [331] are both capable of satisfying these requirements.

In Section 15.4 our discourse evolves further by proposing an enhancement of the SDMD schemes considered by employing both Space-Frequency Interleaving (SFI) and Space-Frequency Walsh-Hadamard Transform (SFWHT)-aided spreading. The performance benefits of employing SFI and SFWHT are quantified in Section 15.4. Finally, our conclusions are summarized in Section 15.6.

Parallel-interference-cancellation-assisted decision-directed channel estimation for OFDM systems using multiple transmit antennas by Münster and Hanzo [299]

Recently, a family of potent Reduced Search Algorithm (RSA) aided Space-Time processing methods has been explored. These new methods utilize the Sphere Decoder (SD) technique introduced by Fincke *et al.* [335]. The SD was first proposed for employment in the context of space-time processing by Damen *et. al.* in [336], where it is utilized for computing the ML estimates of the modulated symbols transmitted simultaneously from multiple transmit antennas. The *complex* version of the sphere decoder was proposed by Hochwald and Brink in [337]. The subject was further investigated by Damen *et al.* in [338]. Subsequently, an improved version of the Complex Sphere Decoder (CSD) was advocated by Pham *et al.* in [339]. Furthermore, CSD-aided detection was considered by Cui and Tellambura in a joint channel estimation and data detection scheme explored in [286], while a revised version of the CSD method, namely the so-called Multistage Sphere Decoding (MSD) was introduced in [340]. The generalized version of the sphere decoder, which is suitable for employment in rank-deficient MIMO systems supporting more

transmitters than the number of receive antennas was introduced by Damen *et al.* in [341] and further refined by Cui and Tellambura in [342]. The so-called *fast* generalized sphere decoding was introduced by Yang *et al.* [343]. Yet another variant of sphere decoder algorithms with improved radius search was introduced by Zhao and Giannakis [344]. The subject of approaching MIMO channel capacity using soft detection on hard sphere decoding was explored by Wang and Giannakis [345]. Iterative detection and decoding in MIMO systems using sphere decoding was considered by Vikalo *et al.* [346].

Consequently, a set of novel OHRSA-aided SDM detection methods are outlined in Section 16.1. Specifically, in Section 16.1.1 we derive the OHRSA-aided ML SDM detector, which benefits from the optimal performance of the ML SDM detector [266], while exhibiting a relatively low computational complexity, which is only slightly higher than that required by the low-complexity MMSE SDM detector [266]. To elaborate a little further, in Section 16.1.2 we derive a bit-wise OHRSA-aided ML SDM detector, which allows us to apply the OHRSA method of Section 16.1 in high-throughput systems, which employ multi-level modulation schemes, such as M-QAM [266].

In Section 16.1.3 our discourse evolves further by deducing the OHRSA-aided Max-Log-MAP SDM detector, which allows for an efficient evaluation of the soft-bit information and therefore results in highly efficient turbo decoding. Unfortunately however, in comparison to the OHRSA-aided ML SDM detector of Section 16.1.2 the OHRSA-aided Max-Log-MAP SDM detector of Section 16.1.3 exhibits a substantially higher complexity. Consequently, in Section 16.1.5 we derive an approximate Max-Log-MAP method, which we refer to as Soft-output OPtimized HIErarchy (SOPHIE) SDM detector. The SOPHIE SDM detector combines the advantages of both the OHRSA-aided ML and OHRSA-aided Max-Log-MAP SDM detectors of Sections 16.1.2 and 16.1.3, respectively. Specifically, it exhibits a similar performance to that of the optimal Max-Log-MAP detector, while imposing a modest complexity, which is only slightly higher than that required by the low-complexity MMSE SDM detector [266]. The computational complexity as well as the achievable performance of the SOPHIE SDM detector of Section 16.1.5 are analysed and quantified in Sections 16.1.5.1 and 16.1.5.2, respectively.

Our conclusions are summarized in Section **??**. Specifically, we report achieving a BER of 10^{-4} at SNRs of $\gamma = 4.2, 9.2$ and 14.5 in high-throughput 8x8 rate-$\frac{1}{2}$ turbo-coded $M = 4, 16$ and 64-QAM systems communicating over dispersive Rayleigh fading channel. Additionally, we report achieving a BER of 10^{-4} at SNRs of $\gamma = 9.5, 16.3$ and 22.8 in high-throughput rank-deficient 4x4, 6x4 and 8x4 rate-$\frac{1}{2}$ turbo-coded 16-QAM systems, respectively.

1.6 Iterative Signal Processing for SDM-OFDM

Figure 1.7: Schematic of a joint iterative receiver comprising channel estimator, SDM detector, as well as turbo decoder employing two RCS serially-concatenated component codes.

In spite of an immense interest from both the academic and the industrial communities, a practical multiple-input multiple-output (MIMO) transceiver architecture, capable of approaching channel capacity boundaries in realistic channel conditions remains largely an open problem. An important overview publication encompassing most major aspects of broadband MIMO-OFDM wireless communications including channel estimation and signal detection, as well as time and frequency syncronization was contributed by Stüber *et al*. [297]. Other important publications considering MIMO systems in realistic conditions include those by Münster and Hanzo [299], Li *et. al.* [296], Mai *et. al.* as well as Qiao *et. al.* [310]. Nevertheless, substantial contributions addressing all the major issues inherent to MIMO transceivers, namely error correction, space-time detection as well as channel estimation in realistic channel conditions remain scarce.

Against this background, in Chapter 17.1 we derive an iterative, so called *turbo* multi-antenna-multi-carrier (MAMC) receiver architecture. Our turbo receiver is illustrated in Figure 1.7. Following the philosophy of turbo processing [316], our turbo SDM-OFDM receiver comprises a succession of detection modules, which iteratively exchange soft bit-related information and thus facilitate a substantial improvement of the overall system performance.

More specifically, our turbo SDM-OFDM receiver comprises three major components, namely, the soft-feedback decision-directed channel estimator, discussed in detail in Section 7.8, followed by the soft-input-soft-output OHRSA Log-MAP SDM detector derived in Section 16.1.3 as well as a soft-input-soft-output serially concatenated turbo code [347]. Consequently, in this chapter we would like to analyze the achievable performance of each individual constituent of our turbo receiver, as well as the achievable performance of the entire iterative system. Our aim is to identify the optimum system configuration, while considering various design trade-offs, such as achievable error-rate performance, achievable data-rate as well as associated computational complexity.

In Section 17.4.2.4 we demonstrate that our turbo SDM-OFDM system employing the MIMO-DDCE scheme of Section 7.8 as well as the OHRSA Log-MAP SDM detector of Section 16.1.3 remains effective in channel conditions associated with high terminal speeds of up to 130 km/h, which corresponds to the OFDM-symbol normalized Doppler frequency of 0.006. Additionally, we report a virtually error-free performance for a rate $1/2$ turbo-coded 8x8-QPSK-OFDM system, exhibiting an effective throughput of 8 MHz $\cdot$ 8 bits/s/Hz=64 Mbps and having a pilot overhead of only 10% at SNR of 7.5dB and a normalized Doppler frequency of 0.003, which corresponds to a mobile terminal speed of about 65 km/h.

1.7 System Model

1.7.1 Channel Statistics

Figure 1.8: Illustration of a wireless multi-path communication link. Note that the non-line of sight paths are randomly faded as a result of the diffraction induced by scattering surfaces.

A Single Input Single Output (SISO) wireless communication link is constituted by a multiplicity of statistically independent components, termed as *paths*. Thus, such a channel is referred to as a *multipath* channel. A *multipath* channel is typically characterized by its Power Delay Profile (PDP), which is a set of parameters constituted by the paths' average powers σ_l^2 and the corresponding relative delays τ_l. Some examples of the commonly used PDPs are illustrated in Figure 1.10. The physical interpretation of each individual path is a single distortionless ray between the transmitter and the receiver antennas. While the term PDP corresponds to the average power values associated with the different multi-path channel components, the term CIR refers to the instantaneous state of the dispersive channel encountered and corresponds to the vector of the instantaneous amplitudes $\alpha_l[n]$ associated with different multi-path components. Thus, the statistical distribution of the CIR is determined by the channel's PDP. In the case of independently Rayleigh fading multiple paths we have $\alpha_l[n] \in \mathcal{CN}(0, \sigma_l^2)$, $l = 1, 2, \cdots, L$, where $\mathcal{CN}(0, \sigma^2)$ is a complex-Gaussian distribution having the mean 0 and the variance of σ^2.

The individual scattered and delayed signal components usually arise as a result of refraction or diffraction from scattering surfaces, as illustrated in Figure 1.8, and are termed as Non-Line-Of-Sight (NLOS) paths. In most recently proposed wireless mobile channel models each such CIR component α_l associated with an individual channel path is modelled by a Wide Sense Stationary (WSS) narrow-band complex Gaussian process [350] having correlation properties characterised by the cross-correlation function

$$r_\alpha[m, j] = E\{\alpha_i[n]\alpha_j^*[n-m]\} = r_{t;i}[m]\delta[i-j]\,, \tag{1.1}$$

Figure 1.9: Illustration of a wireless multi-path communication link. Note that the non-line of sight paths are randomly faded as a result of the diffraction induced by scattering surfaces.

where n is a discrete OFDM-block-related time-domain index and $\delta[\cdot]$ is the Kronecker delta function. The above equation suggests that the different CIR components are assumed to be mutually uncorrelated and each exhibits time-domain autocorrelation properties defined by the time-domain correlation function $r_{t;i}[m]$. The Fourier transform pair of the correlation function $r_t[n]$ associated with each CIR tap corresponds to a band-limited Power Spectral Density (PSD) $p_t(f)$, such that we have $p_t(f) = 0$, if $|f| > f_D$, where Fd is termed as the *maximum Doppler frequency*. The time period $1/f_{\rm D}$ is the so-called *coherence time* of the channel [350] and usually we have: $1/f_{\rm D} \gg T$, where T is the duration of the OFDM block.

A particularly popular model of the time-domain correlation function $r_t[n]$ was proposed by Jakes in [351] and is described by

$$r_t[n] = r_J[n] = J_0(nw_d), \tag{1.2}$$

where $J_0(x)$ is a zero-order Bessel function of the first kind and $w_d = 2\pi T f_D$ is the normalised Doppler frequency. The corresponding U-shaped PSD function, termed as the Jakes-spectrum is given by [351]

$$p_J(w) = \begin{cases} \frac{2}{w_d}\frac{1}{\sqrt{1-(w/w_d)^2}}, & \text{if } |w| < w_d \\ 0, & \text{otherwise.} \end{cases}$$

Generally speaking the Doppler frequencies f_D can assume different values for different signal paths. However, as it was advocated in [261], for the sake of exploiting the time-domain correlation in the context of channel parameters estimation and prediction, it is sufficient to make a worst-case assumption about the nature of time-domain correlation of the channel parameters encountered. The associated worst-case channel time-domain correlation properties can be characterized by an ideally band-limited Doppler PSD function given by [261, 266]

$$p_t(f) = p_{B,unif}(f) = \begin{cases} \frac{1}{2f_D}, & \text{if } |f| < f_D \\ 0, & \text{otherwise}, \end{cases} \tag{1.3}$$

where f_D is the assumed value of the maximum Doppler frequency over all channel paths. The corresponding time-

(a) (b) (c)

Figure 1.10: Power Delay Profiles (PDP) corresponding to three different channel models, namely (a) the Short Wireless Asynchronous Transfer Mode (SWATM) channel model of [266], (b) Bug's channel model [348] and (c) the COST-207 Bad Urban (BU) channel model defined for UMTS-type system, as characterized in [349].

domain correlation function can be described as

$$r_t[m] = r_B[m] = \frac{\sin 2\pi f_D m}{2\pi f_D m}. \tag{1.4}$$

(a) (b)

Figure 1.11: (a) Frequency response and (b) impulse response of an order 8 raised cosine shaping filter with the oversampling rate of 4, the roll-off factor of 0.2 and the delay of 3 samples.

We adopt the complex baseband representation of the continuous-time Channel Impulse Response (CIR), as given by [350]

$$h(t,\tau) = \sum_l \alpha_l(t) c(\tau - \tau_l), \tag{1.5}$$

where $\alpha_l(t)$ is the time-variant complex amplitude of the lth path and the τ_l is the corresponding path delay, while $c(\tau)$ is the aggregate impulse response of the transmitter-receiver pair, which usually corresponds to the raised-cosine Nyquist filter. From (1.5) the continuous Channel Transfer Function (CTF) can be described as in [306]

$$\begin{aligned} H(t,f) &= \int_{-\infty}^{\infty} h(t,\tau)\, e^{-j2\pi f\tau} d\tau \\ &= C(f) \sum_l \alpha_l(t) e^{-j2\pi f \tau_l}, \end{aligned} \tag{1.6}$$

where $C(f)$ is the Fourier transform pair of the transceiver impulse response $c(\tau)$ characterized in Figure 1.11.

As it was pointed out in [261], in OFDM/MC-CDMA systems using a sufficiently long cyclic prefix and adequate synchronisation, the discrete subcarrier-related CTF can be expressed as

$$H[n,k] = H(nT, k\Delta f) = C(k\Delta f) \sum_{l=1}^{L} \alpha_l[n] W_K^{k\tau_l/T_s} \tag{1.7}$$

$$= \sum_{m=0}^{K_0-1} h[n,m] W_K^{km}, \tag{1.8}$$

where $T_s = T/K$ is the baseband sample duration, while K_0 is the length of the cyclic prefix, which normally corresponds to the maximum delay spread encountered, such that we have $K_0 > \tau_{\max}/T_s$. Subsequently

$$h[n,m] = h(nT, mT_s) = \sum_{l=1}^{L} \alpha_l[n] c(mT_s - \tau_l) \tag{1.9}$$

is the Sample-Spaced CIR (SS-CIR) and $W_K = \exp(-\jmath 2\pi/K)$. Note, that in realistic channel conditions associated with non-sample-spaced time-variant path-delays $\tau_l(n)$ the receiver will encounter dispersed received signal components in several neighbouring samples owing to the convolution of the transmitted signal with the system's impulse response, which we refer to as leakage. This phenomenon is usually unavoidable and therefore the resultant SS-CIR $h[n,m]$ will be constituted of numerous correlated non-zero taps described by Equation (1.5) and illustrated in Figure 1.12. By contrast, the Fractionally-Spaced CIR (FS-CIR) $\alpha_l[n] = \alpha_l(nT)$ will be constituted by a lower number of $L \ll K_0 \ll K$ non-zero statistically independent taps associated with distinctive propagation paths, as depicted in Figure 1.12.

(a) (b)

Figure 1.12: The **FS-CIR** (top) and the effective **SS-CIR** (bottom) resulting from the convolution of the original FS-CIR with the raised cosine filter impulse response of Figure 1.11 for the cases of (a) sample-spaced and (b) fractionally-spaced power delay profiles.

As it was shown in [261], the crosscorrelation function $r_H[m,l]$, which characterized both time- and frequency-domain correlation properties of the discrete CTF coefficients $H[n,k]$ associated with different OFDM blocks and subcarriers can be described as

$$r_H[m,l] = \mathrm{E}\left\{H[n+m,k+l]H^*[n,k]\right\}$$
$$= \sigma_H^2 r_t[m] r_f[l], \tag{1.10}$$

where $r_t[m]$ is the time-domain correlation function described by Equation (1.4), while $r_f[i]$ is the frequency-domain correlation functions, which can be expressed as follows [262]

$$r_f[l] = |C(l\Delta f)|^2 \sum_{i=1}^{L} \frac{\sigma_i^2}{\sigma_H^2} e^{-\jmath 2\pi l \Delta f \tau_i}, \tag{1.11}$$

where $\sigma_H^2 = \sum_{i=1}^{L} \sigma_i^2$.

1.7.2 Realistic Channel Properties

The majority of existing advanced channel estimation methods rely on the *a priori* knowledge of the channel statistics commonly characterized by the channel's Power Delay Profile (PDP) for the sake of estimating the instantaneous

Channel Impulse Response (CIR) and the corresponding Channel Transfer Function (CTF). It is evident however, that in realistic wireless mobile channels, where at least one of the communicating terminals is in motion, the channel's PDP will also become time-variant and thus may not be *a priori* known at the receiver.

For the sake of designing as we as characterizing the performance of an efficient and robust channel estimation scheme, which will be suitable for realistic channel conditions, we propose a channel model, which sustains the important characteristics of the realistic wireless mobile channels. More specifically, as opposed to the conventional constant PDP, our channel model is characterized by a time-variant PDP, where both the relative delays τ_l as well as the corresponding average powers σ_l^2 of different PDP taps vary with time.

Our channel model is dynamically generated using a geometric scattering model illustrated in Figure 1.13. More specifically, the individual scatterers associated with different propagation paths are randomly generated using a Marcov statistical model. The corresponding relative delays τ_l and powers σ_l^2 associated with each propagation path are calculated based on the geometrical location of each of the scatterers. Correspondingly, the rate of change in the values of the PDP tap delays τ_l is determined by the speed of the mobile wireless terminal and is characterized by the PDP *tap drift rate* parameter ν_τ. The specific assumptions regarding the practical range of values of the parameter ν_τ is discussed in the next chapter. Furthermore, each propagation path experiences independent fast Rayleigh fading. Finally, the set of parameters characterizing the Marcov model employed is chosen such that the average channel statistics corresponds to the desired static-PDP channel model.

Figure 1.13: PDP examples corresponding.

1.7.3 Baseline Scenario Characteristics

As a baseline scenario we consider a mobile wireless communication system utilizing a frequency bandwidth of $B = 10$ MHz at a carrier frequency of $f_c = 2.5$ GHz. Furthermore, we assume an OFDM system having $K = 128$ orthogonal subcarriers. The corresponding FFT-frame duration is $T_s = K/B = 16$ μs. We assume having a cyclic prefix of $1/4T_s = 4$ μs and thus the total OFDM symbol duration of $T = 20$ μs.

Some other important system-related assumptions include the relative speed of the communicating terminals, which we assume not to exceed $v = 130\ \mathrm{km/h} = 36\ \mathrm{m/s}$. Furthermore, the OFDM-symbol-normalized Doppler

frequency f_D relates to the relative speed of the communicating terminals as follows

$$f_D = T\frac{vf_c}{c}, \tag{1.12}$$

where $c = 3 \cdot 10^8$ m/s denotes the speed of light. The actual Doppler frequency f_D/T encountered in the mobile wireless environment is assumed to be in the range of 3 to 300 Hz, where the maximum value of 300 Hz correponds to the relative terminal speed of $v = 130$ km/h and the carrier frequency of $f_c = 2.5$ GHz. Finally, the OFDM-symbol-normalized PDP tap drift speed ν_τ may be calculated as follows

$$\nu_\tau = T\frac{v}{c}, \tag{1.13}$$

which suggests the that value of the PDP tap drift speed parameter does not exceed the maximum value of $\nu_\tau = 2.4 \cdot 10^{-6}\ \mu\text{s} = T \cdot 0.12\ \mu\text{s/s}$.

Table 1.11: Baseline scenario system characteristics.

Parameter	Value
Carrier frequency f_c	2.5 GHz
Channel bandwidth B	8 MHz
Number of carriers K	128
FFT frame duration T_s	16 μs
OFDM symbol duration T	20 μs (4 μs of cyclic prefix)
Max. delay spread τ_{max}	4 μs
Max. terminal speed v	130 km/h
Norm. Max. Doppler spread f_D	0.006 = $T \cdot 300$ Hz
Norm. Max. PDP tap drift ν_τ	$2.4 \cdot 10^{-6}\ \mu\text{s} = T \cdot 0.12\ \mu\text{s/s}$

The resultant baseline scenario system characteristics are summarized in Table 1.11

1.7.4 MC Transceiver

Figure 1.14: Schematic illustration of a typical OFDM/MC-CDMA system's PHY layer.

The transmitter part of the system is typically constituted of an OFDM / MC-CDMA Encoder and Modulator, the output of which is a complex-valued base-band time-domain signal. The resultant base-band signal is oversampled and pulse-shaped using a Nyquist filter, such as, for example, a root-raised-cosine filter characterized in Figure 1.11. The

resultant oversampled signal is then converted into an analog pass-band signal using a D/A converter and upconverted to the Radio Frequency (RF) band. At the receiver side a reciprocal process is taking place, where the received RF signal is amplified by the RF frontend and downconverted to an intermediate frequency pass-band, then sampled by the A/D converter, downconverted to the base-band, filtered by a matched Nyquist filter and finally decimated. The resultant complex-valued base-band signal is processed by the corresponding OFDM / MC-CDMA Demodulator and Decoder block, where the transmitted information symbols are detected.

In this treatise we consider the link between the output of the MC Modulator and the input of the MC Demodulator of Figure 1.14 as an *Effective Base-Band Channel*. The proof of feasibility for this assumption is beyond the scope this contribution, however it can be found for example in [350, 352].

The discrete frequency-domain model of the OFDM/MC-CDMA system illustrated in Figure 1.14 can be described as in [306]

$$y[n,k] = H[n,k]x[n,k] + w[n,k], \tag{1.14}$$

for $k = 0,\ldots,K-1$ and all n, where $y[n,k]$, $x[n,k]$ and $w[n,k]$ are the received symbol, the transmitted symbol and the Gaussian noise sample respectively, corresponding to the kth subcarrier of the nth OFDM block. Furthermore, $H[n,k]$ represents the complex-valued CTF coefficient associated with the kth subcarrier and time instance n. Note that in the case of an M-QAM modulated OFDM system, $x[n,k]$ corresponds to the M-QAM symbol accommodated by the kth subcarrier, while in a MC-CDMA system, such as a Walsh-Hadamard Transform (WHT) assisted OFDM scheme using G-chip WH spreading code and hence capable of supporting G users [266] we have

$$x[n,k] = \sum_{p=0}^{G-1} c[k,p]s[n,p], \tag{1.15}$$

where $c[k,p]$ is the kth chip of the pth spreading code, while $s[n,p]$ is the M-QAM symbol spread by the pth code. Each of the G spreading codes is constituted by G chips.

1.8 SDM-OFDM System Model

1.8.1 MIMO Channel Model

We consider a MIMO wireless communication system employing m_{t} transmit and n_{r} receive antennas, hence, the corresponding MIMO wireless communication channel is constituted by $(n_{\mathrm{r}} \times m_{\mathrm{t}})$ propagation links, as illustrated in Figure 1.15. Furthermore, each of the corresponding $(n_{\mathrm{r}} \times m_{\mathrm{t}})$ Single Input Single Output (SISO) propagation links comprises a multiplicity of statistically independent components, termed as *paths*. Thus, each of these SISO propagation links can be characterised as a *multipath* SISO channel discussed in detail in Section 1.7.1. Similarly to the SISO case, the multi-carrier structure of our SDM-OFDM transceiver allows us to characterise the broadband frequency-selective channel considered as an OFDM subcarrier-related vector of flat-fading Channel Transfer Function (CTF) coefficients. However, as opposed to the SISO case, for each OFDM symbol n and subcarrier k the MIMO channel is characterized by a $(n_{\mathrm{r}} \times m_{\mathrm{t}})$-dimensional matrix $\mathbf{H}[n,k]$ of the CTF coefficients associated with the different propagation links, such that the element $H_{ij}[n,k]$ of the CTF matrix $\mathbf{H}[n,k]$ corresponds to the propagation link connecting the jth transmit and ith receive antennas.

Furthermore, the correlation properties of the MIMO-OFDM channel can be readily derived as a generalisation of the SISO-OFDM channel scenario discussed in detail in Section 1.7.1. As it was shown in [261], the crosscorrelation function $r_H[m,l]$, which characterizes both the time- and frequency-domain correlation properties of the discrete CTF coefficients $H_{ij}[n,k]$ associated with the particular (i,j)th propagation link of the MIMO channel, as well as with the different OFDM symbol and subcarrier indices n and k can be described as

$$\begin{aligned} r_{H;ij}[m,l] &= \mathtt{E}\left\{H_{ij}^{*}[n+m,k+l], H_{ij}[n,k]\right\} \\ &= \sigma_H^2 r_t[m] r_f[l], \end{aligned} \tag{1.16}$$

where $r_t[m]$ is the time-domain correlation function, which may be characterized by a time-domain correlation model proposed by Jakes in [351], where we have

$$r_t[m] = r_J[m] = J_0(n w_d), \tag{1.17}$$

Figure 1.15: Illustration of a MIMO channel constituted by m_t transmit and n_r receive antennas. The corresponding MIMO channel is characterized by the $(n_r \times m_t)$-dimensional matrix $\mathbf{H}$ of CTF coefficients.

and $J_0(x)$ is a zero-order Bessel function of the first kind, while $w_d = 2\pi T f_D$ is the normalised Doppler frequency. On the other hand, the frequency-domain correlation function $r_f[l]$ can be expressed as follows [262]

$$r_f[l] = |C(l\Delta f)|^2 \sum_{i=1}^{L} \frac{\sigma_i^2}{\sigma_H^2} e^{-j2\pi l \Delta f \tau_i}, \tag{1.18}$$

where $C(f)$ is the frequency response of the pulse-shaping filter employed by the particular system, σ_i^2 and τ_i, $i = 1, \cdots, L$ are the average power and the corresponding delay of the L-tap Power Delay Profile (PDP) encountered, while σ_H^2 is the average power per MIMO channel link, such that we have $\sigma_H^2 = \sum_{i=1}^{L} \sigma_i^2$.

In this report we assume the different MIMO channel links to be mutually uncorrelated. This common assumption is usually valid, if the spacing between the adjacent antenna elements exceeds $\lambda/2$, where λ is the wavelength corresponding to the RF signal employed. Thus, the overall crosscorrelation function between the (i,j)th and (i',j')th propagation links may be described as

$$\begin{aligned} r_{H;ij;i'j'}[m,l] &= \mathrm{E}\left\{ H_{i'j'}^*[n+m, k+l], H_{ij}[n,k] \right\} \\ &= \sigma_H^2 r_t[m] r_f[l] \delta[i-i'] \delta[j-j'], \end{aligned} \tag{1.19}$$

where $\delta[i]$ is the discrete Kronecker Delta function.

1.8.2 Channel Capacity

Whilst most of the multi-path NLOS channel models can be collectively categorized as Rayleigh fading, different channel models characterized by different PDPs exhibit substantial differences in terms of their *information-carrying capacity* and *potential diversity gain*. The channel's capacity determines the upper-bound for the overall system's throughput. On the other hand, the available diversity gain allows the communication system to increase its transmission integrity. Various modulation and coding schemes can be employed by the communication system in order to increase its spectral efficiency and also to take advantage of diversity. Some of these methods are widely discussed in the literature, *e.g.* in [353], and include the employment of antenna arrays, space-time coding, time- and frequency-domain spreading, channel coding, time- and frequency-domain repetition *etc*. The theoretical performance boundaries of such methods are discussed in [267, 354]. Furthermore, the trade-offs between the attainable system capacity gain and the corresponding diversity gain are addressed in [355].

Consequently, the unrestricted capacity of a generic single-carrier ergodic-flat-fading MIMO channel can be expressed as in [337], where we have

$$\mathcal{C} = \mathrm{E}\left\{ \log \det \left[\sigma_w^2 \mathbf{I} + \frac{1}{m_t} \mathbf{H}\mathbf{H}^{\mathrm{H}} \right] \right\}, \tag{1.20}$$

where $\mathbf{H}$ is a $(n_r \times m_t)$-dimensional matrix with independent complex Gaussian distributed entries.

(a) (b)

Figure 1.16: Capacity $\mathcal{C}$ of Equation (1.20) as well as mutual information $I(\mathbf{s};\mathbf{y})$ of Equation (1.21) versus SNR for (a) 1x1 and (2) 2x2 systems in Rayleigh uncorrelated flat fading.

In realistic communication system, however, the achievable throughput is limited by the modulation scheme employed. Some examples of such modulation schemes are Mary PSK or Mary QAM constellation schemes, where M is the number of complex symbols constituting the constellation map corresponding to the particular modulation scheme employed. The upper bound defining the maximum throughput achievable by a particular discrete modulation scheme was first discussed by Shannon in [356] and was shown to be determined by the mutual information $I(\mathbf{s};\mathbf{y})$ exhibited by the modulation scheme employed. The mutual information can be calculated using the following expression

$$I(\mathbf{s};\mathbf{y}) = H(\mathbf{y}) - H(\mathbf{y}|\mathbf{s}), \tag{1.21}$$

where $H(\cdot) = -\mathrm{E}\log p(\cdot)$ denotes the entropy function [356]. In the case of having a Gaussian i.i.d. noise sample vector $\mathbf{w}$ with the corresponding covariance matrix given by $C_w = \sigma_w^2\mathbf{I}$, the constrained entropy constituent $H(\mathbf{y}|\mathbf{s})$ of Equation (1.21) is may be expressed as follows [337]

$$H(\mathbf{y}|\mathbf{x}) = n_\mathrm{r}\log 2\pi\sigma_w^2 e, \tag{1.22}$$

whereas the unconstrained entropy constituent $H(\mathbf{y})$ can be approximated numerically using a Monte-Carlo simulation as in [337], where we have

$$H(\mathbf{y}) = -\mathrm{E}\log\left(\frac{1}{M^{m_\mathrm{t}}(2\pi\sigma_w^2)^{n_\mathrm{r}}}\sum_{\mathbf{s}}\exp\left[-\frac{1}{2\sigma_w^2}\|\mathbf{y}-\mathbf{H}\mathbf{s}\|^2\right]\right), \tag{1.23}$$

where the expectation is taken over the three sources of randomness in the choice of $\mathbf{s}, \mathbf{H}$ and $\mathbf{w}$. Moreover, the summation in Equation (1.23) is carried out over all M^{m_t} possible values of $\mathbf{s}$.

Figures 1.16(a) and 1.16(b) characterize both the capacity $\mathcal{C}$ of Equation (1.20) as well as the mutual information $I(\mathbf{s};\mathbf{y})$ of Equation (1.21) for SISO and 2x2-MIMO systems, respectively. The mutual information plots depicted in both figures correspond to systems employing QPSK as well as 16- and 64-QAM modulations.

1.8.3 SDM-OFDM Transceiver Structure

The schematic of a typical SDM-OFDM system's physical layer is depicted in Figure 1.17. The transmitter of the SDM-OFDM system considered is typically constituted by the Encoder and Modulator seen in Figure 1.17, generating a set of m_t complex-valued base-band time-domain signals [266]. The modulated base-band signals are then processed in parallel. Specifically, they are oversampled and shaped using a Nyquist filter, such as for example a root-raised-cosine filter. The resultant oversampled signals are then converted into an analog pass-band signal using a bank of D/A converters and upconverted to the Radio Frequency (RF) band. At the receiver side of the SDM-OFDM transceiver the inverse process takes place, where the set of received RF signals associated with the n_r receive antenna elements are amplified by the RF amplifier and down-converted to an intermediate frequency pass-band. The resultant pass-band signals are then sampled by a bank of A/D converters, down-converted to the base-band, filtered by a matched Nyquist filter and finally decimated, in order to produce a set of discrete complex-valued base-band signals. The resultant set

Figure 1.17: Schematic of a typical SDM-OFDM system's physical layer.

of discrete signals is processed by the corresponding Demodulator and Decoder module seen in Figure 1.17, where the transmitted information-carrying symbols are detected.

In this treatise we consider the link between the output of the SDM-OFDM Modulator and the input of the corresponding SDM-OFDM Demodulator of Figure 1.17 as an *Effective Base-Band MIMO Channel*. The proof of feasibility for this assumption is beyond the scope this contribution, however it can be found for example in [350, 352]. The structure of the resultant base-band SDM-OFDM system is depicted in Figure 1.18, where the bold grey arrows illustrate subcarrier-related signals represented by the vectors $\mathbf{x}_i$ and $\mathbf{y}_i$, while the black thin arrows accommodate scalar time-domain signals.

Figure 1.18: Schematic of a generic SDM-OFDM BLAST-type transceiver.

The discrete frequency-domain model of the SDM-OFDM system, illustrated in Figure 1.18, may be characterised

as a generalisation of the SISO case described in of Section 1.7.1. Namely, we have

$$y_i[n,k] = \sum_{j=1}^{m_t} H_{ij}[n,k]x_j[n,k] + w_i[n,k], \tag{1.24}$$

where $n = 0,1,\cdots$ and $k = 0,\ldots,K-1$ are the OFDM symbol and subcarrier indices, respectively, while $y_i[n,k]$, $x_j[n,k]$ and $w_i[n,k]$ denote the symbol received at the ith receive antenna, the symbol transmitted from the jth transmit antenna and the Gaussian noise sample encountered at the ith receive antenna, respectively. Furthermore, $H_{ij}[n,k]$ represents the complex-valued CTF coefficient associated with the propagation link connecting the jth transmit and ith receive antennas at the kth OFDM subcarrier and time instance n. Note that in the case of an M-QAM modulated OFDM system, $x_j[n,k]$ corresponds to the M-QAM symbol accommodated by the kth subcarrier of the nth OFDM symbol transmitted from the jth transmit antenna element.

The SDM-OFDM system model described by Equation (1.24) can be interpreted as the per OFDM-subcarrier vector expression of

$$\mathbf{y}[n,k] = \mathbf{H}[n,k]\mathbf{x}[n,k] + \mathbf{w}[n,k], \tag{1.25}$$

where we introduce the space-devision-related vectors $\mathbf{y}[n,k]$, $\mathbf{x}[n,k]$ and $\mathbf{w}[n,k]$, as well as a space-devision-related $(n_r \times m_t)$-dimensional matrix of CTF coefficients $\mathbf{H}[n,k]$. Note that similarly to the SISO case, the multi-carrier structure of the SDM-OFDM transceiver allows us to represent the broadband frequency-selective MIMO channel as a subcarrier-related vector of flat-fading MIMO-CTF matrices $\mathbf{H}[n,k]$.

1.9 Novel Aspects and Outline of the Book

Having briefly reviewed the OFDM, MIMO-OFDM and SDMA-OFDM literature, let us now outline the organization of the monograph.

- **Chapter 3: Channel Coding Assisted STBC-OFDM Systems**
  As an introductory study, in this chapter we discuss various channel coded Space-Time Block Codes (STBCs) in the context of single-user single-carrier and single-user OFDM systems. This work constitutes the background work for the multi-user systems to be investigated in following chapters. More specifically, various Turbo Convolutional (TC) codes, Low Density Parity Check (LDPC) codes and Coded Modulation (CM) schemes are combined with STBCs for improving the performance of the single-user system considered.

- **Chapter 4: Coded Modulation Assisted Multi-User SDMA-OFDM Using Frequency-Domain Spreading**
  In this chapter, we invoke a multi-user MIMO SDMA-OFDM system for uplink communications, where the classic Minimum Mean-Square Error (MMSE) Multi-User Detector (MUD) is employed at the BS for separating the different users' signals. The CM schemes discussed in Chapter 3, namely Trellis Coded Modulation (TCM), Turbo TCM (TTCM), Bit-Interleaved Coded Modulation (BICM) and Iteratively Decoded BICM (BICM-ID), are evaluated and compared in the context of the SDMA-OFDM system. Furthermore, the performance gain arising from invoking Walsh-Hadamard Transform Spreading (WHTS) across a block of OFDM subcarriers in the Frequency Domain (FD) is studied in both the uncoded SDMA-OFDM and the CM-assisted SDMA-OFDM systems.

- **Chapter 5: Hybrid Multi-User Detection for SDMA-OFDM Systems**
  This chapter focuses on the design of MUDs invoked by the SDMA receiver. Specifically, the Maximum Likelihood Detection (MLD) scheme is found to attain the best performance at the cost of a computational complexity that increases exponentially both with the number of users and with the number of Bits Per Symbol (BPS) transmitted by higher-order modulation schemes. By contrast, the MMSE MUD exhibits a lower complexity at the expense of a performance loss. In order to achieve a good performance-complexity tradeoff, Genetic Algorithm (GA) based MUD techniques are proposed for employment in channel coded SDMA-OFDM systems, where TTCM is used. Moreover, a novel Biased Q-function Based Mutation (BQM) assisted iterative GA (IGA) MUD is designed. The performance of the proposed BQM-IGA is compared to both that of the optimum MLD and the linear MMSE MUD in the so-called fully-loaded and overloaded scenarios, respectively, where the number of users is equal to or higher than the number of receiver antenna elements. Additionally, the computational complexity associated with the various MUD schemes is discussed.

- **Chapter 6: Direct-Sequence Spreading and Slow Subcarrier-Hopping Aided Multi-User SDMA-OFDM Systems**

This chapter commences with a short review of conventional SDMA-OFDM systems, followed by an introduction to hybrid SDMA-OFDM arrangements, which incorporate Direct-Sequence Spreading (DSS) and/or Frequency-Hopping (FH) techniques into conventional SDMA-OFDM. A novel FH technique referred to as Slow SubCarrier-Hopping (SSCH) is designed for hybrid DSS/FH SDMA-OFDM systems using a TTCM scheme. Furthermore, two types of SSCH pattern are discussed, namely the Random SSCH (RSSCH) and the Uniform SSCH (USSCH) patterns. The performance of the proposed TTCM-assisted DSS/SSCH SDMA-OFDM system is evaluated and compared to the conventional SDMA-OFDM and various hybrid SDMA-OFDM configurations.

- **Chapter 7: Channel Estimation for OFDM and MC-CDMA**
  We derive an advanced decision directed channel estimation (DDCE) scheme, which is capable of recursive tracking and prediction of the rapidly-fluctuating channel parameters, characterized by time-variant statistics. More specifically, we employ a Projection Approximation Subspace Tracking (PAST) [357] technique for the sake of tracking the channel transfer function's low-rank signal subspace and thus facilitating a high accuracy tracking of the channel's transfer function, while imposing a relatively low computational complexity.

- **Chapter 8: Iterative Joint Channel Estimation and Multi-User Detection for SDMA-OFDM Systems**
  The objective of this chapter is to develop an efficient solution to the channel estimation problem of multi-user MIMO-OFDM systems. It is well-known that compared to Single-Input Single-Output (SISO) systems, channel estimation in the MIMO scenario becomes more challenging, owing to the increased number of independent transmitter-receiver links to be estimated. Against this background, an iterative, joint channel estimation and symbol detection approach is proposed for LDPC-coded MIMO SDMA-OFDM systems. More specifically, the method modifies the GA MUD advocated in Chapter 5 so that it becomes capable of jointly optimizing the Frequency-Domain CHannel Transfer Functions (FD-CHTFs) and the multi-user data symbols. Moreover, an efficient algorithm is derived, which enables the GA to output soft bits for the sake of improving the performance of the LDPC channel decoder.

- **Chapter 9: Reduced-Complexity Sphere Detection for Uncoded SDMA-OFDM Systems**
  The main objective of this chapter is to systematically review the fundamentals of the SD, which is considered to be one of the most proming low-complexity near-optimum detection technique at the time of writing. Furthermore, we address the SD-related complexity reduction issues. Specifically, the principle of the Hard-Input Hard-Output (HIHO) SD is reviewed first in the context of both the depth-first and breadth-first tree search based scenarios, along with that of the GSD, which is applicable to challenging rank-deficient MIMO scenarios. A comprehensive comparative study of the complexity reduction schemes devised for different types of SDs, namely, the conventional depth-first SD, the K-best SD and the novel OHRSA detector, is carried out by analyzing their conceptual similarities and differences. Finally, their achievable performance and th complexity imposed by the various types of SDs are investigated in comparison to each other.

- **Chapter 10: Reduced-Complexity Iterative Sphere Detection for Channel Coded SDMA-OFDM Systems**
  The fundamentals of the LSD scheme are studied at the beginning of this chapter in the context of an iterative detection aided channel coded MIMO-OFDM system. A potentially excessive complexity may be imposed by the conventional LSD, since it has to generate soft information for every transmitted bit, which requires the observation of a high number of hypotheses about the transmitted MIMO symbol. Based on the above-mentioned complexity issue, we contrive a generic center-shifting SD scheme and the so-called *apriori*-LLR-threshold assisted SD scheme with the aid of EXIT chart analysis, both of which are capable of effectively reducing the potentially high complexity imposed by the SD-aided iterative receiver. Moreover, we combine the above-mentioned schemes in the interest of further reducing the complexity imposed. In addition, for the sake of enhancing the achievable iterative detetion gains and hence improving the bandwidth efficiency, a Unity-Rate Code (URC) assisted three-stage serially concatenated transceiver employing the so-called Irregular Convolutional Codes (IrCCs) is devised. Finally, the benefits of the proposed center-shifting SD scheme are also investigated in the context of the above-mentioned three-stage iterative receiver.

- **Chapter 11: Sphere Packing Modulated STBC-OFDM and its Sphere Detection**
  In this chapter we extend the employment of the turbo-detected Sphere Packing (SP) aided Space-Time Block Coding (STBC) scheme to Multi-User MIMO (MU-MIMO) scenarios, because SP was demonstrated to be capable of providing useful performance improvements over conventionally-modulated orthogonal design based STBC schemes in the context of Single-User MIMO (SU-MIMO) systems. For the sake of achieving a near-MAP performance, while imposing a moderate complexity, we specifically design the K-best SD scheme for supporting the operation of the SP-modulated system, since the conventional SD cannot be directly applied to such a system. Consequently, when relying on our SD, a significant performance gain can be achieved by the SP-modulated system over its conventionally-modulated counterpart in the context of MU-MIMO systems.

- **Chapter 12: Multiple-Symbol Differential Sphere Detection for Cooperative OFDM**
  The principle of the MSDSD is first reviewed, which has been recently proposed for mitigating the time-selective-channel-induced performance loss suffered by classic direct transmission schemes employing the Conventional Differential Detection (CDD) scheme. Then, we specifically design the MSDSD for both the Differential Amplify-and-Forward (DAF) and Differential Decode-and-Forward (DDF) assisted cooperative systems based on the multi-dimensional tree search proposed in Chapter 4, which is capable of achieving a significant performance gain for transmission over time-selective channels induced by the relative mobility amongst the cooperating transceivers.

- **Chapter 13: Resource Allocation for the Differentially Modulated Cooperative Uplink**
  In this chapter the theoretical BER performance of both the DAF- and DDF-aided cooperative cellular uplinks are investigated. Then, based on the minimum BER criterion, we design efficient Cooperating-User-Selection (CUS) and Adaptive-Power-Allocation (APA) schemes for the above-mentioned two types of differentially modulated cooperative systems, while requiring no Channel State Information (CSI) at the receiver. Moreover, we investigate the Cooperative-Protocol-Selection (CPS) of the uplink system in conjunction with a beneficial CUS as well as the APA scheme in order to further improve the achievable end-to-end performance, leading to a resource-optimized hybrid cooperative system. Hence, a number of cooperating MSs may be adaptively selected from the available MS candidate pool and the cooperative protocol employed by a specific cooperating MS may also be adaptively selected in the interest of achieving the best possible BER performance.

- **Chapter 14: The Near-Capacity Differentially Modulated Cooperative Cellular Uplink** The DDF-aided cooperative system's DCMC capacity is investigated in comparison to that of its classic direct-transmission based counterpart in order to answer the grave fundamental question, whether it is worth introducing cooperative mechanisms into the development of wireless networks, such as the cellular voice and data networks. Then, we propose a practical framework of designing a cooperative system, which is capable of performing close to the network's corresponding non-coherent DCMC capacity. Based on our low-complexity near-capacity design criterion, a novel Irregular Distributed Hybrid Concatenated Differential (Ir-DHCD) coding scheme is contrived for the DDF cooperative system employing our proposed capacity-achieving low-complexity adaptive-window-aided SISO iterative MSDSD scheme.

- **Chapter 15: Multi-Stream Detection for SDM-OFDM Systems**
  The multi-stream detection problem of SDM-OFDM systems is similar to the MUD techniques of SDMA-OFDM arrangements, which are classified and reviewed in this chapter.

- **Chapter 16: Approximate Log-MAP SDM Detection**
  We propose the novel family of Optimized Hierarchy Reduced Search Algorithm (OHRSA)-aided space-time processing methods, which may be regarded as an advanced extension of the Complex Sphere Decoder (CSD) method, portrayed in [339]. The algorithm proposed extends the potential application range of the CSD methods of [337] and [339], as well as reduces the associated computational complexity. Moreover, the OHRSA-aided SDM detector proposed exhibits the near-optimum performance of the Log-MAP SDM detector, while imposing a substantially lower computational complexity, which renders it an attractive design alternative for practical systems.

- **Chapter 17: Iterative Channel Estimation and Detection for SDM-OFDM**
  Finally, we propose an iterative turbo receiver architecture, which utilises both the soft decision feedback aided MIMO channel estimation scheme of Chapter 7 as well as the Log-MAP SDM detection method derived in Chapter 16. Additionally, we carry out an analysis of the associated design trade-offs.

- **Chapter 18: Conclusions and Future Work**
  The major findings of our work are summarized in this chapter, including our suggestions for future research.

1.10 Chapter Summary

The historic development of various MIMO techniques was briefly summarized in Section 1.1.1.1, followed by a rudimentary introduction to MIMO-OFDM systems in Section 1.1.1.2. In Section 1.1.1.3 a concise review of various SDMA and SDMA-OFDM techniques was given, highlighting the associated signal processing problems.

Chapter 2

OFDM Standards

During the past decades, wireless communication has benefitted from substantial advances and it is considered as the key enabling technique of innovative future consumer products. For the sake of satisfying the requirements of various applications, significant technological achievements are required to ensure that wireless devices have appropriate architectures suitable for supporting a wide range of services delivered to the users.

In the foreseeable future, the large-scale employment of wireless devices and the requirements of high-bandwidth applications are expected to lead to tremendous new challenges in terms of the efficient exploitation of the achievable spectral resources. New wireless techniques, such as Ultra WideBand (UWB) [358], advanced source and channel encoding as well as various smart antenna techniques, for example Space-Time Codes (STCs) [359], Space Division Multiple Access (SDMA) [5] and beamforming, as well as other Multiple-Input Multiple-Output (MIMO) [93] wireless architectures are capable of offering substantial improvements over classic communication systems. Hence researchers have focused their attention on the next generation of wireless broadband communications systems, which aim for delivering multimedia services requiring data rates much higher than existing ones. Undoubtedly, supporting such high data rates, while maintaining a high robustness against radio channel impairments, such as multi-path fading and frequency-selective fading, requires further enhanced system architectures.

The organisation of this chapter is as follows. In Sections 2.1, 2.2 and 2.3, we review various major international standards that adopt OFDM, namely Wi-Fi, the Third-Generation Partnership Project (3GPP) Long-Term Evolution (LTE) and Worldwide Interoperability for Microwave Access (WiMAX) standards, respectively. Finally, we conclude the chapter in Section 2.4.

2.1 Wi-Fi

In 1999, the Wi-Fi Alliance was founded as a global, non-profit organization, aiming for developing a single globally accepted standard for high-speed WLANs. The mission of the Wi-Fi Alliance was to promote the Wi-Fi technology and the corresponding Wi-Fi product certification. The Wi-Fi Alliance has now more than 300 members from more than 20 countries and Wi-Fi has achieved a huge worldwide success. A study [360] released in September 2008 by the Wi-Fi Alliance found that an increased number of consumers in the United States, the United Kingdom and Japan value the Wi-Fi Certified brand. Developed in March 2000, the certification program has approved more than 4,800 products from various vendors worldwide.

2.1.1 IEEE 802.11 Standards

Wi-Fi is based on the IEEE 802.11 standard family. The first version of IEEE 802.11 was released in 1997 [361], which was rectified in 1999 [362]. Then, two further supplements of 802.11-1999 were released, the first one being IEEE 802.11a [363], which provides a bit rate of up to 54 Mbps in the 5 GHz band. In comparison to 802.11-1999, where Frequency-Hopping Spread Spectrum (FHSS) or Direct-Sequence Spread Spectrum (DSSS) are used, 802.11a employs an OFDM scheme, which applies to Wireless Asynchronous Transfer Mode (WATM) networks and access hubs. The second supplement to 802.11-1999 was IEEE 802.11b [364], which has a maximum data rate of 11 Mbps in the 2.4 GHz band and uses the same media access method as that defined in 802.11-1999.

Further enhancements to 802.11 were made later. The IEEE 802.11d-2001 standard [365] introduced the support of international roaming services. The IEEE 802.11g-2003 standard [366], which exploits the same OFDM modulation scheme as 802.11a, provides a data rate of 20-54 Mbps in the 2.4 GHz band. Other improvements include IEEE 802.11h [367], IEEE 802.11i [368] and IEEE 802.11j [369], which introduced spectrum and transmit power management in the 5 GHz band in Europe, security enhancements, and operation in the 4.9-5 GHz band in Japan, respectively. In November 2005, the release of IEEE 802.11e-2005 [370] provided further QoS enhancements.

As the number of standards in the 802.11 family grew up, it was proposed by the working group that a single document combining all up-to-date 802.11 specifications should be provided. This resulted in the IEEE 802.11-2007 standard [371], a new release that includes all previous 802.11 amendments. In 2008, another two amendments were completed. The IEEE 802.11k-2008 [372] extends 802.11 by specifying mechanisms for Radio Resource Measurement (RRM), and the IEEE 802.11r-2008 [373] provides mechanisms for fast Basic Service Set (BSS) transition.

Some of the 802.11 standards are still in the drafting stage, such as the IEEE 802.11n standard [57], which aims for developing next-generation WLANs by incorporating MIMO-OFDM techniques. It is expected to offer high-throughput wireless transmission at 100-200Mbps. The IEEE 802.11y standard [374] will provide support for the operation in the 3650-3700 MHz band in U.S.A.

As a brief summary, we highlight the major 802.11 standards in Tables 2.1, 2.2 and 2.3.

Year	Standard	Title
1997	802.11-1997 [361]	IEEE Standard for Information Technology - Telecommunications and Information Exchange Between Systems - Local and Metropolitan Area Networks - Specific Requirements - Part 11: Wireless LAN Medium Access Control (MAC) and Physical Layer (PHY) Specifications
1999	802.11-1999 [362]	IEEE Standard for Information Technology - Telecommunications and Information Exchange Between Systems - Local and Metropolitan Area Networks - Specific Requirements - Part 11: Wireless LAN Medium Access Control (MAC) and Physical Layer (PHY) Specifications
	802.11a-1999 [363]	Supplement to IEEE Standard for Information Technology - Telecommunications and Information Exchange Between Systems - Local and Metropolitan Area Networks - Specific Requirements - Part 11: Wireless LAN Medium Access Control (MAC) and Physical Layer (PHY) Specifications: High-speed Physical Layer in the 5 GHz Band
	802.11b-1999 [364]	Supplement to IEEE Standard for Information Technology - Telecommunications and Information Exchange Between Systems - Local and Metropolitan Area Networks - Specific Requirements - Part 11: Wireless LAN Medium Access Control (MAC) and Physical Layer (PHY) Specifications: Higher-speed Physical Layer Extension in the 2.4 GHz Band
2001	802.11d-2001 [365]	IEEE Standard for Information Technology - Telecommunications and Information Exchange Between Systems - Local and Metropolitan Area Networks - Specific Requirement - Part 11: Wireless LAN Medium Access Control (MAC) and Physical Layer (PHY) Specification - Amendment 3: Specifications for Operation in Additional Regulatory Domains

Table 2.1: The family of the IEEE 802.11 Standards (1997-2001).

Year	Standard	Title
2003	802.11g-2003 [366]	IEEE Standard for Information Technology - Telecommunications and Information Exchange Between Systems - Local and Metropolitan Area Networks - Specific Requirements - Part 11: Wireless LAN Medium Access Control (MAC) and Physical Layer (PHY) Specifications - Amendment 4: Further Higher Data Rate Extension in the 2.4 GHz Band
	802.11h-2003 [367]	IEEE Standard for Information Technology - Telecommunications and Information Exchange Between Systems - Local and Metropolitan Area Networks - Specific Requirements - Part 11: Wireless LAN Medium Access Control (MAC) and Physical Layer (PHY) Specifications - Amendment 5: Spectrum and Transmit Power Management Extensions in the 5 GHz band in Europe
2004	802.11i-2004 [368]	IEEE Standard for Information Technology - Telecommunications and Information Exchange Between Systems - Local and Metropolitan Area Networks - Specific Requirements - Part 11: Wireless LAN Medium Access Control (MAC) and Physical Layer (PHY) Specifications - Amendment 6: Medium Access Control (MAC) Security Enhancements
	802.11j-2004 [369]	IEEE Standard for Information Technology - Telecommunications and Information Exchange Between Systems - Local and Metropolitan Area Networks - Specific Requirements - Part 11: Wireless LAN Medium Access Control (MAC) and Physical Layer (PHY) Specifications - Amendment 7: 4.9 GHz-5 GHz Operation in Japan
2005	802.11e-2005 [370]	IEEE Standard for Information Technology - Telecommunications and Information Exchange Between Systems - Local and Metropolitan Area Networks - Specific Requirements - Part 11: Wireless LAN Medium Access Control (MAC) and Physical Layer (PHY) Specifications - Amendment 8: Medium Access Control (MAC) Quality of Service Enhancements

Table 2.2: The family of the IEEE 802.11 Standards (2003-2005).

2.2 3GPP Long-Term Evolution

The Third-Generation Partnership Project (3GPP) is an international standardisation body working on the specification of the 3G Universal Terrestrial Radio Access Network (UTRAN) and on the Global System for Mobile communications (GSM). The latest specification that is being studied and developed in 3GPP is an evolved 3G radio access, widely known as the Long-Term Evolution (LTE) or Evolved UTRAN (E-UTRAN), as well as an evolved packet access core network in the System Architecture Evolution (SAE). The initial requirements for LTE were set out in early 2005, which are briefly summarised in Table 2.4 and in [375].

The initial objective of 3GPP was to produce global specifications for a 3G mobile system evolving from the existing GSM core network. This includes the Wideband CDMA (WCDMA) based UTRA Frequency Division Duplex (FDD) mode and the Time Division Code Division Multiple Access (TD-CDMA) based UTRA Time Division Duplex (TDD) mode [377]. In December 2005, it was decided that the LTE radio access should be based on OFDMA in the downlink (DL) and Single-Carrier Frequency Division Multiple Access (SC-FDMA) in the uplink (UL). SC-FDMA is also known as Discrete Fourier Transform Spread OFDMA (DFTS-OFDMA). The main PHY parameters of the LTE DL are summarised in Table 2.5.

Briefly, the objective of the SAE is to migrate circuit-switched networks towards packet-switched networks. This is set out in the recent 3GPP releases, where an Evolved Packet Core was defined. The main targets of SAE can be divided into the following aspects [377]:

Year	Standard	Title
2007	802.11-2007 [371]	IEEE Standard for Information Technology - Telecommunications and Information Exchange Between Systems - Local and Metropolitan Area Networks - Specific Requirements - Part 11: Wireless LAN Medium Access Control (MAC) and Physical Layer (PHY) Specifications
2008	802.11k-2008 [372]	IEEE Standard for Information Technology - Telecommunications and Information Exchange Between Systems - Local and Metropolitan Area Networks - Specific Requirements - Part 11: Wireless LAN Medium Access Control (MAC) and Physical Layer (PHY) Specifications - Amendment 1: Radio Resource Measurement of Wireless LANs (Amendment to IEEE 802.11-2007)
	802.11r-2008 [373]	IEEE Standard for Information Technology - Telecommunications and Information Exchange Between Systems - Local and Metropolitan Area Networks - Specific Requirements - Part 11: Wireless LAN Medium Access Control (MAC) and Physical Layer (PHY) Specifications - Amendment 2: Fast Basic Service Set (BSS) Transition (Amendment to IEEE 802.11-2007 and IEEE 802.11k-2008)
	P802.11n-2008 [57]	Draft IEEE Standard for Information Technology - Telecommunications and Information Exchange Between Systems - Local and Metropolitan Area Networks - Specific Requirements - Part 11: Wireless LAN Medium Access Control (MAC) and Physical Layer (PHY) Specifications - Amendment 4: Enhancements for Higher Throughput
	P802.11y-2008 [374]	Draft IEEE Standard for Information Technology - Telecommunications and Information Exchange Between Systems - Local and Metropolitan Area Networks - Specific Requirements - Part 11: Wireless LAN Medium Access Control (MAC) and Physical Layer (PHY) Specifications - Amendment 3: 3650-3700 MHz Operation in USA (Draft Amendment to IEEE 802.11-2007)

Table 2.3: The family of the IEEE 802.11 Standards (2007-2008).

- high-level user and operational aspects,
- basic capabilities,
- multi-access and seamless mobility,
- man-machine interface aspects,
- performance requirements for the evolved 3GPP,
- security as well as privacy, and
- charging aspects of the system.

2.3 WiMAX Evolution

The rapidly growing demand for flexible, high-speed broadband services requires advanced communication technologies. The more conventional family of high-rate broadband access techniques has relied on wired access, such as Digital Subscriber Line (DSL), cable modems, ethernet and optical fibers. However, the extension of the coverage area results in a significantly increased cost imposed by building and maintaining wired networks. This is particularly true for less densely populated zones, for example suburban and rural areas.

Requirement	Description	
Peak Data Rate	DL	5 bps/Hz (100 Mb/s within 20 MHz)
	UL	2.5 bps/Hz (50 Mb/s within 20 MHz)
Control Plane Latency	$<$ 100 ms (transition time from a camped state)	
	$<$ 50 ms (transition time between dormant states)	
Control Plane Capacity	$\geq$ 200 users per cell	
User Plane Latency	$<$ 5 ms	
Average User Throughput	DL	3 to 4 times over Release 6 [376]
	UL	2 to 3 times over Release 6 [376]
Spectrum Efficiency	DL	3 to 4 times over Release 6 [376]
	UL	3 to 4 times over Release 6 [376]
Mobility	Optimised performance (0-15 km/h), high performance (15-120 km/h), service maintained (120-350 km/h)	
Coverage	5 km cells	Performance targets met
	30 km cells	Slight degradation
	100 km cells	Not precluded
Enhanced MBMS	Enhanced MBMS shall be supported	
Spectral Flexibility	Allocation of different-width bands (1.25-20 MHz) shall be supported. Content can be delivered over an aggregation of resources.	
Coexistence with 3GPP RATs	Coexist with GSM EDGE RAN (GERAN) and UTRAN	
Architecture and Migration	Packet-based single E-UTRAN architecture to support end-to-end QoS and to minimise “single points of failure”	
RRM	Enhanced support for end-to-end QoS, load sharing and policy management	
Complexity	Minimise optional functions and remove redundant mandatory features	

Table 2.4: System requirements for 3GPP LTE [375]. MBMS: Multimedia Broadcast Multicast Service.

Parameters		Values					
System Bandwidth (MHz)		1.25	2.5	5	10	15	20
Timeslot Duration (ms)		0.675					
Subcarrier Spacing (KHz)		15					
Sampling Frequency (MHz)		1.92	3.84	7.68	15.36	23.04	30.72
FFT size		128	256	512	1024	1536	2048
No. of Used Subcarriers		76	151	301	601	901	1201
No. of OFDM Symbols per Time Slot (Short/Long CP)		9/8					
CP Length (μs/samples)	Short	7.29/14	7.29/28	7.29/56	7.29/112	7.29/168	7.29/224
	Long	16.67/32	16.67/64	16.67/128	16.67/256	16.67/384	16.67/512
Timeslot Interval (samples)	Short	18	36	72	144	216	288
	Long	16	32	64	128	192	256

Table 2.5: PHY parameters for 3GPP LTE DL [378].

Hence, Broadband Wireless Access (BWA) techniques have emerged as potent competitors of their conventional wired counterparts, facilitating the provision of broadband services for subscribers that are far from the coverage area of the wired networks. Being flexible, efficient and cost-effective, BWA provides an excellent solution to overcome the above-mentioned coverage problem. During the past decade or so, a number of proprietary wireless access systems have been developed by the wireless industry. Naturally, these proprietary products were based on diverse specifications, which inevitably limited their applications and markets. As a matter of fact, the potential benefits of BWA services were not expected to be widely achieved due to the lack of a common international standard, until the emergence of the Worldwide Interoperability for Microwave Access (WiMAX) standard [379].

WiMAX is one of the most popular BWA technologies available at the time of writing, aiming to provide high-speed broadband wireless access for Wireless Metropolitan Area Networks (WMANs) [380]. As a standardised technology, WiMAX ensures the inter-operability of equipment certified by the WiMAX Forum, resulting in a significant cost reduction for service providers that would like to use products manufactured by diverse vendors. This distinct advantage has paved the way for global broadband wireless services. Another key benefit of WiMAX is that it has been optimised for offering excellent Non-Line-of-Sight (NLOS) coverage with the aid of advanced wireless transmission techniques, such as Multiple-Input Multiple-Output (MIMO) transmit/receive diversity and Automatic Re-transmission Request (ARQ), etc [381], combined with Orthogonal Frequency Division Multiplexing (OFDM) or Orthogonal Frequency Division Multiple Access (OFDMA) [381].

This section is organised as follows. In Section 2.3.1, we first briefly outline the historic background of WiMAX. Specifically, the IEEE 802.16 standard family is reviewed in Section 2.3.1.1, which has tight links to WiMAX, followed by the introduction of the WiMAX Forum in Section 2.3.1.3. Then a brief introduction of the Korean WiMAX standard, Wireless Broadband (WiBro), is provided in Section 2.3.1.4. In Section 2.3.2, we proceed with discussing the technical aspects of WiMAX, including WiMAX-I in Section 2.3.2.1 and WiMAX-II in Section 2.3.2.2, respectively. The trends concerning the future of WiMAX are summarised in Section 2.3.3.

2.3.1 Historic Background

In this section, we will commence by briefly reviewing the IEEE 802.16 standard family in Section 2.3.1.1, and portray the brief history of the WiMAX Forum in Section 2.3.1.3. The connection between WiMAX and WiBro is established in Section 2.3.1.4.

2.3.1.1 IEEE 802.16 Standard Family

WiMAX is closely related to the IEEE 802.16 standard family. Before elaborating on WiMAX, let us first briefly review the history of the IEEE 802.16 Standards outlined in Table 2.6.

The IEEE 802.16 Working Group (WG) was chartered to define the air interface for BWA systems in certain licensed frequency bands. The 802.16 specifications conform to the family of IEEE 802 standards, governing the Local Area Networks (LANs) and Metropolitan Area Networks (MANs) endorsed by the IEEE in 1990 [391]. As opposed to the IEEE 802.11 WG, which focuses on Wireless Local Area Network (WLAN) standards and applications, the IEEE 802.16 WG has been focused on developing cost-efficient point-to-multipoint BWA architectures that enable multimedia broadband services in MANs and Wide Area Networks (WANs) [391].

2.3.1.2 Early 802.16 Standards

As early as in 1998, the IEEE 802.16 group was formed to develop a radio standard for wireless broadband communications. In December 2001, the first member of the IEEE 802.16 standard family was approved, widely referred to as IEEE 802.16-2001 [382]. It focuses on a Line-of-Sight (LOS) based point-to-multipoint wireless broadband system operating in the 10-66 GHz band. It utilises a Single-Carrier (SC) based physical layer (PHY) in conjunction with a burst Time Division Multiplexed (TDM) Media Access Control (MAC) layer [379].

Following the initial release of 802.16-2001, there had been two amendments, namely IEEE 802.16c-2002 [383] in December 2002, which provides detailed system profiles for the 10-66 GHz band, and IEEE 802.16a-2003 [384] in April 2003, which presents some MAC modifications and additional PHY specifications for the 2-11 GHz band. Note that in the standards rectified after 802.16a-2003, in addition to the SC-based PHY, both the OFDM and OFDMA based PHY specifications are also included.

Year	Standard	Title
2001	802.16-2001 [382]	IEEE Standard for Local and Metropolitan Area Networks - Part 16: Air Interface for Fixed Broadband Wireless Access Systems
2002	802.16c-2002 [383]	IEEE Standard for Local and Metropolitan Area Networks - Part 16: Air Interface for Fixed Broadband Wireless Access Systems - Amendment 1: Detailed System Profiles for 10-66 GHz
2003	802.16a-2003 [384]	IEEE Standard for Local and Metropolitan Area Networks - Part 16: Air Interface for Fixed Broadband Wireless Access Systems - Amendment 2: Medium Access Control Modifications and Additional Physical Layer Specifications for 2-11 GHz
2004	802.16d-2004 [56]	IEEE Standard for Local and Metropolitan Area Networks - Part 16: Air Interface for Fixed Broadband Wireless Access Systems
2005	802.16e-2005 [385]	IEEE Standard for Local and Metropolitan Area Networks - Part 16: Air Interface for Fixed and Mobile Broadband Wireless Access Systems - Amendment 2: Physical and Medium Access Control Layers for Combined Fixed and Mobile Operation in Licensed Bands and Corrigendum 1
	802.16f-2005 [386]	IEEE Standard for Local and Metropolitan Area Networks - Part 16: Air Interface for Fixed Broadband Wireless Access Systems - Amendment 1: Management Information Base
2007	802.16k-2007 [387]	IEEE Standard for Local and Metropolitan Area Networks Media Access Control (MAC) Bridges - Amendment 5: Bridging of IEEE 802.16
	802.16g-2007 [388]	IEEE Standard for Local and Metropolitan Area Networks - Part 16: Air Interface for Fixed and Mobile Broadband Wireless Access Systems - Amendment 3: Management Plane Procedure and Services
2008	P802.16h [389]	Draft IEEE Standard for Local and Metropolitan Area Networks - Part 16: Air Interface for Fixed and Mobile Broadband Wireless Access Systems: Improved Coexistence Mechanisms for License-Exempt Operation
	P802.16j [390]	Draft IEEE Standard for Local and Metropolitan Area Networks - Part 16: Air Interface for Fixed and Mobile Broadband Wireless Access Systems Multihop Relay Specification

Table 2.6: The family of the IEEE 802.16 Standards.

2.3.1.2.1 802.16d-2004 - Fixed WiMAX

The IEEE 802.16 standards developed during the early stages tend to describe different parts of the technology. In order to ease future developments, it was decided to merge the previous individual versions into a single one, resulting in IEEE 802.16d-2004 [56], which is also frequently referred to as IEEE 802.16-2004. For operational frequencies spanning from 10-66 GHz, the PHY is based on SC modulation. For NLOS propagation conditions at frequencies below 11 GHz, the design alternatives of SC, OFDM, or OFDMA modulation can be used [56].

Early WiMAX solutions were based on the Wireless Metropolitan Area Network (WirelessMAN) OFDM PHY of 802.16-2004. Therefore, 802.16-2004 is also known as "fixed WiMAX", due to the fact that it does not support mobility.

2.3.1.2.2 802.16e-2005 - Mobile WiMAX

In order to provide mobility support, the IEEE 802.16 working group continued their developments. In December 2005, an amendment of IEEE 802.16-2004 was approved, which is known as IEEE 802.16e-2005 [385] or 802.16e in brief. In addition to numerous corrections to 802.16-2004 regarding stationary operations, a key enhancement of this standard over its ancestors is that it supports subscriber stations moving at vehicular speeds and thereby specifies a system for combined fixed and mobile BWA. The functions required to support higher-layer handover between base stations or sectors are also specified. Its operation is limited to licensed bands suitable for mobility at carrier frequencies below 6 GHz. Furthermore, the previously developed stationary IEEE 802.16 subscriber capabilities are not compromised [385].

Note that 802.16e itself is not a stand-alone document. More specifically, it only includes the differences with respect to the 802.16-2004 document. Although for the sake of simplicity, 802.16e has been widely referred to as if it were a stand-alone standard, it is more natural to combine it with 802.16-2004 into a single consolidated version. This work is being conducted by the IEEE 802.16's Maintenance Task Group under the IEEE P802.16Rev2 Project. This will result in the second revision of 802.16 since the release of 802.16-2001 and 802.16-2004. It will consolidate 802.16-2004, 802.16e as well as other 802.16 standards, such as 802.16f/g [386, 388]. The up-to-date working document for this project is P802.16Rev2/D5 [392], which was released in June 2008.

The 802.16e standard formed the basis of WiMAX for nomadic and mobile applications. It is often referred to as "mobile WiMAX", as compared to "fixed WiMAX", which is synonymous with IEEE 802.16-2004. Since it evolved from 802.16-2004, 802.16e naturally embraces the different options specified in its predecessor, which were designed to suit a variety of applications and deployment scenarios. In Table 2.7, a brief summary of these options is provided.

PHY Profile	Air Interface	Description
WirelessMAN-SC	SC	Operation in the 10-66 GHz frequency band.
WirelessMAN-SCa	SC	For NLOS operation in frequency bands below 11 GHz. For licensed bands, channel bandwidths are limited to the regulatory provisioned bandwidth divided by any power of 2 no less than 1.25 MHz.
WirelessMAN-OFDM	OFDM	For NLOS operation in frequency bands below 11 GHz.
WirelessMAN-OFDMA	OFDMA	For NLOS operation in frequency bands below 11 GHz. For licensed bands, channel bandwidths are limited to the regulatory provisioned bandwidth divided by any power of 2 no less than 1.0 MHz.
WirelessHUMAN	OFDM	Wireless High-speed Unlicensed MAN (WirelessHUMAN) is similar to WirelessMAN-OFDM, but mandates dynamic frequency selection for mainly the Unlicensed National Information Infrastructure (UNII) band [393].

Table 2.7: PHY profiles in IEEE 802.16-2004 and IEEE 802.16e-2005.

Apart from the similarities, there are also numerous differences. Some of the significant changes of 802.16e in comparison to 802.16-2004 are [385, 394]:

- The terminology of Mobile Stations (MS) is introduced. An MS is also a Subscriber Station (SS) as referred to in the standard.
- MAC layer HandOver (HO) procedures are defined, where an MS migrates from the area serviced by one Base Station (BS) to another. In 802.16e, there are two HO variants:
  1. Break-before-make HO ("hard" HO): A HO, where communications with the target BS only commence after relinquishing the link with the previous serving BS.
  2. Make-before-break HO ("soft" HO): A HO, where communications with the target BS start before disconnection of the service with the previous serving BS. Two types of soft HO are defined, namely the Fast BS Switching (FBSS), where the MS may rapidly switch from one BS to another, and the Macro Diversity HandOver (MDHO), where an MS establishes links with more than one BS.

  In order to facilitate power-efficient MS operations and more efficient HOs, two new power-saving modes, namely the sleep mode and the idle mode are introduced as the complement to the active mode already defined in 802.16-2004.
- The concept of Scalable OFDMA (S-OFDMA) is introduced, as part of the significant revision of the original WirelessMAN-OFDMA profile in 802.16-2004. The S-OFDMA architecture supports a wide range of bandwidths, ranging from 1.25 MHz to 20 MHz with a fixed sub-carrier spacing of 10.94 KHz for both fixed and mobile operations. This has the great benefit of flexibly addressing the need for various spectrum allocation schemes, potentially supporting global requirements.
- In addition to the four scheduling services supported in 802.16-2004, which are the Unsolicited Grant Service (UGS), real-time Polling Service (rtPS), non-real-time Polling Service (nrtPS), and Best Effort (BE), a new class referred to as the extended real-time Polling Service (ertPS) is included in 802.16e. The ertPS scheduling mechanism exploits the advantages of both UGS and rtPS. It is capable of avoiding the latency of a bandwidth request, while catering for dynamic resource allocations.
- New Multicast and Broadcast Services (MBSs) are introduced. Two types of access to MBSs may be supported, namely single-BS access and multi-BS access. Single-BS access is implemented for transmission over multicast and broadcast transport connections within the coverage area of one BS, while multi-BS access is implemented by transmitting data from service flows with the aid of multiple BSs.
- The security sublayer is redefined in order to remove some security 'holes' identified in 802.16-2004, for example the non-existence of BS authentication, and to meet dedicated security requirements for mobile services, which are typically more challenging than those designed for stationary scenarios.
- Enhanced PHY technologies. The MIMO and Adaptive Antenna System (AAS) techniques of 802.16-2004 are substantially enhanced with the aid of more detailed implementation guidelines. Low-Density Parity Check (LDPC) codes are included as a further optional channel coding scheme.

2.3.1.2.3 Other 802.16 Standards

Since the publication of 802.16-2004, there have been a few amendments. Besides 802.16e, recently some further amendments have been completed, while others are still progressing at the time of writing, as summarised in Table 2.6. The objective of these amendments of the original 802.16-2004 is to improve specific system-related aspects, such as adding a more efficient handover functionality, or to include other aspects, such as system management information and procedures.

In December 2005, the IEEE 802.16f-2005 standard [386] was approved, which is the first amendment of 802.16-2004. This specification defines a Management Information Base (MIB) for the MAC and PHY layers, together with relevant management procedures, with the aim of providing high-speed unlicensed MAN access.

Other completed 802.16 amendments include the IEEE 802.16k-2007 [387] and IEEE 802.16g-2007 [388], which were approved in August and December 2007, respectively. The former amended the IEEE Standard 802.1D [395] to support bridging of the IEEE 802.16 MAC layer. The latter updates and expands 802.16 by defining further management procedures as enhancements to the air interface specified by IEEE 802.16 for fixed and mobile broadband wireless systems. It specifies the related management functions, interfaces and protocol procedures.

The draft amendments which are still pending include the IEEE P802.16h [389] and P802.16j [390] projects. The latest P802.16h working document Draft 7 was released in June 2008. It specifies improved mechanisms, such as policies and medium access control enhancements, to enable the coexistence of license-exempt systems based on 802.16 and to facilitate the coexistence of these systems with primary users. Furthermore, it aims to improve the coexistence of 802.16 systems in non-exclusively assigned bands. Some of the procedures defined could be applied in other licensing cases, which require improved inter-system coexistence [389].

The P802.16j project, on the other hand, specifies OFDMA PHY and MAC enhancements of 802.16 for licensed bands in order to enable the operation of relay stations. It aims at improving the coverage, throughput and system capacity of 802.16 networks by specifying 802.16 multihop relay capabilities and functionalities of interoperable relay stations and base stations [390]. The subscriber station specifications are not changed. The most recent working document of P802.16j is Draft 5, which was released in May 2008.

2.3.1.3 WiMAX Forum

In 802.16-2004 and 802.16e, SC, OFDM and OFDMA techniques are used, as summarised in Table 2.7. Accordingly, there are multiple choices for the MAC layer structure, duplexing combinations, etc. Although the variety of design options is sufficiently flexible for diverse application and deployment scenarios, it is not feasible to have a single system that is compatible with all these specifications. This inevitably results in an inter-operability problem. To overcome this problem, the standard should have a limited scope, where the number of design and implementation options should be reduced.

Against this background, the WiMAX Forum was established in June 2001. It is an industry-led, not-for-profit organization of more than 520 companies, including over 200 operators [396]. Similar to the Wi-Fi Alliance, which promotes the Wi-Fi standard as well as its product certification, the WiMAX Forum strives to accelerate the global adoption of the WiMAX technology for the provision of broadband wireless services. However, Wi-FI and WiMAX are not direct competitors for wireless broadband subscribers or applications. Although both of them aim for providing wireless connectivity and Internet access, they were designed for different application scenarios and thus become more complementary than competitive. Wi-Fi covers a limited LAN area such as a home or an office, while WiMAX is designed to serve a much larger MAN area with a range of kilometers. Wi-Fi uses unlicensed spectra, in contrast to WiMAX, which typically uses licensed spectra. Furthermore, they have different QoS maintenance mechanisms.

The WiMAX Forum works closely with service providers, regulators, manufacturers, etc. to ensure that WiMAX Forum Certified products are fully interoperable and capable of supporting both fixed and mobile broadband services. Its goal is to certify and promote broadband wireless products based upon the harmonized IEEE 802.16 and European Telecommunications Standards Institute (ETSI) HiperMAN standard [396]. The ETSI HiperMAN [397] is commonly considered as the European equivalent of IEEE 802.16 (or WiMAX), addressing spectrum access in spectral band ranges under 11 GHz. The WiMAX Forum has been using 802.16-2004 and 802.16e to preselect appropriate options and parameter sets, in order to remove the inter-operability barrier and to reduce the associated implementational cost, while remaining compatible with the ETSI HiperMAN standard.

More specifically, this is achieved by defining a few system profiles and certification profiles. A system profile is a collection of specific PHY and MAC layer features, which are selected from the 802.16-2004 or 802.16e standards, respectively. Accordingly, this results in two categories: the fixed WiMAX profiles, which are built upon the WirelessMAN-OFDM PHY of 802.16-2004, and the mobile WiMAX profiles, which are based on the scalable WirelessMAN-OFDMA PHY of 802.16e. It is worth pointing out that the mandatory and optional status of a particular feature within a WiMAX system profile may be different from what it is in the original IEEE standard [379]. On the other hand, a WiMAX certification profile is a particular instantiation of a WiMAX system profile where the operating frequency, channel bandwidth and duplexing mode are also specified. WiMAX equipment are certified based on specific certification profiles for meeting inter-operability requirements [379]. If a device is WiMAX Forum Certified, it is both compliant with the 802.16 standard and with devices from other vendors, provided that they are also WiMAX Forum Certified. This will greatly reduce the cost for service providers, since they can flexibly ‘plug and play’ various certified WiMAX equipment, adapting to new business needs without changing their overall infrastructures.

2.3.1.4 WiMAX and WiBro

The Wireless Broadband (WiBro) system constitutes a wireless Internet technology developed by the Korean telecom industry. In February 2002, the Korean government allocated 100 MHz of spectrum in the 2.3 GHz band, and in late 2004, WiBro Phase 1 was standardized by the Telecommunications Technology Association (TTA) of Korea [391]. In June 2006, the first commercial WiBro service was launched in South Korea, by Korean Telecom and SK Telecom Co.

Ltd. The service was based on Intel's WiMax standard and mainly deployed in and around the Seoul area, the capital of South Korea. It is worth pointing out that WiBro is the synonymy of mobile WiMAX in Korea. It follows the same standard, namely IEEE 802.16e-2005, the same set of system and certification profiles, as well as the same certification processes as required by mobile WiMAX [398]. A brief comparison of WiBro and the 802.16d/e standards is provided in Figure 2.1.

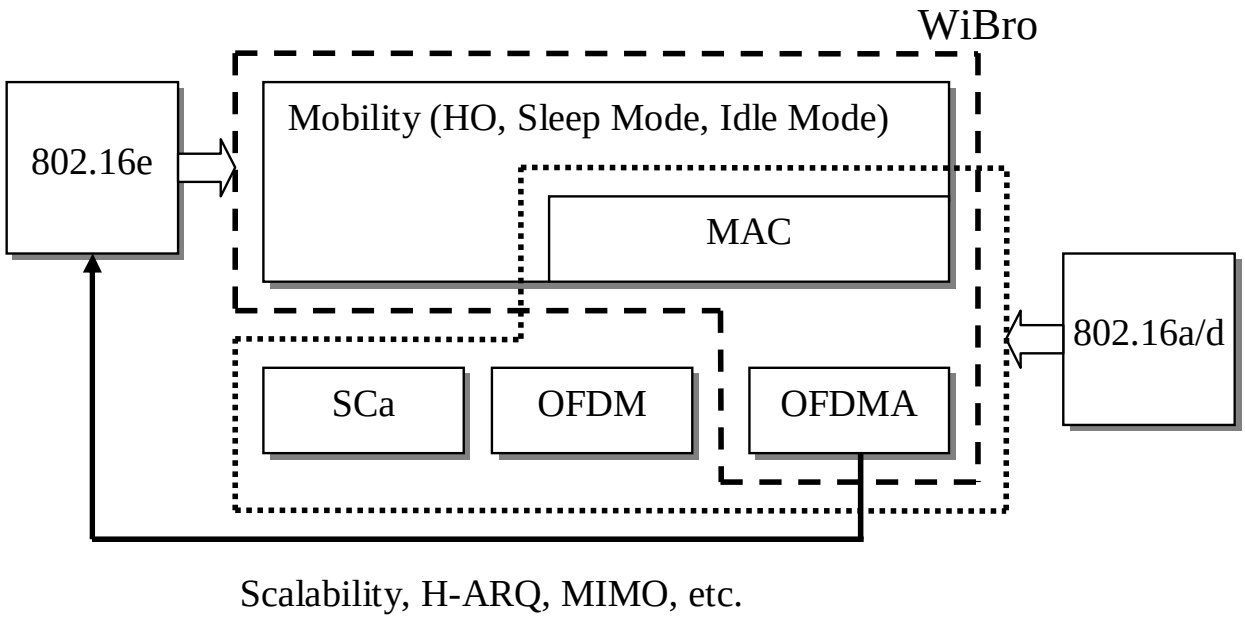

Figure 2.1: WiBro and IEEE 802.16d/e [399].

The features of WiBro, WLAN, and cellular systems are given in Table 2.8. It can be seen that WiBro combines the benefits of WLAN and cellular services, providing high data rates, while improving the coverage and mobility. In the future, it will evolve towards the Fourth-Generation (4G) networks, where the provision of even higher data rates and mobility are expected, as illustrated in Figure 2.2.

	WiBro	WLAN	Cellular
User data rate	about 1 Mbps	over 1 Mbps	about 100 kbps
Velocity	120 km/h	pedestrian	250 km/h
Equipment	laptop/PDA/cell phone	PC/laptop/PDA	PDA/cell phone
Cell radius	about 1km	about 100 m	1∼3 km

Table 2.8: Comparison of WiBro, WLAN and cellular systems.

2.3.2 Technical Aspects of WiMAX

The WiMAX technology has been based on the IEEE 802.16-2004 and IEEE 802.16e-2005 standards, referred to as the fixed WiMAX and mobile WiMAX, respectively. Mobile WiMAX is a broadband wireless solution that enables the convergence of mobile and fixed broadband networks with the aid of a common wide area broadband radio access technology and flexible network architecture [401].

The WiMAX technology is based on the S-OFDMA air interface designed for achieving high spectral efficiency and data rates. WiMAX users benefit from broadband connectivity without the need of LOS communications to the BS. A maximum data rate of up to 75 Mbps can be achieved with sufficient bandwidth, simultaneously supporting hundreds of residential and business areas by a single BS [380].

In the following sections, the technical aspects of WiMAX during its previous and ongoing stages of evolution are summarised.

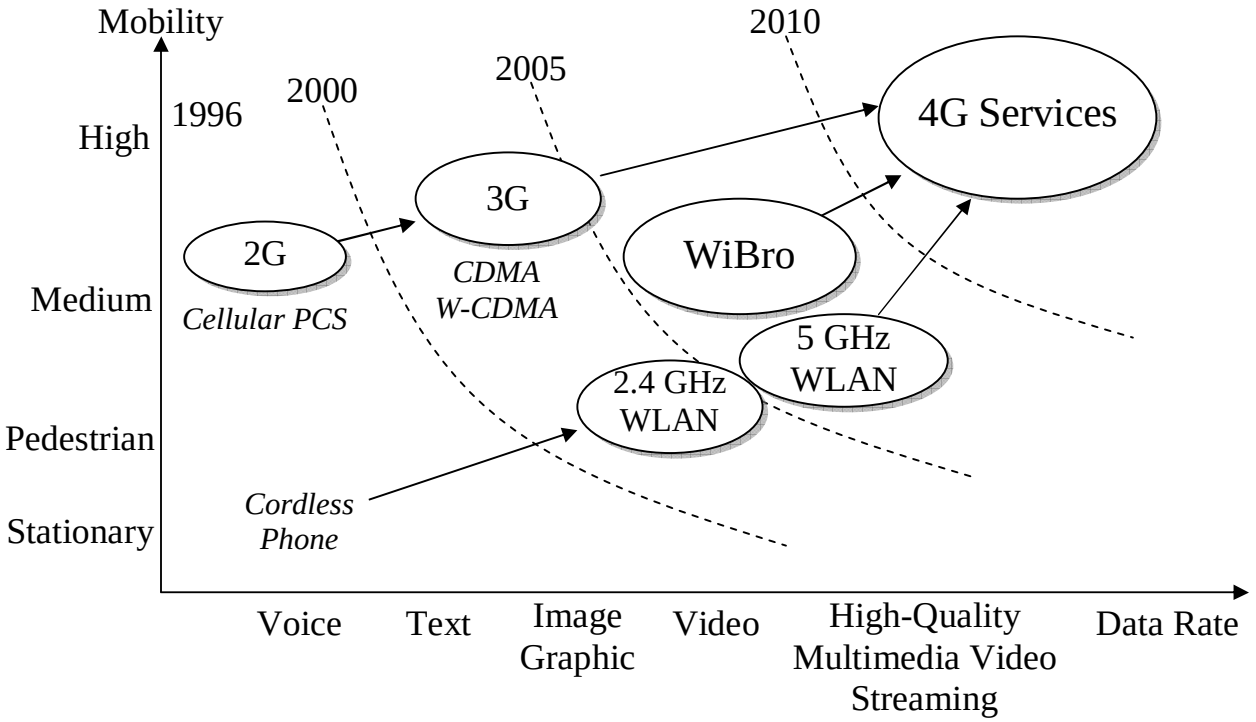

Figure 2.2: WiBro service evolvement [400].

2.3.2.1 WiMAX-I: 802.16-2004 and 802.16e-2005

2.3.2.1.1 OFDMA System Configuration

The concept of scalability was introduced in the IEEE 802.16 WirelessMAN-OFDMA [385] mode by the 802.16 Task Group e (TGe). The S-OFDMA architecture supports a wide range of bandwidth, which spans from 1.25 to 20 MHz combined with fixed subcarrier spacing for both fixed and portable/mobile uses, in order to flexibly address the need for various spectrum allocation and application requirements.

The scalability is achieved by adjusting the Fast Fourier Transform (FFT) size for various channel bandwidths. In addition to this, 802.16e supports Adaptive Modulation and Coding (AMC) subchannels, Hybrid Automatic Repeat Request (HARQ), efficient uplink subchannelisation, MIMO-aided transmit/receive diversity, etc [402]. Table 2.9 summarises the key parameters of 802.16e S-OFDMA [385].

Parameters	Values			
System Channel Bandwidth (MHz)	5	10	8.75	7
Sampling Frequency (F_s in MHz)	5.6	11.2	10	8
FFT Size (N_{fft})	512	1024	1024	1024
Number of Sub-Channels	8	16	16	16
Subcarrier Frequency Spacing (Δf) (KHz)	10.94		9.77	7.81
Useful Symbol Time ($T_b = 1/\Delta f$) (μs)	91.4		102.4	128
Guard Time ($T_g = T_b/8$) (μs)	11.4		12.8	16
OFDMA Symbol Duration ($T_s = T_b + T_g$) (μs)	102.9		115.2	144
Frame Duration (ms)	5		5	5
Number of OFDMA Symbols per Frame	48		43	34

Table 2.9: WiMAX Release-1 parameters.

2.3.2.1.2 Frame Structure

OFDMA is used for both DL and UL transmissions in 802.16e. The OFDMA PHY mode is based on one of the FFT sizes: 2048 (backward compatible to 802.16-2004 [56]), 1024, 512, and 128. This facilitates the support of the various channel bandwidths. The MS may implement a scanning and search mechanism to detect the DL signal, when performing initial network entry, and this may include the detection of the dynamically configured FFT size and the channel bandwidth employed by the BS.

In licensed bands, the duplexing method shall be either FDD or TDD. FDD MSs may be half-duplex FDD (H-FDD). In license-exempt bands, the duplexing method shall be TDD. Figure 2.3 shows an example of an OFDMA frame (with only mandatory zone) in TDD mode. The OFDMA frame may include multiple zones, such as Partial Usage of Subchannels (PUSC), Full Usage of Subchannels (FUSC), PUSC with all subchannels, optional FUSC, AMC, etc. The transition between zones is indicated in the DL-Map by the standardised parameter STC_DL_Zone Information Element (IE) or AAS_DL_IE [385]. No DL-MAP or UL-MAP allocations can span over multiple zones. Figure 2.4 depicts an OFDMA frame with multiple zones.

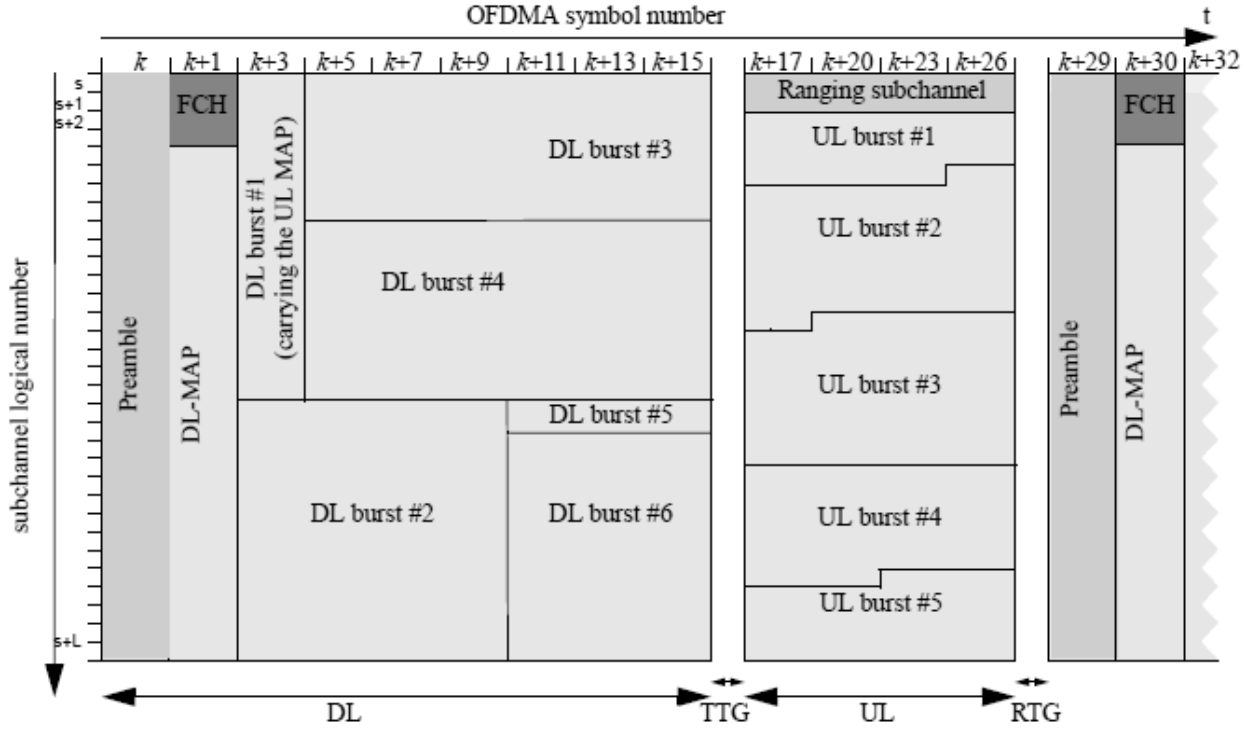

Figure 2.3: Example of a TDD OFDMA frame (with only mandatory zone) [385]. FCH: Feedback Channel; TTG: Transmit Transition Gap; RTG: Receive Transition Gap.

2.3.2.1.3 Subcarrier Mapping

For the OFDMA profile of 802.16e, we have $F_s = floor(n \cdot BW/8000) \cdot 8000$ (Hz), where F_s is the sampling frequency and n is the sampling factor, which is dependent on the bandwidth BW. After removing the frequency-domain guard tones or virtual subcarriers from N_{fft}, which is the FFT size, one obtains the set of "used" subcarriers N_{used}. These used subcarriers are allocated to pilot subcarriers and data subcarriers for both UL and DL.

However, there is a difference between the different possible zones. For the DL FUSC and PUSC, the pilot tones are allocated first, followed by the mapping of data subcarriers to subchannels (i.e. subbands) exclusively allocated for data. For PUSC in the UL, the set of used subcarriers is first partitioned into subchannels and then the pilot subcarriers are allocated from within each subchannel. Thus, in FUSC, there is one set of common pilot subcarriers for the entire frequency band, while in PUSC of the DL, there is one set of common pilot subcarriers in each major group, which is constituted by a few subchannels. By contrast, in PUSC of the UL, each subchannel contains its own set of pilot subcarriers. After mapping all pilots to the associated subchannels, the remaining used subcarriers will be grouped into data subchannels. For the different zones mentioned above, however, the corresponding subcarrier allocation

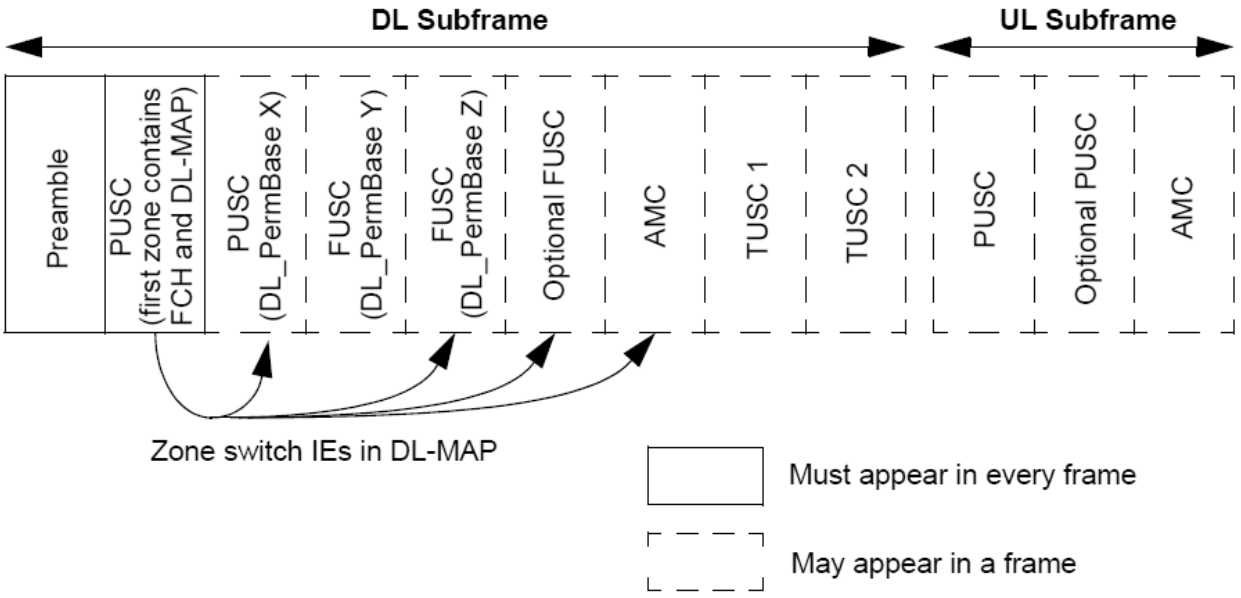

Figure 2.4: Example of a multi-zone OFDMA frame [385]. TUSC: Tile Usage of Subchannels.

or permutation rules are different, although a sufficient level of frequency and/or time diversity should generally be maintained.

2.3.2.1.4 Channel Coding

The coding method used as the mandatory scheme in 802.16e is based on tail-biting Convolutional Coding (CC). Optional coding schemes include the Block Turbo Coding (BTC), Convolutional Turbo Codes (CTC), zero-tailed CC and LDPC codes, which are not included in the earlier 802.16-2004 standard. The encoding block size depends on the number of subchannels allocated and on the modulation scheme specified for the current transmission. For example, the LDPC code specification of 802.16e is summarized in Table 2.10, where n is the codeword length, k is the information block length, and the z factor is the expansion factor which is equal to $n/24$ for a given value of n. Note that due to the associated subchannelization constraints, the combination of coding parameters and modulation schemes is not arbitrary.

2.3.2.1.5 MIMO Support

The Adaptive Antenna System (AAS) constitutes an integral part of 802.16e, which is included in order to attain a significant system capacity improvement. In 802.16e, the AAS may encompass different MIMO techniques, such as Space-Time Block Coding (STBC), beamforming and Spatial Multiplexing (SM). The STBC adopted is the well-known Alamouti code [403]. For the Open-Loop (OL) AAS, the multiple antennas can be used for STBC, SM or for their combinations. When the Closed-Loop (CL) AAS is employed, either because we can exploit the channel's reciprocity in the TDD mode, or because the system has an explicit receiver feedback in the FDD mode, the multiple antennas can be used either for beamforming or for CL MIMO by exploiting transmit antenna precoding techniques.

The general framework of CL MIMO in 802.16e is provided in Figure 2.5. It is constituted by an OL space-time encoding unit and a MIMO precoding unit. The linear precoding matrix spreads the various parallel streams across the various antennas with the aid of appropriate weighting factors. The precoding matrix is then adapted on a regular basis according to the feedback information gleaned from the receiver.

2.3.2.1.6 Other Aspects

In 802.16e, a preamble is used for initial frame timing and frequency synchronisation. Recall that Figure 2.3 shows the OFDMA frame structure in the TDD mode, where the first part of each frame is dedicated to the preamble.

n (bit)	n (byte)	z factor	k (byte)				Number of slots		
			1/2	2/3	3/4	5/6	QPSK	16QAM	64QAM
576	72	24	36	48	54	60	6	3	2
672	84	28	42	56	63	70	7	-	-
768	96	32	48	64	72	80	8	4	-
864	108	36	54	72	81	90	9	-	3
960	120	40	60	80	90	100	10	5	-
1056	132	44	66	88	99	110	11	-	-
1152	144	48	72	96	108	120	12	6	4
1248	156	52	78	104	117	130	13	-	-
1344	168	56	84	112	126	140	14	7	-
1440	180	60	90	120	135	150	15	-	5
1536	192	64	96	128	144	160	16	8	-
1632	204	68	102	136	153	170	17	-	-
1728	216	72	108	144	162	180	18	9	6
1824	228	76	114	152	171	190	19	-	-
1920	240	80	120	160	180	200	20	10	-
2016	252	84	126	168	189	210	21	-	7
2112	264	88	132	176	198	220	22	11	-
2208	276	92	138	184	207	230	23	-	-
2304	288	96	144	192	216	240	24	12	8

Table 2.10: LDPC block sizes and code rates [56].

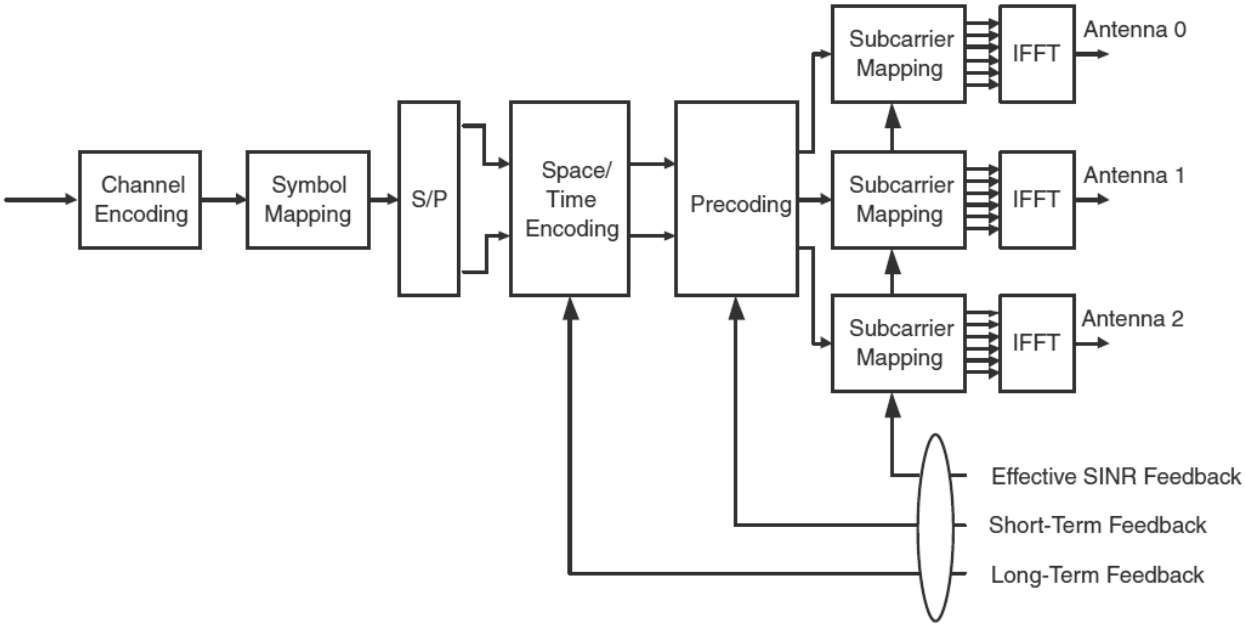

Figure 2.5: The 802.16e-2005 CL MIMO architecture [379].

Synchronisation is activated during the so-called ranging process, where the BS acquires the signals of new subscribers and adjusts the timing of the existing subscribers through the feedback channel. Synchronization is typically achieved by correlating the received signal against known preamble sequences, taking advantage of the deliberately introduced periodicity of the signal. The results of the correlation evaluation are then passed through a detector to determine, whether a legitimate symbol was sent and, if so, to adjust its exact timing.

The development of efficient timing and frequency synchronization algorithms for 802.16e and WiMAX systems is the responsibility of each equipment manufacturer. Some general principles for timing and frequency synchronisation can be found in [379].

The 802.16e standard also specifies optional HARQ support, including the following modes:

- Incremental Redundancy (IR) for CTC;
- IR for CC;
- Chase combining for all coding schemes.

Chase combining and IR are also referred to as type-I and type-II HARQ, respectively. These modes can be specified by the normal map and the HARQ map [385].

Other PHY functionalities, such as control mechanisms, channel quality measurements, transmitter/receiver requirements, as well as the specification of the MAC and upper layers, are also detailed in the standard [385]. For the reader's convenience, we summarise the major PHY features of 802.16e in Table 2.11.

2.3.2.2 WiMAX-II: 802.16m

In the International Telecommunications Union - Radio Communications Sector (ITU-R) WP5D meeting held in Dubai during late June 2008, the technical system performance requirements for the IMT-Advanced radio interface [404] were finalised. All IMT-Advanced proposals will be assessed according to this requirement document. The ITU will then assess all technical submissions, review the assessments, select one or more candidate technologies, and develop as well as rectify standards. The evaluation guidelines are still under development and expected to be finalised in the ITU-R meeting scheduled in October 2008. The selection of IMT-Advanced candidate technologies is expected to be conducted during the first half of 2009, followed by the development of detailed specifications in 2009 or 2010. Vendors may start official implementation between 2010 and 2012, whilst a wide deployment may commence by 2015 [405].

In order to meet the anticipated high requirements of IMT-Advanced, in January 2007 the IEEE started the specification of a new version of the 802.16 standard, which aims at increasing the data transmission rates up to 1 Gbit/s and 100 Mbits/s for fixed and mobile communications, with improved broadcast, multicast and Voice over Internet Protocol (VoIP) performance, while maintaining backward compatibility with existing WiMAX systems. Under the IEEE 802.16 umbrella, the newly formed Task Group m (TGm) is chartered to develop an amendment of the IEEE Standard 802.16, specifying an "Air Interface for Fixed and Mobile Broadband Wireless Access Systems - Advanced Air Interface", which is referred to as the IEEE 802.16m standard. Also known as WiMAX-II, 802.16m is the only 4G approach evolving from an existing OFDMA technology, namely from 802.16e or WiMAX-I, and will be proposed as a 4G candidate for the ITU's IMT-Advanced systems.

2.3.2.2.1 System Requirements

The ultimate mission of the 802.16m project is to draft an 802.16-compatible standard, which will become a candidate for the IMT-Advanced evaluation process conducted by the ITU-R. To achieve this target, a number of high-level system requirements have been identified by TGm, which are summarized in the 802.16m System Requirement Document (SRD) [406] that was finalised in October 2007. However, these requirements will be subject to changes according to the IMT-Advanced requirements, which are expected to be completed in late 2008.

Some of the key 802.16m requirements are [406]:

- *Backward compatibility:* 802.16m shall provide continuing support and inter-operability for legacy WirelessMAN-OFDMA [385] equipments, including both MSs and BSs. More specifically, the legacy 802.16e equipment shall be able to co-exist with 802.16m equipment without any performance degradation. Additionally, 802.16m shall provide the ability to disable legacy support.

Functionality	Configuration/Parameters					
Air Interface	S-OFDMA					
Modulation	QPSK, 16QAM, 64QAM					
System Channel Bandwidth (MHz)	1.25	5	7	8.75	10	20
Sampling Frequency (F_s in MHz)	1.4	5.6	8	10	11.2	22.4
FFT size	128	512	1024	1024	1024	2048
Number of Subchannels	2	8	16	16	16	32
Subcarrier Spacing (Δf) (KHz)	10.94	10.94	7.81	9.77	10.94	10.94
Useful Symbol Time ($T_b = 1/\Delta f$) (μs)	91.4	91.4	128	102.4	91.4	91.4
Guard Time ($T_g = T_b/8$) (μs)	11.4	11.4	16	12.8	11.4	11.4
OFDMA Symbol Duration ($T_s = T_b + T_g$) (μs)	102.9	102.9	144	115.2	102.9	102.9
Number of OFDMA Symbols per Frame	48	48	34	43	48	48
Guard Time ($T_g = T_b/8$) (μs)	11.4	11.4	16	12.8	11.4	11.4
Frame Duration (ms)	5					
Duplexing	FDD, TDD					
Frame Structure	DL - FUSC/PUSC; UL - PUSC					
Channel Coding Rates	CC	1/2, 2/3, 3/4				
	BTC	1/2, 3/4				
	CTC	DL	QPSK (1/2, 3/4), 16QAM (1/2, 3/4), 64QAM (1/2, 2/3, 3/4, 5/6)			
		UL	QPSK (1/2, 3/4), 16QAM (1/2, 3/4)			
	LDPC	1/2, 2/3, 3/4, 5/6				
MIMO Schemes	AAS with STBC/SM/beamforming					
HARQ	IR for CC/CTC					
	Chase combining for all channel coding schemes					
Channel Quality Measurements	Mean and standard deviation of RSSI, SINR					
Spectral Efficiency (bps/Hz)	DL	Raw	2.88			
		Useful	1.15			
	UL	Raw	2.16			
		Useful	0.86			
Spectral Efficiency per Cell (bps/Hz/cell)	DL - 1.2; UL - 0.33					
Peak Data Rates (1×10 MHz 2:1) (Mbps)	DL - 40; UL - 8					
Average Cell Throughput (Mbps)	DL - 8; UL - 1					
VoIP Performance	16 concurrent users/cell/MHz (vehicular speeds up to 120 km/h)					
Maximum Cell Range	$\sim$3.3 Km / $\sim$20 Km^2					
Cell Edge Performance	Steep drop-off towards cell edge - improved with MIMO					
Latency	RTT $<$ 50 ms					

Table 2.11: Major PHY features of IEEE 802.16e-2005.

- *Services:* 802.16m should support legacy services more efficiently than the WirelessMAN-OFDMA Reference System [407] as well as facilitate the introduction of new/emerging types of services. Flexible services having different QoS levels should be supported, as required by next-generation mobile networks.
- *Operating frequencies and bandwidths:* 802.16m systems shall operate at RF frequencies less than 6 GHz and be deployable in licensed spectrum allocated to the mobile and fixed broadband services. It shall be able to operate in frequency bands identified for IMT-Advanced. An 802.16m-compliant system shall be capable of coexisting with other IMT-Advanced or IMT-2000 technologies. Scalable bandwidths ranging from 5 to 20 MHz shall be supported.
- *Support of advanced antenna techniques:* 802.16m shall support MIMO, beamforming operation or other advanced antenna techniques for single-user and multi-user scenarios. The minimum number of transmit and receive antennas for the BS and the MS are 2×2 and 1×2, respectively.
- *Minimum peak data rate:* The baseline DL and UL peak data rates are 8 and 2.8 bps/Hz, respectively. When more antennas are used, the rate requirements become 15 and 5.6 bps/Hz for the DL and UL, respectively.
- *Co-existence and co-deployment with other Radio Access Technologies (RATs):* 802.16m shall support interworking functionality, providing efficient handover and allowing co-deployment with other RATs, including IEEE 802.11 [371], 3GPP GSM/EDGE, UTRA/E-UTRA, and 3GPP2 CDMA2000.
- *Mobility and coverage:* 802.16m shall support vehicular speeds of up to 350 km/h and provide a cell coverage of up to even 100 km. For lower mobility and for areas closer to the cell centre, the system's performance should be optimised and degrade gracefully as a function of the vehicular speed and/or the distance from the cell centre.
- *MBS, Location Based Service (LBS), relaying and self-organisation support:* 802.16m shall support Enhanced Multicast and Broadcast Services (E-MBS) for IMT-Advanced multimedia multicast broadcast services in a spectrally efficient manner, provide mechanisms to enable multi-hop relays including those that may involve advanced multiple antenna techniques, and support self-organizing mechanisms including self-configuration and self-optimisation.

For more details on the various aspects of the 802.16m system requirements, we refer to Tables 2.12, 2.13, 2.14 and 2.15.

2.3.2.2.2 System Description

In January 2008, TGm started to develop the 802.16m System Description Document (SDD) [409], which aims to provide a detailed specification of the 802.16m system that meets the requirements set by 802.16m SRD [406]. Since the commencement of the SDD development, significant efforts have been made by the entire project group. A number of Rapporteur Groups (RG) are formed to focus on dedicated topics, for example the frame structure RG, the multiple access RG, etc. Although technical discussions are still ongoing, some high level descriptions of the 802.16m system are already in place.

The Network Reference Model (NRM) of the 802.16m system is shown in Figure 2.6. The NRM is a logical representation of the overall network architecture. It identifies functional entities and reference points used for ensuring that inter-operability is achieved between functional entities, such as the MS, Access Service Network (ASN) and Connectivity Service Network (CSN) [409]. The ASN is defined as a full set of network functions, including 802.16e/m Layer-1 (L1) and Layer-2 (L2) connectivity between an 802.16m BS and an 802.16e/m MS, transfer of Authentication, Authorization, and Accounting (AAA) messages to an 802.16e/m subscriber's Home Network Service Provider (H-NSP), network discovery and selection of the subscriber's preferred NSP, relay functionality for establishing Layer-3 (L3) connectivity with an 802.16e/m MS, RRM, ASN/CSN anchored mobility, paging, and so on [409].

In Figure 2.7, an illustration of the 802.16m MS's state transition process is provided [409]. When an MS is switched on, it will enter the initialization state, where the cell selection process is performed by scanning and then synchronizing to a BS's preamble, followed by acquiring the system configuration information through the Broadcast Channel (BCH). If this is successful, the MS invokes the network entry procedure, requesting for the entry to the selected BS, which results in a number of access state procedures. More specifically, the ranging process is activated first to attain UL synchronization, followed by a 'capability-negotiation' step with the BS. Then the authentication and authorization process will be invoked and then the MS will be registered by the BS through the allocation of an 802.16m specific ID. Upon successfully performing the access-state operations of Figure 2.7, the MS will enter the connected state, which consists of three modes, namely the sleep mode, the active mode and the scanning mode.

Requirement	Description
Backward compatibility	The legacy 802.16e equipment shall be able to co-exist with 802.16m equipment without performance degradation. 802.16m shall provide the ability to disable legacy support.
Complexity	802.16m should minimize complexity of the architecture and protocols and avoid excessive system complexity. Only the enhancements in those areas where the WirelessMAN-OFDMA Reference System [407] fails to meet the requirements should be provided.
Services	802.16m should support legacy services more efficiently than the WirelessMAN-OFDMA Reference System [407] and facilitate new/emerging services. Flexible services with different QoS levels should be supported.
Operating frequencies	802.16m systems shall operate in RF frequencies less than 6 GHz in licensed spectrum. It shall be able to operate in frequencies identified for IMT-Advanced. An 802.16m compliant system shall be capable of coexisting with other IMT-Advanced or IMT-2000 technologies.
Operating bandwidths	Scalable bandwidths from 5 to 20 MHz shall be supported.
Duplex schemes	Both TDD and FDD shall be supported, where the FDD mode shall support both full-duplex and half-duplex (H-FDD) MS operation.
Support of advanced antenna techniques	802.16m shall support MIMO, beamforming or other advanced antenna techniques for single-user and multi-user scenarios. The minimum number of transmit and receive antennas for BS and MS are 2×2 and 1×2, respectively.

Table 2.12: The major general requirements for IEEE 802.16m.

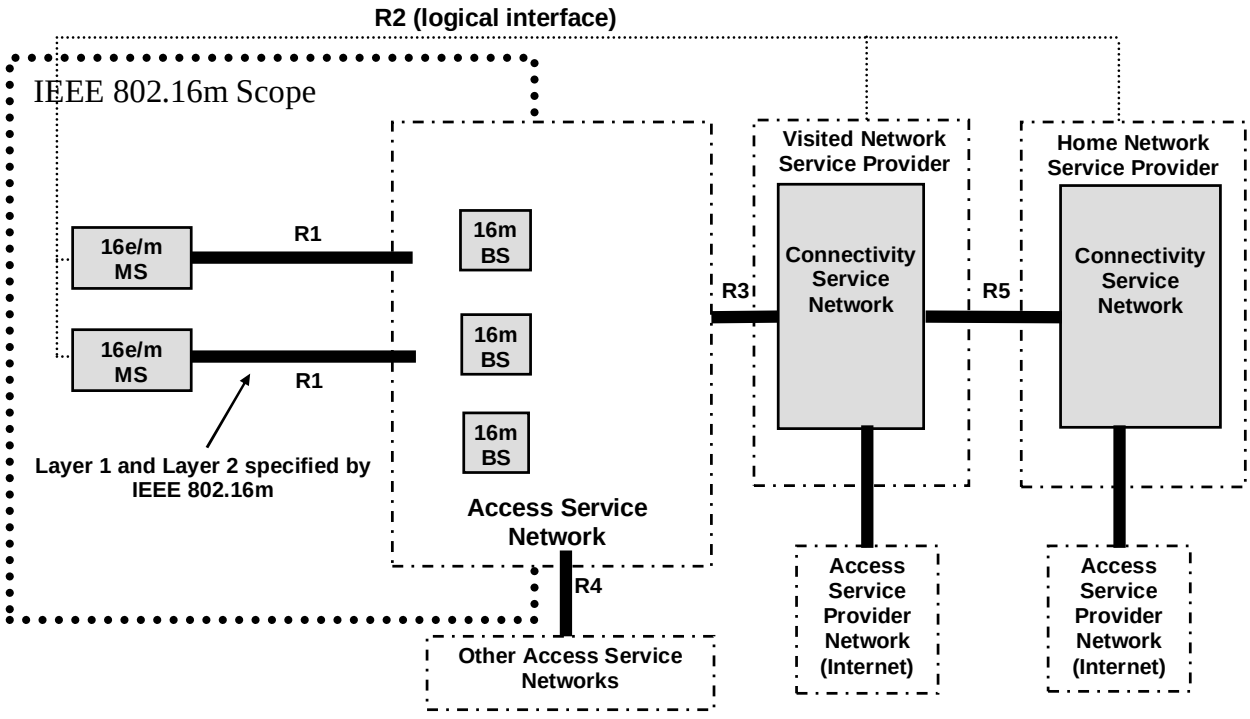

Figure 2.6: The NRM of IEEE 802.16m [409].

Requirement	Description	
Peak data rate (bps/Hz)	Baseline	DL (2×2): 8.0
		UL (1×2): 2.8
	Target	DL (4×4): 15.0
		UL (2×4): 5.6
Latency (ms)	Data latency	10
	State transition latency	100
	Handover interruption time	30 (intra-frequency mode)
		100 (inter-frequency mode)
QoS	802.16m shall support a range of QoS classes and new applications. When possible, the QoS level should be maintained during handover with other RATs.	
RRM	Advanced, efficient RRM shall be supported by 802.16m using appropriate measurement or reporting, interference management and flexible resource allocation mechanisms.	
Handover	Handover between 802.16m, legacy systems, and/or other RATs and IEEE 802.21 Media Independent Handover (MIH) Services [408] shall be supported.	
Broadcast	E-MBS using a dedicated carrier shall be supported. Switching between broadcast and unicast services shall be supported.	
Overhead	802.16m should reduce both user overhead and system overhead when compared to legacy systems without compromising the overall system performance.	
Power efficiency	802.16m shall provide support for enhanced power saving functionality for all services and applications.	
Coexistence with other RATs	802.16m shall support efficient handover to other RATs, including IEEE 802.11 [371], 3GPP GSM/EDGE, UTRA/E-UTRA, and 3GPP2 CDMA2000.	

Table 2.13: The major functional requirements for IEEE 802.16m.

Requirement	Description	
User/Sector throughputs	These should be two times as the WirelessMAN-OFDMA Reference System [407].	
Mobility	0-10 km/h	Optimised system performance
	10-120 km/h	Graceful performance degradation as a function of vehicular speed
	120-350 km/h	Connection should be maintained
Cell coverage	0-5 km	Optimized system performance
	5-30 km	Graceful degradation in system/edge spectral efficiency
	30-100 km	System should be functional (thermal noise limited scenario)
MBS/LBS support	Minimum performance requirements for E-MBS (spectral efficiency over 95% coverage areas) are 4 bps/Hz and 2 bps/Hz for an inter-site distance of 0.5 km and 1.5 km, respectively. Specific LBS requirements should also be met.	

Table 2.14: The major performance requirements for IEEE 802.16m.

Requirement	Description
Relaying	802.16m should provide mechanisms to enable multi-hop relays with and without advanced antenna techniques.
Synchronisation	802.16m shall support synchronisation of frame timing and frame counters across the entire deployed system, including all BSs and MSs regardless of carrier frequencies and operators.
Co-deployment with other networks	802.16m systems shall be able to be co-deployed in the adjacent licensed frequency bands such as CDMA2000 and 3GPP (GSM, UMTS, HSDPA/HSUPA, LTE), and in unlicensed bands such as 802.11 and 802.15.1 networks, or in the same frequency band on an adjacent carrier such as TD-SCDMA.
Self-organization support	802.16m should support self-configuration, enabling real plug-and-play installation of network nodes and cells, and support self-optimization, allowing automated or autonomous optimization of network performance with respect to service availability, QoS, network efficiency and throughput.

Table 2.15: The major operational requirements for IEEE 802.16m.

Furthermore, in order to reduce the power consumption, the MS may enter the idle state, which is constituted by two separate modes, namely the 'paging available' mode and the 'paging unavailable' mode. During the idle state, the MS may switch to the access state, if required [409].

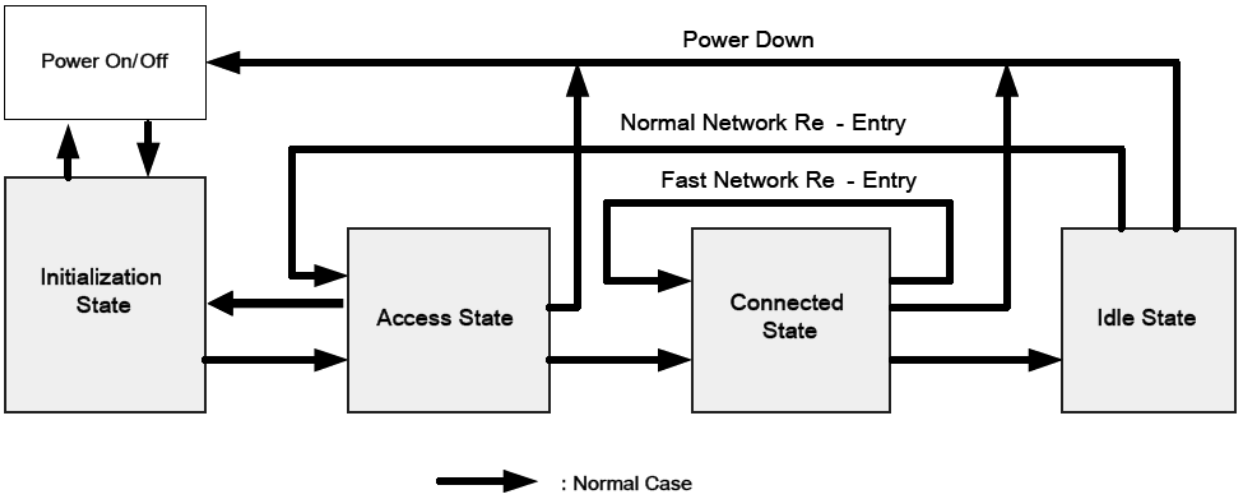

Figure 2.7: The IEEE 802.16m MS state transition diagram [409].

IEEE 802.16m supports both TDD and FDD modes, including H-FDD MS operation, in accordance with the 802.16m SRD [406]. OFDMA is adopted as the multiple access technique in both the DL and UL. Figure 2.8 shows the basic frame structure of 802.16m, where the terminology of superframe and subframe is introduced [409]. Each superframe is of 20 ms and is constituted by four equal-length radio frames of 5 ms each. Each 5 ms radio frame consists of eight subframes SF0, . . ., SF7, as seen in Figure 2.8. Two types of subframes are supported, depending on the length of the cyclic prefix. The so-called type-1 and type-2 subframes are formed by six and seven OFDMA symbols, respectively. The basic frame structure of Figure 2.8 is applied to both TDD and FDD modes, including the H-FDD MS operation. The number of DL/UL switching points in each TDD radio frame is either two or four. The transmission gaps between DL and UL (and vice versa) are required to allow the settling of transients following the switching of the transmitter and receiver circuitry [409].

In order to ensure backward compatibility with legacy 802.16 equipment, the concept of time zone is introduced in 802.16m, which is applied to both the TDD and FDD modes. The time zone is defined in terms of a non-zero integer number of consecutive subframes [409]. An example of TDD time zones is portrayed in Figure 2.9. More specifically,

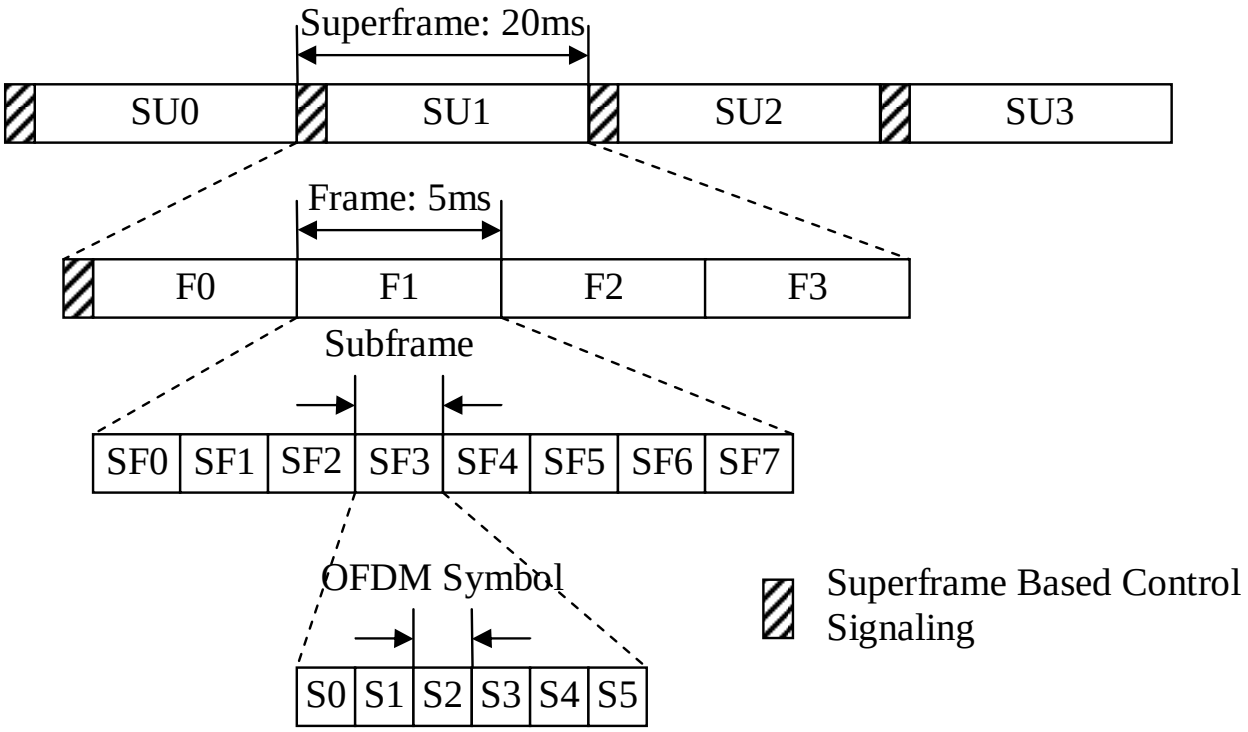

Figure 2.8: The IEEE 802.16m frame structure [409].

two zones are multiplexed in the time domain for the DL, one for 802.16m and the other for legacy systems. For UL transmissions, these will be multiplexed in both the time and frequency domains. Note that the legacy MS can only be scheduled in the legacy zones, whilst the 802.16m MS can be scheduled in both zones. If there is no legacy system in the network, the legacy zones will be replaced by the expanded 802.16m zone for maximising the system's efficiency [409].

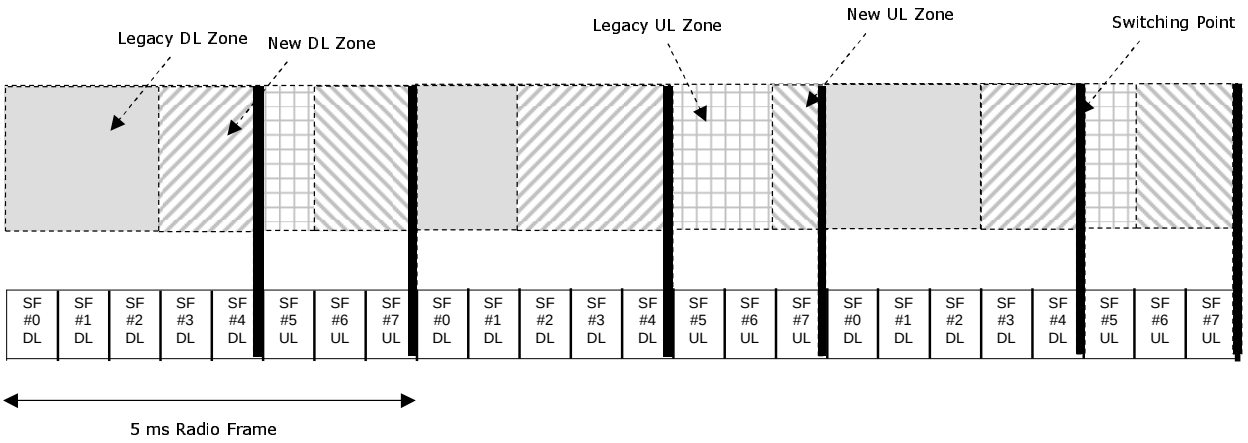

Figure 2.9: The time zones in the IEEE 802.16m TDD mode [409].

Other system specifications, such as MIMO transmission schemes, physical structure, control structure, the support of multi-hop relaying, etc. are still under intensive discussions within TGm. Further details are expected to be available during the first half of 2009.

2.3.3 The Future of WiMAX

In October 2007, ITU formally accepted IEEE 802.16e-2005 based Mobile WiMAX as the sixth standardised terrestrial radio interface. This specific implementation, known as "IMT-2000 OFDMA TDD WMAN", is the version of

IEEE 802.16 standard supported in a profile developed for certification purposes by the WiMAX Forum [410]. This will encourage its acceptance by regulatory authorities and operators for allocating cellular spectrum and for future WiMAX deployment.

New products and impressive technical deployments have been stimulating the penetration of WiMAX across the globe. Its rapid speed is driven by new equipment arriving from leading manufacturers and suppliers, as well as by an increasing number of WiMAX trials and deployments supported by telecom service providers. This list includes Alcatel-Lucent, Alvarion, AT&T, BT, Clearwire, Fujitsu, Intel, Korea Telecom, Motorola, Nokia, Nortel, Redline Communications, Samsung, Sequans, SR Telecom, Verizon, etc., who are actively paving the way for the WiMAX evolution. It is forecast that by 2010 the worldwide WiMAX market will be reaching $3.5 billion and account for 4 percent of all broadband usage [405].

At the end of 2007, there have been a total of 181 WiMAX operators globally. The WiMAX forum expects this number to rise to 538 by 2012. Among the total of 234 countries in the world, the number of those using WiMAX is anticipated to rise from 94 at the end of 2007 to 201 in 2012 [411]. It is also forecast that by 2012 there will be about 134 million WiMAX users world wide, with the main growth coming from the Asia Pacific and North America regions, as shown in Figure 2.10 [411].

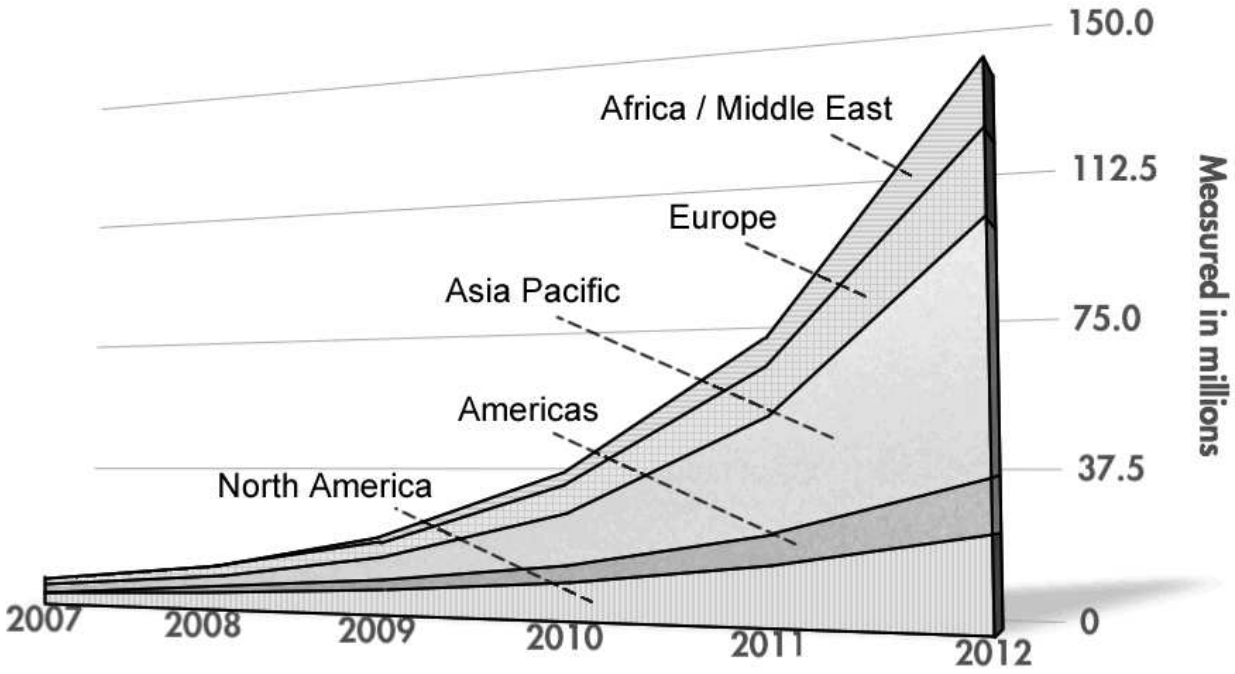

Figure 2.10: Forecast of WiMAX users by region 2007-2012 [411].

In June 2008, the WiMAX Forum announced the first WiMAX Forum Certified Mobile WiMAX products, including four base stations and six mobile terminals, provided by eight WiMAX Forum member companies, namely Airspan Networks, Alvarion, Beceem, Intel, Motorola, Samsung, Sequans, and ZyXEL [412]. The products are designed for the 2.5 GHz profile. The WiMAX Forum also revealed its roadmap for 3.5 and 2.3 GHz equipment certification, with plans for equipment in the 3.5 GHz band to achieve certification by the end of 2008 [412].

The latest official schedule for the IEEE 802.16m standardisation project was released in July 2008. According to the schedule, TGm will commence working on the detailed specification in November 2008 and will start the sponsor ballot in September 2009, with a target of completing the standard in March 2010. It aims to be in line with ITU's time line of call for IMT-Advanced proposals - a critical time for the further success of WiMAX in the future.

2.4 Chapter Summary

In this chapter, we have reviewed a range of major international standards that adopt OFDM. We first briefly considered the history, milestones and main contributions in the OFDM literature in Section 1.1. Then in Section 2.1 we reviewed the Wi-Fi standard family, followed by Section 2.2 where the 3GPP LTE cellular standard was highlighted. A more

detailed introduction of WiMAX was presented in Section 2.3. More specifically, we briefly reviewed the history of WiMAX in Section 2.3.1, spanning from the early IEEE 802.16 standards in Section 2.3.1.2 to their recent amendments in Sections 2.3.1.2.1, 2.3.1.2.2, and 2.3.1.2.3. Early WiMAX solutions were based on the WirelessMAN OFDM PHY of 802.16-2004, which is also known as "fixed WiMAX". By contrast, as the successor of 802.16-2004, the 802.16e standard incorporates mobility support and thus it is referred to as "mobile WiMAX". In Section 2.3.1.3, the historic background of the WiMAX Forum was summarized, where its mission and achievements were briefly reviewed. Furthermore, we provided a brief introduction of the Korean WiMAX standard WiBro in Section 2.3.1.4. Being the world's largest commercial mobile WiMAX deployment, the WiBro network is accelerating its evolution towards the 4G era.

In Section 2.3.2, we focused our attention on the technical aspects of WiMAX. More specifically, the major PHY specifications of WiMAX-I, which were based on 802.16-2004 and 802.16e, was provided in Section 2.3.2.1. These included the OFDMA system configuration, frame structure, subcarrier mapping, channel coding, MIMO support, etc. Moreover, in Section 2.3.2.2 the technical requirements and system description of the 802.16m draft standard was presented. It is expected that the 802.16m standard will be finalised in March 2010, although it is still in its infancy at the time of writing. Finally, a brief discussion of the progress and future of WiMAX was offered in Section 2.3.3.

Part I

Coherently Detected SDMA-OFDM Systems

Chapter 3

Channel Coding Assisted STBC-OFDM Systems

3.1 Introduction

Increasing market expectations for third-generation mobile radio systems show a great demand for a wider range of services spanning from voice to high-rate data services required for supporting mobile multimedia communications. This leads to higher technical specifications for existing and future communication systems, which have to support data rates as high as 144Kb/s in vehicular, 384Kb/s in outdoor-to-indoor and 2Mb/s in indoor and picocelluar environments [413].

The employment of multiple antennas constitutes an effective way of achieving an increased capacity. The classic approach is to use multiple receiver antennas and exploit Maximum Ratio Combining (MRC) of the received signals for the sake of improving the system's performance [414, 415]. However, the performance improvement of MRC is achieved at the cost of increasing the complexity of the Mobile Stations (MSs). Alternatively, MRC may be employed at the Base Stations (BSs), which support numerous MSs. While this scheme provides diversity gain for the BSs' receivers, the MSs cannot benefit from it.

Employing multiple transmitters, rather than receiver antennas at the BSs constitutes a further design option in this context. Since transmitter diversity techniques are proposed for employment at the BSs, it is possible to enhance the system's integrity by upgrading the BSs. Alamouti [403] introduced an attractive scheme, which uses two transmitters in conjunction with an arbitrary number of receivers for communications in non-dispersive Rayleigh fading channels. Tarokh *et al.* [416, 417] generalized Alamouti's scheme to an arbitrary number of transmitters. These schemes introduced Space-Time Block Codes (STBCs), which show remarkable encoding and decoding simplicity, while achieving a good performance.

3.2 Space-Time Block Codes

In this section we will present the basic principles of space-time block codes. Before providing more details, let us first consider a simple space-time block coded system communicating over uncorrelated Rayleigh fading channels, as shown in Figure 3.1.

3.2.1 Alamouti's G_2 Space-Time Block Code

The system contains two transmitter antennas and one receiver antenna. The philosophy of Alamouti's G_2 space-time block code is as follows.

In a conceptually simple approach we could argue that the achieveable throughput of the system may be doubled with the aid of the two transmitter antennas, if their signal could be separated by the receiver. This task may be viewed as analogous to multiuser detection, where the two signals would arrive at the BS's receiver from two geographically

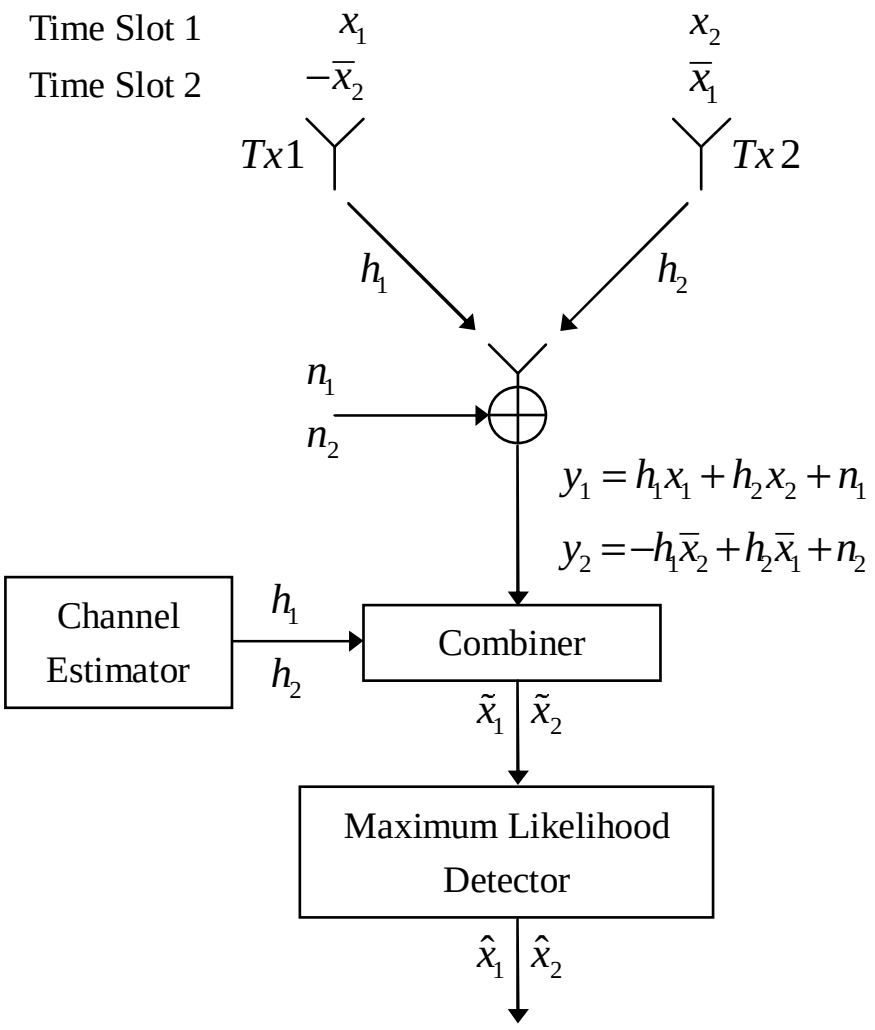

Figure 3.1: Schematic of Alamouti's G_2 space-time block code.

separated users. From a simple conceptual perspective the Bell Labs Layered Space-Time (BLAST) transmission scheme [106] adopts a similar principle for increasing the achievable throughput of multiple transmitter antenna based systems.

By contrast, Alamouti's approach is different, since the aim is to achieve a diversity gain rather than to increase the achievable throughput. This is achieved by extending the duration of time allocated to the transmission of a symbol by a factor of two and transmitting two independently faded and 'appropriately transformed' replicas of the symbol using each of the two antennas. The independence of the two channels may be ascertained by positioning the transmitter antennas Tx 1 and Tx 2 sufficiently far apart, for example at a distance of 10λ, where λ is the wavelength. Thus, during the first time slot, the information symbols x_1 and x_2 are transmitted by transmitter antenna Tx 1 and Tx 2, respectively, and again each of the two symbols is transmitted through an independently faded channel. For the sake of avoiding the channel-induced inter-symbol interference between the two time slots, both channels' path gains are assumed to be constituted by a single propagation path given by:

$$h_1 = |h_1|\, e^{j\alpha_1} \tag{3.1}$$

$$h_2 = |h_2|\, e^{j\alpha_2}, \tag{3.2}$$

where $|h_1|$, $|h_2|$ are the fading magnitudes and α_1, α_2 are the corresponding phase rotations. The complex fading envelopes are assumed to remain constant during the two consecutive time slots [359], which is expressed as:

$$h_1 = h_1(t = 1) = h_1(t = 2) \tag{3.3}$$

$$h_2 = h_2(t = 1) = h_2(t = 2). \tag{3.4}$$

Therefore we receive the composite signal y_1 constituted by the superposition of the two transmitted symbols through both channels:

$$y_1 = h_1 x_1 + h_2 x_2 + n_1, \tag{3.5}$$

where n_1 is a complex noise sample. As mentioned above, during the second time slot, a transformed version of the signals x_1 and x_2 is transmitted. Since the consecutive time slots are not faded independently, no diversity gain would be achieved, if we mapped these 'transformed' replicas of x_1 and x_2 to the same transmitter antenna as during the first time slot. Hence we now swap the assignment of the time slots to transmitter antennas, since this way their independent fading may be ascertained. More explicitly, during the second time slot, the negative version of the conjugate of x_2 and the conjugate of x_1 are sent by transmitter antenna Tx 1 and Tx 2, respectively. However, as mentioned above, the envelopes of each of the channels associated with the two transmitters are assumed to be the same as during the first time slot, hence we get the second transmitter's signal y_2 as:

$$y_2 = -h_1 \bar{x}_2 + h_2 \bar{x}_1 + n_2, \tag{3.6}$$

where n_2 is a complex noise sample. If the channels' characteristics are known to the receiver, i.e. we have a perfect channel estimator, the information symbols x_1 and x_2 can be readily separated in the combiner of Figure 3.1, yielding:

$$\begin{aligned} \tilde{x}_1 &= \bar{h}_1 y_1 + h_2 \bar{y}_2 \\ &= \bar{h}_1 h_1 x_1 + \bar{h}_1 h_2 x_2 + \bar{h}_1 n_1 - h_2 \bar{h}_1 x_2 + h_2 \bar{h}_2 x_1 + h_2 \bar{n}_2 \\ &= \left(|h_1|^2 + |h_2|^2 \right) x_1 + \bar{h}_1 n_1 + h_2 \bar{n}_2 \end{aligned} \tag{3.7}$$

$$\begin{aligned} \tilde{x}_2 &= \bar{h}_2 y_1 - h_1 \bar{y}_2 \\ &= \bar{h}_2 h_1 x_1 + \bar{h}_2 h_2 x_2 + \bar{h}_2 n_1 + h_1 \bar{h}_1 x_2 - h_1 \bar{h}_2 x_1 - h_1 \bar{n}_2 \\ &= \left(|h_1|^2 + |h_2|^2 \right) x_2 + \bar{h}_2 n_1 - h_1 \bar{n}_2, \end{aligned} \tag{3.8}$$

where $\tilde{x}_1$ and $\tilde{x}_2$ are the extracted noisy signals. Then $\tilde{x}_1$ and $\tilde{x}_2$ will be forwarded to the maximum likelihood detector of Figure 3.1, which determines the most likely transmitted symbols, namely $\hat{x}_1$ and $\hat{x}_2$ by simply outputting the specific legitimate transmitted symbol, which has the lowest Euclidean distance from the received channel-impaired symbol [359].

The equations above, which are based on the one-receiver scheme, can be generalized to multiple-receiver aided schemes, where the received signal y_t^j arriving at receiver j during time slot t is [359]:

$$y_t^j = \sum_{i=1}^{p} h_{i,j} x_t^i + n_t^j, \tag{3.9}$$

where p is the number of transmitters, $h_{i,j}$ is the complex-valued path gain between the transmitter i and receiver j, x_t^i is the space-time coded symbol transmitted by transmitter i during time slot t, and n_t^j is the noise sample at receiver j in time slot t. Accordingly, the extracted noisy signals become [359]:

$$\tilde{x}_1 = \sum_{j=1}^{q} \left[\left(\left| h_{1,j} \right|^2 + \left| h_{2,j} \right|^2 \right) x_1 + \bar{h}_{1,j} n_1^j - h_{2,j} \bar{n}_2^j \right] \tag{3.10}$$

$$\tilde{x}_2 = \sum_{j=1}^{q} \left[\left(\left| h_{1,j} \right|^2 + \left| h_{2,j} \right|^2 \right) x_2 + \bar{h}_{2,j} n_1^j - h_{1,j} \bar{n}_2^j \right]. \tag{3.11}$$

3.2.2 Encoding Algorithm

In last section, we have provided an example of a simple space-time block coded communication system. Let us now discuss space-time block codes in more depth.

3.2.2.1 Transmission Matrix

A generic space-time block code is defined by a $(n \times p)$-dimensional transmission matrix G, where the entries of the matrix G are linear combinations of the k input symbols $x_1, x_2, \cdots, x_k$ and their conjugates. Each symbol

x_i $(i = 1, \cdots, k)$ conveys b original information bits according to the relevant signal constellation that has $M = 2^b$ constellation points, and hence can be regarded as information symbols. Thus, $(k \times b)$ input bits are conveyed by each $(n \times p)$ block. The general form of the transmission matrix of space-time block codes is given by Equation (3.12):

$$G = \begin{bmatrix} g_{11} & g_{12} & \cdots & g_{1p} \\ g_{21} & g_{22} & \cdots & g_{2p} \\ \cdots & \cdots & \cdots & \cdots \\ g_{n1} & g_{n2} & \cdots & g_{np} \end{bmatrix}, \tag{3.12}$$

where the entries g_{ij} $(i = 1, \cdots, n;\ j = 1, \cdots, p)$ represent the linear combinations of the information symbols x_i $(i = 1, \cdots, k)$ and their conjugates. In the transmission matrix G, which can be viewed as a space-time encoding block, the number of rows (namely n) is equal to the number of time slots, while the number of columns (namely p) is equal to the number of transmitter antennas. For example, during time slot $i = 1$, the encoded symbols $g_{11}, g_{12}, \cdots, g_{1p}$ are transmitted simultaneously from transmitter antennas $Tx\ 1, Tx\ 2, \cdots, Tx\ p$, respectively.

References [403,416] have defined a range of space-time block codes. Different designs of the transmission matrix seen in Equation (3.12) will result in different encoding algorithms and code rates. Generally, the code rate is defined as:

$$R = k/n, \tag{3.13}$$

where k is the number of possible input information symbols, and n is the number of time slots.

3.2.2.2 Encoding Algorithm of the Space-Time Block Code G_2

From Section 3.2.1 and Equation (3.12) we can readily derive the G_2 transmission matrix in the form of:

$$G_2 = \begin{bmatrix} g_{11} & g_{12} \\ g_{21} & g_{22} \end{bmatrix} \tag{3.14}$$

or more specifically, as:

$$G_2 = \begin{bmatrix} x_1 & x_2 \\ -\bar{x}_2 & \bar{x}_1 \end{bmatrix}. \tag{3.15}$$

From Equation (3.15), it can be readily seen that there are $n = 2$ rows in the G_2 matrix associated with two time slots and $p = 2$ columns corresponding to two transmitter antennas, as we have already seen in the example of Figure 3.1. Since there are $k = 2$ input symbols, namely x_1 and x_2, the code rate of G_2 is $R = k/n = 1$.

3.2.2.3 Other Space-Time Block Codes

The G_2 space-time block code was first proposed by Alamouti [403] in 1998. This code has attracted much attention because of its appealing simplicity compared to the family of Space-Time Trellis Codes (STTCs) proposed in [418–421], although this simplicity was achieved at the cost of a performance loss. Later, Tarokh *et al.* [416] extended Alamouti's scheme to multiple transmitters, which led to other space-time block codes, such as the three-transmitter code G_3 and four-transmitter code G_4. The transmission matrix of G_3 [416] is defined as:

$$G_3 = \begin{bmatrix} x_1 & x_2 & x_3 \\ -x_2 & x_1 & -x_4 \\ -x_3 & x_4 & x_1 \\ -x_4 & -x_3 & x_2 \\ \bar{x}_1 & \bar{x}_2 & \bar{x}_3 \\ -\bar{x}_2 & \bar{x}_1 & -\bar{x}_4 \\ -\bar{x}_3 & \bar{x}_4 & \bar{x}_1 \\ -\bar{x}_4 & -\bar{x}_3 & \bar{x}_2 \end{bmatrix}, \tag{3.16}$$

and the transmission matrix of G_4 [416] is defined as:

$$G_4 = \begin{bmatrix} x_1 & x_2 & x_3 & x_4 \\ -x_2 & x_1 & -x_4 & x_3 \\ -x_3 & x_4 & x_1 & -x_2 \\ -x_4 & -x_3 & x_2 & x_1 \\ \bar{x}_1 & \bar{x}_2 & \bar{x}_3 & \bar{x}_4 \\ -\bar{x}_2 & \bar{x}_1 & -\bar{x}_4 & \bar{x}_3 \\ -\bar{x}_3 & \bar{x}_4 & \bar{x}_1 & -\bar{x}_2 \\ -\bar{x}_4 & -\bar{x}_3 & \bar{x}_2 & \bar{x}_1 \end{bmatrix}. \tag{3.17}$$

From Equations (3.16) and (3.17), we may notice that the code rates of G_3 and G_4 are reduced to a half, which degrades the bandwidth efficiency. However, the space-time block codes H_3 and H_4 of [416] mitigate this problem, since their code rate is $3/4$. The transmission matrices of H_3 and H_4 [416] are defined as follows:

$$H_3 = \begin{bmatrix} x_1 & x_2 & \frac{x_3}{\sqrt{2}} \\ -\bar{x}_2 & \bar{x}_1 & \frac{x_3}{\sqrt{2}} \\ \frac{\bar{x}_3}{\sqrt{2}} & \frac{\bar{x}_3}{\sqrt{2}} & \frac{(-x_1-\bar{x}_1+x_2-\bar{x}_2)}{2} \\ \frac{\bar{x}_3}{\sqrt{2}} & -\frac{\bar{x}_3}{\sqrt{2}} & \frac{(x_2+\bar{x}_2+x_1-\bar{x}_1)}{2} \end{bmatrix} \tag{3.18}$$

$$H_4 = \begin{bmatrix} x_1 & x_2 & \frac{x_3}{\sqrt{2}} & \frac{x_3}{\sqrt{2}} \\ -\bar{x}_2 & \bar{x}_1 & \frac{x_3}{\sqrt{2}} & -\frac{x_3}{\sqrt{2}} \\ \frac{\bar{x}_3}{\sqrt{2}} & \frac{\bar{x}_3}{\sqrt{2}} & \frac{(-x_1-\bar{x}_1+x_2-\bar{x}_2)}{2} & \frac{(-x_2-\bar{x}_2+x_1-\bar{x}_1)}{2} \\ \frac{\bar{x}_3}{\sqrt{2}} & -\frac{\bar{x}_3}{\sqrt{2}} & \frac{(x_2+\bar{x}_2+x_1-\bar{x}_1)}{2} & \frac{(-x_1-\bar{x}_1-x_2+\bar{x}_2)}{2} \end{bmatrix}. \tag{3.19}$$

In conclusion, the parameters of the space-time block codes mentioned above are summarized in Table 3.1.

Space-time block code	Code rate (R)	Number of transmitters (p)	Number of input symbols (k)	Number of time slots (n)
G_2	1	2	2	2
G_3	1/2	3	4	8
G_4	1/2	4	4	8
H_3	3/4	3	3	4
H_4	3/4	4	3	4

Table 3.1: Parameters of the space-time block codes.

3.2.3 Decoding Algorithm

In this section, two algorithms are briefly discussed, which are widely used for decoding space-time block codes. The maximum likelihood (ML) decoding algorithm generates hard-decision outputs, while the Maximum-A-Posteriori (MAP) decoding algorithm is capable of providing soft outputs, which readily lend themselves to channel coding for the sake of achieving further performance improvements.

3.2.3.1 Maximum Likelihood Decoding

Maximum Likelihood (ML) decoding of space-time block codes can be achieved using simple linear processing at the receiver, thus maintaining a low decoding complexity. As mentioned in Section 3.2.1, when the space-time coded symbols are transmitted over different channels and arrive at the receiver during time slot t $(t = 1, \cdots, n)$, we will have the received signal y_t^j expressed in Equation (3.9). With the proviso of having a perfect channel estimator, the receiver computes the decision metric

$$\sum_{t=1}^{n} \sum_{j=1}^{q} \left| y_t^j - \sum_{i=1}^{p} h_{i,j} x_t^i \right|^2 \tag{3.20}$$

over all indices $i = 1, \cdots, n$; $j = 1, \cdots, p$ and decides in favor of the specific entry that minimizes the sum.

Alamouti [403] first proposed a simple maximum likelihood decoding algorithm for the G_2 space-time block code. Tarokh *et al.* [417] extended it for the space-time block codes summarized in Table 3.1. The algorithm exploits the orthogonal structure of the space-time block codes for decoupling the signals transmitted from different antennas rather than requiring their joint detection. According to [417], low complexity signal processing may be invoked for separating the channel-impaired transmitted signal y_t^j into k decision metrics, each of which corresponding to

the channel-impaired version of a specific information symbol of the set x_i, $i = 1, \cdots, k$. For example, for the G_2 space-time block code, we will minimize the decision metric

$$\left| \left[\sum_{j=1}^{q} \left(y_1^j \bar{h}_{1,j} + \bar{y}_2^j h_{2,j} \right) \right] - x_1 \right|^2 + \left(\sum_{j=1}^{q} \sum_{i=1}^{2} |h_{i,j}|^2 - 1 \right) |x_1|^2 \tag{3.21}$$

for decoding x_1 and the decision metric

$$\left| \left[\sum_{j=1}^{q} \left(y_1^j \bar{h}_{2,j} - \bar{y}_2^j h_{1,j} \right) \right] - x_2 \right|^2 + \left(\sum_{j=1}^{q} \sum_{i=1}^{2} |h_{i,j}|^2 - 1 \right) |x_2|^2 \tag{3.22}$$

for decoding x_2. The relevant decision metrics for decoding other STBC codes can be found in [417].

3.2.3.2 Maximum-A-Posteriori Decoding

As seen in Equations (3.21) and (3.22), hard decisions would have to be made in order to generate the decoded outputs, which are the most likely transmitted information symbols. In other words, the usual ML detection is a hard-decoding method. However, in most practical systems various channel codes, such as Low Density Parity Check (LDPC) codes [422] or turbo codes [359, 423, 424], may have to be combined with STBC codes for the sake of further improving the system's performance. In this case, the space-time decoder must provide soft outputs, which can be efficiently utilized by the channel decoder.

Bauch [425] presented a simple symbol-by-symbol Maximum-A-Posteriori (MAP) algorithm for decoding space-time block codes. According to [425], the aposteriori probability of each information symbol x_i $(i = 1, \cdots, k)$ is:

$$\ln P\left(x_i \left| \mathrm{y}_1, \mathrm{y}_2, \cdots, \mathrm{y}_q \right.\right) = \text{const} + \ln P\left(\mathrm{y}_1, \mathrm{y}_2, \cdots, \mathrm{y}_q \left| x_i \right.\right) + \ln P\left(x_i\right), \tag{3.23}$$

where $\mathrm{y}_j = [\, y_1^j,\, y_2^j,\, \cdots,\, y_n^j \,]$ $(j = 1, \cdots, q)$ represents the received signal vector at receiver j during the period spanning from time slot 1 to time slot n. For example, for the space-time block code G_2 $(k = 2, n = 2)$ the aposteriori probabilities are:

$$\begin{aligned} &\ln P\left(x_1 \left| \mathrm{y}_1, \mathrm{y}_2, \cdots, \mathrm{y}_q \right.\right) = \text{const} + \\ &-\frac{1}{2\sigma^2} \left\{ \left| \left[\sum_{j=1}^{q} \left(y_1^j \bar{h}_{1,j} + \bar{y}_2^j h_{2,j} \right) \right] - x_1 \right|^2 + \left(\sum_{j=1}^{q} \sum_{i=1}^{2} |h_{i,j}|^2 - 1 \right) |x_1|^2 \right\} + \ln P\left(x_1\right) \end{aligned} \tag{3.24}$$

$$\begin{aligned} &\ln P\left(x_2 \left| \mathrm{y}_1, \mathrm{y}_2, \cdots, \mathrm{y}_q \right.\right) = \text{const} + \\ &-\frac{1}{2\sigma^2} \left\{ \left| \left[\sum_{j=1}^{q} \left(y_1^j \bar{h}_{2,j} - \bar{y}_2^j h_{1,j} \right) \right] - x_2 \right|^2 + \left(\sum_{j=1}^{q} \sum_{i=1}^{2} |h_{i,j}|^2 - 1 \right) |x_2|^2 \right\} + \ln P\left(x_2\right). \end{aligned} \tag{3.25}$$

We notice that Equations (3.24) and (3.25) are quite similar to Equations (3.21) and (3.22), respectively. In fact, it can be shown that Bauch's MAP algorithms can be extended for decoding other space-time block codes, such as the G_3, G_4, H_3 and H_4 and the corresponding algorithms also resemble the ML algorithms [359] discussed in Section 3.2.3.1. Given the aposteriori probabilities of the symbols, we can derive the corresponding aposteriori probabilities of the bits (i.e. the corresponding soft outputs) using the symbol-to-bit probability conversion of:

$$P\left(d_i = 0\right) = \sum_{j} P\left(x_j \left| \mathrm{y}_1, \mathrm{y}_2, \cdots, \mathrm{y}_q \right.\right), \quad \forall x_j = \left(d_1 \cdots d_i \cdots d_b\right), \quad d_i = 0, \tag{3.26}$$

$$P\left(d_i = 1\right) = \sum_{j} P\left(x_j \left| \mathrm{y}_1, \mathrm{y}_2, \cdots, \mathrm{y}_q \right.\right), \quad \forall x_j = \left(d_1 \cdots d_i \cdots d_b\right), \quad d_i = 1, \tag{3.27}$$

where $P(d_i = 0)$ or $P(d_i = 1)$ represents the probability of the i^{th} bit, namely d_i, of the b-bit symbol being zero and one, respectively. Let us consider the QPSK modulation scheme for example. The phasor constellation of QPSK is shown in Figure 3.2:

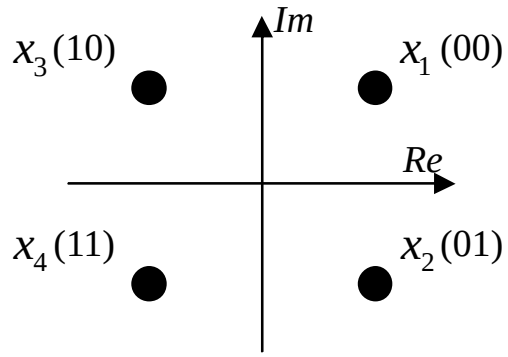

Figure 3.2: Gray-coded QPSK constellation.

As seen in Figure 3.2, each constellation point consists of two bits, hence the constellation points can be represented as:

$$x_j = (d_2 d_1), \quad j = \{1, \cdots, 4\}, \tag{3.28}$$

where $d_i = \{0, 1\}$. With the aid of Equations (3.26) and (3.27), we generate the aposteriori probabilities of each bit, taking into account that d_1 assumes a value of zero only in x_1 and x_3, while d_2 in x_1 and x_2, etc. yielding:

$$\begin{cases} P(d_1 = 0) = P\left(x_1 \left| \mathrm{y}_1, \mathrm{y}_2, \cdots, \mathrm{y}_q \right.\right) + P\left(x_3 \left| \mathrm{y}_1, \mathrm{y}_2, \cdots, \mathrm{y}_q \right.\right) \\ P(d_1 = 1) = P\left(x_2 \left| \mathrm{y}_1, \mathrm{y}_2, \cdots, \mathrm{y}_q \right.\right) + P\left(x_4 \left| \mathrm{y}_1, \mathrm{y}_2, \cdots, \mathrm{y}_q \right.\right) \\ P(d_2 = 0) = P\left(x_1 \left| \mathrm{y}_1, \mathrm{y}_2, \cdots, \mathrm{y}_q \right.\right) + P\left(x_2 \left| \mathrm{y}_1, \mathrm{y}_2, \cdots, \mathrm{y}_q \right.\right) \\ P(d_2 = 1) = P\left(x_3 \left| \mathrm{y}_1, \mathrm{y}_2, \cdots, \mathrm{y}_q \right.\right) + P\left(x_4 \left| \mathrm{y}_1, \mathrm{y}_2, \cdots, \mathrm{y}_q \right.\right) \end{cases}. \tag{3.29}$$

Then the relevant soft outputs can be forwarded to the channel decoders, which will make a hard decision to finally decode the received signals.

In practical applications, however, the Max-Log-MAP [426, 427] or Log-MAP [428] algorithms are usually preferred [359], since either can lower the computational complexity to some degree. The Max-Log-MAP algorithm was proposed by both Koch and Baier [426] and Erfanian *et al.* [427] for reducing the complexity of the MAP algorithm. This technique transfers the computation into the logarithmic domain and invokes an approximation for dramatically reducing the complexity imposed. As a consequence of using an approximation, its performance is sub-optimal. However, Robertson *et al.* [428] later proposed the Log-MAP algorithm, which partially corrected the approximation invoked in the Max-Log-MAP algorithm. Hence the performance of the Log-MAP algorithm is similar to that of the MAP algorithm, which is achieved at a significantly lower complexity. More details of the Max-Log-MAP and Log-MAP algorithms may be found in [359]. In our STBC soft decoder, the Log-MAP algorithm is employed. In the rest of this section we will characterize the achievable performance of a range of space-time block coding schemes.

3.2.4 System Overview

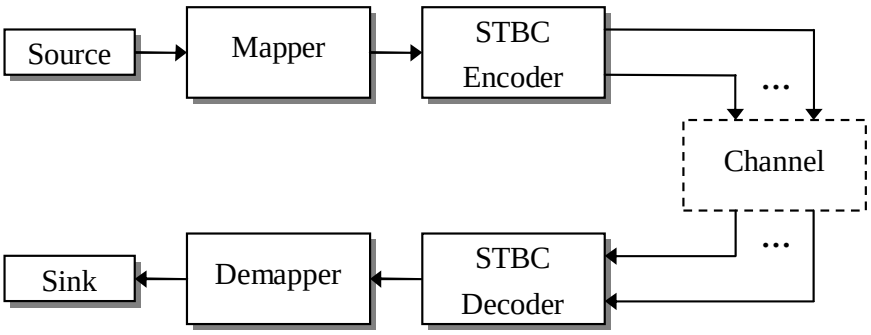

Figure 3.3: Schematic diagram of a simple system employing space-time block codes.

Figure 3.3 shows the structure of the simulation system used. As seen in the figure, the mapper maps the source information bits to relevant phasor constellation points employed by the specific modulation scheme used. Then

the symbols are forwarded to the space-time encoder. The encoded symbols are then transmitted through different antennas and arrive the receiver(s), where the received signals will be decoded by the space-time decoder. Finally, the demapper converts the STBC-decoded symbols back to the information bits and the Bit Error Ratio (BER) is calculated. The parameters of all the space-time block codes studied are summarized in Table 3.1. There following assumptions were used:

- Signals are transmitted over uncorrelated Rayleigh fading channels;
- The channels are quasi-static so that the path gains are constant across n consecutive time slots, corresponding to the n rows of the space-time block codes' transmission matrix;
- The average signal power received from each transmitter antenna is the same;
- The receiver has a perfect knowledge of the channels' fading amplitudes.

These assumptions simplify the simulations to a degree, therefore the system concerned is not a realistic one. However, since the experimental circumstances are identical for all performance comparisons, the results characterize the relative performance of various space-time block codes.

3.2.5 Simulation Results

In the past sections, the basic principles of space-time block codes as well as the simulation conditions were presented. In this section, our simulation results will be provided for the sake of comparatively studying the performance of the various STBCs of Table 3.1.

3.2.5.1 Performance over Uncorrelated Rayleigh Fading Channels

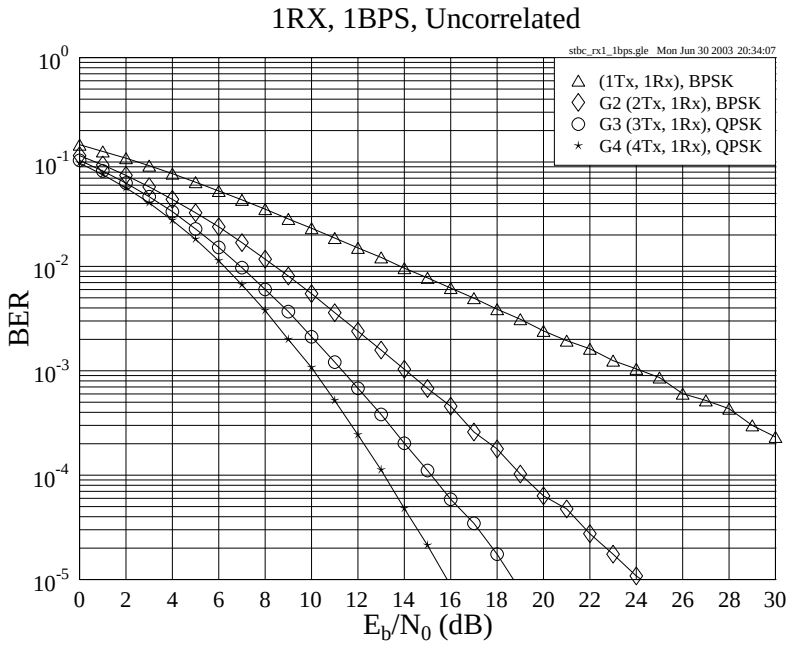

Figure 3.4: The BER versus E_b/N_0 performance of the $\mathbf{G_2}$, $\mathbf{G_3}$, and $\mathbf{G_4}$ space-time block codes of Table 3.1 at an effective throughput of **1 BPS** using **one receiver** over **uncorrelated** Rayleigh fading channels.

Performance at the Throughput of 1 BPS Figure 3.4 compares the performance of the G_2, G_3, and G_4 space-time block codes in conjunction with one receiver at the throughput of 1 BPS over the uncorrelated Rayleigh fading channel. Binary Phase-Shift Keying (BPSK) modulation is employed in conjunction with the space-time code G_2, while QPSK modulation is considered with the half-rate space-time codes G_3 and G_4 so that the system throughput remains 1 BPS. From Figure 3.4 we can see that at the BER of 10^{-5} the G_3 and G_4 codes provide an approximately 5.5 and 7.5 dB gain over the G_2 code, respectively. If we add one more receiver in the context of all of these schemes,

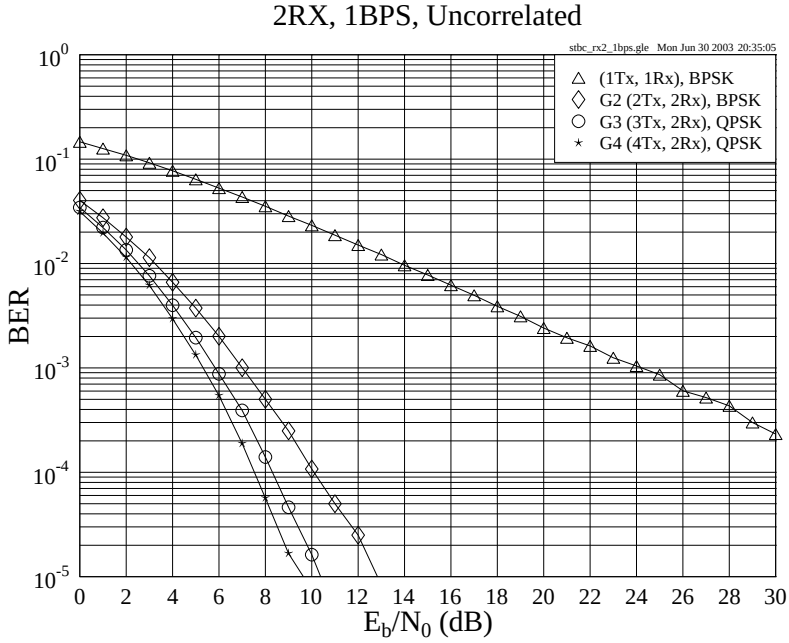

Figure 3.5: The BER versus E_b/N_0 performance of the $\mathbf{G_2}$, $\mathbf{G_3}$, and $\mathbf{G_4}$ space-time block codes of Table 3.1 at an effective throughput of **1 BPS** using **two receivers** over **uncorrelated** Rayleigh fading channels.

as seen in Figure 3.5, the relevant E_b/N_0 gain of the G_3 and G_4 schemes over the G_2 arrangement reduces to 2.5 and 3.5 dB, respectively. This may suggest that the G_2 code using two receivers has achieved most of the attainable diversity gain [359], and hence even if we further increase the number of transmitter antennas, the performance cannot be significantly improved.

Performance at the Throughput of 2 BPS In Figure 3.6 the performances of the space-time block codes using one receiver and having a throughput of about 2 BPS over uncorrelated Rayleigh fading channels are compared. In order to meet the 2 BPS throughput criteria, QPSK modulation is used for the G_2 code, while 16QAM modulation is employed for the G_3 and G_4 arrangements, as the latter ones are half rate codes. However, for the $\frac{3}{4}$-rate codes H_3 and H_4, an exact throughput of 2 BPS cannot be achieved. Thus we chose 8PSK and the throughput of the H_3 and H_4 schemes became 2.25 BPS, which is close to 2 BPS.

From Figure 3.6 we can see that when the Signal-to-Noise Ratio (SNR) is low, i.e. E_b/N_0 is below 12.5 dB, the space-time block code G_2 performs better than other codes, although the performance difference is not significant. When E_b/N_0 increases to a value higher than 12.5 dB, however, the G_4 code outperforms other codes, having an approximately 1 dB gain over the H_4 code at the BER of 10^{-5}. Similarly, the G_3 code achieves an approximately 1 dB gain over the H_3 code at the BER of 10^{-5}. We may note that although the G_3 and G_4 codes employ a higher-order 16QAM modulation scheme, which is more vulnerable to channel effects than the lower-order 8PSK modulation scheme used by the H_3 and H_4 codes, the former performs slightly better than the latter.

In the scenario of using two receivers, however, the G_2 code stands out in comparison to all the candidates, as Figure 3.7 indicates. This result suggests that the attainable diversity gain has already been achieved by the G_2 code using two receivers. Furthermore, the potential benefit of using more transmitters is eroded by the employment of higher throughput, but more vulnerable modulation schemes, which are more prone to transmission errors.

Performance at the Throughput of 3 BPS The performances of the space-time block codes using one receiver and having a throughput of 3 BPS over uncorrelated Rayleigh fading channels are compared in Figure 3.8. Again, similarly to the scenario of having a throughput of 2 BPS, the G_2 code performs best at a low SNR, namely below about 10 dB, although the performance difference between G_2 and other codes is even smaller than it is in Figure 3.6. As shown in Figure3.8, at the BER of 10^{-5}, the H_3 and H_4 codes achieve a gain of about 3 dB over the G_3 and G_4 codes, respectively. Since the space-time block codes themselves do not have an error-correction capability which would allow them to correct the extra errors induced by employing a more vulnerable, higher-order modulation scheme [359], this results in a poorer performance. Furthermore, since the relative increase of the constellation density when changing from 16QAM to 64QAM is higher than that from 8PSK to 16QAM, the performance degradation imposed by reverting from 16QAM to 64QAM is more severe than that imposed by opting for 16QAM instead of 8PSK. Therefore it is not

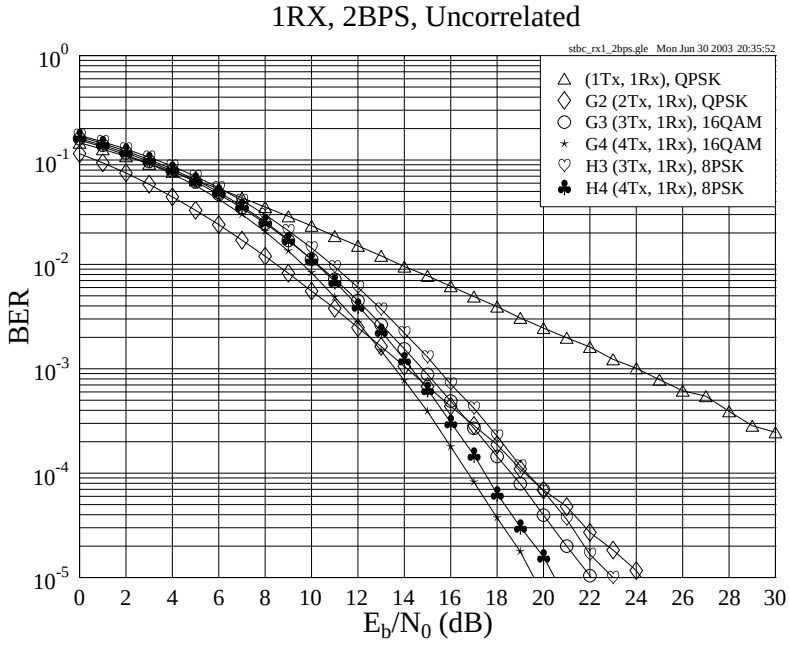

Figure 3.6: The BER versus E_b/N_0 performance of the $\mathbf{G_2}$, $\mathbf{G_3}$, $\mathbf{G_4}$, $\mathbf{H_3}$, and $\mathbf{H_4}$ space-time block codes of Table 3.1 at an effective throughput of about **2 BPS** using **one receiver** over **uncorrelated** Rayleigh fading channels.

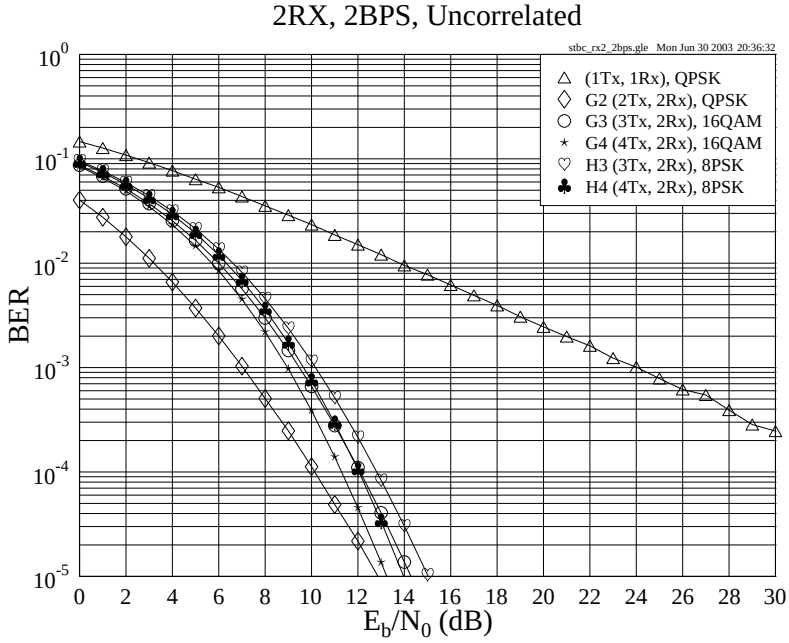

Figure 3.7: The BER versus E_b/N_0 performance of the $\mathbf{G_2}$, $\mathbf{G_3}$, $\mathbf{G_4}$, $\mathbf{H_3}$, and $\mathbf{H_4}$ space-time block codes of Table 3.1 at an effective throughput of about **2 BPS** using **two receivers** over **uncorrelated** Rayleigh fading channels.

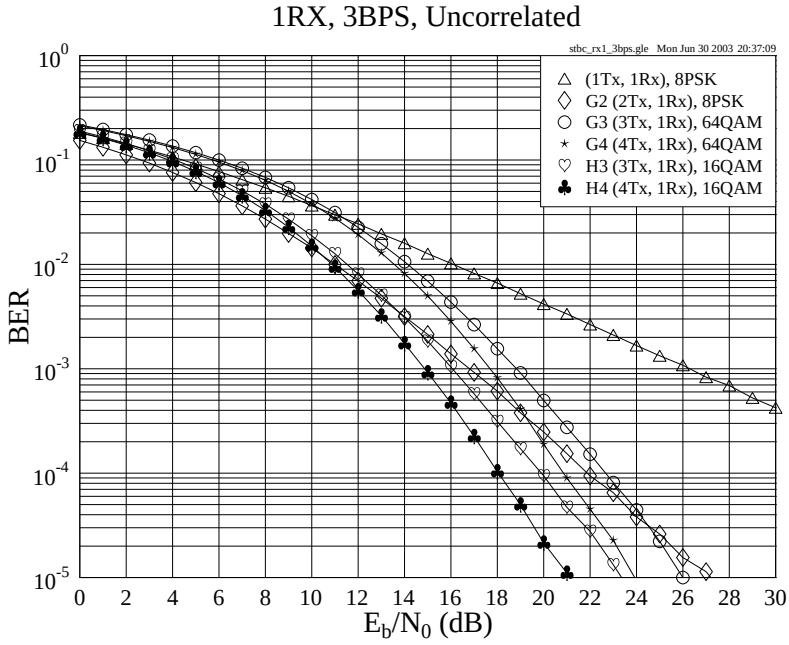

Figure 3.8: The BER versus E_b/N_0 performance of the $\mathbf{G_2}$, $\mathbf{G_3}$, $\mathbf{G_4}$, $\mathbf{H_3}$, and $\mathbf{H_4}$ space-time block codes of Table 3.1 at an effective throughput of **3 BPS** using **one receiver** over **uncorrelated** Rayleigh fading channels.

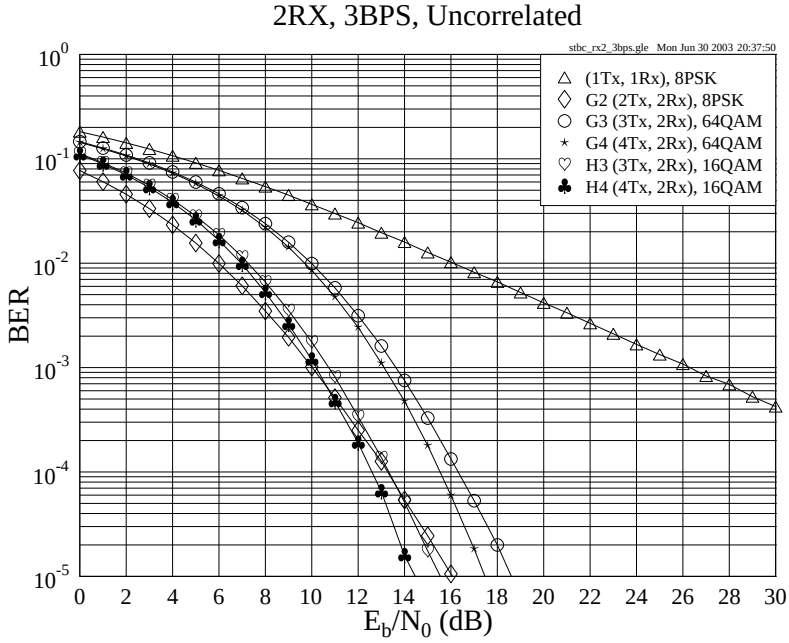

Figure 3.9: The BER versus E_b/N_0 performance of the $\mathbf{G_2}$, $\mathbf{G_3}$, $\mathbf{G_4}$, $\mathbf{H_3}$, and $\mathbf{H_4}$ space-time block codes of Table 3.1 at an effective throughput of **3 BPS** using **two receivers** over **uncorrelated** Rayleigh fading channels.

surprising that the best code to be used for high-SNR situations becomes the H_4 instead of the G_4 code, which was the best code according to Figure 3.6 at high-SNR scenarios, since the G_4 and H_4 codes are used in conjunction with 64QAM and 16QAM, respectively. Moreover, we note that the H_3 code gives approximately 0.4 dB gain over the G_4 code, although the former has a lower diversity order.

If the number of receivers is doubled, as seen in Figure 3.9, the performance degradations of the G_3 and G_4 codes are much more dramatic. In this scenario, even the lower-diversity space-time code G_2 is capable of outperforming the space-time code G_4 having a higher-order diversity by about 1.7 dB at the BER of 10^{-5}.

3.2.5.2 Performance over Correlated Rayleigh Fading Channel

We have compared the performances of the space-time block codes of Table 3.1 for transmission over uncorrelated Rayleigh fading channels in Section 3.2.5.1. In this section, the performance of the STBCs will be studied based on the same assumptions noted on page 66, except that the channel is assumed to be a correlated Rayleigh fading channel associated with the normalized Doppler frequency of 3.25×10^{-5}.

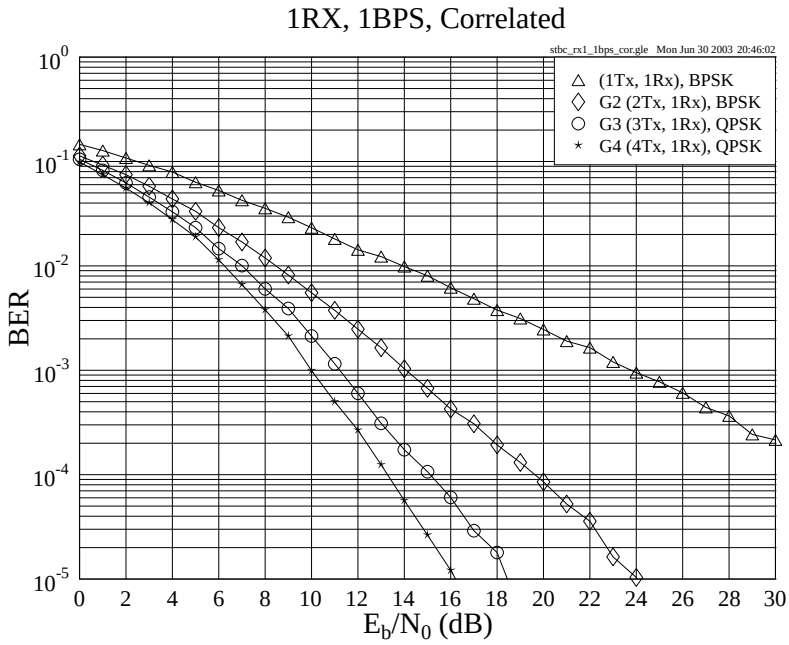

Figure 3.10: The BER versus E_b/N_0 performance of the $\mathbf{G_2}$, $\mathbf{G_3}$, and $\mathbf{G_4}$ space-time block codes of Table 3.1 at an effective throughput of **1 BPS** using **one receiver** over **correlated** Rayleigh fading channels. The normalized Doppler frequency is 3.25×10^{-5}.

Specifically, Figure 3.10 compares the performance of the G_2, G_3, and G_4 space-time block codes in conjunction with one receiver at the throughput of 1 BPS, when communicating over a correlated Rayleigh fading channel. If we compare Figure 3.10 with Figure 3.4, which shows the relevant codes' performance over uncorrelated Rayleigh fading channels, we will note that the performances recorded in these cases are almost the same. This is because the receiver is aided by a perfect channel estimator that provides full knowledge of the path gains, and thus the effect imposed on the transmitted signals by the different path gains, regardless whether they are correlated or uncorrelated, is efficiently counteracted. When the throughput increases to 2 BPS and even further to 3 BPS, it can also be shown that the achievable performances of STBC codes communicating over a correlated Rayleigh channel are the same as those of their corresponding counterparts transmitting over uncorrelated Rayleigh channels, respectively.

3.2.6 Conclusions

From the discussions and simulation results of Sections 3.2.5.1 and 3.2.5.2, several conclusions can be inferred. Firstly, the encoding and decoding of space-time block codes has a low complexity. At the receiver end, the maximum likelihood decoder requires low-complexity linear processing for decoding.

Secondly, from Figures 3.4, 3.6 and 3.8 we note that when the effective throughput is increased, the phasor-constellation has to be extended for accommodating the increased number of bits. Hence the performances of the half-rate codes G_3 and G_4 degrade in comparison to that of the unity-rate code G_2.

Thirdly, at the even higher effective throughput of 3 BPS, the H_3 and H_4 codes perform better than the G_3 and G_4 codes, respectively, as shown in Figure 3.8. Moreover, according to Figures 3.4, 3.5, 3.8 and 3.9, when the number of receivers is increased, the performance gain of the G_3, G_4, H_3 and H_4 codes over the G_2 code becomes more modest because much of the attainable diversity gain has already been achieved using the G_2 code employing two receivers.

Last but not least, it was also found that the performances of the space-time codes communicating over uncorrelated and correlated Rayleigh fading channels are similar, provided that the effective throughput is the same.

The achievable coding gains of the space-time block codes are summarized in Table 3.2. The coding gain is defined as the E_b/N_0 difference, expressed in terms of decibels, at a BER of 10^{-5} between the various space-time block coded and uncoded single-transmitter systems having the same throughput. The best schemes at the effective throughput of 1, 2, and 3 BPS are printed in bold, respectively.

BPS	Code	Code Rate	Modem	E_b/N_0 (dB)		Gain (dB)	
				BER			
				10^{-3}	10^{-5}	10^{-3}	10^{-5}
1.00	Uncoded	1	BPSK	24.22	44.00	0.00	0.00
	G_2	1	BPSK	14.08	24.22	10.14	19.78
	G_3	1/2	QPSK	11.33	18.71	12.89	25.29
	G_4	1/2	QPSK	**10.10**	**15.85**	**14.12**	**28.15**
2.00	Uncoded	1	QPSK	24.22	44.00	0.00	0.00
	G_2	1	QPSK	14.12	24.22	10.10	19.78
	G_3	1/2	16QAM	14.78	22.06	9.44	21.94
	G_4	1/2	16QAM	**13.61**	**19.58**	**10.61**	**24.42**
2.25	H_3	3/4	8PSK	15.43	23.00	8.79	21.00
≈ 2.00	H_4	3/4	8PSK	14.31	20.48	9.91	23.52
3.00	Uncoded	1	8PSK	26.30	46.26	0.00	0.00
	G_2	1	8PSK	16.80	27.21	9.50	19.05
	G_3	1/2	64QAM	18.83	26.00	7.47	20.26
	G_4	1/2	64QAM	17.69	23.92	8.61	22.34
	H_3	3/4	16QAM	16.06	23.36	10.24	22.90
	H_4	3/4	16QAM	**14.87**	**21.10**	**11.43**	**25.16**

Table 3.2: Coding gains of the space-time block codes using one receiver when communicating over uncorrelated and correlated Rayleigh fading channels. The performance of the best scheme for a specific effective throughput is printed in bold.

3.3 Channel Coded Space-Time Block Codes

In Section 3.2, we have presented the basic concepts of the space-time block codes and provided a range of characteristic performance results. Furthermore, the MAP algorithm invoked for decoding STBC codes has also been briefly highlighted. This enables a space-time decoder to provide soft outputs that can be exploited by concatenated channel decoders for further improving the system's performance. In this section, we will concatenate the space-time block codes with various Low Density Parity Check (LDPC) channel codes [422] and with a Turbo Convolutional (TC) code [423, 424]. The performances of the different schemes will also be evaluated.

3.3.1 Space-Time Block Codes with LDPC Channel Codes

LDPC codes were devised by Gallager [422] in 1962. During the early evolutionary phase of channel coding, LDPC schemes made a limited impact on the research of the channel coding community, although they showed an unprecedented performance prior to the turbo coding era. This was because LDPC codes required a relatively high storage space and complexity. However, owing to their capability of approaching Shannon's predicted performance limits [429], research interests in LDPC codes have been rekindled during recent years [429–433].

LDPC codes [422] belong to the family of linear block codes, which are defined by a parity check matrix having M rows and N columns. The column weight j and row weight k is typically significantly lower than the dimension M and N of the parity check matrix. The construction of the parity check matrix is referred to as regular or irregular, depending on whether the Hamming weight per column or row is identical. Reference [431] shows that carefully designed irregular LDPC codes may perform better than their regular counterparts. Furthermore, when the block length is increased, irregular LDPC codes may become capable of outperforming turbo codes [429] at the cost of a higher complexity. Since the details of the decoding of LDPC codes can be found in [434], in the forthcoming sections we are more interested in the performance of LDPC codes than the LDPC decoding algorithm itself.

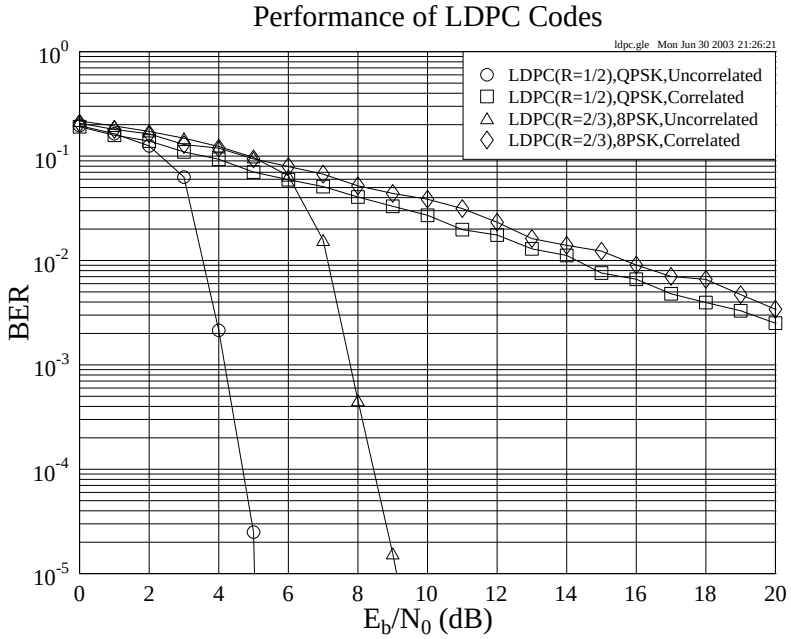

Figure 3.11: The BER versus E_b/N_0 performance of several LDPC codes communicating over both uncorrelated and correlated Rayleigh fading channels. The parameters of the LDPC codes are given in Tables 3.3 and 3.4. The normalized Doppler frequency of the correlated Rayleigh fading channels was 3.25×10^{-5}. The effective throughput of the QPSK and 8PSK schemes were 1 BPS and 2 BPS, respectively.

The number of columns N is given by the number of coded bits hosted by a LDPC codeword, while the number of rows M corresponds to the number of parity check constraints imposed by the design of the LDPC code. The number of information bits encoded by a LDPC codeword is denoted by $K = N - M$, yielding a coding rate of K/M [434]. Thus, the LDPC code rate can be adjusted by changing K and/or M.

Figure 3.11 characterizes the performance of several LDPC codes for transmission over both uncorrelated and correlated Rayleigh fading channels. The normalized Doppler frequency of the correlated Rayleigh channel was 3.25×10^{-5}. It was found that the LDPC codes perform far better over uncorrelated than over correlated Rayleigh channels, since the codeword length is short. This characteristic predetermines the expected performance of the LDPC-STBC coded concatenated system to be introduced in the next section and characterized in Section 3.3.1.2.2.

3.3.1.1 System Overview

Figure 3.12 shows the schematic diagram of the system. The source bits are first encoded by the LDPC encoder, whose outputs are modulated and forwarded to the STBC encoder. At the receiver, the noise-contaminated received symbols are decoded by the STBC soft decoder. As discussed in Section 3.2.3.2, the soft outputs constituted by the aposteriori

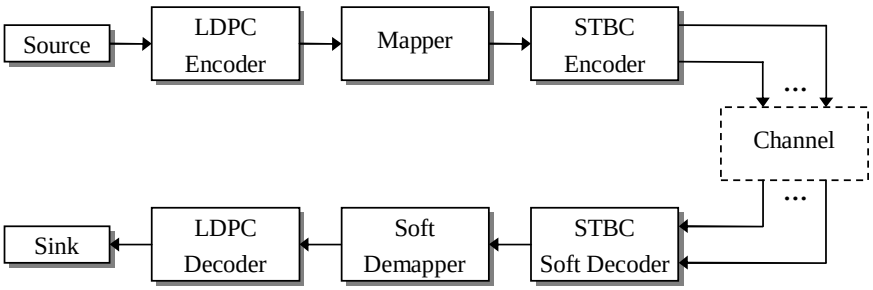

Figure 3.12: System overview of LDPC channel coding aided space-time block codes.

probabilities of the STBC-decoded symbols will be passed on to the soft demapper, where the symbol probabilities are used for generating the resultant bit probabilities. Finally, the LDPC decoder decodes the soft inputs and the channel decoded information bits are obtained.

In Section 3.3.1.2, we will provide a range of simulation results and compare the achievable performances of the different schemes designed for transmission over both uncorrelated and correlated Rayleigh fading channels. According to [434], when using different column weights j and/or a different number of LDPC decoding iterations, the performance of LDPC codes will change correspondingly. In our system, we fix the column weight and the number of iterations to 3 and 25, respectively. For the scenarios of communicating over correlated Rayleigh fading channels, a fix-length random channel interleaver was used. Furthermore, for the sake of fair comparisons, we comply with the assumptions outlined on page 66 so that the simulation results of Section 3.2.5 remain comparable in this new context.

The parameters used in our LDPC-STBC coded concatenated system are given in Tables 3.3 and 3.4, while the parameters of the space-time block codes have been given in Table 3.1. For the sake of maintaining the same effective throughput, the LDPC codec's parameters have to be harmonized with the STBC codec's parameters.

3.3.1.2 Simulation Results

Similarly to Section 3.2.5, we will compare the performances of different schemes in the context of the same effective throughput, when communicating over both uncorrelated and correlated Rayleigh fading channels.

3.3.1.2.1 Performance over Uncorrelated Rayleigh Fading Channels

Performance at the Throughput of 1 BPS Figure 3.13 compares the achievable performance of the G_2, G_3, G_4, H_3 and H_4 space-time block codes, which are combined with various LDPC codes, in the context of using one receiver and maintain a throughput of 1 BPS, while communicating over uncorrelated Rayleigh fading channels. We can see that when E_b/N_0 is lower than about 2.7dB, the half-rate space-time bock code G_4 using QPSK modulation, which constituted the best system at the throughput of 1 BPS according to Table 3.2, gives the best performance. But when the SNR increases, the situation reverses since the performance of the LDPC-assisted STBC codes becomes significantly better than that of the G_4 scheme using no channel coding. Moreover, the scheme constituted by the G_2 code and half-rate LDPC code excels among all the LDPC-coded STBC schemes by a margin of about 2dB gain over others. Note that in order to maintain the same effective throughput of 1 BPS, the unity-rate space-time block code G_2 is combined with the half-rate LDPC code employing QPSK modulation, while the half-rate space-time codes G_3 and G_4 assisted by half-rate LDPC code use 16QAM modulation. For the $\frac{3}{4}$-rate codes H_3 and H_4, the $\frac{2}{3}$-rate LDPC code is introduced and QPSK modulation is used for meeting the criteria of having the same throughput of 1 BPS.

From Figure 3.13, we may arrive at the following conclusions. Provided that a fixed block size of the LDPC codeword is used, a lower LDPC code rate implies that more parity check bits are attached to the original bits sequence, which leads to a better performance. On the other hand, as seen in Figure 3.13, when QPSK modulation is used, the G_2 code employing the half-rate LDPC code outperforms the H_3 and H_4 codes in conjunction with the $\frac{2}{3}$-rate LDPC code, despite the fact that the former has a lower diversity order. Therefore we may surmise for the set of LDPC-coded STBC schemes considered that when using a specific modulation scheme, the system's performance is predominantly determined by the LDPC code employed instead of the space-time code's diversity order. Another observation informed from the figure is, that the number of bits per symbol used by the specific modulation scheme is a more decisive factor in terms of determining the achievable performance, than the diversity order, when the same LDPC code is used. In other words, if we want to improve the system's performance, it is more beneficial to reduce

BPS	STBC		LDPC					Modem
	Code	Code Rate	Code Rate	Input Bits Block Size	Output Bits Block Size	Column Weight	Iter-ations	
1.00	G_2	1	1/2	1008	2016	3	20	QPSK
	G_3	1/2	1/2	1008	2016	3	20	16QAM
	G_4	1/2	1/2	1008	2016	3	20	16QAM
	H_3	3/4	2/3	1344	2016	3	20	QPSK
	H_4	3/4	2/3	1344	2016	3	20	QPSK
2.00	G_2	1	2/3	1344	2016	3	20	8PSK
	G_2	1	1/2	1008	2016	3	20	16QAM
	G_2	1	1/3	672	2016	3	20	64QAM
	G_3	1/2	2/3	1344	2016	3	20	64QAM
	G_4	1/2	2/3	1344	2016	3	20	64QAM
2.25	H_3	3/4	1/2	1008	2016	3	20	64QAM
$\approx$ 2.00	H_4	3/4	1/2	1008	2016	3	20	64QAM
3.00	G_2	1	3/4	1512	2016	3	20	16QAM
	G_2	1	1/2	1008	2016	3	20	64QAM
	H_3	3/4	2/3	1344	2016	3	20	64QAM
	H_4	3/4	2/3	1344	2016	3	20	64QAM

Table 3.3: The parameters used in the LDPC-STBC coded concatenated schemes for transmissions over **uncorrelated** Rayleigh fading channels.

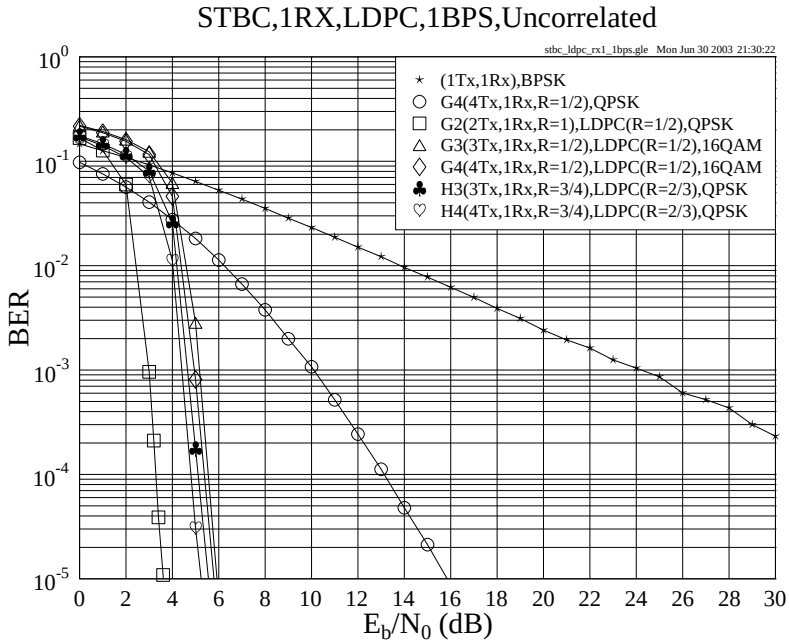

Figure 3.13: The BER versus E_b/N_0 performance of the $\mathbf{G_2}$, $\mathbf{G_3}$, $\mathbf{G_4}$, $\mathbf{H_3}$ and $\mathbf{H_4}$ space-time block codes of Table 3.1 in conjunction with the different-rate LDPC codes of Table 3.3 at an effective throughput of **1 BPS** using **one receiver** over **uncorrelated** Rayleigh fading channels.

BPS	STBC		LDPC					Channel Interleaver Depth	Modem
	Code	Code Rate	Code Rate	Input Bits Block Size	Output Bits Block Size	Column Weight	Iterations		
1.00	G_2	1	1/2	10080	20160	3	20	20160	QPSK
	G_3	1/2	1/2	10080	20160	3	20	20160	16QAM
	G_4	1/2	1/2	10080	20160	3	20	20160	16QAM
	H_3	3/4	2/3	13440	20160	3	20	20160	QPSK
	H_4	3/4	2/3	13440	20160	3	20	20160	QPSK
2.00	G_2	1	2/3	13440	20160	3	20	20160	8PSK
	G_2	1	1/2	10080	20160	3	20	20160	16QAM
	G_2	1	1/3	6720	20160	3	20	20160	64QAM
	G_3	1/2	2/3	13440	20160	3	20	20160	64QAM
	G_4	1/2	2/3	13440	20160	3	20	20160	64QAM
2.25 $\approx$ 2.00	H_3	3/4	1/2	10080	20160	3	20	20160	64QAM
	H_4	3/4	1/2	10080	20160	3	20	20160	64QAM
3.00	G_2	1	3/4	15120	20160	3	20	20160	16QAM
	G_2	1	1/2	10080	20160	3	20	20160	64QAM
	H_3	3/4	2/3	13440	20160	3	20	20160	64QAM
	H_4	3/4	2/3	13440	20160	3	20	20160	64QAM

Table 3.4: The parameters used in the LDPC-STBC coded concatenated schemes for transmissions over **correlated** Rayleigh fading channels.

the number of bits per symbol instead of increasing the number of transmitter antennas. For example, when employing a half-rate LDPC code, the G_3 and G_4 space-time codes employing 16QAM perform about 2.2dB worse than the G_2 code employing QPSK, despite that the fact that the former one has a higher diversity order.

Performance at the Throughput of 2 BPS In Figure 3.14 the performance of the LDPC-aided space-time block codes using one receiver and having a throughput of about 2 BPS, while communicating over uncorrelated Rayleigh fading channels is studied. Specially, the $\frac{3}{4}$-rate codes H_3 and H_4 are employed in conjunction with the half-rate LDPC code using 64QAM modulation, and thus achieve an effective throughput of 2.25 BPS, which is close to our target of 2 BPS.

The curves seen in Figure 3.14 can be divided into two groups based on their relative performances. The first group contains the three schemes employing the G_2 code in conjunction with various LDPC codes and gives an average gain of about 3dB over the members of the second group, in which the $G_3/G_4/H_3/H_4$ schemes are grouped. The performance difference between the two groups tallies with our conclusions derived in the case of aiming for a throughput of 1 BPS. As seen in Figure 3.14, the schemes of the second group suffer performance degradations as a consequence of employing the densely-packed 64QAM constellation, which is more prone to transmission errors than the other modulation schemes. Furthermore, the 64QAM-based scheme of the first group, i.e. the arrangement employing the G_2 code as well as the $\frac{1}{3}$-rate LDPC code, also performs better than any member scheme of the second group as a benefit of its lower LDPC code rate.

Ass seen in Figure 3.14, in all the three G_2-based schemes of the superior group, the best design option is the compromise scheme employing the half-rate LDPC-aided G_2 code using 16QAM modulation. The reason for this phenomenon can be explained from two different aspects. On one hand, when the number of bits per symbol is moderate, as in relatively lower-order 8PSK and 16QAM, for example, the performance trends imposed by the different LDPC codes outweigh those caused by the different modulation schemes. In this case, as expected, if the system uses

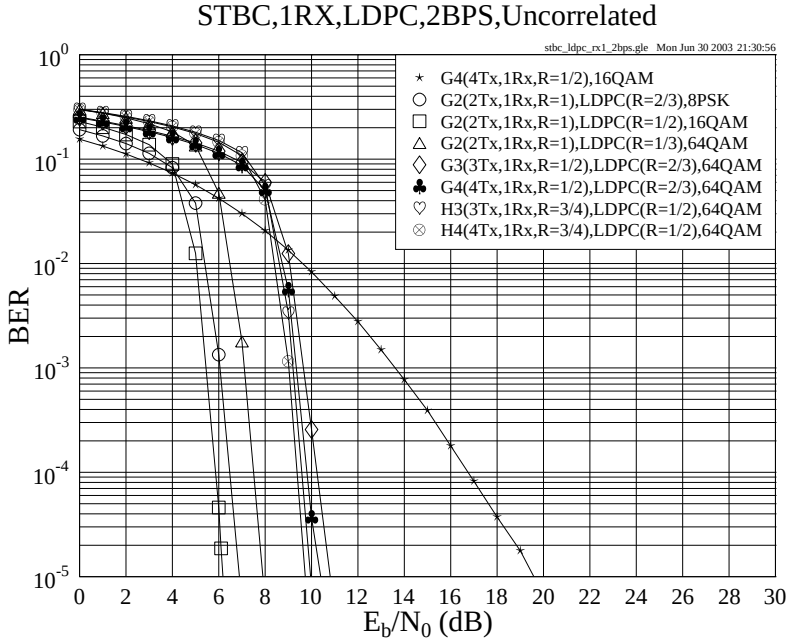

Figure 3.14: The BER versus E_b/N_0 performance of the $\mathbf{G_2}$, $\mathbf{G_3}$, $\mathbf{G_4}$, $\mathbf{H_3}$ and $\mathbf{H_4}$ space-time block codes of Table 3.1 in conjunction with the different-rate LDPC codes of Table 3.3 at an effective throughput of about **2 BPS** using **one receiver** over **uncorrelated** Rayleigh fading channels.

a lower-rate LDPC code, it will achieve a better performance. This is why the half-rate LDPC coded scheme using 16QAM modulation is superior to the $\frac{2}{3}$-rate LDPC coded scheme using 8PSK modulation, as seen in Figure 3.14. On the other hand, when the modulation level is increased to 64, for example, as in 64QAM, the situation is reversed and the number of bits per symbol conveyed by the modulation schemes will become the predominant factor. In this case, the combination of lower-rate LDPC codes with high-order modulation arrangements will no longer outperform the scheme that uses higher-rate LDPC codes in conjunction with lower-order modulation constellations. Hence the $\frac{1}{3}$-rate LDPC coded 64QAM modulation scheme is outperformed by the half-rate LDPC coded 16QAM modulation arrangement, as indicated by Figure 3.14.

Performance at the Throughput of 3 BPS The performance of the LDPC-assisted space-time block codes using one receiver and having a throughput of 3 BPS for transmissions over uncorrelated Rayleigh fading channels is shown in Figure 3.15. When the half-rate space-time codes G_3 and G_4 are used in conjunction with LDPC codes, even if we employ a high-throughput 64QAM scheme, the system's effective throughput will be lower than 3 BPS, because the code rate of the LDPC code is below unity. For employment in conjunction with the G_3 and G_4 codes, a high-rate LDPC code has to be used in order to maintain a throughput close to 3 BPS. However, as discussed before, when the high-order 64QAM scheme is used, the achievable performance improvement of LDPC coding remains modest, regardless of the rate of the LDPC code. Hence in this scenario the performance of the LDPC-aided G_3 and G_4 codes is not considered here.

In Figure 3.15, similarly to the 2-BPS throughput scenario, it is also found that the four LDPC-aided STBC schemes can be divided into two groups. The G_2 space-time code aided by the $\frac{3}{4}$-rate LDPC code using 16QAM performs best in high SNR situations and it only suffers a low performance degradation over the scheme using no channel coding when SNR is low.

When we increase the number of receiver antennas, the performance gap between the two groups remains still obvious as shown in Figure 3.16. In this scenario, the best scheme is again the one employing the half-rate LDPC-aided G_2 code using 16QAM. However, the gain achieved by the best LDPC-STBC scheme over the best unprotected STBC scheme using two receivers decreases to about 10dB compared to the 12.5dB achieved, while using a single receiver.

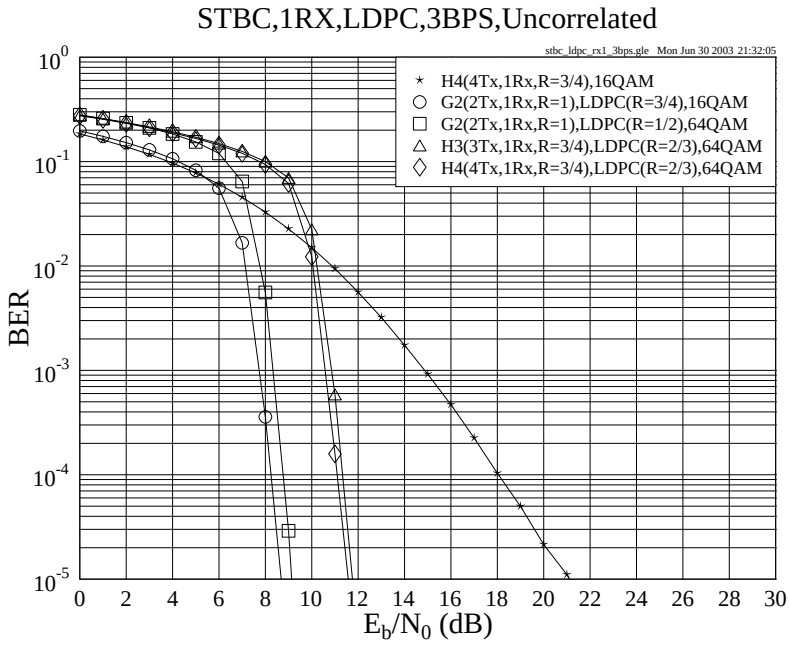

Figure 3.15: The BER versus E_b/N_0 performance of the $\mathbf{G_2}$, $\mathbf{H_3}$, and $\mathbf{H_4}$ space-time block codes of Table 3.1 in conjunction with the different-rate LDPC codes of Table 3.3 at an effective throughput of **3 BPS** using **one receiver** over **uncorrelated** Rayleigh fading channels.

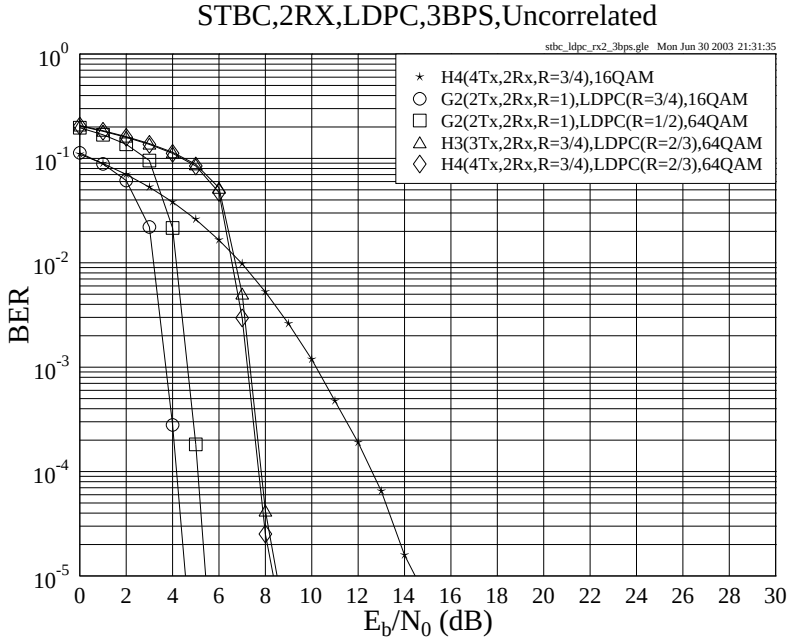

Figure 3.16: The BER versus E_b/N_0 performance of the $\mathbf{G_2}$, $\mathbf{H_3}$, and $\mathbf{H_4}$ space-time block codes of Table 3.1 in conjunction with the different-rate LDPC codes of Table 3.3 at an effective throughput of **3 BPS** using **two receivers** over **uncorrelated** Rayleigh fading channels.

3.3.1.2.2 Performance over Correlated Rayleigh Fading Channels

We have compared the performance of the LDPC-aided space-time block codes when communicating over uncorrelated Rayleigh fading channels in Section 3.3.1.2.1. In this section, the performance of the STBC codes will be studied based on the same assumptions summarized on page 66, except that the channel is assumed to be a correlated Rayleigh fading channel obeying the normalized Doppler frequency of 3.25×10^{-5}. The corresponding parameters are given in Table 3.4.

In Section 3.2.5.2 it was found that if the effective throughput is a fixed constant, the performance of the various space-time codes used for transmission over uncorrelated and correlated Rayleigh fading channels is similar. However, in the context of the LDPC-assisted STBC-coded system, the achievable performances are different over uncorrelated and correlated Rayleigh fading channels. This can be clearly seen by comparing Figures 3.17, 3.18 and 3.19 of this section to Figures 3.13, 3.14 and 3.15 of Section 3.3.1.2.1, respectively. The reason for this phenomenon is that the LDPC codes perform better over uncorrelated rather than correlated Rayleigh fading channels, unless their codeword length is extremely high or long channel interleavers are used. This will be demonstrated during our further discourse.

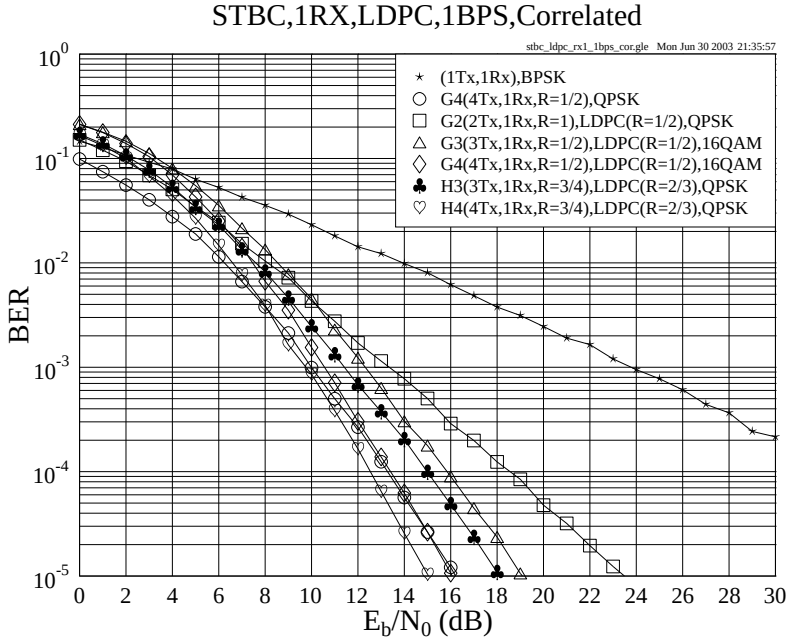

Figure 3.17: The BER versus E_b/N_0 performance of the $\mathbf{G_2}$, $\mathbf{G_3}$, $\mathbf{G_4}$, $\mathbf{H_3}$, and $\mathbf{H_4}$ space-time block codes of Table 3.1 in conjunction with the different-rate LDPC codes of Table 3.4 at an effective throughput of **1 BPS** using **one receiver** over **correlated** Rayleigh fading channels. The normalized Doppler frequency is 3.25×10^{-5}.

Performance at the Throughput of 1 BPS Figure 3.17 shows the achievable performance of the LDPC-assisted G_2, G_3, G_4, H_3 and H_4 codes of Table 3.1 using one receiver at the effective throughput of 1 BPS when communicating over correlated Rayleigh fading channels. We can see that the $\frac{2}{3}$-rate LDPC-coded H_4 and H_3 codes outperform the $\frac{2}{3}$-rate LDPC-coded G_4 and G_3 codes by about 1dB, respectively. However, when E_b/N_0 is lower than about 8dB, we notice that the scheme employing the unprotected G_4 code, which is the best design option at the throughput of 1 BPS according to Table 3.2, performs better than the scheme employing the $\frac{2}{3}$-rate LDPC-aided H_4 code. When the SNR is increased to 15dB, the situation is reversed, since the unprotected G_4 scheme is outperformed by the best LDPC-STBC scheme, namely the $\frac{2}{3}$-rate LDPC-assisted H_4 coded scheme, with about 1dB E_b/N_0 degradation at the BER of 10^{-5}.

Performance at the Throughput of 2 BPS At an effective throughput of approximately 2 BPS, the relevant schemes' performances are given in Figure 3.18. It is seen in the figure that the performance of the schemes employing the H_4 and H_3 codes of Table 3.1 is similar to those of the schemes employing the G_4 and G_3 codes, respectively, although we may bear in mind that the $\frac{3}{4}$-rate H_4 and H_3 codes have an effective throughput of 2.25 BPS, rather than exactly 2 BPS. Furthermore, an important phenomenon found in Figure 3.18 is that the best unprotected STBC scheme of Figure 3.6 also attains the best performance in this new scenario.

This result may be explained as follows. The performance of the unprotected space-time block codes remains similar over uncorrelated or correlated Rayleigh fading channels, as it was indicated in Section 3.2.5.2. Furthermore,

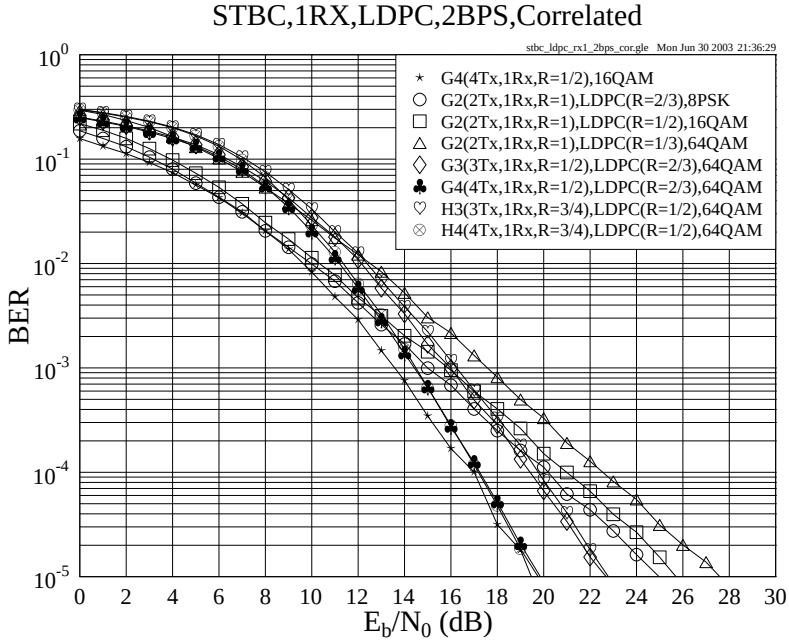

Figure 3.18: The BER versus E_b/N_0 performance of the $\mathbf{G_2}$, $\mathbf{G_3}$, $\mathbf{G_4}$, $\mathbf{H_3}$, and $\mathbf{H_4}$ space-time block codes of Table 3.1 in conjunction with the different-rate LDPC codes of Table 3.4 at an effective throughput of about **2 BPS** using **one receiver** over **correlated** Rayleigh fading channels. The normalized Doppler frequency is 3.25×10^{-5}.

the performance of the LDPC codes degrades when communicating over correlated rather than uncorrelated Rayleigh fading channels, as seen in Figure 3.11. Hence it is not surprising that the LDPC-STBC coded concatenated system will suffer a performance degradation in the context of correlated Rayleigh channels. In this case, the LDPC codes' relatively poor performance recorded over correlated Rayleigh channels disadvantageously affects the entire system. In other words, the LDPC codes improve the system's performance less dramatically over correlated Rayleigh fading channels than over uncorrelated Rayleigh fading channels, unless the LDPC codeword length is very high or long interleavers are used.

Performance at the Throughput of 3 BPS The performance of the LDPC-assisted space-time block codes using one receiver and having a throughput of 3 BPS while communicating over correlated Rayleigh fading channel is portrayed in Figure 3.19. Similar to Figure 3.15, the schemes which employ the half-rate space-time codes G_3 and G_4 of Table 3.1 are not considered in this scenario, since they are incapable of achieving an effective throughput of 3 BPS, nor can they achieve a better performance than the candidate schemes characterized in Figure 3.19.

As Figure 3.19 shows, the unprotected STBC H_4 using 16QAM modulation performs best, giving an approximately 1dB gain over the best LDPC-aided scheme, namely the STBC H_4 combined with the $\frac{2}{3}$-rate LDPC code using 64QAM modulation at the BER of 10^{-5}. Similar to the scenario maintaining an effective throughput of 2 BPS, at a relatively lower E_b/N_0 value, i.e. below 14.5dB, the best STBC-LDPC concatenated scheme is the one that employs the G_2 ST code combined with a low-order modulation, namely the $\frac{3}{4}$-rate LDPC-coded 16QAM.

Furthermore, when the number of receivers is increased to two, the $\frac{3}{4}$-rate LDPC-assisted G_2 code outperforms all the other schemes considered, provided that the E_b/N_0 value is below 12dB, as observed in Figure 3.20. At even higher E_b/N_0 values, namely in excess of 12dB, the $\frac{2}{3}$-rate LDPC-assisted H_4 code exhibits the best performance, although it uses the highest-order 64QAM modem. It can be also observed from Figure 3.20 that the curves are significantly closer to one another compared to the scenario of using one receiver, which is shown in Figure 3.19.

3.3.1.3 Complexity Issues

In Section 3.3.1.2, we have compared the performance of various LDPC-STBC coded concatenated systems. The best scheme was also identified for each scenario. However, these choices have been made based purely on the achievable performance, and the complexity issue of implementation has not been taken into consideration. In this section, we will briefly address the associated complexity issues.

As discussed in Section 3.2.3.2, the soft decoder of the space-time block codes employs the Log-MAP algorithm

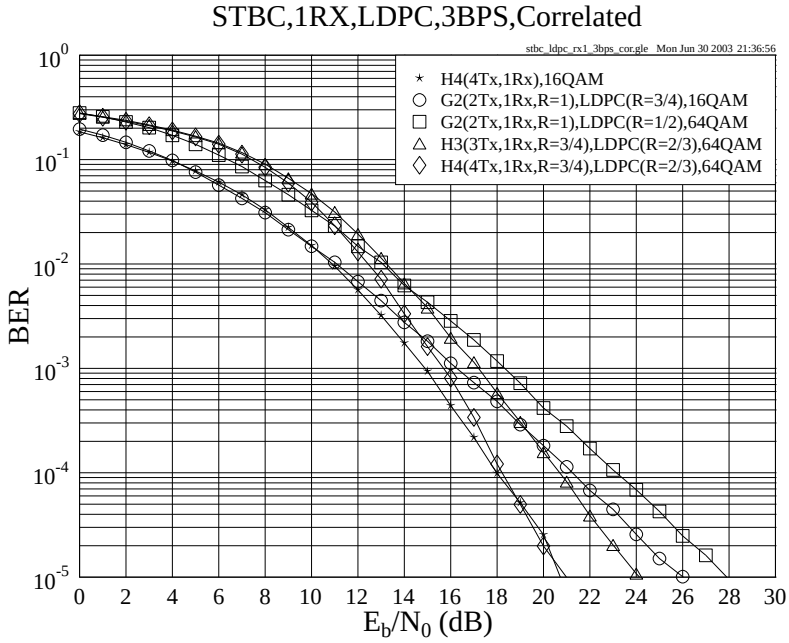

Figure 3.19: The BER versus E_b/N_0 performance of the $\mathbf{G_2}$, $\mathbf{H_3}$, and $\mathbf{H_4}$ space-time block codes of Table 3.1 in conjunction with the different-rate LDPC codes of Table 3.4 at an effective throughput of **3 BPS** using **one receiver** over **correlated** Rayleigh fading channels. The normalized Doppler frequency is 3.25×10^{-5}.

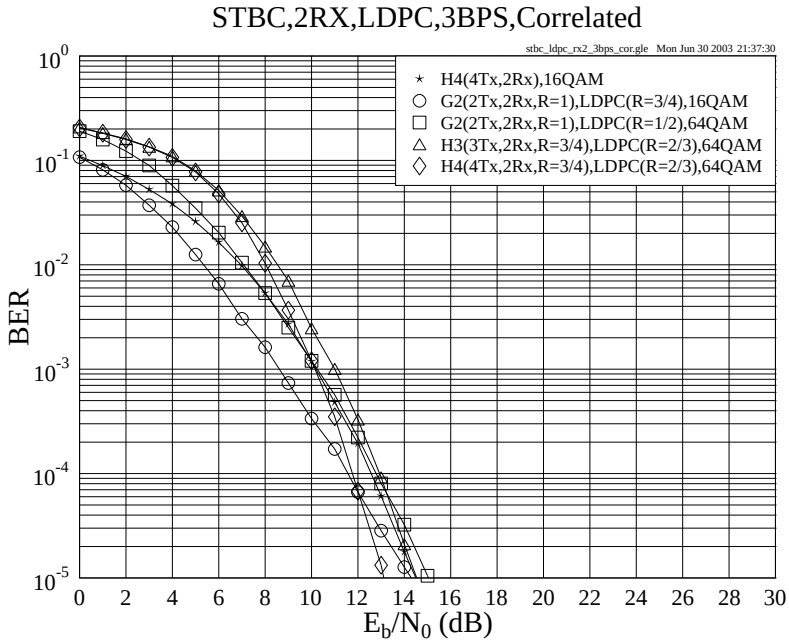

Figure 3.20: The BER versus E_b/N_0 performance of the $\mathbf{G_2}$, $\mathbf{H_3}$, and $\mathbf{H_4}$ space-time block codes of Table 3.1 in conjunction with the different-rate LDPC codes of Table 3.4 at an effective throughput of **3 BPS** using **two receivers** over **correlated** Rayleigh fading channels. The normalized Doppler frequency is 3.25×10^{-5}.

summarized for example in [359]. With the advent of the Log-MAP algorithm, the high-complexity complicated exponential operations are substituted by additions and subtractions carried out in the logarithmic domain. Hence the complexity of the STBC decoder is significantly reduced, while closely matching the performance of the MAP algorithm. In our following discussions, the decoding complexity of the space-time bock codes is considered to be sufficiently low for it to be ignored for the sake of simplifying our comparisons. This will not affect our conclusions, since we will show in the rest of this section that the LDPC-assisted G_2 code, which has the lowest decoding complexity among all the space-time block codes of Table 3.1, gives the best performance as seen in Figures 3.21, 3.22 and 3.23. Hence, even if the decoding complexity of the space-time block codes is considered, the G_2 code will still be superior to the other STBCs in the context of the coding gain versus complexity performance.

The decoding complexity per information bit per iteration of the LDPC codes can be calculated as follows [434]:

$$comp\{LDPC\} = \left(\frac{5-R}{1-R}\right) \cdot j^2, \tag{3.30}$$

where R is the LDPC code's code rate and j is the column weights of the parity check matrix. In our system the value of column weights was fixed to 3, thus Equation (3.30) is simplified to:

$$comp\{LDPC\} = \left(\frac{45-9R}{1-R}\right). \tag{3.31}$$

According to Equation (3.31), the decoding complexity is essentially based on the code rate of the LDPC code employed. Thus for the rate 1/3, 1/2, 2/3 and 3/4 LDPC codes used in our system, the associated decoding complexity per bit per iteration becomes 63, 81, 117 and 153 additions and subtractions, respectively, as summarized in Table 3.5.

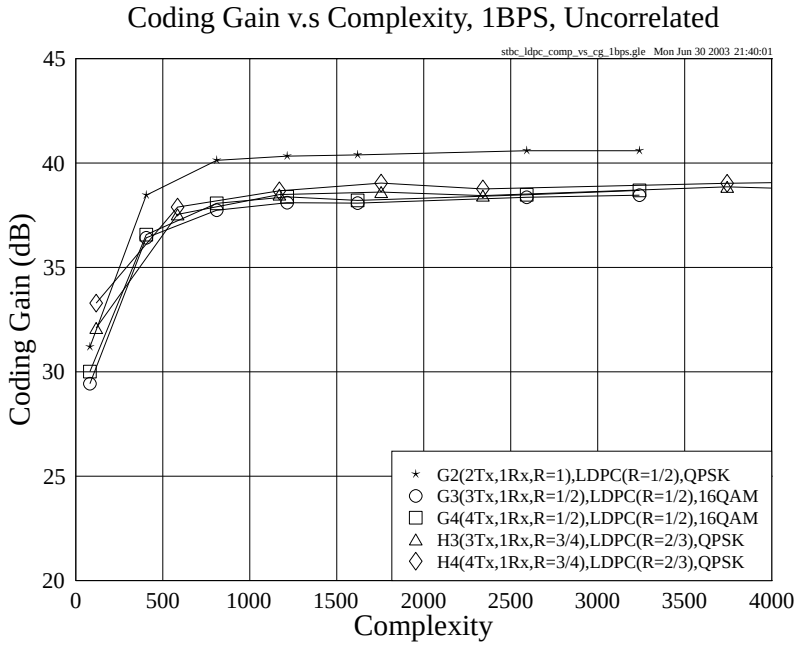

Figure 3.21: Coding gain versus estimated complexity for the LDPC-STBC coded concatenated schemes using one receiver, when communicating over uncorrelated Rayleigh fading channels at the effective throughput of **1 BPS**. The simulation parameters are given in Table 3.3.

Let us now compare the coding gain versus complexity characteristics of the different schemes considered, as seen from Figures 3.21 to 3.23, where the parameters used are given in Table 3.3. The coding gain here is defined as the E_b/N_0 difference, expressed in terms of decibels, at a BER of 10^{-5} between the various channel codes assisted space-time block coded systems and the uncoded single-transmitter systems having the same throughput. All the estimated implementational complexities were calculated based on Equation (3.31), using different number of iterations ranging from 1 to 40 with a step of about 5.

At an effective throughput of 1 and 2 BPS, as seen in Figures 3.21 and 3.22, it was found that the best scheme was the half-rate LDPC-coded G_2 space-time code. In the scenario of having an effective throughput of 3 BPS, the performance curves of the half-rate and $\frac{3}{4}$-rate LDPC-coded G_2 space-time code are close to each other, although the former performs slightly better. We may also note that the coding gain increases dramatically in the low-complexity range

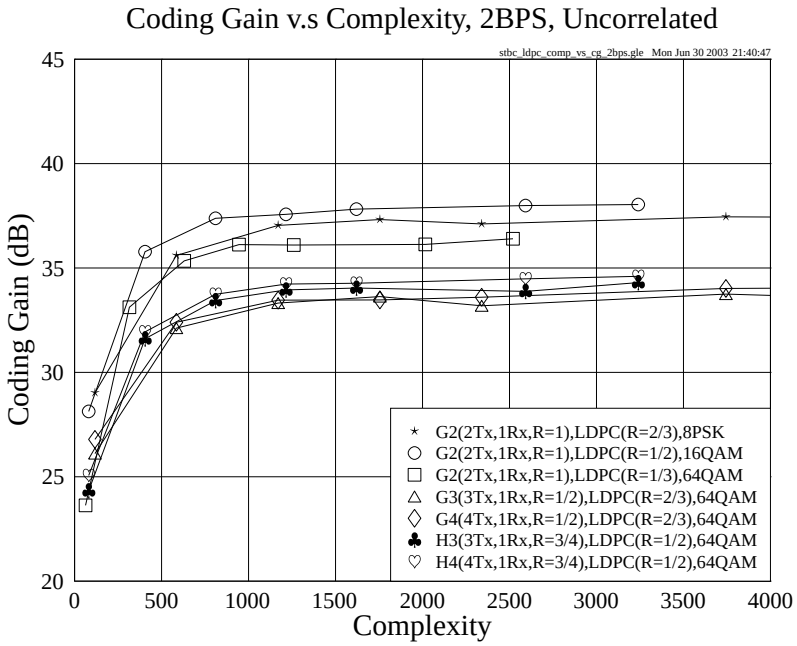

Figure 3.22: Coding gain versus estimated complexity for the LDPC-STBC coded concatenated schemes using one receiver, when communicating over uncorrelated Rayleigh fading channels at the effective throughput of **2 BPS**. The simulation parameters are given in Table 3.3.

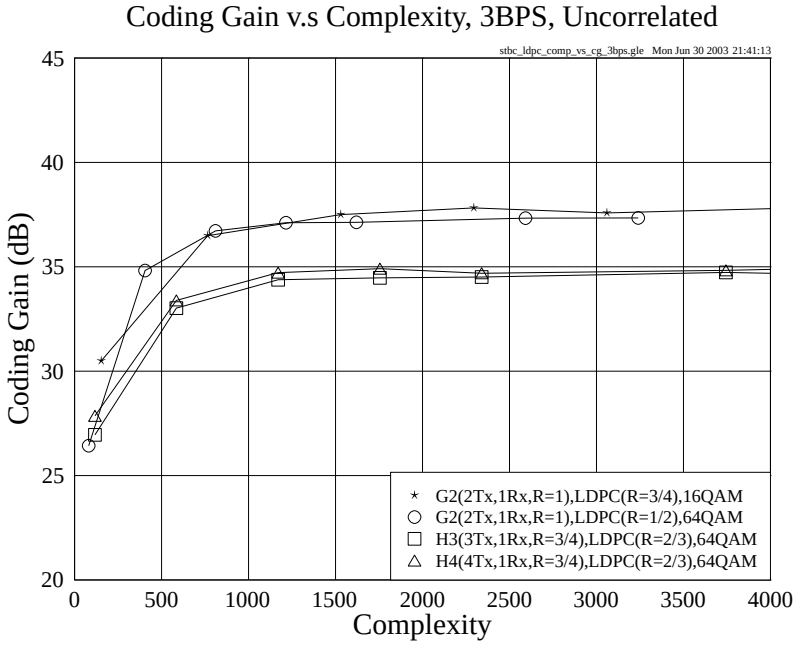

Figure 3.23: Coding gain versus estimated complexity for the LDPC-STBC coded concatenated schemes using one receiver, when communicating over uncorrelated Rayleigh fading channels at the effective throughput of **3 BPS**. The simulation parameters are given in Table 3.3.

and tends to saturate in the vicinity of an estimated complexity of about 1200, which corresponds to approximately 19, 15, 10 and 8 iterations for the LDPC codes having a code rate of $\frac{1}{3}$, $\frac{1}{2}$, $\frac{2}{3}$ and $\frac{3}{4}$, respectively. As Figure 3.24 shows, for example, when the number of iterations is increased to about 10 in terms of the half-rate LDPC-aided G_2 code, the performance is already close to the achievable maximum coding gain. This result can be considered as a rule of thumb for setting the number of iterations for the LDPC-STBC coded concatenated schemes, when aiming for a good tradeoff in terms of the achievable performance-to-complexity relationships.

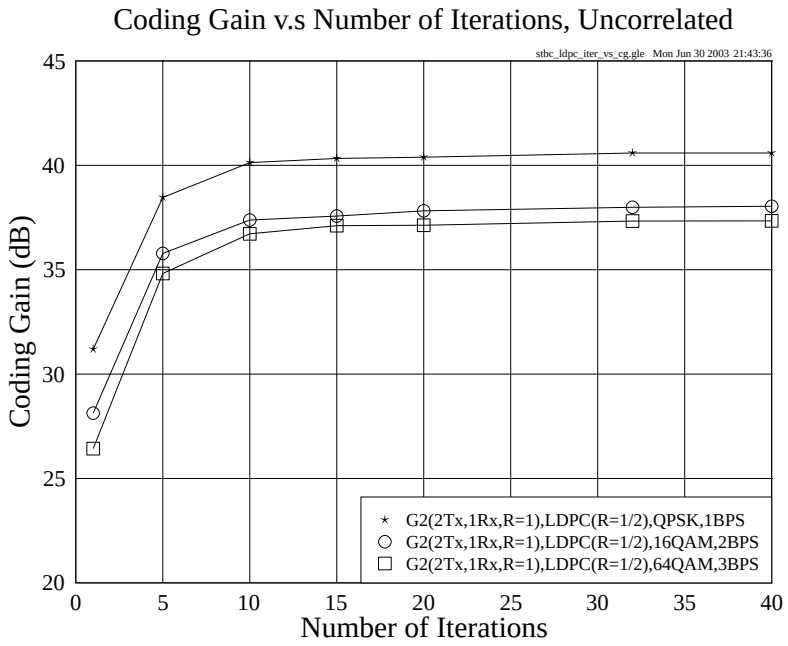

Figure 3.24: Coding gain versus the number of iterations for the half-rate LDPC-assisted G_2 space-time block coded schemes using one receiver, when communicating over uncorrelated Rayleigh fading channels at the effective throughput of 1, 2 and 3 BPS. The parameters used are given in Table 3.3.

In Figure 3.25, we show the E_b/N_0 value required for maintaining a BER of 10^{-5} versus the effective throughput BPS for the unprotected space-time block codes and the half-rate LDPC-assisted G_2 code, while the associated simulation parameters are summarized in Tables 3.1 and 3.3. The simulation results were obtained using one receiver for communicating over uncorrelated Rayleigh fading channels. It can be observed in Figure 3.25 that the E_b/N_0 value required for maintaining a BER of 10^{-5} increases near-linearly, as the effective BPS throughput increases. This conclusion was valid for both the unprotected STBC-aided schemes and for the half-rate LDPC-assisted G_2 coded scheme. Furthermore, the half-rate LDPC-G_2 concatenated scheme achieves a gain of about 15dB over the best unprotected STBC scheme at the effective throughput values of 1, 2 and 3 BPS, respectively.

3.3.1.4 Conclusions

Having studied Figures 3.13 to 3.19, we may arrive at the following conclusions. First of all, as expected, the LDPC-aided STBC-coded schemes perform significantly better than the unprotected STBC schemes, when transmitting over uncorrelated Rayleigh fading channels. However, over correlated Rayleigh fading channels the performance improvements achieved by the LDPC codes are not as significant as in uncorrelated Rayleigh fading channels, as seen in Figures 3.17 to 3.20. This is because the LDPC codes suffer from their finite codeword length and for a limited tolerable channel interleaver delay, as evidenced by Figure 3.11. This affects the attainable performance of the LDPC-STBC coded concatenated system to some degree. If we use an extremely long codeword or employ a long channel interleaver, however, the achievable performance of the LDPC-STBC concatenated schemes can be improved in the context of correlated Rayleigh fading channels.

Another observation inferred from Figures 3.13 to 3.19 is that when the number of receiver antennas is increased, most of the attainable diversity gain has already been achieved by the LDPC-G_2 coded concatenated schemes. Hence, the employment of a space-time block code using more transmitter antennas will introduce a higher-throughput modulation mode, which in turn will require an increased E_b/N_0 value and hence degrades the achievable performance.

Furthermore, in the context of uncorrelated Rayleigh fading channels and using a specific modulation scheme,

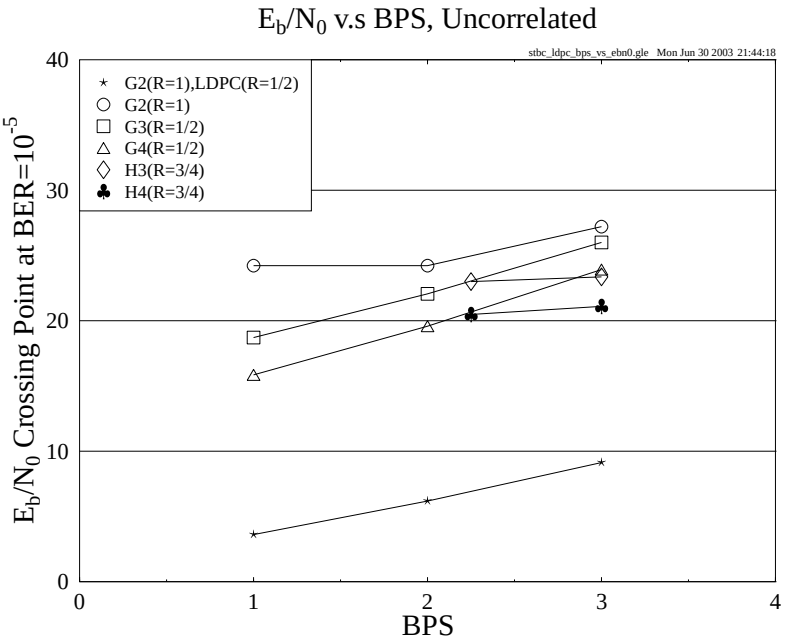

Figure 3.25: The E_b/N_0 value required for maintaining BER=10^{-5} versus the effective BPS throughput for the space-time block codes of Table 3.1 and for the half-rate LDPC-assisted G_2 code of Table 3.3, when using one receiver and communicating over uncorrelated Rayleigh fading channels.

the LDPC-STBC coded system's performance is mainly decided by the code-rate and error correction capability of the LDPC code employed, instead of the space-time codes' diversity order. In this case, using a lower-rate LDPC code will achieve a more substantial performance improvement than increasing the number of transmitters and the associated diversity gain. On the other hand, if the same LDPC code is employed, the throughput of the modulation scheme has more influence on the system's performance than the diversity order. In other words, the benefits brought about by the employment of low-throughput modulation schemes will be more substantial than that offered by a high-order space-time block code, provided that both schemes are assisted by the same LDPC code. The reason behind this phenomenon is that when the higher-order STBC codes are used in conjunction with a high number of antennas, more vulnerable high-throughput modulation schemes have to be used, for the sake of maintaining the same effective throughput. Therefore the employment of the latter scenario would result in performance degradations. In summary, the best candidate schemes are the ones using the LDPC-aided G_2 code when communicating over uncorrelated Rayleigh fading channels. When using the same space-time block code, the complexity of the STBC code can be ignored during our comparisons.

Another useful conclusion can be drawn from Figure 3.24. As seen in the figure, the coding gains of the LDPC-aided schemes tend to remain unimproved, even if the affordable complexity increases to a certain degree, although the validity of this statement depends on the specific choice of the LDPC code used. This result assists us in deciding on the appropriate number of iterations to be used by the LDPC-STBC concatenated schemes, so that the achievable best possible performance-to-complexity tradeoff can be achieved.

Before concluding this section, we summarize the achievable performance of the different schemes used in our various candidate systems communicating over uncorrelated Rayleigh fading channels in Table 3.5. For the scenarios of having an effective throughput of 1, 2 and 3 BPS, respectively, the corresponding bold numbers denote the best scheme based on the criterion of achieving the best coding gain versus complexity tradeoff, as seen in Figures 3.21, 3.22 and 3.23. As a result, the half-rate LDPC-coded space-time block code G_2 was found to be the best scheme in the scenarios having an effective throughput of 1 and 2 BPS, while the $\frac{3}{4}$-rate LDPC-coded G_2 code performs best in the scenario of having an effective throughput of 3 BPS.

3.3.2 LDPC-Aided and TC-Aided Space-Time Block Codes

In Section 3.3.1, we have studied the performance of various LDPC-aided space-time block coded systems. It has been found that the LDPC codes considerably improve the STBC-coded system's performance over uncorrelated Rayleigh fading channels. However, besides LDPC channel codes, the space-time block codes can also be concatenated with

BPS	STBC Code	LDPC Rate	LDPC *Compl.*	E_b/N_0 (dB) BER 10^{-3}	E_b/N_0 (dB) BER 10^{-5}	Gain (dB) BER 10^{-3}	Gain (dB) BER 10^{-5}	Modem
1.00	Uncoded	-	-	24.22	44.00	0.00	0.00	BPSK
	G_4	-	-	10.10	15.85	14.12	28.15	QPSK
	G_2	1/2	81	**2.99**	**3.61**	**21.23**	**40.39**	QPSK
	G_3	1/2	81	5.17	5.92	19.05	38.08	16QAM
	G_4	1/2	81	4.95	5.79	19.27	38.21	16QAM
	H_3	2/3	117	4.65	5.56	19.57	38.44	QPSK
	H_4	2/3	117	4.41	5.24	19.81	38.76	QPSK
2.00	Uncoded	-	-	24.22	44.00	0.00	0.00	QPSK
	G_4	-	-	13.61	19.58	10.61	24.42	16QAM
	G_2	2/3	117	6.05	6.89	18.17	37.11	8PSK
	G_2	1/2	81	**5.45**	**6.18**	**18.77**	**37.82**	16QAM
	G_2	1/3	63	7.10	7.90	17.12	36.10	64QAM
	G_3	2/3	117	9.65	10.81	14.57	33.19	64QAM
	G_4	2/3	117	9.34	10.40	14.88	33.60	64QAM
2.25 $\approx$ 2.00	H_3	1/2	81	9.20	9.96	15.02	34.04	64QAM
	H_4	1/2	81	9.02	9.73	15.20	34.27	64QAM
3.00	Uncoded	-	-	26.30	46.26	0.00	0.00	8PSK
	H_4	-	-	14.87	21.10	11.43	25.16	16QAM
	G_2	3/4	153	**7.73**	**8.68**	**18.57**	**37.58**	16QAM
	G_2	1/2	81	8.33	9.13	17.97	37.13	64QAM
	H_3	2/3	117	10.85	11.75	15.45	34.51	64QAM
	H_4	2/3	117	10.58	11.57	15.72	34.69	64QAM

Table 3.5: Coding gains of the LDPC-STBC coded concatenated schemes using one receiver, when communicating over uncorrelated Rayleigh fading channels. With reference to Figures 3.21, 3.22 and 3.23, the performance of the best scheme is printed in bold for the scenarios of having different effective throughputs, respectively.

a range of other channel codes, such as Convolutional Codes (CC), Turbo Convolutional (TC) codes [423, 424], Turbo Bose-Chaudhuri-Hocquenghem (TBCH) codes [435], etc. The performance of these various channel-coded G_2 schemes designed for transmission over uncorrelated Rayleigh fading channels has been studied in [359], where the best scheme found was the half-rate TC(2,1,4) code in conjunction with the space-time block code G_2. Hence, in this section, we will compare the performance of the best LDPC-STBC coded concatenated scheme found in Section 3.3.1.2, namely that of the half-rate LDPC-aided G_2 code, with the half-rate TC(2,1,4)-aided space-time block coded schemes.

3.3.2.1 System Overview

In 1993, Berrou *et al.* [423, 424] proposed a novel channel code, referred to as a turbo code. As detailed in [359], the turbo encoder consists of two component encoders. Generally, convolutional codes are used as the component encoders and the corresponding turbo codes are termed here as TC codes. For a TC(n, k, K) code, the three parameters n, k and K have the same meaning as in a convolutional code CC(n, k, K), where k is the number of input bits, n is the number of coded bits and K is the constraint length of the code. More details about TC codes can be found in [359]. The schematic of our experimental system, where the half-rate TC(2,1,4) code is employed, is given in Figure 3.26.

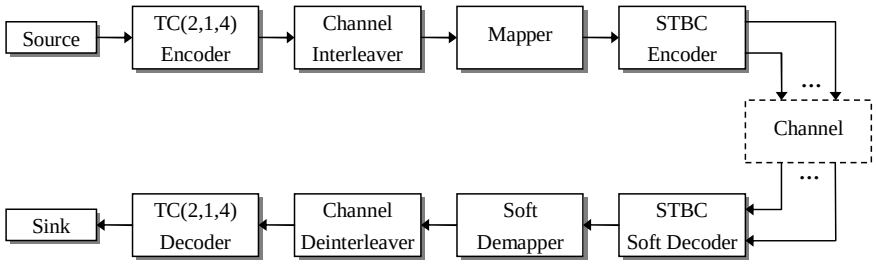

Figure 3.26: Overview of the space-time block coded and TC(2,1,4) channel coded system.

The source bits are first encoded by the half-rate TC(2,1,4) encoder. The Log-MAP decoding algorithm [359] is utilized for iterative turbo decoding, since it operates in the logarithmic domain and thus significantly reduces the computational complexity imposed by the MAP algorithm [428]. The number of turbo iterations is set to eight, since this yields a performance close to the achievable performance associated with an infinite number of iterations. The TC-encoded bits will be interleaved by the channel interleaver, as seen in Figure 3.26. In this case, a random interleaver having a depth of about 20,000 is used. The interleaved bits will then be forwarded to the mapper, followed by the STBC encoder. At the receiver side, the corresponding inverse operations are invoked, as seen in Figure 3.26. The simulation parameters of the TC-STBC coded concatenated system are given in Table 3.6.

BPS	STBC		TC(2,1,4)						Modem
	Code	Code Rate	Random Turbo Interleaver Depth	Random Channel Interleaver Depth	Code Rate	Puncturing Pattern	Iterations	Total *Compl.*	
1.00	G_2	1	10000	20000	1/2	10,01	8	2576	QPSK
	G_3	1/2	10000	20000	1/2	10,01	8	2576	16QAM
	G_4	1/2	10000	20000	1/2	10,01	8	2576	16QAM
2.00	G_2	1	10000	20000	1/2	10,01	8	2576	16QAM
3.00	G_2	1	10002	20004	1/2	10,01	8	2576	64QAM

Table 3.6: The parameters used in the TC(2,1,4)-STBC coded concatenated schemes.

3.3.2.2 Complexity Issues

For the sake of fair comparisons, we should calculate and take into account the complexity of the LDPC and TC(2,1,4) codes. The total estimated complexity of the TC codes per information bit per iteration in terms of additions and subtractions to be carried out is [436]:

$$comp\left\{TC\left(n,1,K\right)\right\} = 40\left(2^{K-1}\right) + 12n - 22. \tag{3.32}$$

According to Equation (3.32), the complexity of the TC(2,1,4) code is 322 per information bit per iteration. Since the number of iterations has been set to eight, the total complexity of the TC(2,1,4) code per bit is $322 \times 8 = 2576$ in the context of additions and subtractions, as shown in Table 3.6.

On the other hand, the complexity of the LDPC codes per information bit per iteration can be calculated according to Equation (3.31). Therefore, we can multiply the result of Equation (3.31) with the appropriately selected number of iterations required by the different-rate LDPC codes, so that a similar complexity per bit is used for both the LDPC codes and for the TC(2,1,4) code. For the half-rate LDPC-coded G_2 scheme, the number of iterations was set to 32 so that the total complexity becomes $81 \times 32 = 2592$, which is close to the estimated complexity of 2576 encountered by the TC(2,1,4) scheme. The parameters of the LDPC-G_2 coded concatenated scheme used in this new scenario are given in Table 3.7.

BPS	STBC		LDPC						Inter-leaver Depth	Modem
	Code	Code Rate	Code Rate	Input Bits Block Size	Output Bits Block Size	Column Weight	Iter-ations	Total *Compl.*		
1.00	G_2	1	1/2	10000	20000	3	32	2592	20000	QPSK
2.00	G_2	1	1/2	10000	20000	3	32	2592	20000	16QAM
3.00	G_2	1	1/2	10002	20004	3	32	2592	20004	64QAM

Table 3.7: The parameters used in the LDPC-G_2 coded concatenated schemes invoked for comparison with the TC(2,1,4)-G_2 coded concatenated schemes.

3.3.2.3 Simulation Results

In this section, the performance of the LDPC- and TC-aided space-time block coded schemes communicating over uncorrelated Rayleigh fading channels will be studied and compared. The parameters of the space-time block codes, the half-rate TC(2,1,4) code and the LDPC codes are given in Tables 3.1, 3.6 and 3.7, respectively. The simulation results are based on the same assumptions which were outlined in Section 3.2.4 on page 66.

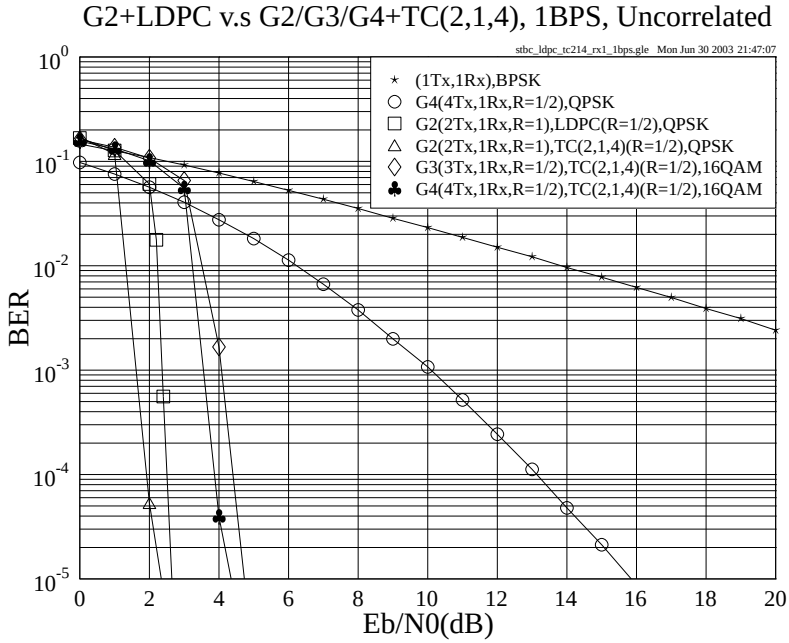

Figure 3.27: The BER versus E_b/N_0 performance of the $\mathbf{G_2}$, $\mathbf{G_3}$ and $\mathbf{G_4}$ space-time block codes of Table 3.1 in conjunction with the LDPC codes of Table 3.7 or the half-rate TC(2,1,4) code of Table 3.6 at an effective throughput of **1 BPS** using one receiver over uncorrelated Rayleigh fading channels.

Figure 3.27 compares the performance of the candidate schemes using the parameters summarized in Tables 3.6 and 3.7 operating at an effective throughput of 1 BPS over uncorrelated Rayleigh fading channels. For the half-rate TC(2,1,4) coded scheme combined with the half-rate G_3 and G_4 codes, the 16QAM modem is used for maintaining a throughput of 1 BPS. As seen in Figure 3.27, the TC(2,1,4)-aided G_2 code outperforms the others. However, at the BER of 10^{-5}, it only provides an approximately 0.1dB gain over the LDPC-aided G_2 code, which is the best LDPC-STBC coded concatenated scheme according to Table 3.5. It is also observed that the schemes in which the G_3 and G_4 codes are employed exhibit an inferior performance in comparison to their G_2-code based counterpart as well as in comparison to the LDPC-aided scheme, because the more densely-packed 16QAM phasor constellation is used.

Figure 3.28 compares the performance of the candidate schemes using the parameters summarized in Tables 3.6

and 3.7 operating at an effective throughput of 2 and 3 BPS over uncorrelated Rayleigh fading channels. As suggested by Figure 3.28, the TC(2,1,4)-aided schemes perform slightly better, than the LDPC-aided schemes providing an approximately 0.1dB and 0.4dB gain at the BER of 10^{-5} in the scenarios of having a throughput of 2 and 3 BPS, respectively.

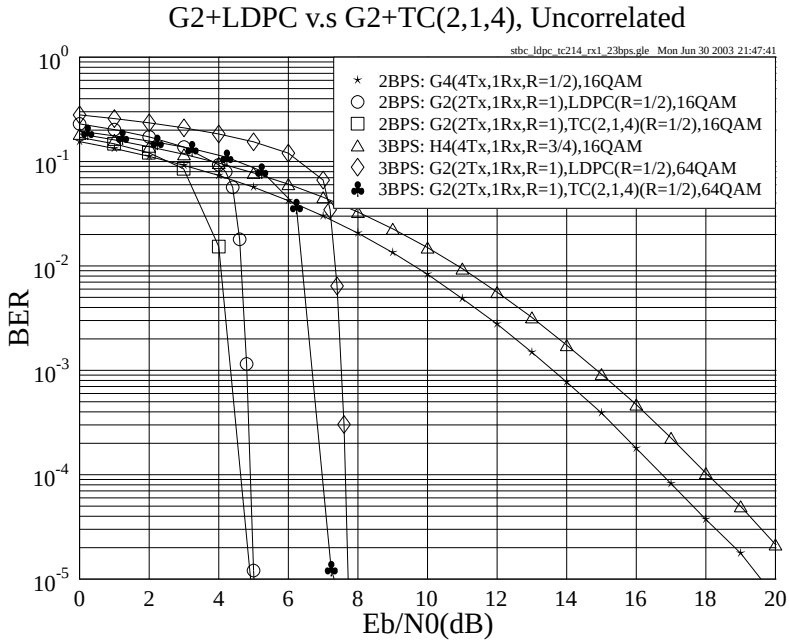

Figure 3.28: The BER versus E_b/N_0 performance of the $\mathbf{G_2}$ space-time block code of Table 3.1 in conjunction with the LDPC codes of Table 3.7 or the half-rate TC(2,1,4) code of Table 3.6 at an effective throughput of **2** and **3 BPS** using one receiver over uncorrelated Rayleigh fading channels.

In Figure 3.29 the achievable coding gain versus complexity is characterized. The coding gains were recorded at the BER of 10^{-5}, as presented in Section 3.3.1.3. From Figure 3.29, we infer that the curves associate with the TC(2,1,4) code are close to those of the LDPC codes, although the former ones perform slightly better than the latter ones in the context of having the same effective throughput of 1, 2 and 3 BPS, respectively. However, in the low complexity range, namely in the complexity range spanning from 0 to 600, the LDPC codes perform better than the TC(2,1,4) code. On one hand, the achievable lowest complexity of the half-rate TC(2,1,4) code is 322, which is attained when the number of iterations is set to one, while the LDPC codes are capable of providing an even lower complexity down to 81, again, as seen in Figure 3.29. On the other hand, for the LDPC schemes, the achievable coding gain dramatically increases, when the affordable complexity is increased within the range spanning from 0 to about 600. Therefore, the employment of the LDPC-aided schemes may be more attractive in scenarios, where the affordable complexity is the most important concern, while the system's performance does not necessarily have to be the best.

3.3.2.4 Conclusions

In Section 3.3.2.3 we have presented a range of performance comparisons in the context of the attainable coding gain versus complexity for the various TC(2,1,4)-STBC and the LDPC-STBC coded concatenated schemes for transmission over uncorrelated Rayleigh fading channels. As a conclusion, the TC(2,1,4)-assisted space-time block code G_2 outperforms its LDPC-assisted counterparts for all the three scenarios having different effective throughputs. However, it was found that the associated performance difference is insignificant, namely less than 0.3dB. Furthermore, the LDPC-STBC coded concatenated schemes considered may be preferred for employment in systems, where the severity of complexity constraint outweighs the importance of achieving the highest possible performance.

Finally, the performance of the different schemes studied is summarized in Table 3.8. All the results were generated using a single receiver, when communicating over uncorrelated Rayleigh fading channels. The performance of the best scheme at the effective throughputs of 1, 2 and 3 BPS is printed in bold, respectively.

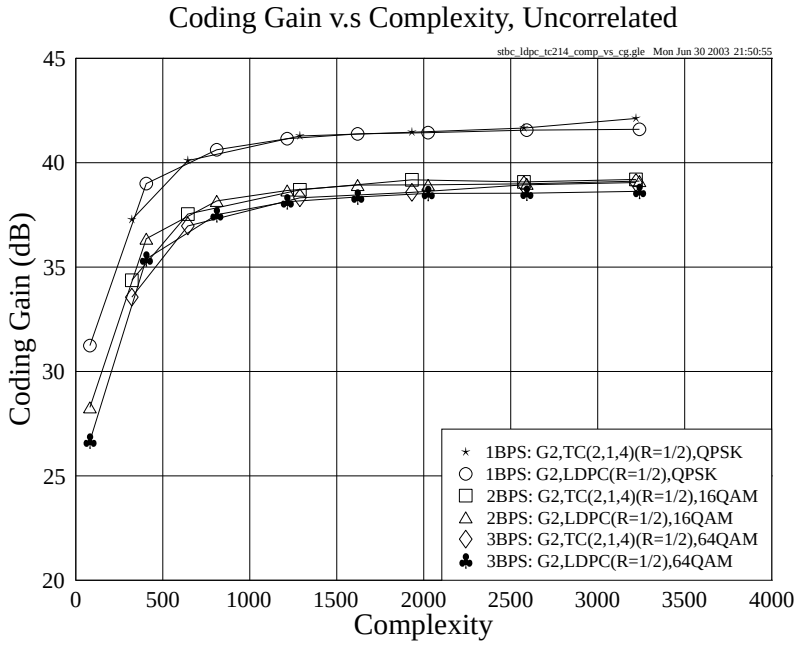

Figure 3.29: Coding gain versus complexity for the LDPC-G_2 concatenated arrangements and for the TC(2,1,4)-G_2 concatenated schemes using one receiver for communicating over uncorrelated Rayleigh fading channels. The associated parameters are given in Tables 3.6 and 3.7.

BPS	STBC Code	LDPC Rate	TC(2,1,4) Rate	E_b/N_0 (dB) BER 10^{-3}	E_b/N_0 (dB) BER 10^{-5}	Gain (dB) BER 10^{-3}	Gain (dB) BER 10^{-5}	Modem
1.00	Uncoded	-	-	24.22	44.00	0.00	0.00	BPSK
	G_4	-	-	10.10	15.85	14.12	28.15	QPSK
	G_2	1/2	-	2.36	2.44	21.86	41.56	QPSK
	G_2	-	1/2	**1.62**	**2.34**	**22.60**	**41.66**	QPSK
	G_3	-	1/2	4.07	4.73	20.15	39.27	16QAM
	G_4	-	1/2	3.55	4.35	20.67	39.65	16QAM
2.00	Uncoded	-	-	24.22	44.00	0.00	0.00	QPSK
	G_4	-	-	13.61	19.58	10.61	24.42	16QAM
	G_2	1/2	-	4.81	5.01	19.41	38.99	16QAM
	G_2	-	1/2	**4.34**	**4.92**	**19.88**	**39.08**	16QAM
3.00	Uncoded	-	-	26.30	46.26	0.00	0.00	8PSK
	H_4	-	-	14.87	21.10	11.43	25.16	16QAM
	G_2	1/2	-	7.52	7.72	18.78	38.54	64QAM
	G_2	-	1/2	**6.68**	**7.32**	**19.62**	**38.94**	64QAM

Table 3.8: Coding gains of the LDPC-STBC concatenated schemes and the TC(2,1,4)-STBC concatenated schemes using one receiver for communicating over uncorrelated Rayleigh fading channels. For the scenarios having different effective throughputs, the performance of the best scheme is printed in bold.

3.4 Channel Coding Aided Space-Time Block Coded OFDM

In Section 3.3, we have investigated various LDPC channel coding assisted space-time block coded schemes communicating over narrowband fading channels, followed by the performance study of LDPC-aided and TC-aided STBC schemes. Naturally, a range of channel codes can also be combined with the family of space-time block codes for the sake of improving the system's performance. In this section, various Coded Modulation (CM) [359] assisted STBC schemes will be studied for transmission over multipath Rayleigh fading channels. Specifically, Trellis-Coded Modulation (TCM) [359, 437], Turbo Trellis-Coded Modulation (TTCM) [359, 438], Bit-Interleaved Coded Modulation (BICM) [359, 439] and iterative joint decoding and demodulation assisted BICM (BICM-ID) [359, 440] will be investigated. Furthermore, the above CM-assisted STBC aided schemes will be studied in the context of a single-user Orthogonal Frequency Division Multiplexing (OFDM) [3–6] system. As a well-established technique, OFDM has exhibited a number of advantages over more traditional multiplexing techniques, and has been adopted for both Digital Audio and Video Broadcasting (DAB and DVB) in Europe. It has also been selected as the IEEE 802.11 standards for Wireless Local Area Network (WLAN). Let us now embark on the investigation of the CM-assisted space-time coded single-user OFDM system.

3.4.1 Coded Modulation Assisted Space-Time Block Codes

Since the signal bandwidth available for wireless communications is limited, one of the most important objectives in the design of digital mobile systems is to make the most of the attainable bandwidth, for example with the aid of the CM schemes.

3.4.1.1 Coded Modulation Principles

The basic principle of CM [359] is that we attach a parity bit to each uncoded information symbol formed by m information bits according to the specific modulation scheme used, hence doubling the number of constellation points to 2^{m+1} compared to that of 2^m in the original modem constellation. This is achieved by extending the modulation constellation, rather than expanding the required bandwidth, while maintaining the same effective throughput of m bits per symbol, as in the case of no channel coding. In other words, the signalling rate remains the same, since the redundant parity bit can be absorbed by the expansion of the constellation. Therefore, when the achievable coding gain of the CM scheme becomes higher than the E_b/N_0 degradation imposed by the more vulnerable higher-order modulation scheme employed, a useful effective coding gain can be achieved.

Among the various CM schemes, TCM [437] was originally designed for transmission over Additive White Gaussian Noise (AWGN) channels. TTCM [438] is a more recent joint coding and modulation scheme which has a structure similar to that of the family of binary turbo codes, but employs TCM schemes as component codes. Both TCM and TTCM employ set partitioning based constellation mapping [359], while using symbol-based turbo interleavers and channel interleavers. Another CM scheme referred to as BICM [439], invokes bit-based channel interleavers in conjunction with gray constellation mapping. Furthermore, iteratively decoded BICM [440] using set partitioning was also proposed. More details about the various CM schemes used can be found in [359]. In this section, we will mostly focus on the performance of the proposed CM-assisted STBC coded OFDM schemes communicating over wideband Rayleigh fading channels.

3.4.1.2 Inter-Symbol Interference and OFDM Basics

If the modulation bandwidth exceeds the coherence bandwidth of the channel, Inter-Symbol Interference (ISI) will be introduced and the consecutive transmitted symbols are distorted, since the past and current symbols of the signals are overlapped. Hence, at the receiver, channel equalizers have to be employed for the sake of removing the effects of ISI [359].

An alternative way of mitigating the effects of ISI is to employ OFDM, which effectively mitigates the detrimental effects of the frequency-selective fading, when transmitting over high-rate wideband channels. The basic principle of OFDM is to split a high-rate data stream into a number of low-rate streams which are transmitted simultaneously over a number of subcarriers. Hence the symbol duration is rendered longer for each of the parallel subcarriers, and thus the relative effects of imposed by the multipath channel's delay spread is reduced. In other words, since the system's data throughput is the sum of all the parallel sub-channels' throughputs, the data rate per sub-channel is only a small fraction of the total data rate of a conventional single-carrier system having the same throughput. This results

in the phenomenon that the symbol duration becomes significantly longer than the channel's impulse response, thus it has the potential to disperse with channel equalization. Specifically, if an appropriate-duration cyclic OFDM symbol extension is selected, the ISI between consecutive OFDM symbols can be almost completely eliminated. Furthermore, for a given delay spread, the implementation complexity of an OFDM modem may be significantly lower than that of a single carrier system employing an equalizer [6].

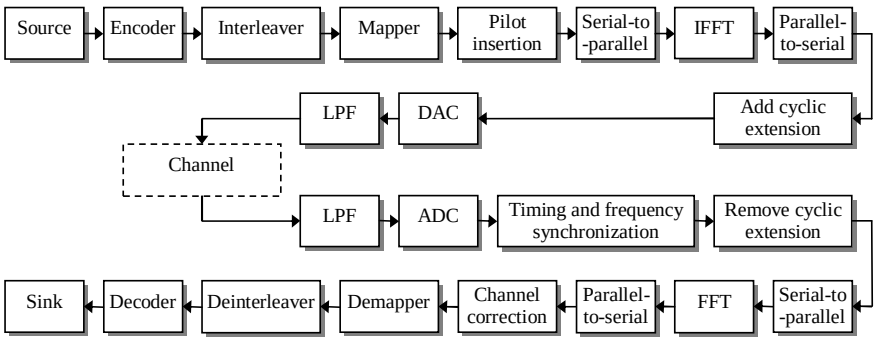

Figure 3.30: Schematic diagram of an OFDM modem.

The schematic of an OFDM modem is shown in Figure 3.30. The source bit stream is first encoded by a STBC or channel encoder and forwarded to the interleaver and the mapper, where the bits are interleaved and may be mapped to non-binary symbols. Some pilot subcarriers may be inserted for the sake of assisting the estimation of the channel's frequency-domain transfer function, which is required for the receiver to counteract the effects of the channel's frequency-domain fading. The serial data stream is then converted into a parallel symbol sequence and forwarded to the Inverse Fast Fourier Transform (IFFT) modulator for the sake of forming the time-domain modulated signal. Again, in order to eliminate the ISI between consecutive OFDM symbols a cyclic extension has to be added to each OFDM symbol. Then the Digital-to-Analogue Converter (DAC) converts the cyclically extended OFDM signal to the analogue domain, which is finally filtered by a Low-Pass Filter (LPF) and transmitted through the wideband channel. At the receiver side, the Analogue-to-Digital Converter (ADC) converts the LPF-filtered received signal to the digital domain, where symbol timing and frequency synchronization are the first processing steps [6]. Then the cyclic extension attached to each OFDM symbol is removed and the recovered signal is forwarded to the Fast Fourier Transform (FFT) based demodulator, whose output will be processed by the pilot-based frequency-domain channel equalizer in order to compensate the frequency-domain fading imposed by the channel. After symbol-demapping and deinterleaving the received signal is finally passed to the space-time or channel decoder, which outputs the decoded information bits.

3.4.1.3 System Overview

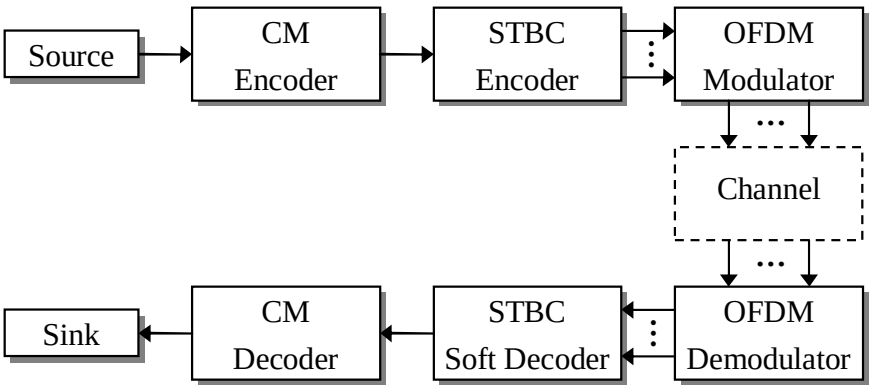

Figure 3.31: Schematic diagram of the proposed CM-assisted space-time block coded OFDM system.

Figure 3.31 shows the schematic of the CM-assisted space-time block coded OFDM system investigated [5, 359]. As observed in Figure 3.31, the source information bits are first encoded and modulated by the CM encoder followed by the space-time encoder. In our schemes, the space-time block code employed was the G_2 code of Table 3.1,

which invokes two transmitter antennas, and the two space-time coded samples are mapped to two consecutive OFDM subcarriers and OFDM modulated. Then the frequency-domain symbols are converted to time-domain OFDM symbols by the IFFT-based modulator and the cyclic extension is appended to each individual OFDM symbol. The OFDM symbols are then transmitted via the multipath fading channel, and the received noise-contaminated symbols are forwarded to the OFDM demodulator, where the FFT operation will be employed for converting the channel-impaired time-domain symbols to their frequency-domain counterparts. The recovered signal is then space-time soft-decoded and the soft outputs are fed to the CM decoder for recovering the most-likely transmitted information bits.

3.4.1.3.1 Complexity Issues

In order to compare the different candidate schemes under fair conditions, we chose the system parameters so that the decoding complexity of the various CM schemes employed became similar. The complexity imposed by the STBC codec was neglected, since the same G_2 space-time block code was used for all the CM-STBC concatenated schemes.

The symbol-based Log-MAP decoder [359] is utilized in all the CM schemes considered in our system, namely in the TCM, TTCM, BICM and BICM-ID codecs, for the sake of reducing the computational complexity imposed by the MAP algorithm [359]. Therefore, the multiplication and and addition operations are substituted by additions and by the Jacobian sum operations [428] carried out in the logarithmic domain, respectively. As a result, in terms of the number of additions and subtractions, the total decoding complexity per bit per iteration for the TTCM scheme studied is as follows [434]:

$$comp\{TTCM\} = \frac{10M\left(2^{\nu+1}-1\right)}{m}, \tag{3.33}$$

where m is the number of information bits in a coded information symbol, $M = 2^m$ is the number of legitimate symbols in the mapping constellation set, and ν is the code memory. For example, for the QPSK-based TTCM scheme having a code memory of $\nu = 3$, the associated complexity per bit per iteration is $\frac{10\cdot 2^1\cdot\left(2^{3+1}-1\right)}{1} = 300$, since in this case m is equal to 1. If the number of iterations is 4, the total decoding complexity per bit becomes $300 \cdot 4 = 1200$, as seen in Table 3.9. For the remaining CM schemes used, namely for TCM/BICM/BICM-ID, the corresponding decoding complexity per bit per iteration is:

$$comp\{TCM/BICM/BICM-ID\} = \frac{5M\left(2^{\nu+1}-1\right)}{m}, \tag{3.34}$$

which is half the complexity of that in Equation (3.33). The reason for this is that the TTCM scheme utilizes two Log-MAP decoders, while TCM/BICM/BICM-ID schemes only use one [359], hence the associated complexity of TTCM is doubled. The parameters used by the various CM-STBC concatenated schemes investigated are provided in Table 3.9. From the table, we may see that the total decoding complexity per bit - rather than per bit per iteration - of the four CM schemes are similar.

3.4.1.3.2 Channel Model

As mentioned earlier, we will investigate the proposed system when communicating over dispersive wideband Rayleigh fading channels. Specifically, we consider the Short Wireless Asynchronous Transfer Mode (SWATM) Channel Impulse Response (CIR) given on page 78 of [5], although the Doppler frequency may assume a range of different values. The three-tap SWATM channel is a truncated version of the five-tap Wireless Asynchronous Transfer Mode (WATM) CIR, retaining only the first three impulses [5]. This reduces the total length of the impulse response, where the last path arrives at a delay of 48.9ns, which corresponds to 11 sample periods. For our simulations each of the three paths experiences independent Rayleigh fading having the normalized Doppler frequency of $f'_d = 1.235 \times 10^{-5}$. Figure 3.32 displays the impulse response of the SWATM channel, while the associated parameters are given in Table 3.10.

For the sake of combating the effects of ISI when communicating over the multipath Rayleigh fading channel, as discussed in Section 3.4.1, we employ an OFDM modem having 512 subcarriers, while each OFDM symbol is extended by a cyclic prefix of $512/8 = 64$ time-domain samples [5]. Therefore, the length of an OFDM symbol becomes $512 + 64 = 576$ samples. Since the number of subcarriers is sufficiently high, we may assume that each OFDM subcarrier experiences narrowband channel conditions in the frequency domain.

BPS	STBC		CM							Modem
	Code	Code Rate	CM Scheme	Code Rate	Data Bits	ν	Iter-ations	Symbol-based Cw. Length	Total *Compl.*	
1.00	G_2	1	-	-	-	-	-	1024	-	QPSK
	G_2	1	TCM	1/2	1	6	-	1024	1270	QPSK
	G_2	1	TTCM	1/2	1	3	4	1024	1200	QPSK
	G_2	1	BICM	1/2	1	6	-	1024	1270	QPSK
	G_2	1	BICMID	1/2	1	3	8	1024	1200	QPSK
2.00	G_2	1	-	-	-	-	-	1024	-	8PSK
	G_2	1	TCM	2/3	2	6	-	1024	1270	8PSK
	G_2	1	TTCM	2/3	2	3	4	1024	1200	8PSK
	G_2	1	BICM	2/3	2	6	-	1024	1270	8PSK
	G_2	1	BICMID	2/3	2	3	8	1024	1200	8PSK
3.00	G_2	1	-	-	-	-	-	1024	-	16QAM
	G_2	1	TCM	3/4	3	6	-	1024	1693	16QAM
	G_2	1	TTCM	3/4	3	3	4	1024	1600	16QAM
	G_2	1	BICM	3/4	3	6	-	1024	1693	16QAM
	G_2	1	BICMID	3/4	3	3	8	1024	1600	16QAM

Table 3.9: The parameters of the various CM-assisted space-time block coded schemes. The parameters of the STBC G_2 are given in Table 3.1.

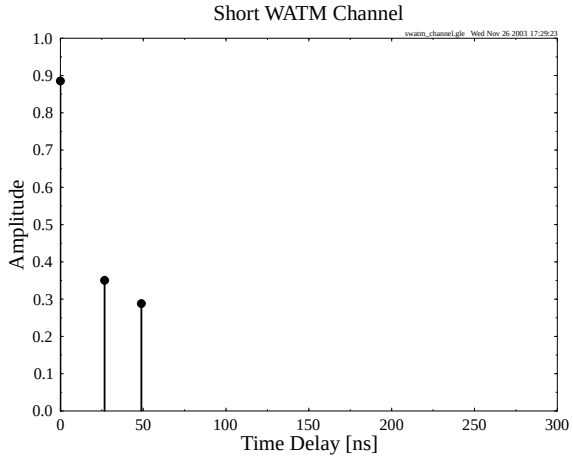

Figure 3.32: The impulse response of the SWATM channel [5]. The corresponding parameters of the channel are summarized in Table 3.10.

$1/T_s$	τ_{max}	f_d	f'_d	n	K	cp
225 MHz	48.9 ns	2278 Hz	1.235×10^{-5}	3	512	64

Table 3.10: Sampling Rate $1/T_s$, maximum path delay τ_{max}, maximum Doppler frequency f_d, normalized Doppler frequency f'_d, number of paths n, FFT length K and cyclic prefix length cp of the SWATM channel of Figure 3.32.

3.4.1.3.3 Assumptions

When the space-time block codes were employed for transmissions over uncorrelated Rayleigh fading channels, as mentioned in Section 3.2.4, we assumed that the channel was quasi-static so that its path gains remained constant across for example $n = 2$ consecutive STBC time slots for the G_2 space-time block code, corresponding to the $n = 2$ rows of the G_2 code's transmission matrix. However, in this new context we can no longer assume that the corresponding frequency-domain subcarrier gains remain identical as a consequence of the wideband channel's frequency-domain fading profile, an issue, which will be further discussed in Section 3.4.1.4. This results in a residual error floor for the unprotected G_2 space-time block coding scheme, as seen for example in Figure 3.35. For the concatenated CM-STBC schemes, however, the error floor experienced may be significantly reduced to a neglectable level.

In Section 3.4.1.4, the performance of the proposed CM-assisted space-time block coded OFDM schemes will be compared. All our simulation results achieved were based on the following assumptions:

- Each path of the multipath channel employed experiences independent Rayleigh fading;
- The average signal power received from each transmitter antenna is the same;
- The receiver has a perfect knowledge of the channels' fading amplitudes.

These assumptions simplify the simulations to a degree, therefore the system concerned is not a realistic one. However, again, since the experimental circumstances are identical for all performance comparisons, the results may be expected to adequately characterize the relative performance of the various schemes used.

3.4.1.4 Simulation Results

In this section, the performance of the CM-assisted space-time block coded OFDM system considered will be studied. The simulation parameters have been given in Table 3.9. All schemes utilized two transmitter antennas for the G_2 space-time block code and one receiver antenna. Each OFDM symbol has 512 subcarriers and a cyclic extension of 64 samples.

Performance at an effective throughput of 1 BPS Figure 3.33 shows the performance of the various CM-assisted G_2 space-time block coded OFDM schemes communicating over the SWATM channel. In our system, we employ gray-coding based constellation mapping for the BICM scheme, while using set-partitioning based constellation mapping for the TCM, TTCM and BICM-ID arrangements [359]. For the sake of achieving an effective throughput of 1 BPS, QPSK modulation is used for all the half-rate CM-assisted schemes. As seen in Figure 3.33, the CM-G_2 coded concatenated schemes perform significantly better than the unprotected G_2 scheme, achieving an E_b/N_0 gain of about 14dB at the BER of 10^{-5}. Among all the CM-assisted schemes, the TTCM-aided arrangement gives the best performance by achieving about 0.5dB to 1dB gain over the other CM-assisted schemes at the BER of 10^{-5}.

Performance at an effective throughput of 2 BPS The performance comparison of the different CM-STBC concatenated schemes having an effective throughput of 2 BPS for transmissions over the SWATM channel is shown in Figure 3.34. It is seen in Figure 3.34 that when the E_b/N_0 value encountered is relatively low, namely below about 7.5dB, the unprotected G_2 scheme performs better than the CM-assisted G_2 schemes. However, when the E_b/N_0 value experienced is higher than approximate 7.5dB, the TTCM-aided G_2 scheme outperforms all the other candidates, achieving a gain of about 1.3dB and 12.5dB over the other CM-aided G_2 schemes and over the unprotected G_2 scheme, respectively, at the BER of 10^{-5}.

Performance at an effective throughput of 3 BPS If we increase the system's effective throughput to 3 BPS, a residual BER of approximate 6×10^{-5} is observed for the performance curve of the unprotected G_2 scheme, as seen in Figure 3.35. This phenomenon can be explained as follows. In the context of the single-path uncorrelated Rayleigh fading channels mentioned in Section 3.2.4, we assumed that the channel is quasi-static so that the channel's path gains are constant across n consecutive STBC time slots. For example, we have $n = 2$ for the G_2 space-time block code, corresponding to the $n = 2$ rows of the space-time block codes' transmission matrix. In the context of wideband channels, for instance the SWATM channel of Figure 3.32, however, the channel's delay spread will have an effect on the associated frequency-domain transfer functions. More specifically, the fading amplitudes vary more rapidly, when the delay spread is increased [359]. Since the maximum delay spread of the SWATM channel is as high as $\tau_{max} = 48.9ns$, the variation of the frequency-domain fading amplitudes is so dramatic that we can no longer assume that the path gains remain constant during two consecutive STBC time slots. In this case, for the unprotected STBC schemes, the rapid variation of the channel's frequency-domain fading envelope will seriously

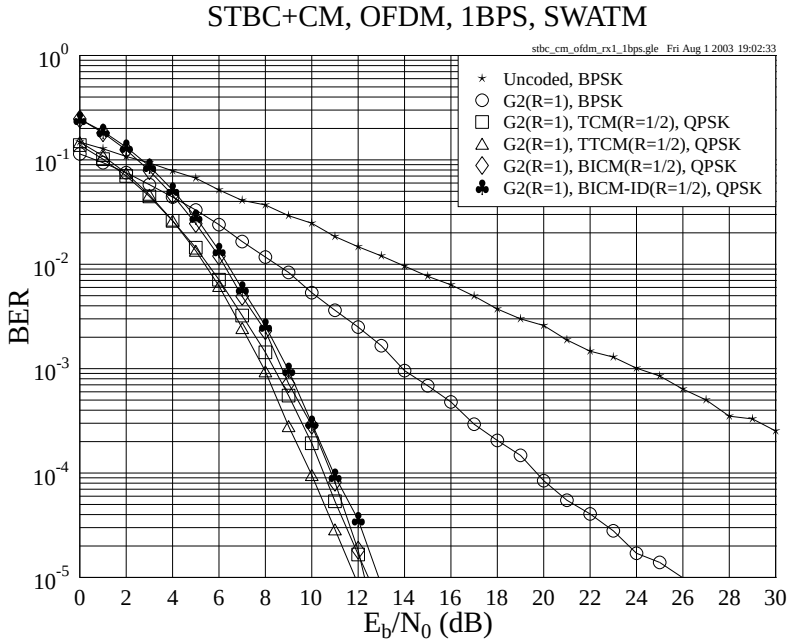

Figure 3.33: The BER versus E_b/N_0 performance of the G_2 space-time block code of Table 3.1 in conjunction with the various Coded Modulation schemes of Table 3.9 at an effective throughput of **1 BPS** using one receiver when communicating over the SWATM channel. An OFDM scheme having 512 subcarriers and a cyclic extension of 64 samples is employed.

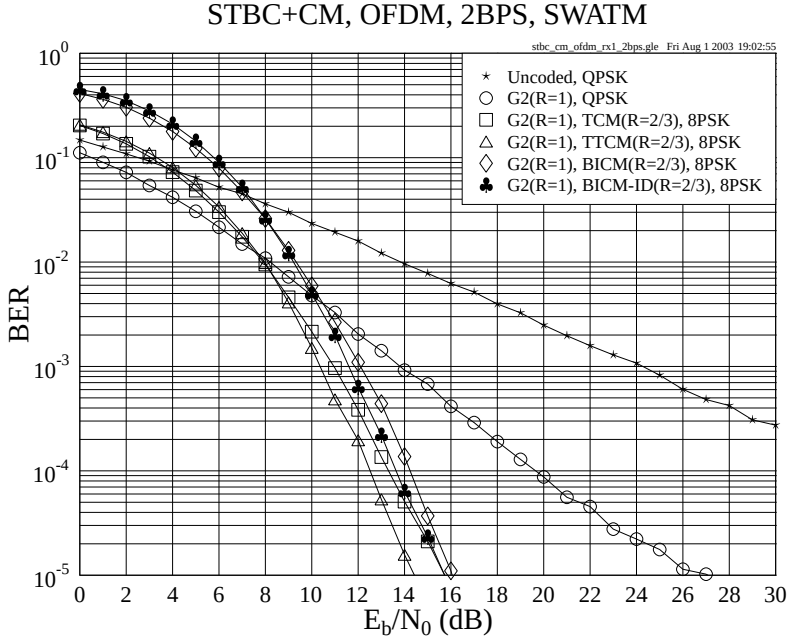

Figure 3.34: The BER versus E_b/N_0 performance of the G_2 space-time block code of Table 3.1 in conjunction with the various Coded Modulation schemes of Table 3.9 at an effective throughput of **2 BPS** using one receiver when communicating over the SWATM channel. An OFDM scheme having 512 subcarriers and a cyclic extension of 64 samples is employed.

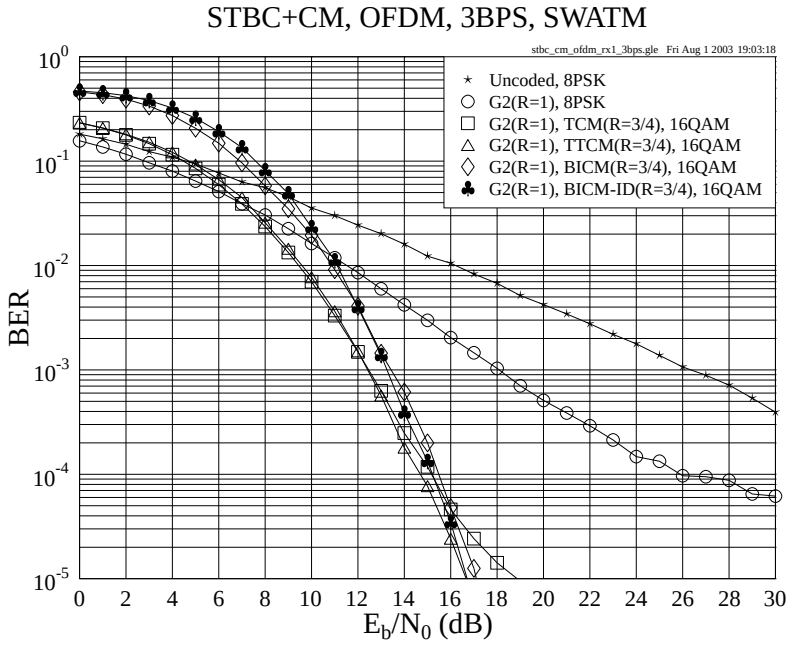

Figure 3.35: The BER versus E_b/N_0 performance of the G_2 space-time block code of Table 3.1 in conjunction with the various Coded Modulation schemes of Table 3.9 at an effective throughput of **3 BPS** using one receiver when communicating over the SWATM channel. An OFDM scheme having 512 subcarriers and a cyclic extension of 64 samples is employed.

erode the orthogonality of the G_2 space-time block code's two components, resulting in a residual error floor, as seen for example in Figure 3.35.

Furthermore, if a higher-order modulation scheme such as 16QAM is employed, as shown in Figure 3.35, since the signal is mapped to more densely-packed constellation phasors which are prone to transmission errors, the error floor imposed by the channel is expected to be higher than that in the scenarios, where a lower-order modulation scheme, such as QPSK or 8PSK is used, as exhibited by Figures 3.33 and 3.34. More explicitly, comparing Figures 3.33 and 3.34 to Figure 3.35, we can see that the BER error floors observed in Figures 3.33 and 3.34 are below 10^{-5}, while in Figure 3.35 the error floor encountered is about 6×10^{-5}.

With the advent of employing the CM schemes, however, the error floor can be eliminated or reduced to a significantly lower level. As Figure 3.35 shows, the CM schemes significantly improve the space-time block coded OFDM system's performance and the BER error floor exhibited by the unprotected G_2 scheme has been essentially eliminated. Similar to the scenarios of having an effective throughput of 1 and 2 BPS, the TTCM-G_2 concatenated scheme was found to give the best performance among all the CM-assisted schemes studied, although the E_b/N_0 gain achieved over the other candidate schemes is not significant.

3.4.1.5 Conclusions

In the previous sections we have investigated the achievable performance of the various CM-assisted space-time block coded OFDM schemes for transmissions over the SWATM channel. We first briefly reviewed the basic principles of the CM schemes in Section 3.4.1.1. In Section 3.4.1.2 a rudimentary introduction to OFDM was provided, which was followed by the overview of the simulation arrangement, as detailed in Section 3.4.1.3. Our performance analysis was presented in Section 3.4.1.4, where the CM-assisted STBC schemes were found to significantly improve the system's achievable performance, eliminating the BER floor of the unprotected STBC scheme. Furthermore, the TTCM-STBC coded concatenated scheme was observed to give the best performance among all the CM-STBC coded concatenated schemes.

In conclusion, we summarized the performance of the evaluated CM-STBC concatenated schemes in Table 3.11. The coding gains summarized in Table 3.11 were defined as the E_b/N_0 difference, expressed in terms of decibels, at a BER of 10^{-5} between the various channel coding assisted space-time block coded OFDM systems and the uncoded single-transmitter OFDM system having the same effective throughput. All the results were recorded by using one

receiver, while communicating over the SWATM channel of Section 3.4.1.3.2.

BPS	STBC Scheme	CM Scheme	CM Code Rate	E_b/N_0 (dB) BER 10^{-3}	E_b/N_0 (dB) BER 10^{-5}	Gain (dB) BER 10^{-3}	Gain (dB) BER 10^{-5}	Modem
1.00	Uncoded	-	-	24.06	44.27	0.00	0.00	BPSK
	G_2	-	-	13.92	25.97	10.14	18.30	BPSK
	G_2	TCM	1/2	8.38	12.44	15.68	31.83	QPSK
	G_2	TTCM	1/2	**7.94**	**11.87**	**16.12**	**32.40**	QPSK
	G_2	BICM	1/2	8.72	12.28	15.34	31.99	QPSK
	G_2	BICM-ID	1/2	8.96	12.89	15.10	31.38	QPSK
2.00	Uncoded	-	-	24.06	44.27	0.00	0.00	QPSK
	G_2	-	-	13.81	27.08	10.25	17.19	QPSK
	G_2	TCM	2/3	10.95	15.73	13.11	28.54	8PSK
	G_2	TTCM	2/3	**10.36**	**14.43**	**13.70**	**29.84**	8PSK
	G_2	BICM	2/3	12.10	16.05	11.96	28.22	8PSK
	G_2	BICM-ID	2/3	11.60	15.73	12.46	28.54	8PSK
3.00	Uncoded	-	-	26.36	47.17	0.00	0.00	8PSK
	G_2	-	-	18.09	-	8.27	-	8PSK
	G_2	TCM	3/4	12.46	18.86	13.90	28.31	16QAM
	G_2	TTCM	3/4	**12.42**	**16.67**	**13.94**	**30.50**	16QAM
	G_2	BICM	3/4	13.43	17.11	12.93	30.06	16QAM
	G_2	BICM-ID	3/4	13.25	16.71	13.11	30.46	16QAM

Table 3.11: Performance of the CM-STBC concatenated OFDM schemes using one receiver, when communicating over the SWATM channel. The STBC and CM parameters were given in Table 3.1 and Table 3.9, respectively. An OFDM scheme having 512 subcarriers and a cyclic extension of 64 samples was employed. For the scenarios of having a different effective throughput, the performance of the best scheme is printed in bold.

3.4.2 CM-Aided and LDPC-Aided Space-Time Block Coded OFDM Schemes

In Section 3.4.1, we have studied the performance of different CM-assisted space-time block coded schemes for transmissions over the SWATM channel [5] of Figure 3.32. Instead of the joint coding modulation schemes of Table 3.9, separate channel codes such as LDPC codes [422], can also be incorporated into our space-time block coded OFDM system for the sake of improving the achievable performance. Hence, in this section we will compare the CM-assisted G_2 space-time coded schemes of Section 3.4.1 to those in which the LDPC codes are combined with the space-time block code G_2.

3.4.2.1 System Overview

The LDPC-assisted space-time block coded OFDM system's schematic is given in Figure 3.36. Compared to Figure 3.31, where the CM-assisted space-time block coded OFDM system was introduced, we substituted the CM encoder and decoder by a LDPC encoder and decoder, respectively. For the CM schemes, the associated symbol-based channel interleaver and deinterleaver have been integrated in the CM encoder and decoder, respectively. For the LDPC schemes, however, an external bit-based channel interleaver and deinterleaver has to be employed for the sake of further improving the system's performance, as seen in Figure 3.36.

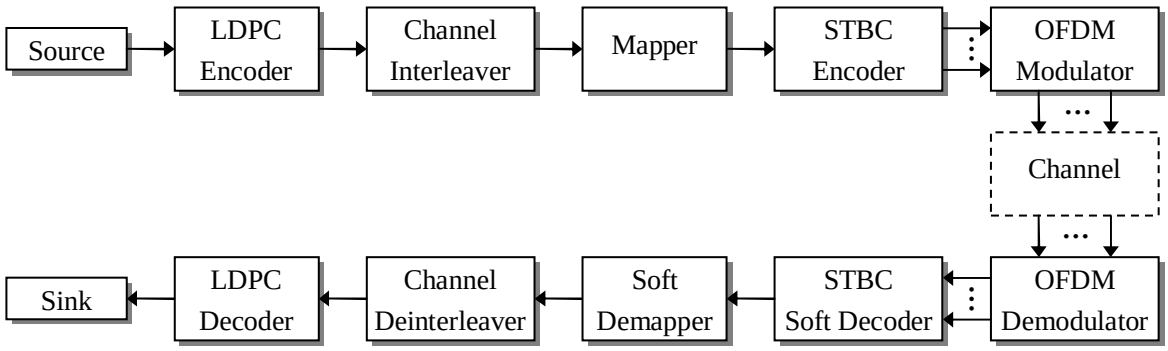

Figure 3.36: Schematic diagram of the proposed LDPC-assisted space-time block coded OFDM system.

Assisted by Equations (3.31), (3.33), and (3.34), we can calculate the corresponding decoding complexity per bit per iteration for the LDPC and CM schemes, respectively. For the sake of fair comparisons, we have to select the appropriate parameters, so that the CM-STBC schemes and the LDPC-STBC schemes exhibit a similar decoding complexity. Specifically, similar to Section 3.4.1.3, the space-time block code was also chosen to be the G_2 code in all the LDPC-STBC concatenated OFDM schemes investigated, and thus again the related decoding complexity of the G_2 code was neglected in order to simplify our comparisons. Furthermore, the symbol-based codeword length of the LDPC-STBC concatenated schemes was fixed to 1024, which is equal to that of the CM-STBC concatenated schemes. Specifically, the same channel model, namely the SWATM channel of Section 3.4.1.3, and the same OFDM modem having 512 subcarriers and a cyclic prefix of 64 samples were employed in this new context.

As mentioned in Section 3.4.1.4, at a specific effective throughput, it was found that the TTCM-assisted G_2 coded scheme gave the best performance. Hence we used the TTCM scheme as the representative of the CM family, while half-rate and $\frac{3}{4}$-rate LDPC codes were chosen for representing the LDPC code family. As a summary, the parameters of the various CM-STBC concatenated OFDM systems are given in Table 3.9, while the parameters of the LDPC-STBC concatenated OFDM systems are provided in Table 3.12.

BPS	STBC		LDPC								Modem
	Code	Code Rate	Code Rate	Column Weight	Iter-ations	In. Bits Block Size	Out. Bits Block Size	Inter-leaver Depth	Symbol-based Cw. Length	Total *Compl.*	
1.00	G_2	1	1/2	3	15	1024	2048	2048	1024	1215	QPSK
2.00	G_2	1	1/2	3	15	2048	4096	4096	1024	1215	16QAM
3.00	G_2	1	3/4	3	10	3072	4096	4096	1024	1530	16QAM

Table 3.12: Parameters of the various LDPC-assisted space-time block coded OFDM schemes. The parameters of the G_2 space-time block code are given in Table 3.1.

3.4.2.2 Simulation Results

In this section we compare the TTCM- and LDPC-assisted space-time block coded OFDM schemes, which are characterized in Figure 3.37. All schemes utilized two transmitter antennas for the G_2 space-time block code and one receiver antenna. All simulation results were generated based on the assumptions outlined in Section 3.4.1.3.

As seen from Figure 3.37, the TTCM- and LDPC-assisted G_2 coded OFDM schemes have a similar performance. Specifically, when the effective throughput is 1 BPS, the TTCM-assisted scheme performs slightly better than the LDPC-aided candidate system. In the scenario of having an effective throughput of 2 BPS, the former outperforms the latter again. In this context, however, we may see that the performance gap between the two competing schemes is larger than that in the scenario of having a throughput of 1 BPS. This is because in order to achieve the same effective throughput of 2 BPS, the TTCM-aided scheme employs 8PSK modulation in conjunction with set partitioning, while the LDPC-aided candidate has to employ the more vulnerable 16QAM gray mapping based constellation, since the

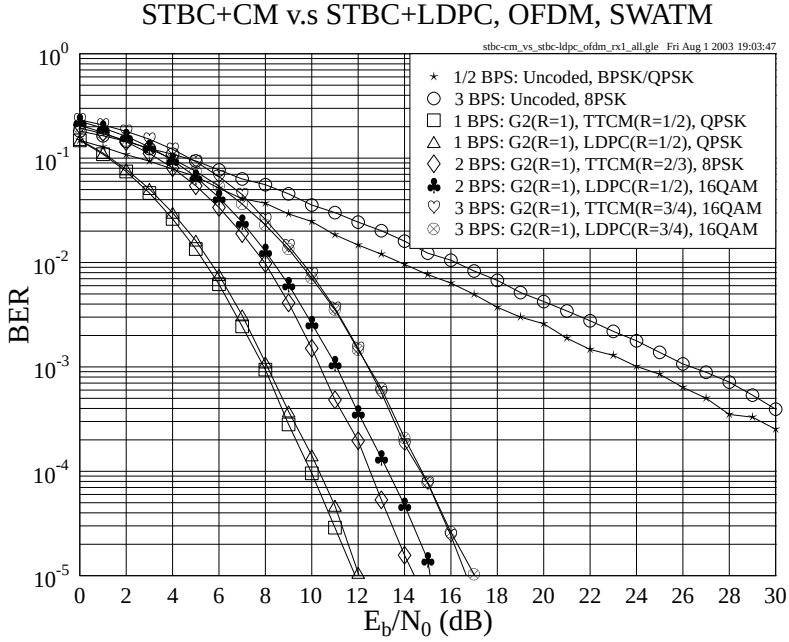

Figure 3.37: The BER versus E_b/N_0 performance of the G_2 space-time block code of Table 3.1 in conjunction with the TTCM of Table 3.9 or the LDPC codes of Table 3.12 at different effective throughputs using one receiver when communicating over the SWATM channel of Figure 3.32. An OFDM scheme having 512 subcarriers and a cyclic extension of 64 samples is employed.

code rate of the TTCM and the LDPC code are $\frac{2}{3}$ and $\frac{1}{2}$, respectively. Nonetheless, it is found in Figure 3.37 that the two corresponding competitors exhibit a similar performance, when the throughput is increased to 3 BPS. In this case, however, the LDPC-aided scheme is marginally superior to the TTCM-aided scheme, when the E_b/N_0 value is relatively low, namely below 11dB.

In Figure 3.38, the associated coding gain versus complexity results are provided. The coding gain was defined in Section 3.4.1.5, while the complexity of the CM schemes and LDPC codes can be calculated with the aid of Equations (3.33) and (3.31), respectively. Given the same effective throughput, it is found that the coding gain performance of the TTCM-aided G_2 schemes surpasses that of the LDPC-aided G_2 schemes, when the affordable complexity is higher than approximate 500, as observed in Figure 3.38. At a low complexity, namely below a value of about 500, however, the LDPC-aided schemes tend to achieve a higher coding gain than the TTCM-aided schemes at the specific throughput values considered.

3.4.2.3 Conclusions

In Section 3.4.2.2 the performance of the different TTCM- and LDPC-assisted G_2 coded OFDM schemes has been studied and compared. As seen from Figure 3.37, the TTCM-assisted G_2 scheme gives a better performance than the LDPC-assisted G_2 scheme. Furthermore, in the context of the achievable coding gain versus complexity performance, it was found that the TTCM-assisted schemes are capable of achieving higher coding gains in the relatively high complexity range, than the LDPC-assisted candidate schemes.

In conclusion, we summarize the achievable performance of the various schemes discussed in Table 3.13.

3.5 Chapter Summary

The state-of-the-art of various transmission schemes based on multiple transmitters and receivers was briefly reviewed in Section 3.1. A simple communication system invoking the space-time block code G_2 was introduced in Section 3.2.1, leading to further discussions on various other space-time block codes. More specifically, Section 3.2.2.1 defined the STBC transmission matrix, while the encoding algorithm of the G_2 and a range of other space-time block codes was given in Sections 3.2.2.2 and 3.2.2.3, respectively. Section 3.2.3 presented the decoding algorithm of the

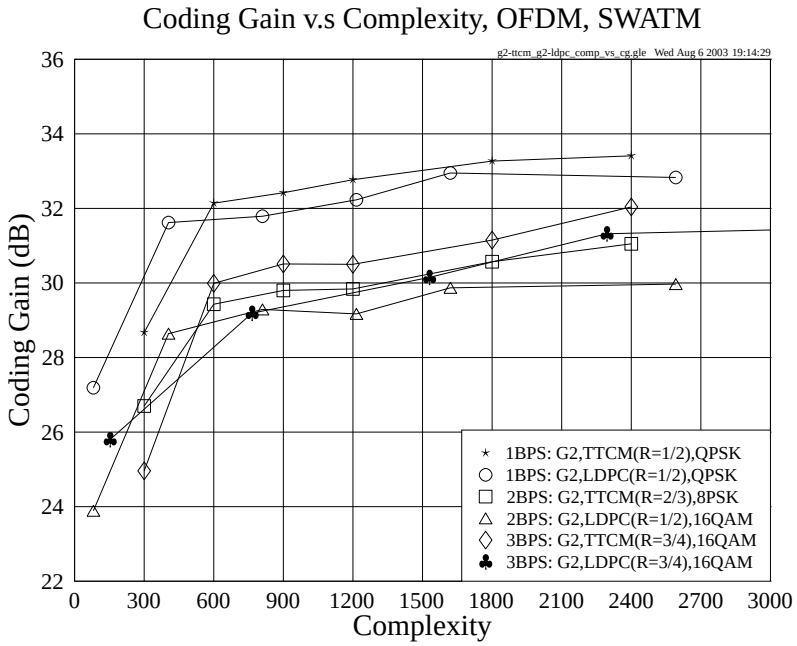

Figure 3.38: Coding gain versus complexity for the TTCM-G_2 concatenated and LDPC-G_2 concatenated schemes using one receiver, when communicating over the SWATM channel of Figure 3.32. An OFDM scheme having 512 subcarriers and a cyclic extension of 64 samples is employed. The simulation parameters are given in Tables 3.9 and 3.12.

BPS	STBC Scheme	TTCM Code Rate	LDPC Code Rate	E_b/N_0 (dB) BER 10^{-3}	E_b/N_0 (dB) BER 10^{-5}	Gain (dB) BER 10^{-3}	Gain (dB) BER 10^{-5}	Modem
1.00	Uncoded	-	-	24.06	44.27	0.00	0.00	BPSK
	G_2	-	-	13.92	25.97	10.14	18.30	BPSK
	G_2	1/2	-	**7.94**	**11.87**	**16.12**	**32.40**	QPSK
	G_2	-	1/2	8.09	12.04	15.97	32.23	QPSK
2.00	Uncoded	-	-	24.06	44.27	0.00	0.00	QPSK
	G_2	-	-	13.81	27.08	10.25	17.19	QPSK
	G_2	2/3	-	**10.36**	**14.43**	**13.70**	**29.84**	8PSK
	G_2	-	1/2	11.07	15.10	12.99	29.17	16QAM
3.00	Uncoded	-	-	26.36	47.17	0.00	0.00	8PSK
	G_2	-	-	18.09	-	8.27	-	8PSK
	G_2	3/4	-	**12.42**	**16.67**	**13.94**	**30.50**	16QAM
	G_2	-	3/4	12.44	17.02	13.92	30.15	16QAM

Table 3.13: Performance of the TTCM- and LDPC-STBC coded concatenated OFDM schemes using one receiver, when communicating over the SWATM channel of Figure 3.32. The STBC, CM and LDPC parameters were given in Tables 3.1, 3.9 and 3.12, respectively. An OFDM scheme having 512 subcarriers and a cyclic extension of 64 samples was employed. For the scenarios of having a different effective throughput, the performance of the best scheme is printed in bold.

space-time block codes considered. More specifically, Section 3.2.3.1 introduced the Maximum Likelihood algorithm, while Section 3.2.3.2 discussed the Maximum-A-Posteriori algorithm, which enables the STBC decoder to provide soft outputs. Thus various channel codes can be concatenated with the space-time block codes for the sake of improving the system's performance. In Section 3.2.4, the schematic of the proposed system was presented, and some assumptions used in our simulations were outlined.

The performances of the various space-time block codes were studied and compared in Section 3.2.5. Specifically, in Sections 3.2.5.1 and 3.2.5.2 the performances of different space-time block coded schemes communicating over both uncorrelated and correlated Rayleigh fading channels were compared, respectively. It was found that the performances of the half-rate codes G_3 and G_4 degraded in comparison to that of the unity-rate code G_2, when the effective throughput was increased. The reason is that in order to maintain the same effective throughput, higher-throughput modulation schemes have to be employed in conjunction with the half-rate codes G_3 and G_4 which are more vulnerable to errors. This hence degrades the performance of the system. The $\frac{3}{4}$-rate codes H_3 and H_4 suffer a lower degradation in this case, as their code rate is higher than that of the G_3 and G_4 codes, therefore a moderate-throughput modulation scheme can be employed. This in turn assists in maintaining the performance advantage achieved by the space-time codes. Additionally, when the number of receivers is increased, the achievable performance gain of the G_3, G_4, H_3 and H_4 codes over the G_2 code becomes lower, as seen in Figures 3.4, 3.5, 3.8 and 3.9. This is because much of the attainable diversity gain has already been achieved using the G_2 code employing two receivers. Another important conclusion is that the performances of the space-time codes communicating over both uncorrelated and correlated Rayleigh fading channels are the same, provided that the effective throughput is the same. The performances of all the space-time block codes are summarized in Table 3.2 at the end of Section 3.2.6.

The schemes employing space-time block codes in conjunction with channel codes were studied in Section 3.3, which were divided into two parts, namely the performance study of LDPC-aided space-time block codes was presented in Section 3.3.1, while our performance comparisons between LDPC-assisted and TC(2,1,4)-aided STBC schemes were provided in Section 3.3.2.

In Section 3.3.1.1 the LDPC-based system was introduced and the associated simulation parameters were given. The performances of the LDPC-STBC concatenated schemes were provided in Section 3.3.1.2, including the scenarios of both uncorrelated and correlated Rayleigh fading channels in Section 3.3.1.2.1 and Section 3.3.1.2.2, respectively. The implementation complexity issues of the schemes studied were discussed in Section 3.3.1.3, where the coding gain versus complexity at different effective throughputs was shown in Figures 3.21, 3.22 and 3.23. It was found that the LDPC-aided STBC schemes performed significantly better than the STBC-only schemes when communicating over uncorrelated Rayleigh fading channels, while the achievable performance improvement was insignificant, when communicating over correlated Rayleigh fading channels. This is because the attainable performances of the LDPC codes were found to be worse, when comminucating over correlated Rayleigh channels than over uncorrelated Rayleigh channels, unless the LDPC codeword length was sufficiently long enough or a sufficiently long channel interleaver was used. The phenomenon of achieving different performances over uncorrelated and correlated Rayleigh fading channels was also observed in the context of the LDPC-STBC concatenated system. On the other hand, when the number of receiver antennas was increased, the schemes employing a space-time block code of a higher-diversity order were found to provide an inferior performance, since most of the attainable diversity gain has already been achieved by the LDPC-aided G_2 coded scheme. It was also found that for transmission over the uncorrelated Rayleigh fading channels, when the same modulation scheme was used, a lower-rate LDPC code benefited the system more than a space-time code of a higher-diversity order did. Furthermore, when the same LDPC code was used, a lower-order modulation scheme tended to offer a higher performance improvement, than a space-time block code of a higher diversity order did. The performance of different LDPC-aided space-time block coded schemes was summarized in Table 3.5, where the half-rate LDPC-coded space-time block code G_2 was found to be the best option among all the LDPC-STBC concatenated schemes.

Following Section 3.3.1, where the LDPC-aided space-time coded system was studied, our comparative study between LDPC-aided and TC(2,1,4)-assisted STBC schemes transmitting over uncorrelated Rayleigh fading channels was presented in Section 3.3.2. The TC(2,1,4)-aided system was introduced in Section 3.3.2.1, while the associated complexity issues were discussed in Section 3.3.2.2, which was followed by the performance analysis in Section 3.3.2.3. From our coding gain versus complexity performance comparisons, it was concluded that the half-rate TC(2,1,4)-assisted space-time block code G_2 slightly outperforms the LDPC-assisted space-time block coded schemes. However, the LDPC-STBC concatenated schemes may be considered as better design options for complexity-sensitive systems, where the achievable performance does not necessarily have to be the highest possible, since the LDPC-aided schemes are capable of maintaining a lower complexity than the TC(2,1,4)-aided scheme is. In conclusion, the performance of the different schemes studied was summarized in Table 3.8.

Furthermore, channel coding assisted space-time block coded single-user OFDM systems were studied in Section 3.4. This research was divided into two parts. The first part is the investigation of the various CM-assisted

space-time block coded OFDM schemes detailed in Section 3.4.1. The basic OFDM system was introduced in Section 3.4.1.2, followed by the whole system's overview in Section 3.4.1.3. More specifically, a brief complexity analysis was provided in Section 3.4.1.3.1, and the introduction of the SWATM channel model was the subject of Section 3.4.1.3.2. Our simulation results were discussed in Section 3.4.1.4, which were summarized in Table 3.11. The latter part of Section 3.4 focused on the performance comparison of the CM- and LDPC-assisted space-time block coded systems considered, which was detailed in Section 3.4.2. The BER versus E_b/N_0 as well as the coding gain versus complexity performances of the two groups of candidate schemes were compared in Section 3.4.2.2, followed by our conclusions in Section 3.4.2.3, where the results were summarized in Table 3.13.

The family of STBCs is readily applicable to employment in downlink systems, where the multiple transmitter antennas are installed at the BS. However, in the context of uplink systems it is impractical to use high-order STBCs at the MSs, since the MSs are expected to have a low implementation complexity and thus cannot afford the added cost of a high number of transmitter antennas. In the next chapter, Space Division Multiple Access (SDMA) type uplink multi-user OFDM systems will be investigated, which invoke multiple receiver antenna elements for supporting a multiplicity of MSs, each of which employs a single transmitter antenna only.

Chapter 4

Coded Modulation Assisted Multi-User SDMA-OFDM Using Frequency-Domain Spreading

4.1 Introduction

In recent years Orthogonal Frequency Division Multiplexing (OFDM) [3, 5, 6, 26] has emerged as a successful air-interface technology for both broadcast and Wireless Local Area Network (WLAN) applications, whilst Wideband Code Division Multiple Access (WCDMA) has emerged as the winning candidate for 3G mobile systems. Our research therefore includes an exploration of the performance versus complexity tradeoffs of a generic class of Multi-Carrier Code Division Multiple Access (MC-CDMA) [40] systems, which are capable of supporting the interworking of existing as well as future broadcast and personal communication systems.

Space Division Multiple Access (SDMA) based OFDM [5, 194, 441] communication invoking Multi-User Detection (MUD) [442] techniques has recently attracted intensive research interests. In SDMA Multiple-Input Multiple-Output (MIMO) systems the transmitted signals of L simultaneous uplink mobile users - each equipped with a single transmitter antenna - are received by the P different receiver antennas of the base station (BS). At the BS the individual users' signals are separated with the aid of their unique, user-specific spatial signature constituted by their channel transfer functions or, equivalently, Channel Impulse Responses (CIRs). A variety of MUD schemes, such as the Least-Squares (LS) [5, 442, 443] and Minimum Mean-Square Error (MMSE) [5, 194, 198, 442, 443] detectors, or Successive Interference Cancellation (SIC) [5, 194, 198, 442–444], Parallel Interference Cancellation (PIC) [5, 442, 444, 445] and Maximum Likelihood Detection (MLD) [5, 194, 198, 199, 442] schemes may be invoked for the sake of separating the different users at the BS on a per-subcarrier basis. Among these schemes, the MLD arrangement was found to give the best performance, although this was achieved at the cost of a dramatically increased computational complexity, especially in the context of a high number of users and higher-order modulation schemes, such as 16QAM [444]. By contrast, MMSE combining exhibits the lowest complexity in this set of detectors, while suffering from a performance loss [5, 444].

In order to improve the achievable performance by exploiting the multi-path diversity potential offered by wideband channels, a further technique that is often used in the context of CDMA systems is constituted by the spreading of the subcarrier signals over a number of adjacent subcarriers with the aid of orthogonal spreading codes, such as Walsh-Hadamard Transform (WHT) based codes [34]. This technique may also be employed in multi-user SDMA-OFDM systems in the context of spreading across all or a fraction of the subcarriers [446]. Spreading across all subcarriers using a single Walsh-Hadamard Transform Spreading (WHTS) [5] code is expected to result in a better averaging of the bursty error effects at the cost of a higher WHT complexity.

Furthermore, the achievable performance can be significantly improved, if Forward Error Correction (FEC) schemes, such as for example Turbo Convolutional (TC) codes are incorporated into the SDMA system [5]. Among a number of FEC schemes, Trellis Coded Modulation (TCM) [359, 437], Turbo TCM (TTCM) [359, 438], Bit-Interleaved Coded Modulation (BICM) [359, 439] and Iteratively Decoded BICM (BICM-ID) [359, 440] have attracted intensive research interests, since they are capable of achieving a substantial coding gain without bandwidth expansion.

In this section, we combine the above-mentioned various Coded Modulation (CM) schemes with a multi-user SDMA-OFDM system, in which WHT-based subcarrier spreading is used. The structure of this section is as follows. The SDMA MIMO channel model is described in Section 4.2.1, while an overview of the CM-assisted multi-user SDMA-WHTS-OFDM system is provided in Section 4.2.2, where the basic principles of CM, MUD and WHT-based spreading (WHTS) are also introduced. Our simulation results are provided in Section 4.3, while our conclusions are summarized in Section 4.4.

4.2 System Model

4.2.1 SDMA MIMO Channel Model

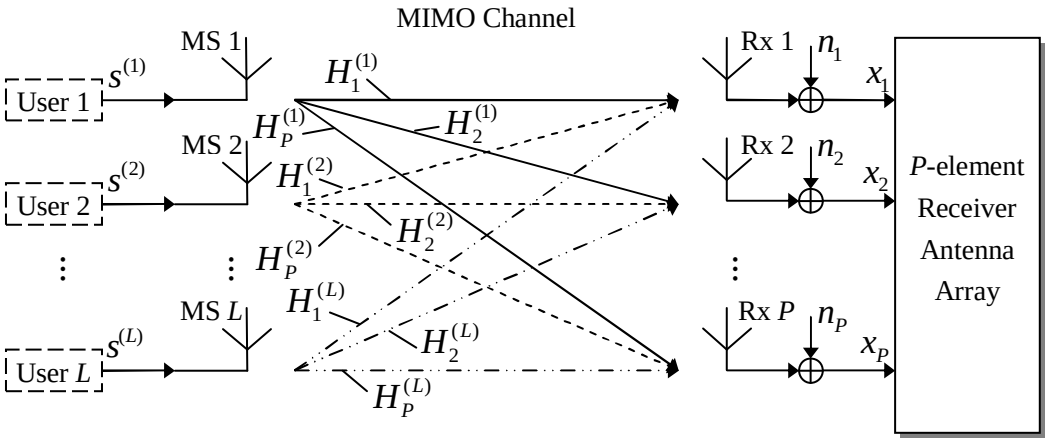

Figure 4.1: Schematic of the SDMA uplink MIMO channel model [5], where each of the L mobile users is equipped with a single transmitter antenna and the BS's receiver is assisted by a P-element antenna front-end.

Figure 4.1 shows a SDMA uplink MIMO channel model, where each of the L simultaneous mobile users employs a single transmitter antenna at the mobile station (MS), while the BS's receiver exploits P antennas. At the k^{th} subcarrier of the n^{th} OFDM symbol received by the P-element receiver antenna array we have the complex received signal vector $\mathbf{x}[n,k]$, which is constituted by the superposition of the independently faded signals associated with the L mobile users and contaminated by the Additive White Gaussian Noise (AWGN), expressed as:

$$\mathbf{x} = \mathbf{H}\mathbf{s} + \mathbf{n}, \tag{4.1}$$

where the $(P \times 1)$-dimensional vector $\mathbf{x}$, the $(L \times 1)$-dimensional vector $\mathbf{s}$ and the $(P \times 1)$-dimensional vector $\mathbf{n}$ are the received, transmitted and noise signals, respectively. Here we have omitted the indices $[n,k]$ for each vector for the sake of notational convenience. Specifically, the vectors $\mathbf{x}$, $\mathbf{s}$ and $\mathbf{n}$ are given by:

$$\mathbf{x} = \left[x_1, x_2, \cdots, x_P \right]^T, \tag{4.2}$$

$$\mathbf{s} = \left[s^{(1)}, s^{(2)}, \cdots, s^{(L)} \right]^T, \tag{4.3}$$

$$\mathbf{n} = \left[n_1, n_2, \cdots, n_P \right]^T. \tag{4.4}$$

The $(P \times L)$-dimensional matrix $\mathbf{H}$, which contains the Frequency-Domain CHannel Transfer Functions (FD-CHTFs) of the L users, is given by:

$$\mathbf{H} = \left[\mathbf{H}^{(1)}, \mathbf{H}^{(2)}, \cdots, \mathbf{H}^{(L)} \right], \tag{4.5}$$

where $\mathbf{H}^{(l)}$ $(l = 1, \cdots, L)$ is the vector of the FD-CHTFs associated with the transmission paths from the l^{th} user's transmitter antenna to each element of the P-element receiver antenna array, which is expressed as:

$$\mathbf{H}^{(l)} = \left[H_1^{(l)}, H_2^{(l)}, \cdots, H_P^{(l)} \right]^T, \quad l = 1, \cdots, L. \tag{4.6}$$

In Equations (4.1) to (4.6), we assume that the complex signal $s^{(l)}$ transmitted by the l^{th} user has zero-mean and a variance of σ_l^2. The AWGN noise signal n_p also exhibits a zero-mean and a variance of σ_n^2. The FD-CHTFs $H_p^{(l)}$ of the different receivers or users are independent, stationary, complex Gaussian distributed processes with zero-mean and unit variance [446].

4.2.2 CM-assisted SDMA-OFDM Using Frequency Domain Spreading

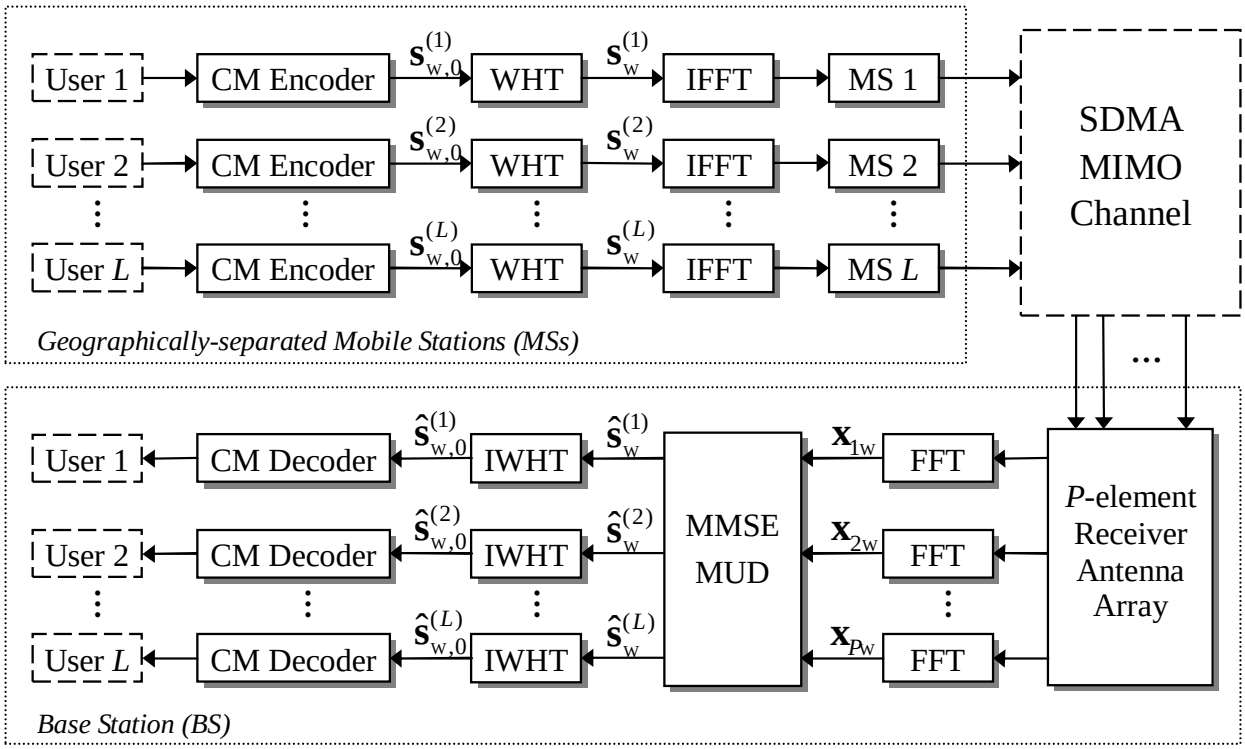

Figure 4.2: Schematic of the CM-assisted and multi-user detected SDMA-OFDM uplink system employing subcarrier-based WHT spreading.

In Section 4.2.1 we have briefly reviewed the SDMA MIMO channel model, as shown in Figure 4.1. In Figure 4.2, we present the schematic of the proposed CM-assisted and multi-user detected SDMA-OFDM uplink system employing WHT spreading. At the transmitter end, as seen at the top of Figure 4.2, the information bit sequences of the geographically-separated L simultaneous mobile users are forwarded to the CM encoders, where they are encoded into symbols. Each user's encoded signal is divided into a number of WHT signal blocks, denoted by $\mathbf{s}_{w,0}^{(l)}$ $(l = 1, \cdots, L)$, which are then forwarded to the subcarrier-based WHT spreader, followed by the OFDM-related Inverse Fast Fourier Transform (IFFT) based modulator, which converts the frequency-domain signals to the time-domain modulated OFDM symbols. The OFDM symbols are then transmitted by the MSs to the BS over the SDMA MIMO channel. Then each element of the receiver antenna array shown at the bottom of Figure 4.2 receives the superposition of the AWGN-contaminated transmitted signals and performs Fast Fourier Transform (FFT) based OFDM demodulation. The demodulated outputs $\mathbf{x}_{p_w}$ $(p = 1, \cdots, P)$ seen in Figure 4.2 are forwarded to the multi-user detector for separating the different users' signals. The separated signals $\hat{\mathbf{s}}_{w}^{(l)}$ $(l = 1, \cdots, L)$, namely the estimated versions of the transmitted signals, are independently despread based on the inverse WHT (IWHT), resulting in the despread signals of $\hat{\mathbf{s}}_{w,0}^{(l)}$ $(l = 1, \cdots, L)$ which are then decoded by the CM decoders of Figure 4.2.

The further structure of this section is as follows. A brief description of the MMSE MUD employed in our SDMA-OFDM system is given in Section 4.2.2.1. The subcarrier-based WHTS is then introduced in Section 4.2.2.2.

4.2.2.1 Minimum Mean-Square Error Multi-User Detector

As mentioned earlier, MUD schemes have to be invoked at the receiver of the SDMA-OFDM system for the sake of detecting the received signals of different users. From the family of various MUD techniques, represented for example by the Maximum Likelihood Detection (MLD) [5, 194, 198, 199, 442], Parallel Interference Cancellation (PIC) [5, 442, 444, 445], Successive Interference Cancellation (SIC) [5, 194, 198, 442–444], Minimum Mean-Square Error (MMSE) [5, 194, 198, 442, 443] and Least-Squares (LS) [5, 442, 443] detectors, ML detection is known to exhibit the optimum performance, although this is achieved at the highest complexity. In order to avoid the potentially excessive complexity of optimum ML detection, sub-optimum detection techniques such as the MMSE-MUD have been devised. Specifically, the MMSE detector exhibits the lowest detection complexity in the set of detectors mentioned

above, although this comes at the cost of a Bit Error Ratio (BER) degradation [5, 444].

In the MMSE-based MUD the estimates of the different users' transmitted signals are generated with the aid of the linear MMSE combiner. More specifically, the estimated signal vector $\hat{\mathbf{s}} \in \mathbb{C}^{(L\times 1)}$ generated from the transmitted signal $\mathbf{s}$ of the L simultaneous users, as shown in Figure 4.2, is obtained by linearly combining the signals received by the P different receiver antenna elements with the aid of the array weight matrix, as follows [5]:

$$\hat{\mathbf{s}} \quad = \quad \mathbf{W}_{\text{MMSE}}^{H}\mathbf{x}, \tag{4.7}$$

where the superscript H denotes the Hermitian transpose, and $\mathbf{W}_{\text{MMSE}} \in \mathbb{C}^{(P\times L)}$ is the MMSE-based weight matrix given by [5]:

$$\mathbf{W}_{\text{MMSE}} = (\mathbf{H}\mathbf{H}^{H} + \sigma_n^2\mathbf{I})^{-1}\mathbf{H}, \tag{4.8}$$

while $\mathbf{I}$ is the identity matrix and σ_n^2 is the AWGN noise variance.

4.2.2.2 Subcarrier-based Walsh-Hadamard Transform Spreading

In single- and multi-carrier CDMA systems, the employment of orthogonal codes is vital for the sake of supporting multiple access [34]. In the context of multi-user SDMA-OFDM systems, orthogonal codes may be employed for the sake of randomizing the wideband channel's frequency-selective fading, rather than for supporting multiple users, since the multiple users are supported with the aid of the SDMA-OFDM system employing a P-element antenna array and appropriate multi-user detection techniques.

A prominent class of orthogonal codes often used in CDMA systems is the family of orthogonal Walsh codes [34], which are particularly attractive, since the operation of spreading with the aid of these codes can be implemented in form of a 'fast' transform, which takes advantage of the codes' recursive structure, similarly to the FFT [5].

Let us now provide a deeper insight into the operation of the subcarrier-based WHTS [5]. During every OFDM symbol period prior to transmission of the independent user signals, the K data samples associated with the subcarriers, where K is the FFT length, may be spread with the aid of the WHT having a block size of K. This is achieved by left-multiplying the WHT signal block $\mathbf{s}_{\text{w},0}^{(l)}$ $(l = 1, \cdots, L)$ of Figure 4.2 with the K-order WHT matrix $\mathbf{U}_{\text{WHT}_K}$ for each user separately:

$$\mathbf{s}_{\text{w}}^{(l)} \quad = \quad \mathbf{U}_{\text{WHT}_K}\mathbf{s}_{\text{w},0}^{(l)}, \quad l = 1, \cdots, L, \tag{4.9}$$

where $\mathbf{s}_{\text{w}}^{(l)}$ is the l^{th} user's spread signal block, and $\mathbf{U}_{\text{WHT}_K}$ is given in a recursive form as:

$$\mathbf{U}_{\text{WHT}_K} = \frac{1}{\sqrt{2}}\begin{bmatrix} 1\cdot\mathbf{U}_{\text{WHT}_{K/2}} & 1\cdot\mathbf{U}_{\text{WHT}_{K/2}} \\ 1\cdot\mathbf{U}_{\text{WHT}_{K/2}} & -1\cdot\mathbf{U}_{\text{WHT}_{K/2}} \end{bmatrix}, \tag{4.10}$$

while the lowest-order WHT unitary matrix is defined by:

$$\mathbf{U}_{\text{WHT}_2} = \frac{1}{\sqrt{2}}\begin{bmatrix} 1 & 1 \\ 1 & -1 \end{bmatrix}. \tag{4.11}$$

When the WHT block size is long, for example identical to the FFT length of $K = 512$, the computational complexity imposed by the length-K WHTS may be very high. Therefore a more practical solution is to further divide the K samples into K/M_{WHT} number of interleaved blocks, each of which has a block size of $M_{\text{WHT}} < K$. Specifically, the i^{th} WHT block is constituted by the samples selected from the subcarriers having the indices [5, 446]:

$$j = i + r\frac{K}{M_{\text{WHT}}},\ 0 \le i \le \frac{K}{M_{\text{WHT}}} - 1,\ 0 \le r \le M_{\text{WHT}} - 1, \tag{4.12}$$

where i is the index of the WHT blocks within the same OFDM symbol. In Figure 4.3 we illustrate the operation of the subcarrier-based WHTS, where the number of OFDM subcarriers is 512 and the WHT block size is 32. Therefore in each OFDM symbol we have $512/32 = 16$ frequency-domain interleaved WHT blocks. At the top of Figure 4.3 an OFDM symbol is shown with the subcarriers' indices displayed, while the bottom illustration of the figure shows the WHT blocks generated, which contain subcarriers of the specified indices, as given by Equation (4.12). As Figure 4.3 shows, for example, the signal sample carried by the second ($r = 1$) slot within the WHT block of index $i = 0$ is selected from the subcarrier of index $j = 16$ within the original OFDM symbol. After the WHT blocks are formed, the WHTS is then invoked with the aid of the length-M_{WHT} WHT matrix given in Equation (4.10).

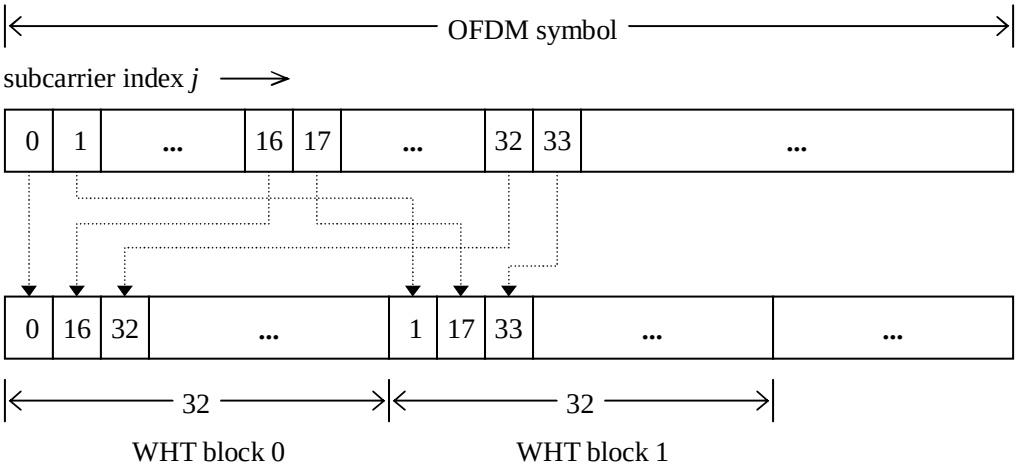

Figure 4.3: Example of the subcarrier-based WHT blocks' generation using a WHT block size of 32, where the total number of OFDM subcarriers is 512.

At the BS receiver seen in Figure 4.2, the despreading operation follows the inverse procedure of that portrayed in Figure 4.3, which is invoked independently for the separated signal of each user. More specifically, we have:

$$\hat{\mathbf{s}}_{\mathrm{w},0}^{(l)} = \mathbf{U}_{\mathrm{WHT}_K} \hat{\mathbf{s}}_{\mathrm{w}}^{(l)}, \quad l = 1, \cdots, L, \tag{4.13}$$

where $\hat{\mathbf{s}}_{\mathrm{w},0}^{(l)}$ and $\hat{\mathbf{s}}_{\mathrm{w}}^{(l)}$ are the estimated version of $\mathbf{s}_{\mathrm{w},0}^{(l)}$ and $\mathbf{s}_{\mathrm{w}}^{(l)}$, respectively, while $\hat{\mathbf{s}}_{\mathrm{w}}^{(l)}$ is achieved by applying Equation (4.7) at each subcarrier of every length-M_{WHT} WHT block. Upon employing the WHTS technique, the detrimental effects imposed on the system's average BER performance by the specific subcarriers corrupted by deep frequency-domain channel fades can be potentially improved, since the effects of the fades are spread over the entire WHT block. Hence the receiver has a high chance of recovering the impaired transmitted signals of the badly affected subcarriers.

4.3 Simulation Results

In this section, we characterize the performance of the proposed CM-assisted MMSE-SDMA-OFDM schemes in conjunction with WHTS. The channel is assumed to be OFDM-symbol-invariant, implying that the taps of the impulse response are assumed to be constant for the duration of one OFDM symbol, but they are faded at the beginning of each symbol [4]. Each user's associated transmit power or signal variance is assumed to be the same and normalized to unity, while the complex-valued fading envelope of the different users' signal is assumed to be uncorrelated. For the sake of simplifying the experimental conditions, the channel's frequency-domain transfer function is assumed to be perfectly known in all simulations. Nonetheless, these performance trends are expected to remain unchanged in case of imperfect channel estimation, in particular, when the turbo-style PIC aided Recursive Least-Squares (RLS) channel estimators of Chapter 16 in reference [5] are used. This may be made plausible by noting that turbo-style iterative detection techniques have been reported to be capable of achieving a virtually indistinguishable performance from the idealistic system using perfect channel estimation [5, 359].

4.3.1 MMSE-SDMA-OFDM Using WHTS

We commence by considering a multi-user SDMA-OFDM system operating without the assistance of CM communicating over the Short Wireless Asynchronous Transfer Mode (SWATM) channel of [4]. The impulse response of the three-tap SWATM channel was given in Figure 3.32, while the specific channel parameters used were given in Table 3.10. Each of the three paths experiences independent Rayleigh fading having the same normalized Doppler frequency of $f_d' = 1.235 \times 10^{-5}$. A total of 512 subcarriers and a cyclic prefix of 64 samples were used for the OFDM modem.

Figure 4.4 compares the BER versus E_b/N_0 performance of the MMSE-SDMA-OFDM system equipped with two receiver antenna elements, while supporting one or two users both with and without WHTS, respectively. Furthermore, the performance of the unprotected single-user BPSK scheme communicating over an AWGN channel is also provided for reference. As expected, the WHTS-assisted schemes perform better than their non-spread counterparts, both for

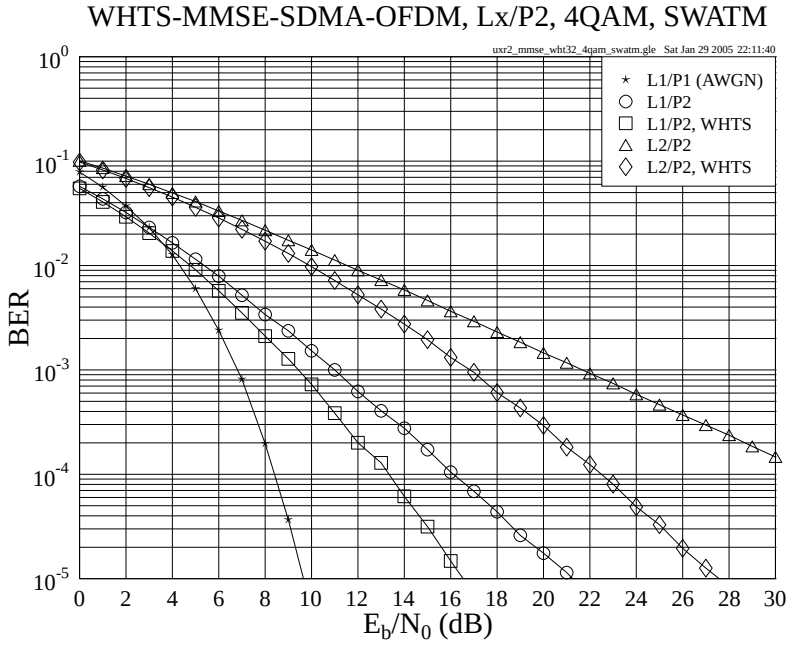

Figure 4.4: BER versus E_b/N_0 performance of the **WHTS-assisted MMSE-SDMA-OFDM** system employing a 4QAM scheme for transmission over the **SWATM** channel, where **L=1, 2** users are supported with the aid of **P=2** receiver antenna elements. The WHT block size used is **32**.

one and two users. It is also beneficial to view the subcarrier BERs as a function of both the subcarrier index and the E_b/N_0, which was portrayed in Figure 4.5 for the SDMA-OFDM system equipped with two BS receiver antennas for supporting two users. The subcarrier BER is defined as the BER averaged over a specific subcarrier of all the consecutive OFDM symbols transmitted by the users. It was found that at a specific E_b/N_0 value, the subcarrier BER curves shown at the top of Figures 4.5, exhibit undulations across the frequency domain owing to deep channel fades at certain subcarriers, which could be potentially eliminated with the aid of WHTS, as observed at the bottom of the figure. This suggests that the system's average BER performance can be potentially improved by using WHTS, since the bursty subcarrier errors can be effectively spread across the subcarriers of the entire WHT block.

4.3.2 CM- and WHTS-assisted MMSE-SDMA-OFDM

Similarly to the previous sections, let us first investigate the SDMA-OFDM system's performance while communicating over the SWATM channel [4].

4.3.2.1 Performance Over the SWATM Channel

For the various CM schemes used, we select the parameters so that all schemes have the same effective throughput and the same number of decoding states, hence have a similar decoding complexity. More specifically, the code memory ν is fixed to 6 for the non-iterative TCM and BICM schemes, so that the number of decoding states becomes $S = 2^\nu = 64$. For the iterative TTCM and BICM-ID schemes, however, ν is fixed to 3, while the number of iterations for these schemes is set to 4 and 8, respectively. Hence the total number of trellis states is $2^3 \cdot 4 \cdot 2 = 64$ for TTCM and $2^3 \cdot 8 \cdot 1 = 64$ for BICM-ID, since there are two 8-state decoders, which are invoked in four iterations in the scenario of TTCM, while only one 8-state decoder is employed in the context of BICM-ID. The generator polynomials expressed in octal format for TCM, TTCM, BICM and BICM-ID are $[117 \quad 26]$, $[13 \quad 6]$, $[133 \quad 171]$ and $[15 \quad 17]$, respectively. The parameters of the various CM schemes used are summarized in Table 4.1.

4.3.2.1.1 Two Receiver Antenna Elements

In Section 4.3.1 the beneficial effects of WHTS on the MMSE-SDMA-OFDM system's performance have been demonstrated. Let us now combine the various CM schemes considered with the multi-user MMSE-SDMA-OFDM

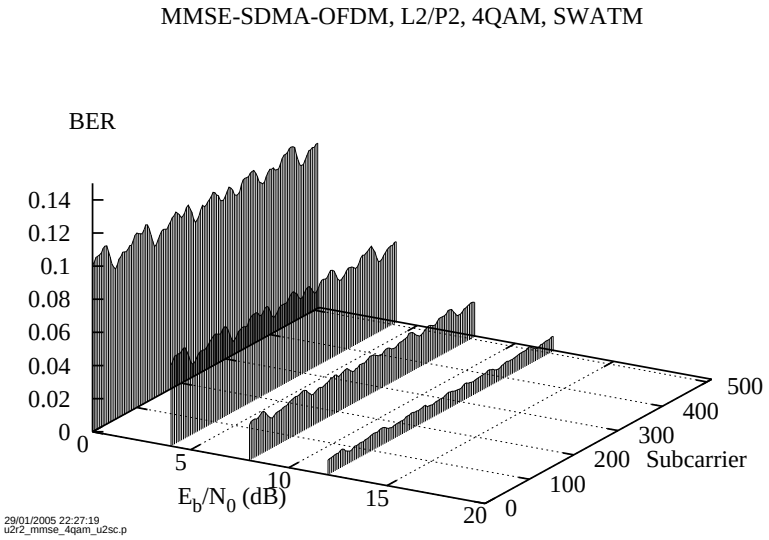

Figure 4.5: BER versus E_b/N_0 performance as a function of the subcarrier index of the **MMSE-SDMA-OFDM (top)** and **WHTS-assisted MMSE-SDMA-OFDM (bottom)** systems employing a 4QAM scheme for transmission over the **SWATM** channel, where **L=2** users are supported with the aid of **P=2** receiver antenna elements. The WHT block size used is **32**.

CM Scheme	Code Rate	Data Bits	Parity Bits	Code Memory	Iterations	Codeword Length	Modem
TCM	1/2	1	1	6	-	1024	4QAM
TTCM	1/2	1	1	3	4	1024	4QAM
BICM	1/2	1	1	6	-	1024	4QAM
BICMID	1/2	1	1	3	8	1024	4QAM

Table 4.1: The parameters of the various CM schemes used in the multi-user SDMA-OFDM system for communicating over the SWATM channel of Figure 3.32.

system. The corresponding simulation results are portrayed in Figure 4.6, where the top and bottom of the figure illustrate the BER and CodeWord Error Ratio (CWER) versus E_b/N_0 performance of the proposed CM-MMSE-SDMA-OFDM schemes, respectively.

Here we define the user load of an L-user and P-receiver SDMA-OFDM system as:

$$\alpha_P = \frac{L}{P}, \tag{4.14}$$

which assumes a value of unity in case of full user load, when the number of users is equal to the number of receiver antenna elements. The simulation results generated in the context of $\alpha_2 = 0.5$ and $\alpha_2 = 1$ are plotted at the left and right side of Figure 4.6, respectively. The BER performance of the 32-state TC code assisted MMSE-SDMA-OFDM [5] system is also portrayed as a reference. Furthermore, the performance of the unprotected 4QAM SDMA-OFDM system and that of the single-user BPSK scheme communicating over an AWGN channel is also provided as a benchmarker. As observed in Figure 4.6, the TC-assisted arrangement and the various CM-assisted schemes provide a similar BER performance in both scenarios. As expected, all the FEC-aided schemes perform significantly better than their unprotected counterparts in the BER performance investigations. Furthermore, the TTCM-aided scheme is found to give the best CWER performance from the set of all CM-aided schemes in both the half-loaded and fully-loaded scenarios, where α_2 is equal to 0.5 and 1, respectively. This suggests that more transmission errors can be eliminated by TTCM than by the other three CM schemes, although the burst errors inflicted by deep frequency-domain channel fades cannot be recovered completely. However, this effect may be potentially mitigated by employing WHTS, as discussed in Section 4.2.2.2.

As expected, for each of the schemes evaluated, we may notice that the performance achieved in the context of $\alpha_2 = 0.5$, is better than that attained, when we have $\alpha_2 = 1$. This phenomenon may be explained as follows. Since P receiver antenna elements are invoked at the BS, there are P uplink paths for each MS user having one transmitter antenna. Hence the achievable spatial diversity order provided by the P paths remains the same for each user, regardless of the total number of simultaneous users supported. However, when the user load is lower, i.e. the number of users supported is lower, the MMSE combiner will benefit from a higher degree of freedom in terms of the choice of the array weights optimized for differentiating the different users' transmitted signal, and thus the system becomes more efficient in terms of suppressing the reduced Multi-User Interference (MUI).

In Figure 4.7, we provide the subcarrier based BER versus E_b/N_0 performance of the TTCM-assisted MMSE-SDMA-OFDM system in the context of two users and two receiver antenna elements. Comparing Figure 4.5 to Figure 4.7, where the beneficial effects of WHTS have been characterized, we may notice that the achievable performance improvement attained by TTCM, or more generally by the CM schemes, is typically higher than that achieved by WHTS.

Having discussed the beneficial effects of WHTS and those of CM on the SDMA-OFDM system, as described in Section 4.3.1 and earlier in this section, respectively, we now combine the MMSE-SDMA-OFDM system with CM and WHTS. The corresponding simulation results are portrayed in Figure 4.8, where the left and right side of the figure illustrate the scenarios of $\alpha_2 = 0.5$ and $\alpha_2 = 1$, while the top and bottom of the figure shows the BER and CWER performance, respectively. Again, the TTCM-aided scheme was found to give the best CWER performance among all the CM-aided schemes considered. Comparison of Figure 4.6 and Figure 4.8 shows that in the CM-aided MMSE-SDMA-OFDM system the employment of WHTS having a block size of 32 only insignificantly improves the system's BER and CWER performance, since most of the achievable diversity gain may have already been achieved by using the CM schemes. However, the employment of WHTS has the potential of further enhancing the CM-SDMA-OFDM system's performance in highly-dispersive propagation environments, an issue which will be further discussed in Section 4.3.2.2.

Furthermore, if a longer CM codeword length is used, the system's performance can be further improved at the cost of a higher computational complexity. The effects of different CM codeword lengths can be seen in Figure 4.9. As expected, when a higher codeword length is employed, the system's performance becomes better, since a longer CM codeword is capable of better averaging the bursty error effects. However this performance improvement is achieved at a substantially higher complexity. For examples of the associated complexity issues, the interested reader is referred to Chapter 9 of [359].

4.3.2.1.2 Four Receiver Antenna Elements

In Section 4.3.2.1.1, we have compared the various CM- and WHTS-aided schemes in the context of one or two users and two receiver antenna elements. In this section, we investigate a higher-order spatial diversity assisted scenario by increasing the number of receiver antenna elements, and thus supporting a higher number of simultaneous users.

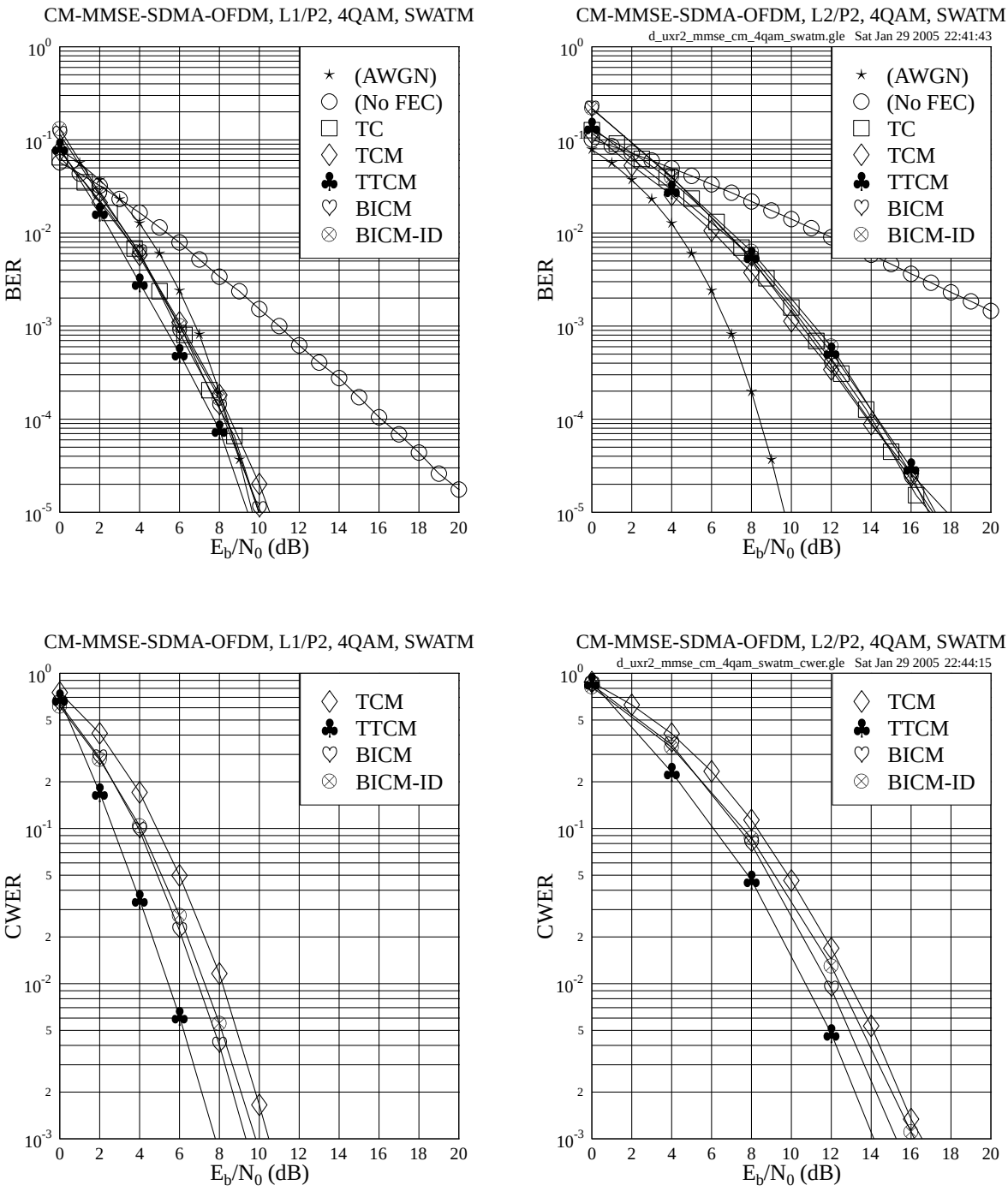

Figure 4.6: BER (top) and **CWER (bottom)** versus E_b/N_0 performance of the **CM-assisted MMSE-SDMA-OFDM** system employing a 4QAM scheme for transmission over the **SWATM** channel, where **L=1 (left)** or **L=2 (right)** users are supported with the aid of **P=2** receiver antenna elements. The CM parameters are given in Table 4.1. The CM codeword length is **1024** symbols. The BER performance of the same 4QAM MMSE-SDMA-OFDM system assisted by the half-rate TC code [5] (the curves with the legend of □) is also provided for reference.

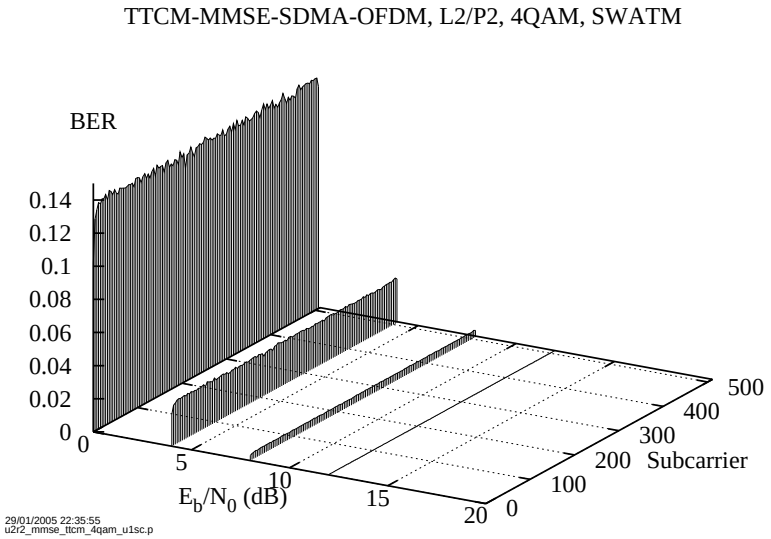

Figure 4.7: BER versus E_b/N_0 performance as a function of the subcarrier index of the **TTCM-assisted MMSE-SDMA-OFDM** system employing a 4QAM scheme for transmission over the **SWATM** channel, where **L=2** users are supported with the aid of **P=2** receiver antenna elements. The TTCM codeword length is **1024** symbols.

Figures 4.10 and 4.11 show the BER and CWER performance achieved by the CM- and WHTS-aided MMSE-SDMA-OFDM schemes in the scenario, where there are four receivers supporting a maximum number of four users. The BER performance of the 32-state TC code assisted MMSE-SDMA-OFDM [5] system is also provided as a reference. As seen in Figure 4.10, similar to the two-receiver scenario of Figure 4.8, the TC-assisted arrangement and the various CM-aided schemes achieve a similar BER performance at a specific user load. However, again, the TTCM-aided scheme stands out of all CM-aided schemes by attaining a better CWER performance.

Furthermore, comparing Figure 4.8 to Figure 4.10, where there are two receivers supporting a maximum of two users, we find that at the same user load level, for example at $\alpha_4 = \alpha_2 = 0.5$ or $\alpha_4 = \alpha_2 = 1.0$, the E_b/N_0 performance achieved by the four-receiver system is approximately 4.5dB better than that of the two-receiver system, provided that the same CM-assisted scheme is used. This is because, when the number of the BS receiver antenna elements is increased, the SDMA-MIMO system becomes capable of providing a higher diversity gain, which may be expected to improve the system's performance for each user.

4.3.2.2 Performance Over the COST207 HT Channel

In this section, we will investigate the performance of the CM- and WHTS-assisted MMSE-SDMA-OFDM schemes, while communicating over a more dispersive channel, namely over the 12-path COST207 [447] Hilly Terrain (HT) channel. The impulse response of the channel model is portrayed in Figure 4.12, while the specific channel parameters are given in Table 4.2. Each of the twelve paths experiences independent Rayleigh fading having the same normalized Doppler frequency of $f'_d = 1.0 \times 10^{-5}$. Compared to the 512-subcarrier OFDM modem used for communication over the SWATM channel investigated in Section 4.3.2.1, we now employ a higher number of 2048 subcarriers and a cyclic prefix of 256, since the maximum path delay of the COST207 HT channel is longer than that of the SWATM channel, hence it requires a longer cyclic prefix for combatting the effects of Inter-Symbol Interference (ISI) [5, 26].

In Sections 4.3.2.2.1 and 4.3.2.2.2, we will compare the corresponding performance of the various CM- and WHTS-assisted MMSE-SDMA-OFDM schemes, when communicating over the COST207 HT channel. The parameters of the CM schemes used are summarized in Table 4.3.

4.3.2.2.1 Two Receiver Antenna Elements

We present the BER and CWER performance of the CM-assisted MMSE-SDMA-OFDM system dispensing with WHTS for transmission over the COST207 HT channel at the top of Figures 4.13 and 4.14, respectively. Two receiver

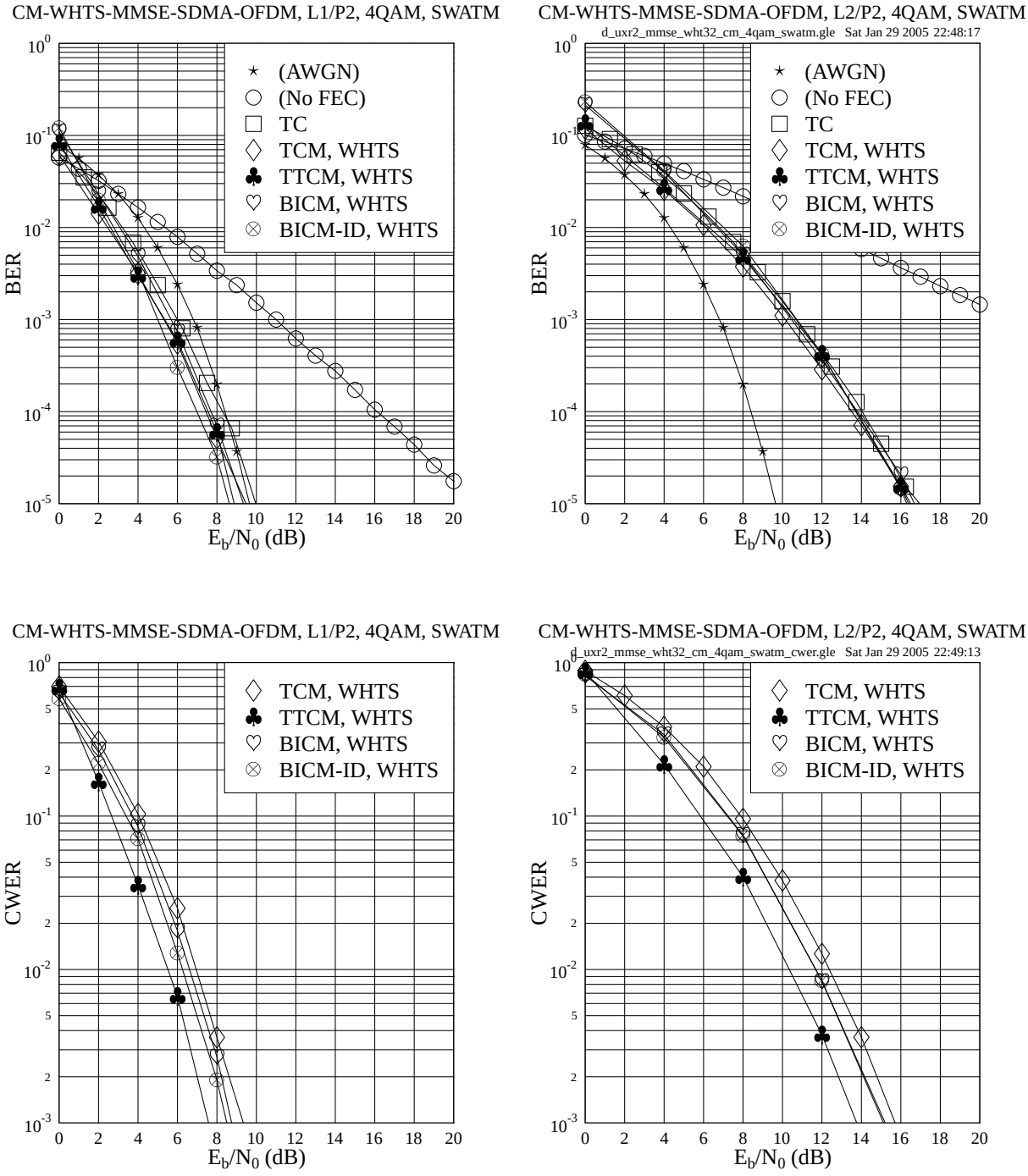

Figure 4.8: BER (top) and **CWER (bottom)** versus E_b/N_0 performance of the **CM- and WHTS-assisted MMSE-SDMA-OFDM** system employing a 4QAM scheme for transmission over the **SWATM** channel, where **L=1 (left)** or **L=2 (right)** users are supported with the aid of **P=2** receiver antenna elements. The CM parameters are given in Table 4.1. The CM codeword length is **1024** symbols and the WHT block size used is **32**. The BER performance of the 4QAM MMSE-SDMA-OFDM system assisted by the half-rate TC code [5] (the curves with the legend of □) is also provided for reference.

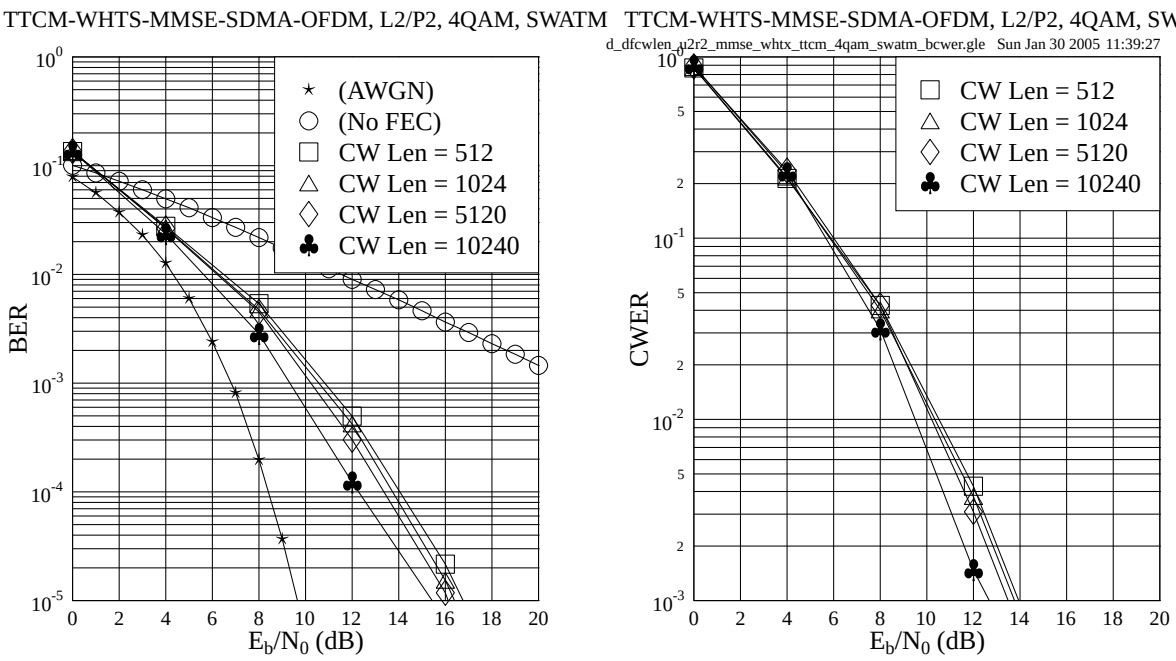

Figure 4.9: BER (left) and **CWER (right)** versus E_b/N_0 performance of the **TTCM- and WHTS-assisted MMSE-SDMA-OFDM** system employing a 4QAM scheme for transmission over the **SWATM** channel, where **L=2** users are supported with the aid of **P=2** receiver antenna elements. The TTCM parameters are given in Table 4.1, although a range of **different codeword lengths** is employed. The WHT block size used is **32**.

$1/T_s$	τ_{max}	f_d	f'_d	n	K	cp
9.14 MHz	19.9 μs	92.6 Hz	1.0×10^{-5}	12	2048	256

Table 4.2: Sampling Rate $1/T_s$, maximum path delay τ_{max}, maximum Doppler frequency f_d, normalized Doppler frequency f'_d, number of paths n, FFT length K and cyclic prefix length cp of the COST207 Hilly Terrain (HT) channel of Figure 4.12.

CM Scheme	Code Rate	Data Bits	Parity Bits	Code Memory	Iterations	Codeword Length	Modem
TCM	1/2	1	1	6	-	2048	4QAM
TTCM	1/2	1	1	3	4	2048	4QAM
BICM	1/2	1	1	6	-	2048	4QAM
BICMID	1/2	1	1	3	8	2048	4QAM

Table 4.3: The parameters of the various CM schemes used in the multi-user SDMA-OFDM system communicating over the COST207 HT channel of Figure 4.12.

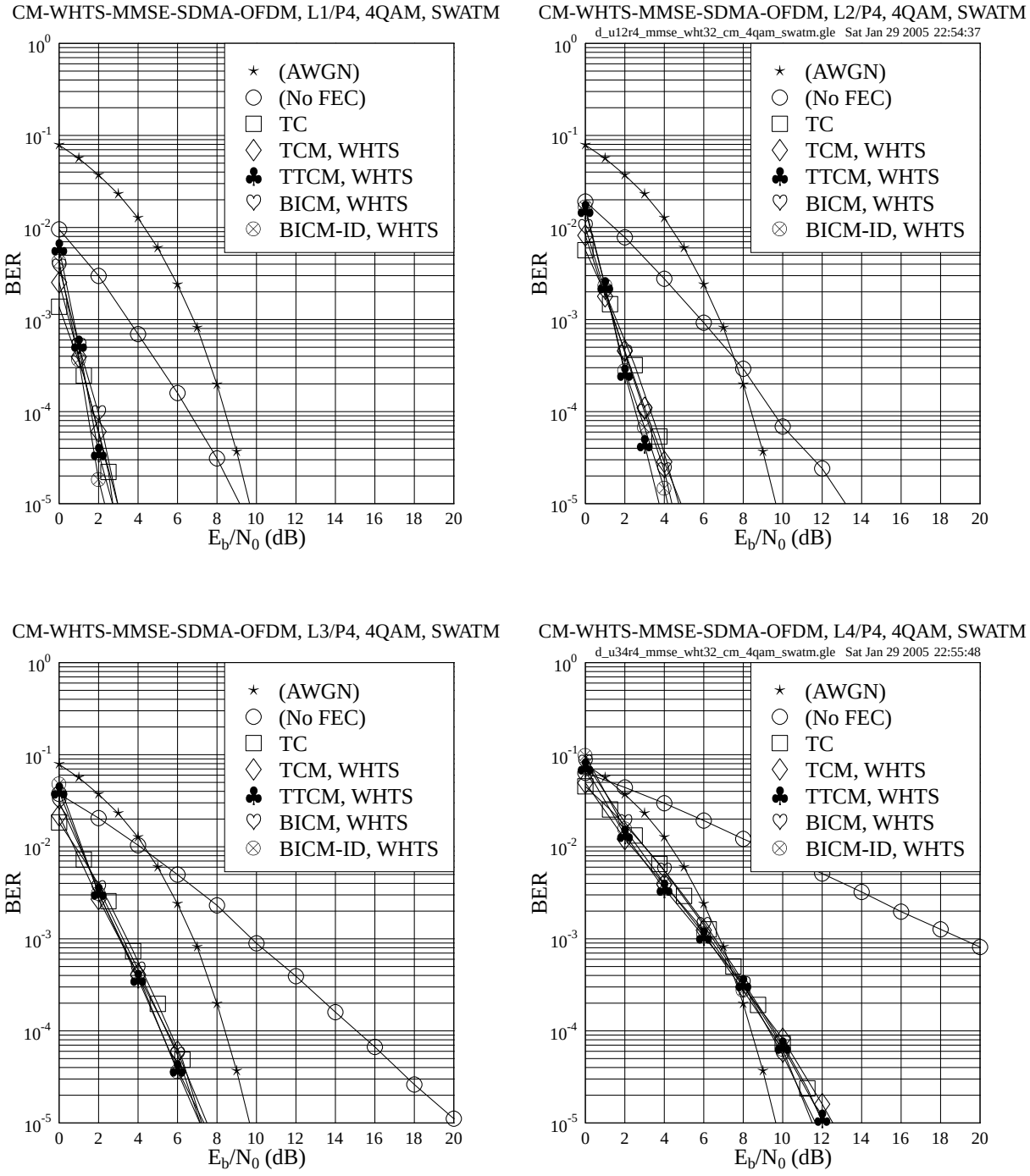

Figure 4.10: BER versus E_b/N_0 performance of the **CM- and WHTS-assisted MMSE-SDMA-OFDM** system employing a 4QAM scheme for transmission over the **SWATM** channel, where **L=1 (top left)**, **L=2 (top right)**, **L=3 (bottom left)** or **L=4 (bottom right)** users are supported with the aid of **P=4** receiver antenna elements. The CM parameters are given in Table 4.1. The CM codeword length is **1024** symbols and the WHT block size used is **32**. The BER performance of the 4QAM MMSE-SDMA-OFDM system assisted by the half-rate TC code [5] (the curves with the legend of □) is also provided for reference.

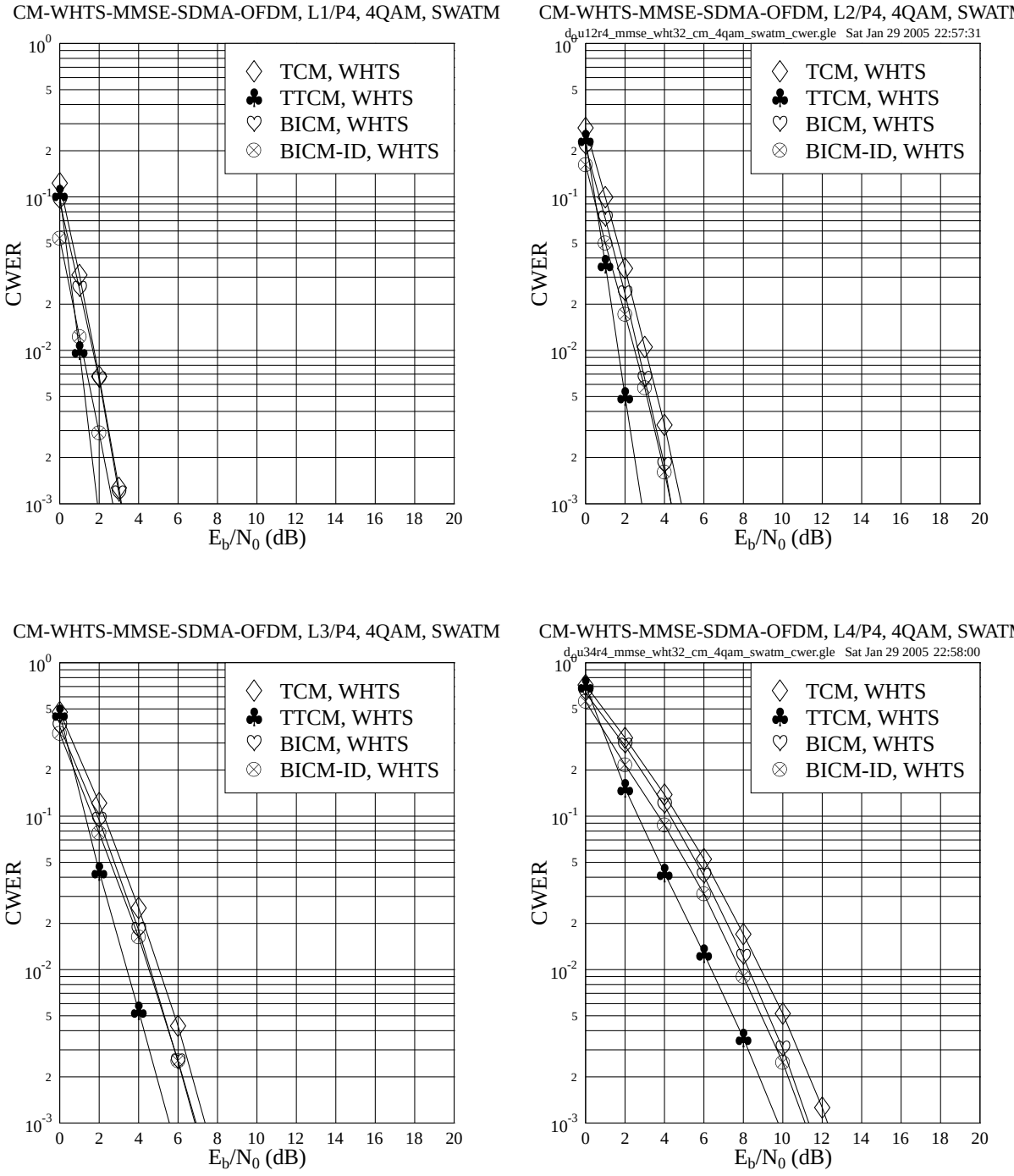

Figure 4.11: CWER versus E_b/N_0 performance of the **CM- and WHTS-assisted MMSE-SDMA-OFDM** system employing a 4QAM scheme for transmission over the **SWATM** channel, where **L=1 (top left)**, **L=2 (top right)**, **L=3 (bottom left)** or **L=4 (bottom right)** users are supported with the aid of **P=4** receiver antenna elements. The CM parameters are given in Table 4.1. The CM codeword length is **1024** symbols and the WHT block size used is **32**.

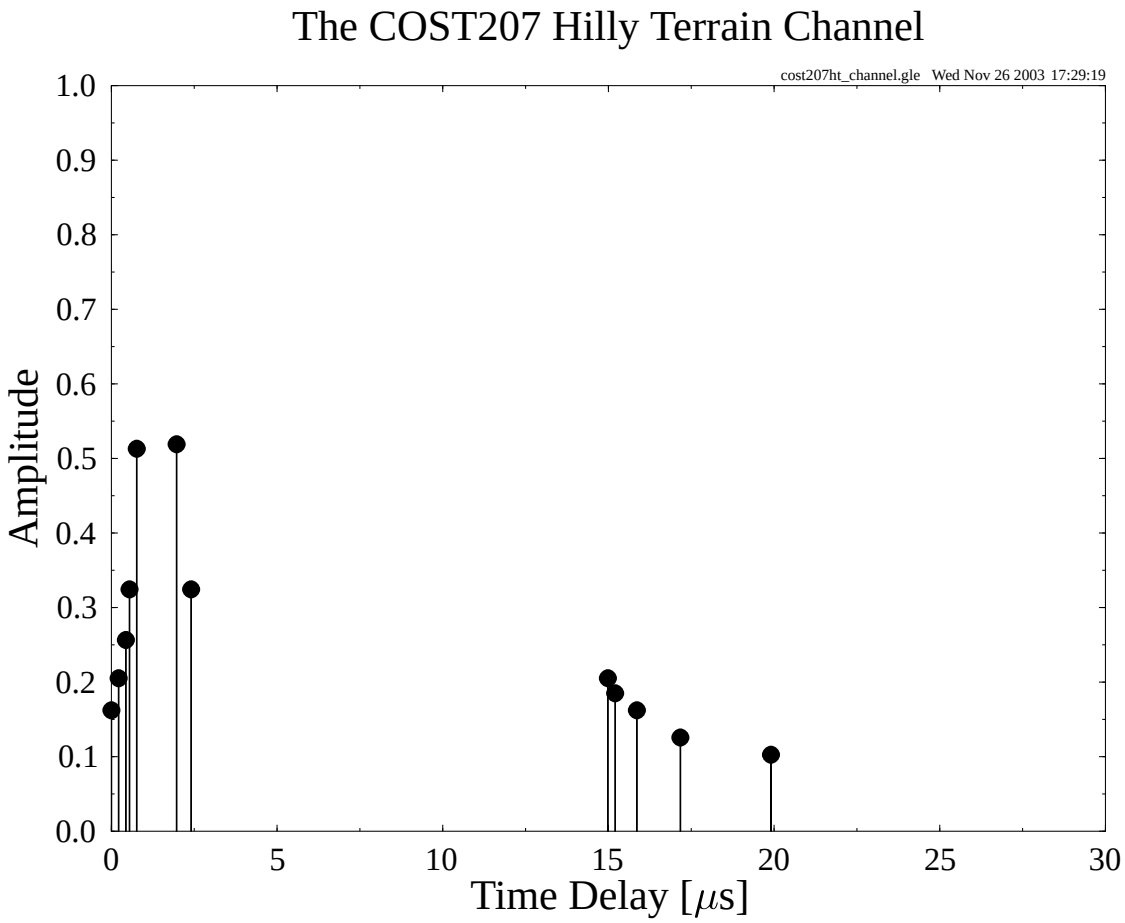

Figure 4.12: COST207 Hilly Terrain (HT) channel impulse response. The corresponding parameters of the channel are summarized in Table 4.2.

antenna elements are employed for supporting a maximum of two users. The simulation results show that the TTCM-aided scheme constitutes the best design option in terms of both the BER and CWER, attaining a coding gain ranging from 2dB to 4dB over the other three CM-aided schemes at the BER of 10^{-5} without the assistance of WHTS. Furthermore, when WHTS is incorporated into the CM-MMSE-SDMA-OFDM system, as seen in the bottom of Figures 4.13 and 4.14, a further useful E_b/N_0 gain is achieved by most of the four schemes, especially by the TCM-aided arrangement. However, recall that in Section 4.3.2.1 where the SWATM channel was employed, the additional E_b/N_0 gain achieved by spreading in the context of the various CM- and WHTS-assisted schemes was rather modest. This result may suggest that in highly dispersive environments, such as that characterized by the 12-path COST207 HT channel, the channel-coded SDMA-OFDM system's performance may be further improved by employing WHTS. This spreading-induced E_b/N_0 gain was achieved, because the detrimental effects imposed on the system's average BER performance by the deeply-faded subcarriers has been spread over the entire WHT block, and these randomized or dispersed channel errors may be more readily corrected by the CM decoders.

It transpires from Figures 4.13 and 4.14 that the four CM-aided schemes communicating over the COST207 HT channel attain a different performance. This observation is different from what was noted in Figures 4.6 and 4.8, where the performance of the various CM-aided schemes communicating over the SWATM channel was more similar. The reason for this phenomenon is that the amplitude variation of the FD-CHTFs becomes both more frequent and more dramatic, when the channel exhibits a longer path delay [359]. Since the COST207 HT channel's maximum path delay is $19.9\mu s$, which is significantly longer than the $48.9ns$ maximum dispersion of the SWATM channel, the fades occur more frequently in the FD-CHTF of the COST207 HT channel, as indicated by Figure 4.15. Apparently, in the COST207 HT channel displayed at the left hand side of Figure 4.15, the frequency domain separation between the neighbouring fades is proportionately lower than that in the SWATM channel shown at the right side of Figure 4.15. This characteristic will result in more uniformly distributed corrupted subcarrier symbols which can be more readily corrected by the channel codes. More specifically, when a deep fade occurs in the FD-CHTF of the SWATM channel, a number of consecutive subcarriers which are located in the corresponding faded block of subcarriers may be seriously

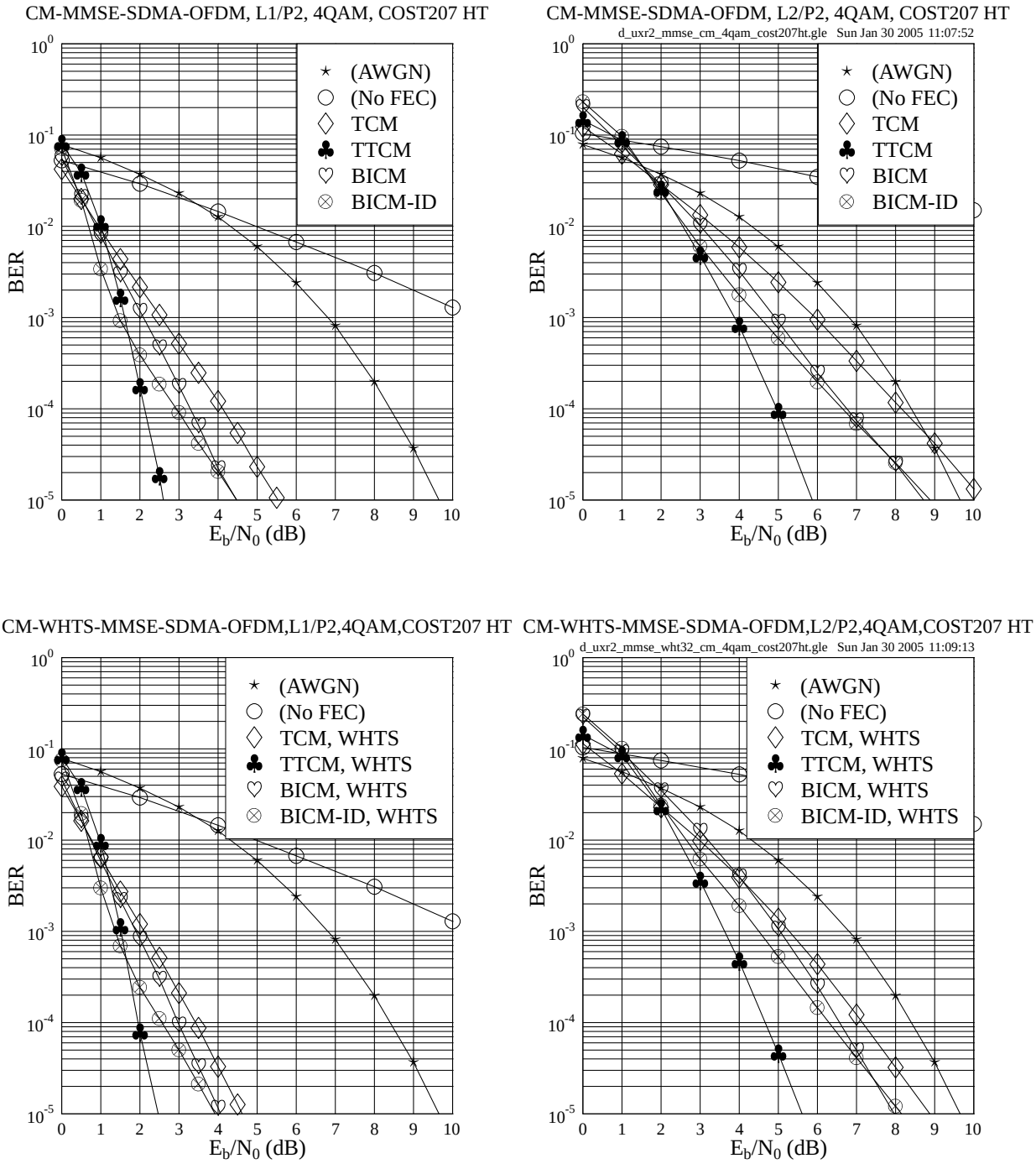

Figure 4.13: BER versus E_b/N_0 performance of the **CM-assisted MMSE-SDMA-OFDM (top)** and **CM- and WHTS-assisted MMSE-SDMA-OFDM (bottom)** systems employing a 4QAM scheme for transmission over the **COST207 HT** channel, where **L=1 (left)** or **L=2 (right)** users are supported with the aid of **P=2** receiver antenna elements. The CM parameters are given in Table 4.3. The CM codeword length is **2048** symbols and the WHT block size used is **32**.

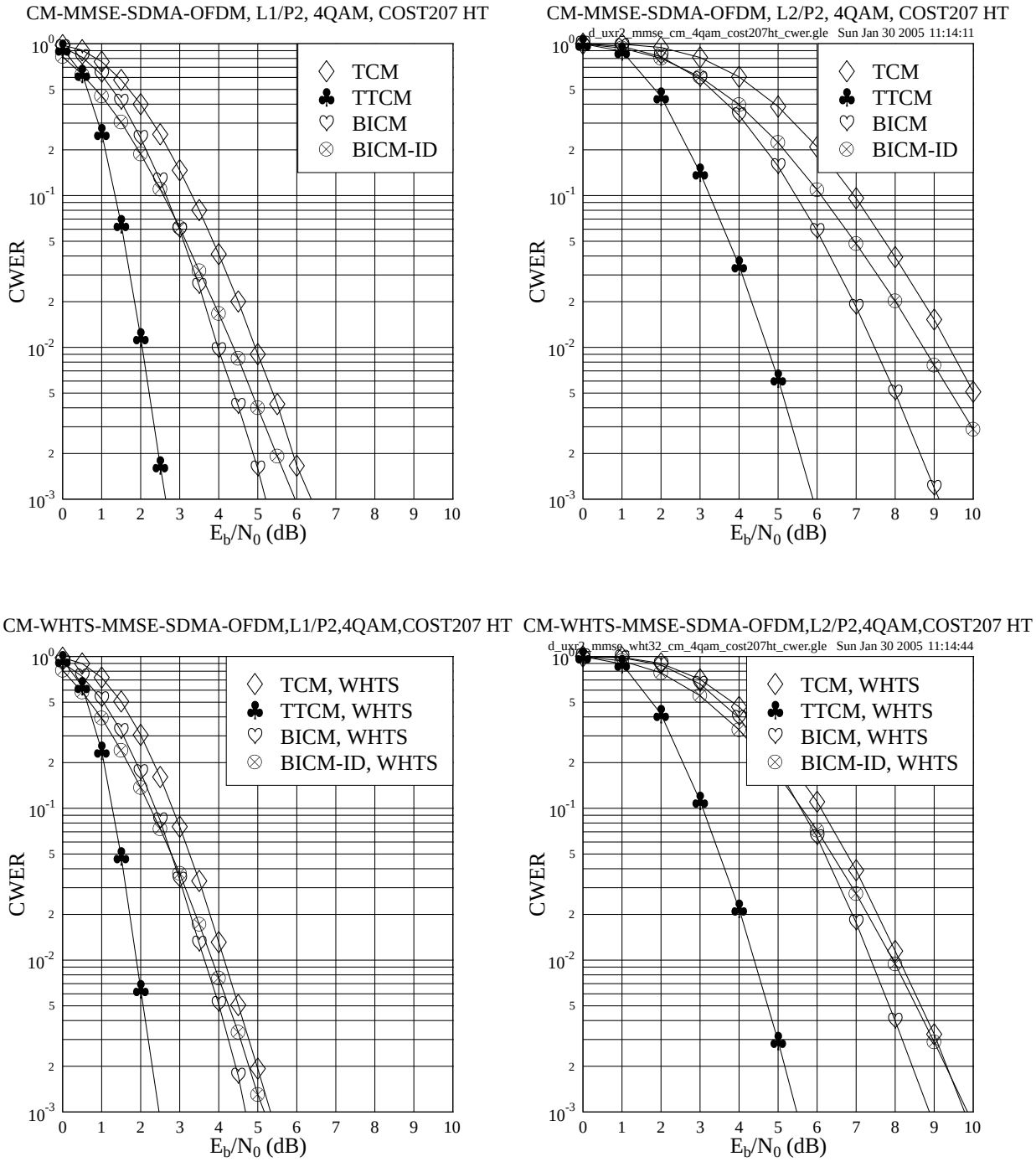

Figure 4.14: CWER versus E_b/N_0 performance of the **CM-assisted MMSE-SDMA-OFDM (top)** and **CM- and WHTS-assisted MMSE-SDMA-OFDM (bottom)** systems employing a 4QAM scheme for transmission over the **COST207 HT** channel, where **L=1 (left)** or **L=2 (right)** users are supported with the aid of **P=2** receiver antenna elements. The CM parameters are given in Table 4.3. The CM codeword length is **2048** symbols and the WHT block size used is **32**.

affected by the fade.

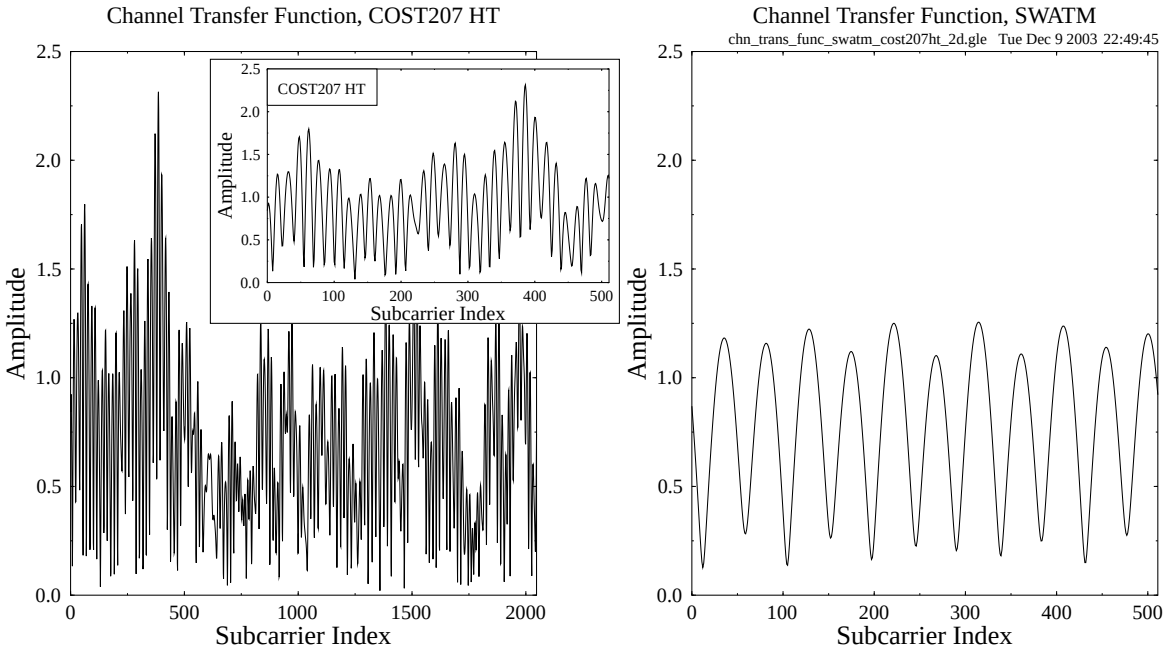

Figure 4.15: The FD-CHTF amplitudes of the **COST207 HT (left)** and **SWATM (right)** channels plotted for the duration of one OFDM symbol.

This implies that the channel codes, for example one of the four CM schemes, may have a lower chance of correcting less-frequently occurring but prolonged error bursts, than more frequently encountered isolated errors. The more prolonged error bursts imposed by the SWATM channel often overload the error correction capability of the CM schemes, regardless of which of the four CM schemes is used, since owing to the preponderance of transmission errors their trellis decoder often opts for choosing the wrong trellis path. This is particularly true for CM schemes using short channel interleavers. Therefore, this phenomenon results in a similar performance for the various CM-aided schemes, when communicating over the SWATM channel, as seen in Figures 4.6 and 4.8.

By contrast, in the context of the COST207 HT channel such prolonged error bursts are unlikely to occur, since the faded subcarriers result in more frequent but less prolonged error bursts, which are reminiscent of the error distributions experienced in AWGN channels and therefore may have a higher chance of being corrected by the CM decoders used at the receiver. Hence, the different error-correcting capability of the various CM schemes becomes more explicit, as revealed in Figures 4.13 and 4.14.

4.3.2.2.2 Four Receiver Antenna Elements

As mentioned in Section 4.3.2.1.2, when the number of receiver antenna elements is increased to four, the performance of the system becomes better, than that experienced in the two-receiver scenario, which was discussed in Section 4.3.2.2.1. In Figures 4.16 and 4.17, we compare both the BER and CWER performance of the different CM- and WHTS-assisted schemes for transmissions over the COST207 HT channel, while employing four receiver antenna elements at user loads of $\alpha_4 = 0.5$ and $\alpha_4 = 1.0$, as shown at the left and right hand sides of Figures 4.16 and 4.17, respectively. Again, it can be seen in the figures that the performance achieved by the four-receiver SDMA-OFDM system, which has a higher diversity order, is better than that attained by the two-receiver system both at the user loads of $\alpha_{2,4} = 0.5$ and $\alpha_{2,4} = 1.0$, averaging at an approximately 3dB E_b/N_0 improvement for a specific CM-aided scheme. Hence a plausible conclusion is that at a specific user load α_P, the more receivers the SDMA-MIMO system employs, the higher attainable grade of diversity and thus an improved performance may be achieved. However, the relative performance improvement achieved by an already high-order system upon doubling the number of receivers is expected to be lower than that in a lower-order system, since most of the attainable gain may have already been achieved, which results in a near-Gaussian performance.

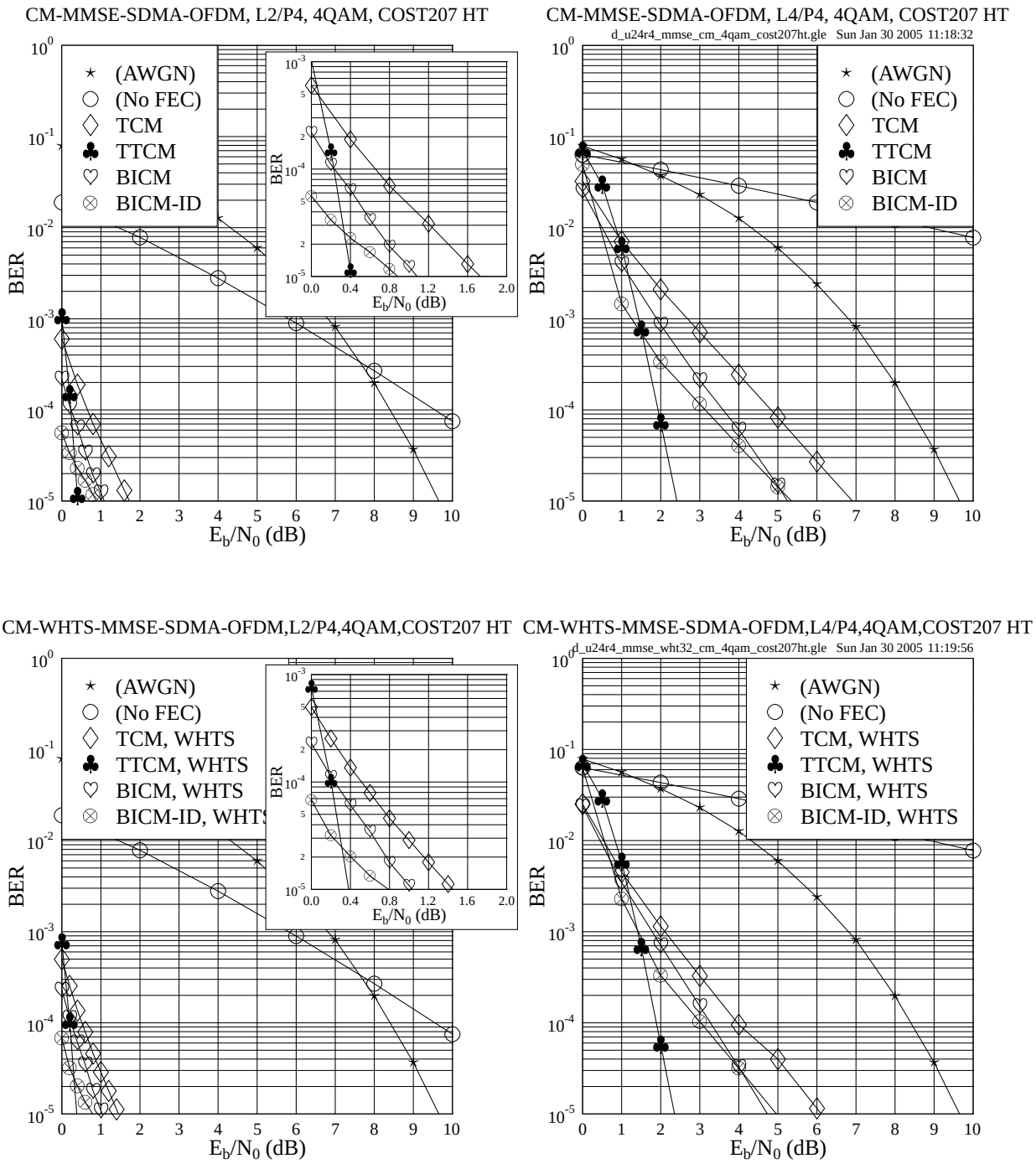

Figure 4.16: **BER** versus E_b/N_0 performance of the **CM-assisted MMSE-SDMA-OFDM (top)** and **CM- and WHTS-assisted MMSE-SDMA-OFDM (bottom)** systems employing a 4QAM scheme for transmission over the **COST207 HT** channel, where **L=2 (left)** or **L=4 (right)** users are supported with the aid of **P=4** receiver antenna elements. The CM parameters are given in Table 4.3. The CM codeword length is **2048** symbols and the WHT block size used is **32**.

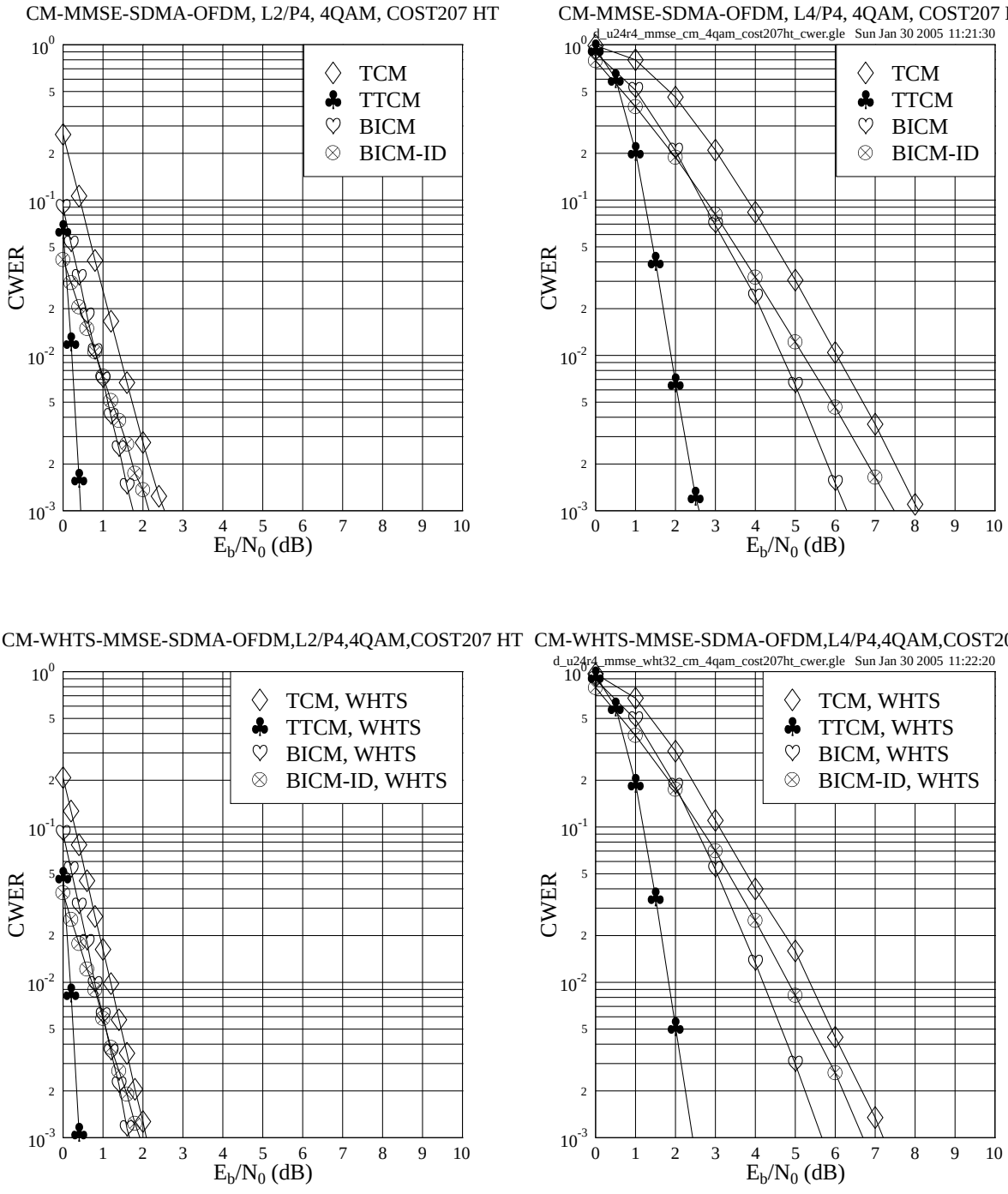

Figure 4.17: CWER versus E_b/N_0 performance of the **CM-assisted MMSE-SDMA-OFDM (top)** and **CM- and WHTS-assisted MMSE-SDMA-OFDM (bottom)** systems employing a 4QAM scheme for transmission over the **COST207 HT** channel, where **L=2 (left)** or **L=4 (right)** users are supported with the aid of **P=4** receiver antenna elements. The CM parameters are given in Table 4.3. The CM codeword length is **2048** symbols and the WHT block size used is **32**.

4.3.2.2.3 Performance Comparisons

CM Schemes	Spreading	$\alpha_{2,4} = 0.5$		$\alpha_{2,4} = 1.0$	
		U1R2	U2R4	U2R2	U4R4
(No FEC)	No WHTS	20.85	12.99	41.97	38.85
	WHTS	14.53	9.53	23.30	20.78
	E_b/N_0 *Gain*	**6.32**	**3.46**	**18.67**	**18.07**
TCM	No WHTS	5.53	1.73	10.28	6.91
	WHTS	4.62	1.45	8.88	6.11
	E_b/N_0 *Gain*	**0.91**	**0.28**	**1.40**	**0.80**
TTCM	No WHTS	2.60	0.41	5.87	2.41
	WHTS	2.47	0.38	5.61	2.35
	E_b/N_0 *Gain*	**0.13**	**0.03**	**0.26**	**0.06**
BICM	No WHTS	4.47	1.08	8.72	5.25
	WHTS	4.06	1.03	7.97	4.73
	E_b/N_0 *Gain*	**0.41**	**0.05**	**0.75**	**0.52**
BICM-ID	No WHTS	4.48	0.88	8.89	5.35
	WHTS	3.92	0.79	8.15	4.96
	E_b/N_0 *Gain*	**0.56**	**0.09**	**0.74**	**0.39**

Table 4.4: The E_b/N_0 values required and the spreading-induced gains achieved at the BER of 10^{-5} of the various CM- and WHTS-assisted MMSE-SDMA-OFDM schemes for communicating over the COST207 HT channel. The CM parameters are given in Table 4.3. The CM codeword length is 2048 symbols and the WHT block size used is 32. All data are in dB.

Table 4.4 summarizes the E_b/N_0 values required by the various CM- and WHTS-assisted MMSE-SDMA-OFDM schemes for achieving a BER of 10^{-5}. The corresponding spreading-induced E_b/N_0 gains achieved by the WHTS-assisted schemes are also provided, which are defined as the E_b/N_0 difference, expressed in terms of dBs, at a BER of 10^{-5} between the WHTS-assisted and the unspreading system having the same effective throughput.

Several useful points can be concluded from Table 4.4. Firstly, when we have a specific user load, the spreading-induced E_b/N_0 gain achieved by a system having a lower diversity order is higher, regardless whether CM is employed or not. For example, when we have a user load of $\alpha_{2,4} = 0.5$, the spreading-induced E_b/N_0 gains achieved in the No-FEC-, TCM-, TTCM-, BICM- and BICM-ID-assisted two-receiver systems are 6.32, 0.91, 0.13, 0.41 and 0.56dB, respectively. By contrast, lower spreading-induced E_b/N_0 gains of 3.46, 0.28, 0.03, 0.05 and 0.09dB are achieved in the corresponding four-receiver systems, respectively. In other words, in relatively lower diversity-order scenarios, the subcarrier-based WHTS technique may be expected to attain a higher system performance improvement.

Furthermore, if the number of users supported is fixed but the number of receiver antenna elements is varied, similar conclusions may be drawn. When there are two simultaneous users, for example, the spreading-induced E_b/N_0 gains achieved in the two-receiver scenario, are higher than those achieved in the four-receiver scenario, as observed in Table 4.4. A plausible explanation for this fact may be as follows. In the SDMA-MIMO system, when a higher number of receiver antenna elements is employed, a potentially higher space diversity can be achieved. In this scenario, the benefits of spreading may be less substantial, especially in the CM-aided system, since most of the attainable gain has already been achieved by using the channel codes.

Secondly, when the BS employs a given number of receiver antenna elements, the spreading-induced E_b/N_0 gains achieved in the context of the fully-loaded systems are higher than in the half-loaded systems, regardless of the employment of channel codes. For instance, if we have two receivers installed in the BS, the various schemes having a user load of $\alpha_2 = 1.0$ attain a higher spreading-induced E_b/N_0 gain, than their half-loaded counterparts, as seen in Table 4.4. This suggests that more benefits may arise from WHTS, especially in the fully-loaded scenarios, where the MUD suffers from a relatively low efficiency in differentiating the different users' signals. Furthermore, if

a longer WHT block size is used, the E_b/N_0 gain of WHTS may even be higher, since the detrimental bursty error effects degrading the system's average BER performance will be spread over a higher block length, hence increasing the chances of correcting a higher number of errors, as it will be presented in Section 4.3.2.3.

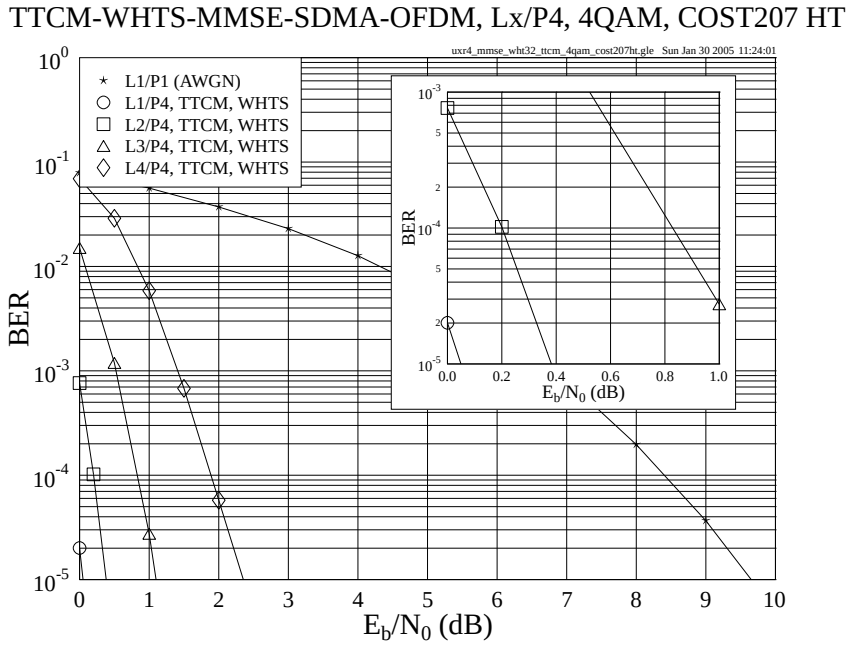

Figure 4.18: BER versus E_b/N_0 performance of the **TTCM- and WHTS-assisted MMSE-SDMA-OFDM** system employing a 4QAM scheme for transmission over the **COST207 HT** channel, where **L=1, 2, 3, 4** users are supported with the aid of **P=4** receiver antenna elements. The TTCM parameters are given in Table 4.3. The TTCM codeword length is **2048** symbols and the WHT block size used is **32**.

In order to characterize the system's performance at different user loads, as an example, we portray the BER performance of the TTCM- and WHTS-aided scheme at a range of different user loads in Figure 4.18. As expected, the system's performance improves, when the user load is lower, since the MUD will have a better chance of separating the different users' signals. It is also observed in Figure 4.18 that the relevant E_b/N_0 gain achieved by a lower-load scheme over a higher-load arrangement reduces, when the user load decreases. This again shows that most of the achievable E_b/N_0 gain has already been attained at a medium user load.

Figure 4.19 shows the E_b/N_0 crossing points of the various CM-WHTS-MMSE-SDMA-OFDM schemes at the BER of 10^{-5}. It is shown explicitly that the performance gap between the different CM-aided schemes increases as the user load increases. Furthermore, from Figure 4.19 we see that the TTCM-aided scheme performs best in high user-load scenarios, namely for $\alpha_4 \geq 0.5$. In other words, the other three CM schemes, namely the TCM, BICM and BICM-ID arrangements will suffer a higher performance degradation than TTCM, when the MUD's user-separation capability erodes owing to the increased MUI.

In Figure 4.20 we compare the total gain achieved by the four different CM-aided schemes, which includes both the coding gain and the spreading-induced E_b/N_0 gain. As the figure indicates, the TTCM-aided scheme achieved a further E_b/N_0 gain of 3.76dB, 2.38dB and 2.61dB over the TCM, BICM and BICM-ID aided schemes in the fully-loaded scenario, respectively. At a relatively low user load, namely for $\alpha_4 \leq 0.5$, the various schemes provide a similar performance, because most of the attainable gain in the four-receiver SDMA-OFDM system has already been achieved, as discussed earlier in this section.

4.3.2.3 Effects of the WHT Block Size

In Sections 4.3.2.1 and 4.3.2.2 we have investigated the CM- and WHTS-assisted MMSE-SDMA-OFDM system for transmission over the SWATM and COST207 HT channel, respectively. In this section, we will study how the variation of the WHT block size affects the system's performance, when communicating over the above two channel models.

As mentioned in Section 4.3.2.2.3, when a larger WHT block size is used for the SDMA-OFDM system, the system's performance may potentially be improved, since the signals carried by the subcarriers that are badly-affected

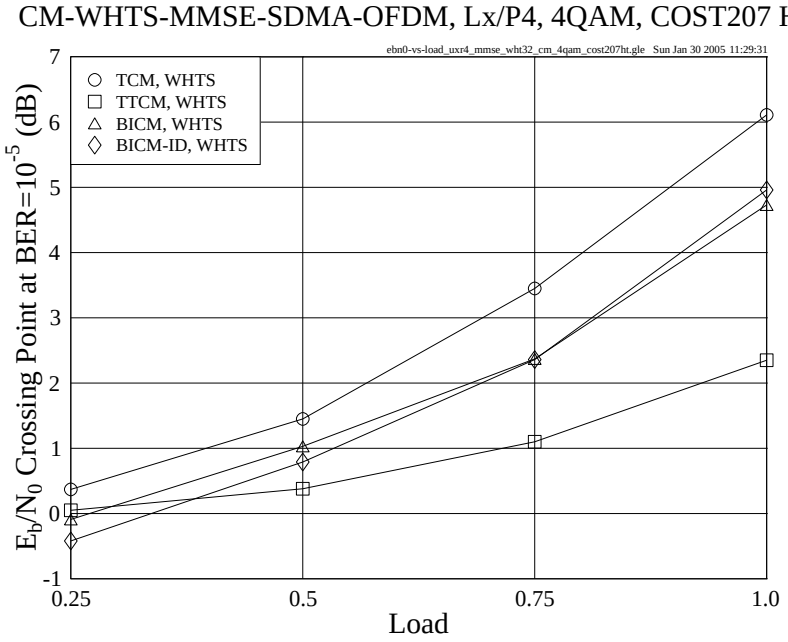

Figure 4.19: E_b/N_0 Crossing Point at the BER of 10^{-5} versus user load performance of the **CM- and WHTS-assisted MMSE-SDMA-OFDM** system employing a 4QAM scheme for transmission over the **COST207 HT** channel, where **L=1, 2, 3, 4** users are supported with the aid of **P=4** receiver antenna elements. The CM parameters are given in Table 4.3. The CM codeword length is **2048** symbols and the WHT block size used is **32**.

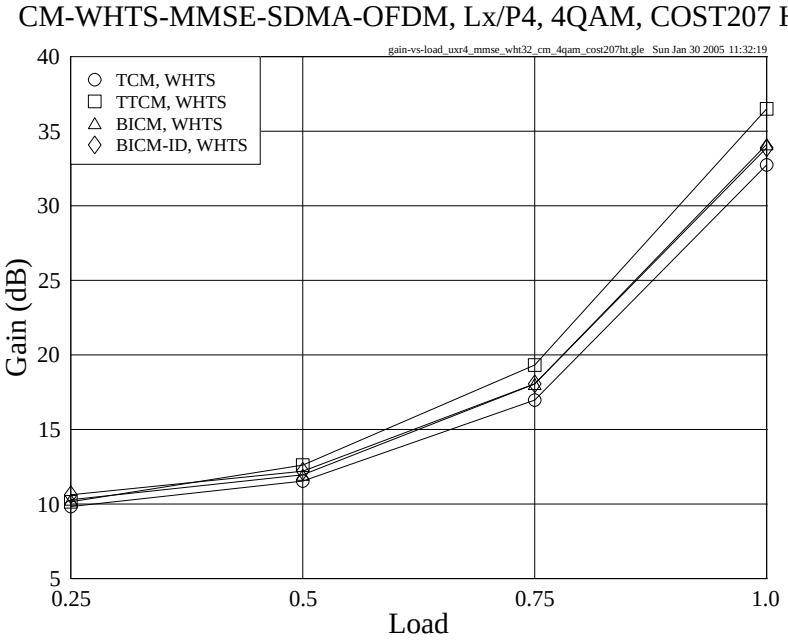

Figure 4.20: Gain at the BER of 10^{-5} versus user load performance of the **CM- and WHTS-assisted MMSE-SDMA-OFDM** system employing a 4QAM scheme for transmission over the **COST207 HT** channel, where **L=1, 2, 3, 4** users are supported with the aid of **P=4** receiver antenna elements. The CM parameters are given in Table 4.3. The CM codeword length is **2048** symbols and the WHT block size used is **32**.

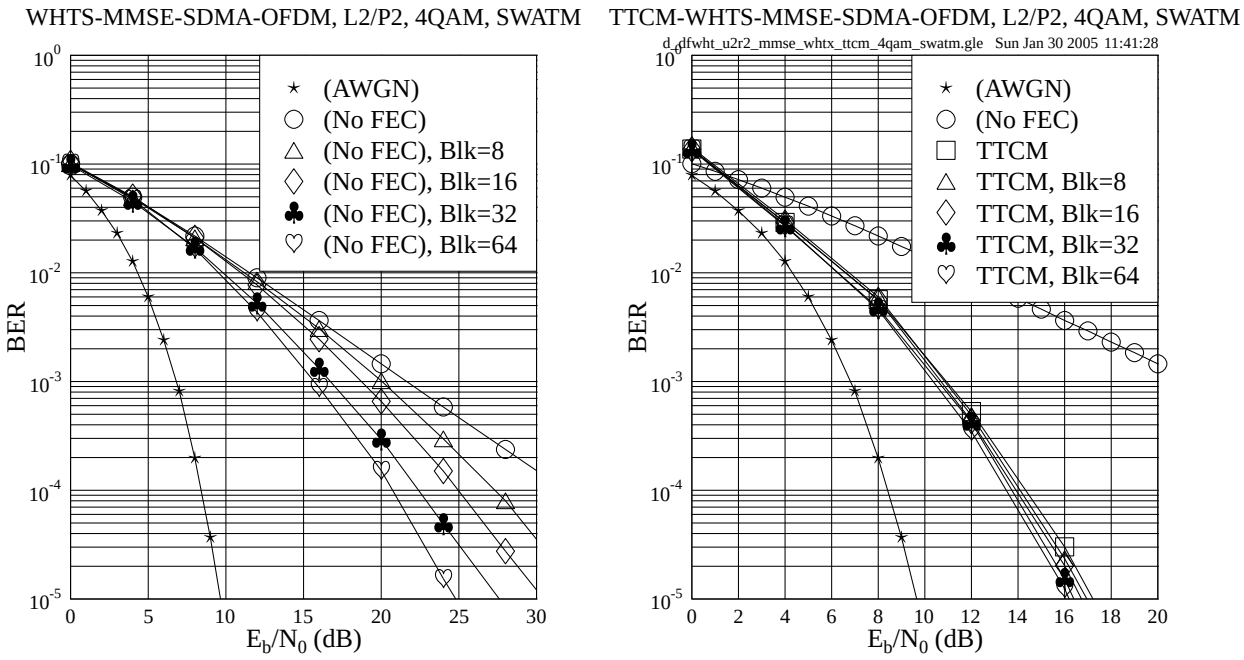

Figure 4.21: BER versus E_b/N_0 performance of the **WHTS-assisted MMSE-SDMA-OFDM (left)** and **TTCM- and WHTS-assisted MMSE-SDMA-OFDM (right)** systems using **different WHT block size** and employing a 4QAM scheme for transmission over the **SWATM** channel, where **L=2** users are supported with the aid of **P=2** receiver antenna elements. The TTCM parameters are given in Table 4.1 and the TTCM codeword length is **1024** symbols.

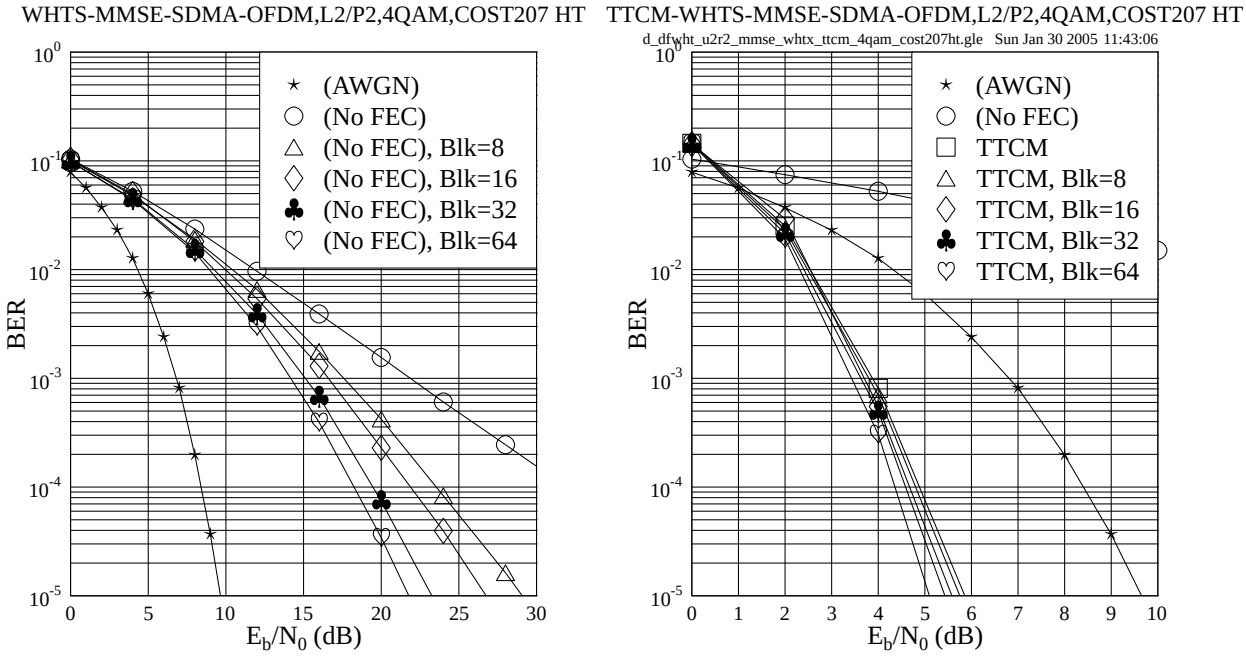

Figure 4.22: BER versus E_b/N_0 performance of the **WHTS-assisted MMSE-SDMA-OFDM (left)** and **TTCM- and WHTS-assisted MMSE-SDMA-OFDM (right)** systems using **different WHT block size** and employing a 4QAM scheme for transmission over the **COST207 HT** channel, where **L=2** users are supported with the aid of **P=2** receiver antenna elements. The TTCM parameters are given in Table 4.3 and the TTCM codeword length is **2048** symbols.

by deep channel fades could be spread over a larger set of subcarriers, which may mitigate the detrimental channel effects and thus assists the receiver in achieving a better performance. In order to show the effects imposed by different-length WHTS schemes, we provide simulation results generated in the context of different WHT block sizes in both the No-CM and CM-aided scenarios, as shown in the left and right hand sides of Figure 4.21, respectively. As expected, the system's performance was improved upon increasing the WHT block size, regardless whether CM was employed or not. In the context of the COST207 HT channel of Figure 4.12, similarly, a performance improvement is observed, when an increased WHT block size is employed as portrayed in Figure 4.22.

Furthermore, we may notice that the spreading-induced E_b/N_0 gains achieved by the No-CM schemes, when using a larger WHT block size, are significantly higher than those attained by the TTCM-aided schemes, as observed in Figures 4.21 and 4.22. This suggests that in the SDMA-OFDM system employing no CM, the performance improvement potential owing to the employment of a larger WHT block size is higher than that in the CM-aided system, where most of the achievable diversity gain has been attained by the time-diversity of the CM schemes. However, as suggested by Table 4.2, the other three CM-aided schemes, for example the TCM-aided arrangement, may be capable of achieving a higher spreading-induced gain than the TTCM-aided scheme with the aid of WHTS. Therefore, owing to their lower time-diversity and relatively more modest unspread performance, a potentially higher spreading-induced E_b/N_0 gain may be achieved by combining WHTS with the TCM, BICM and BICM-ID assisted schemes than in conjunction with the TTCM-aided arrangement, when a larger WHT block size is used. Having studied the effects of different WHT block sizes, let us now consider the impact of varying the Doppler frequency.

4.3.2.4 Effects of the Doppler Frequency

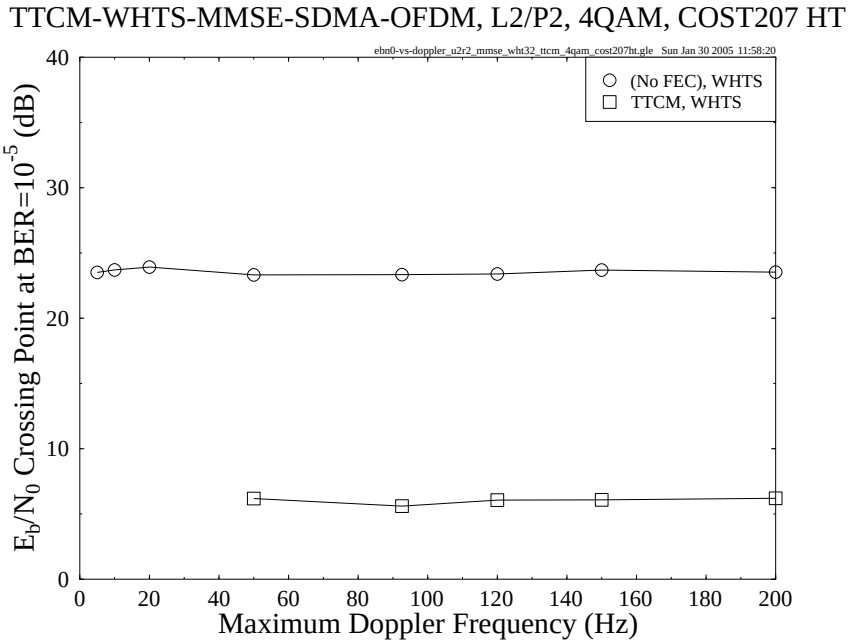

Figure 4.23: $\mathbf{E_b/N_0}$ Crossing Point at the BER of 10^{-5} versus maximum Doppler frequency performance of the **TTCM- and WHTS-assisted MMSE-SDMA-OFDM** system employing a 4QAM scheme for transmission over the **COST207 HT** channel, where **L=2** users are supported with the aid of **P=2** receiver antenna elements. The TTCM parameters are given in Table 4.3. The TTCM codeword length is **2048** symbols and the WHT block size used is **32**.

In our further investigations we have generated the BER versus E_b/N_0 curves of the TTCM- and WHTS-assisted MMSE-SDMA-OFDM system communicating over the COST207 HT channel, when the maximum Doppler frequency was fixed to a range of different values. For simplicity, here we have assumed perfect channel estimation. As before, the CIR of the 12-path COST207 HT channel of Figure 4.12 was used. For the sake of presenting these results in a compact form, the E_b/N_0 values required for maintaining a BER of 10^{-5} were extracted. In Figure 4.23, we show the E_b/N_0 crossing point at BER=10^{-5} versus the maximum Doppler frequency for the WHTS-assisted MMSE-SDMA-OFDM system both with and without the aid of TTCM, where two receivers were used for supporting two users. We conclude from the near-horizontal curves shown in Figure 4.23 that the maximum Doppler frequency does not significantly affect the performance of the WHTS-assisted MMSE-SDMA-OFDM system, regardless of the employment of TTCM. This may be a desirable benefit of the error-randomizing effect of WHTS, resulting in a robust-

ness against the variation of the mobile speed. Moreover, as expected, the performance of the TTCM-aided scheme was consistently better, than that of the scheme using no channel coding, as evidenced by Figure 4.23.

It is worth noting that when the channel's Doppler frequency is high, the effects of Inter-Carrier Interference (ICI) may become significant[1], as argued on page 81 of [5]. In this case for example the ICI-cancellation techniques of Chapter 4 in [5] may be invoked for combating the ICI effects.

4.4 Chapter Summary

The system model of our multi-user uplink SDMA-based OFDM system was presented in Section 4.2, where the SDMA-MIMO channel model was introduced in Section 4.2.1, followed by the detailed description of the CM-assisted multi-user SDMA-OFDM system employing the frequency-domain subcarrier-based WHTS scheme of Section 4.2.2. The theoretical foundations of the Minimum Mean-Square Error based Multi-User Detector were provided in Section 4.2.2.1. Furthermore, a detailed discussion of the WHTS technique was presented in Section 4.2.2.2.

In Section 4.3 the performance of the various CM- and WHTS-assisted MMSE-SDMA-OFDM schemes was studied and compared. The uncoded MMSE-SDMA-OFDM system was first investigated in Section 4.3.1, where it was found that WHTS was capable of improving the system's performance, since the bursty subcarrier errors can be pseudo-randomly spread across the subcarriers of the entire WHT block. In the investigations outlined in Section 4.3.2 our performance comparison among the different CM- and WHTS-assisted MMSE-SDMA-OFDM schemes was detailed. Specifically, the unspread CM-aided SDMA-OFDM system using two receiver antenna elements was studied in Section 4.3.2.1.1, whose performance was compared to that of the WHTS-assisted system dispensing with the employment of CM. Firstly, it was found that the performance achieved by all half-loaded schemes was better than that attained by the fully-loaded arrangements. This is because, when the user load is lower, the MUD will achieve a higher efficiency in differentiating the different users' transmitted signal, since the multi-user interference is lower. Therefore, the system becomes more efficient in terms of suppressing the detrimental fading channel effects. Secondly, it was also noticed that the achievable performance improvement attained by CM was typically higher than that achieved by WHTS, as evidenced by comparing Figure 4.5 to Figure 4.7.

Furthermore, we combined the MMSE-SDMA-OFDM system with both CM and WHTS in Section 4.3.2.1.1. The corresponding simulation results portrayed in Figure 4.8 showed that the TTCM-aided scheme achieved the best CWER performance among all the CM- and WHTS-assisted schemes considered. Moreover, the comparison of Figure 4.6 and Figure 4.8 suggested that in the CM-aided MMSE-SDMA-OFDM system the employment of WHTS having a block size of 32 subcarriers only insignificantly improved the system's BER and CWER performance, since most of the achievable diversity gain may have already been achieved by the time-diversity of the CM schemes. It was also found that when a higher CM codeword length was used, the system's performance was further improved, as observed in Figure 4.9, since a longer CM codeword is capable of more efficiently dispersing and averaging the bursty error effects.

In Section 4.3.2.1.2, the system's performance evaluated in the four-receiver CM scenarios was compared, when communicating over the SWATM channel of Figure 3.32. Comparing Figure 4.8 to Figure 4.10, we found that at the same user load level, for example at $\alpha_4 = \alpha_2 = 0.5$ or $\alpha_4 = \alpha_2 = 1.0$, the E_b/N_0 performance achieved by the four-receiver system was better than that of the two-receiver system, provided that the same CM-assisted scheme was used. The reason for this phenomenon is that when the SDMA-MIMO system's space-diversity order is increased by employing a higher number of receiver antenna elements, it becomes capable of providing a higher diversity gain, which may be expected to improve the system's performance for each user.

The performance of the various CM- and WHTS-assisted MMSE-SDMA-OFDM systems was evaluated in the context of the COST207 HT channel of Figure 4.12 in Section 4.3.2.2, which included the two- and four-receiver scenarios in Section 4.3.2.2.1 and Section 4.3.2.2.2, respectively. It was found that without the assistance of WHTS the TTCM-aided scheme constituted the best design option in terms of both the BER and CWER in comparison to the other three CM-aided schemes. When WHTS was incorporated into the CM-MMSE-SDMA-OFDM system, a further E_b/N_0 gain was achieved by all the schemes, which was different from the scenario of Section 4.3.2.1 recorded for transmission over the SWATM channel, where the additional E_b/N_0 gain achieved by WHTS in the context of the various CM- and WHTS-assisted schemes was rather modest. This may suggest that in highly dispersive environments, such as that characterized by the 12-path COST207 HT channel of Figure 4.12, the channel-coded SDMA-OFDM

[1] Since the ICI is caused by the variation of the channel impulse response during the transmission of each OFDM symbol, we introduce the OFDM-symbol-normalized Doppler frequency F_d [5]. In the case of a maximum Doppler frequency of 200Hz, for example, the corresponding OFDM-symbol-normalized Doppler frequency F_d will become as high as $F_d = f_d \cdot NT_s = f'_d \cdot N = 0.023$, where N is the cyclically-extended OFDM symbol's total duration expressed as $N = K + cp$, while the associated values of f_d, f'_d, T_s, K and cp are given in Table 4.2.

system's performance may be further improved by employing WHTS. This is because the detrimental fading-induced bursty error effects degrading the system's average BER performance owing to the deeply-faded subcarriers can be spread over the entire WHT block, and these dispersed and randomized channel errors may be more readily corrected by the CM decoder.

Furthermore, the four CM-aided schemes communicating over the COST207 HT channel of Figure 4.12 attain a different performance, as shown in Figures 4.13 and 4.14. This conclusion is different from what was noted in Figures 4.6 and 4.8, where the performance of the various CM-aided schemes communicating over the SWATM channel of Figure 3.32 was more similar. This is owing to the more frequent and more dramatic amplitude variation of the FD-CHTF in the COST207 HT channel, which exhibits a significantly longer maximum path delay than that of the SWATM channel, as indicated by Figure 4.15. This characteristic resulted in more randomly dispersed rather than burstily corrupted subcarrier symbols, which can be more readily corrected by the channel codes. Hence, in the context of the COST207 HT channel of Figure 4.12, the different error-correcting capability of the various CM schemes becomes more explicit, than that exhibited in the scenario of the SWATM channel of Figure 3.32.

In Table 4.4 of Section 4.3.2.2.3 we summarized the E_b/N_0 values required by the various CM- and WHTS-assisted MMSE-SDMA-OFDM schemes for achieving a BER of 10^{-5}, also showing the corresponding gains attained by the WHTS-assisted schemes. We observed that on one hand, when we had a specific user load, the spreading-induced E_b/N_0 gain achieved by a system having a lower diversity order was higher, regardless of the employment of CM. In other words, the subcarrier-based WHTS technique may be expected to attain a higher system performance improvement in relatively lower diversity-order scenarios. Moreover, if we supported a fixed number of users but varied the number of receiver antenna elements, similar conclusions may be drawn. A plausible explanation for this fact may be that in the SDMA-MIMO system, a potentially higher space diversity gain may be achieved, when a higher number of receiver antenna elements is employed, and thus the benefits of WHTS may be less substantial. This may be particularly true in the context of the CM-aided systems, since most of the attainable gain has already been achieved by using the channel codes. On the other hand, when a given number of receiver antenna elements was used, the spreading-induced E_b/N_0 gains achieved in the context of the fully-loaded systems were higher than in the half-loaded systems, regardless of the employment of channel codes. This suggests that more benefits may arise from WHTS, especially in the fully-loaded scenarios, where the MUD suffers from a relatively low efficiency in differentiating the different users' signals.

Additionally, we provided the E_b/N_0 crossing points and the corresponding total gain achieved by the various CM-WHTS-MMSE-SDMA-OFDM schemes at the BER of 10^{-5}, in Figures 4.19 and 4.20 of Section 4.3.2.2.3, respectively. It was demonstrated that the performance gap between the different CM-aided schemes increased, as the user load increased. Furthermore, it was observed in Figures 4.19 and 4.20 that the TCM, BICM and BICM-ID-aided schemes suffered a higher performance degradation than the TTCM arrangement, when the MUD's user-separation capability eroded owing to the increased multi-user interference. At a relatively low user load the various schemes provided a similar performance, because most of the attainable gain of the four-receiver SDMA-OFDM system had already been achieved, as discussed earlier in Section 4.3.2.2.3.

The effects of using different WHT block sizes was studied in Section 4.3.2.3, in both the SWATM and COST207 HT channel scenarios, as seen in Figures 4.21 and 4.22, respectively. As expected, it was found that the system's performance was improved, while the WHT block size used was increased. This is because when a larger WHT block size is used by the SDMA-OFDM system, the data symbols carried by the subcarriers that are badly-affected by deep channel fades could be spread over a larger WHT length, which may mitigate the detrimental channel effects and thus assists the receiver in terms of achieving a better error correction capability. Furthermore, it was suggested by the simulation results of Section 4.3.2.3 that in the SDMA-OFDM system operating without the aid of CM, the performance improvement potential owing to the employment of a larger WHT block size was higher than that in the CM-aided system, where most of the achievable diversity gain has been attained by using CM.

Finally, we studied the effects of the Doppler frequency in Section 4.3.2.4. It was concluded that the maximum Doppler frequency does not significantly affect the performance of the WHTS-assisted MMSE-SDMA-OFDM system, regardless of the employment of CM, as for example portrayed in Figure 4.23.

From the investigations conducted, we conclude that the various CM schemes, namely TCM, TTCM, BICM and BICM-ID are capable of substantially improving the achievable performance of SDMA-OFDM systems. The employment of WHTS has the potential of further enhancing the system's performance in highly dispersive propagation environments. As a result, the TTCM- and WHTS-assisted scheme was found to have the best CWER performance in all the scenarios investigated. Furthermore, it was also the best design option in terms of the achievable E_b/N_0 gain expressed in dB, when communicating in highly dispersive environments, for example over the COST207 HT channel of Figure 4.12, while carrying a high user load of $\alpha_P \geq 0.5$.

In the next chapter, our research is targeted at contriving a more sophisticated MUD, namely the Genetic Algorithm

(GA) assisted MUD, in order to further improve the SDMA-OFDM system's achievable performance.

Chapter 5

Hybrid Multi-User Detection for SDMA-OFDM Systems

5.1 Introduction

In the previous chapter, the MMSE MUD has been investigated in the context of various CM schemes assisted SDMA-OFDM systems. Furthermore, the WHT-based frequency-domain spreading technique has been incorporated into the CM-assisted MMSE-SDMA-OFDM system for the sake of attaining performance enhancements. However, the SDMA system's performance is somewhat limited due to the employment of the low-complexity MMSE MUD, which is devised based on the sub-optimal linear MMSE algorithm. On the other hand, the high-complexity optimum Maximum Likelihood (ML) MUD is capable of achieving the best performance owing to invoking an exhaustive search. However, the computational complexity of the ML MUD typically increases exponentially with the number of simultaneous users supported by the SDMA-OFDM system, which may render its implementation prohibitive. In the literature, a range of sub-optimal nonlinear MUDs have been proposed, such as for example the MUDs based on Successive Interference Cancellation (SIC) [5, 194, 198, 442–444] or Parallel Interference Cancellation (PIC) [5, 442, 444, 445] techniques. Instead of detecting and demodulating the users' signals in a sequential manner, as the MMSE MUD does, the PIC and SIC MUDs invoke an iterative processing technique that combines detection and demodulation. More specifically, the output signal generated during the previous detection iteration is demodulated and fed back to the input of the MUD for the next iterative detection step. Similar techniques invoking decision-feedback have been applied also in the context of classic channel equalization. However, since the philosophy of both the PIC and SIC MUDs is based on the principle of removing the effects of the interfering users during each detection stage, they are prone to error propagation occurring during the consecutive detection stages due to the erroneously detected signals of the previous stages [5]. In order to mitigate the effects of error propagation, an attractive design alternative is to *simultaneously* detect all the users' signals, rather than invoking iterative interference cancellation schemes. Recently, another branch of multi-user detection schemes referred to as Sphere Decoder (SD) [448–454] has also been proposed for multi-user systems, which is capable of achieving ML performance at a lower complexity.

As far as we are concerned, most of the above-mentioned techniques were proposed for the systems, where the number of users is less than or equal to the number of receivers, referred to here as the underloaded or fully-loaded scenarios, respectively. However, in practical applications it is possible that the number of users L to be supported exceeds that of the receiver antennas P, which is often referred to as an *overloaded* scenario. In overloaded systems, the $(P \times L)$-dimensional MIMO channel matrix representing the $(P \times L)$ number of channel links becomes singular, thus rendering the degree of freedom of the detector insufficient. This will catastrophically degrade the performance of numerous known detection approaches, such as for example the Vertical Bell Labs Layered Space-Time architecture (V-BLAST) [106, 109, 455] detector of [136], the MMSE algorithm of [5, 442] and the QR Decomposition combined with the M-algorithm (QRD-M) algorithm of [173].

Based on this motivation, in this chapter a sophisticated nonlinear MUD is devised, which exploits the power of genetic algorithms. Genetic Algorithms (GAs) [456–460] have been applied to a number of problems, such as machine learning and modeling adaptive processes. Moreover, GA-based multiuser detection has been proposed by Juntti *et al.* [461] and Wang *et al.* [462], where the analysis was based on the AWGN channel in the absence of diversity techniques. The proposal by Ergün *et al.* [463] utilized GAs as the first stage of a multistage multiuser detector, in

order to provide good initial guesses for the subsequent stages. Its employment in Rayleigh fading channels was considered by Yen *et al.* in [40, 464] and [40, 465] in diverse scenarios both with and without the aid of diversity techniques, respectively.

However, most of the GA-aided transceiver research mentioned above was conducted in the context of Code Division Multiple Access (CDMA) systems [40, 466]. By contrast, in this chapter, we apply GAs in the context of multi-user OFDM schemes, rather than CDMA systems. More specifically, we combine GAs with the MMSE MUD for the sake of contriving a more powerful concatenated MMSE-GA MUD, which is capable of maintaining near-optimum performance in the above-mentioned overloaded systems. Furthermore, TTCM is selected as the FEC scheme for the proposed MMSE-GA multi-user detected SDMA-OFDM system, since it generally provides the best performance in the family of CM schemes in the context of MMSE-SDMA-OFDM systems, as demonstrated in Chapter 4. We will show in this chapter that the proposed MMSE-GA assisted TTCM-SDMA-OFDM system is capable of achieving a similar performance to that attained by its optimum ML MUD assisted counterpart at a significantly lower computational complexity, especially at high user loads. Furthermore, the performance of the proposed GA-aided system can be further improved, if an enhanced iterative GA MUD is employed. This improvement is achieved at the cost of an increased complexity, which is however still substantially lower than that imposed by the ML MUD.

The structure of this chapter is as follows. The overview of the GA-assisted TTCM-aided MMSE-SDMA-OFDM system is given in Section 5.2.1, followed by the introduction of the basic principles of the concatenated MMSE-GA MUD of Section 5.2.2. Our simulation results are provided in Section 5.2.3, while the associated complexity issues are discussed in Section 5.2.4. The enhanced GA MUD is introduced in Section 5.3, including the improved mutation scheme of Section 5.3.1 and the enhanced GA MUD framework of Section 5.3.2, while the associated simulation results are provided in Sections 5.3.1.3 and 5.3.2.2, respectively, followed by the associated complexity analysis in Section 5.3.3. Our final conclusions are summarized in Section 5.4.

5.2 Genetical Algorithm Assisted Multi-User Detection

5.2.1 System Overview

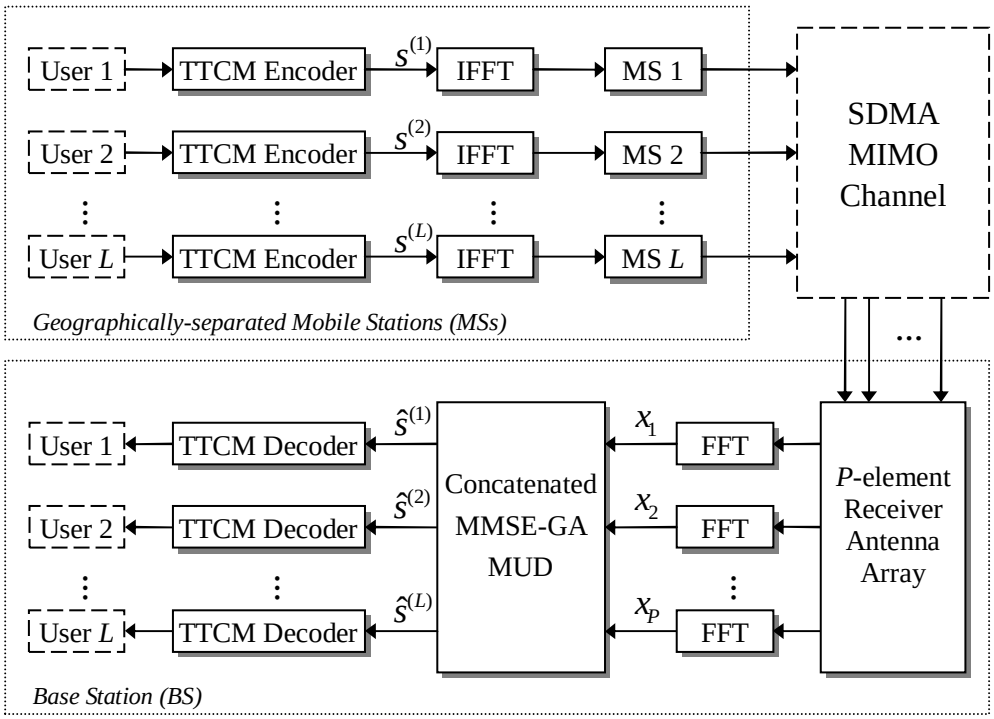

Figure 5.1: Schematic of the MMSE-GA-concatenated multi-user detected SDMA-OFDM uplink system.

In Figure 5.1, we present the schematic of the proposed concatenated MMSE-GA MUD aided SDMA-OFDM uplink system. At the transmitter end, as seen at the top of Figure 5.1, the information bit sequences of the geographically separated L simultaneous mobile users are forwarded to the TTCM [359] encoders, where they are encoded into

symbols. The encoded signals $s^{(l)}$ $(l = 1, \cdots, L)$ of the L users are then forwarded to the OFDM-related Inverse Fast Fourier Transform (IFFT) based modulator, which converts the frequency-domain signals to the time-domain modulated OFDM symbols. The OFDM symbols are then transmitted by the independent Mobile Stations (MSs) to the Base Station (BS) over the SDMA MIMO channel, which has been presented in Section 4.2.1. Then each element of the receiver antenna array shown at the bottom of Figure 5.1 receives the superposition of the transmitted signals faded and contaminated by the channel and performs Fast Fourier Transform (FFT) based OFDM demodulation. The demodulated outputs x_p $(p = 1, \cdots, P)$ seen in Figure 5.1 are forwarded to the proposed concatenated MMSE-GA MUD for separating the different users' signals. The separated signals $\hat{s}^{(l)}$ $(l = 1, \cdots, L)$, namely the estimated versions of the L users' transmitted signals, are then independently decoded by the TTCM decoders of Figure 5.1.

5.2.2 MMSE-GA-concatenated Multi-User Detector

5.2.2.1 Optimization Metric for the GA MUD

The optimum ML MUD [5] uses an exhaustive search for finding the most likely transmitted signals. More explicitly, for a ML-detection assisted SDMA-OFDM system supporting L simultaneous users, a total of 2^{mL} metric evaluations has to be invoked, where m denotes the number of bits per symbol (BPS), in order to detect the L-user symbol vector $\hat{\mathbf{s}}_{\text{ML}}$ that consists of the most likely transmitted symbols of the L users at a specific subcarrier, given by:

$$\hat{\mathbf{s}}_{\text{ML}} = \arg\left\{ \min_{\check{\mathbf{s}} \in \mathcal{M}^L} ||\mathbf{x} - \mathbf{H}\check{\mathbf{s}}||^2 \right\}, \tag{5.1}$$

where the $(P \times 1)$-dimensional received signal vector $\mathbf{x}$ and the $(P \times L)$-dimensional Frequency-Domain CHannel Transfer Function (FD-CHTF) matrix $\mathbf{H}$ are defined by Equations (4.2) and (4.5), respectively. The set $\mathcal{M}^L$ in Equation (5.1), which is constituted by 2^{mL} number of trial vectors, is formulated as:

$$\mathcal{M}^L = \left\{ \check{\mathbf{s}} = \left[\check{s}^{(1)}, \check{s}^{(2)}, \cdots, \check{s}^{(L)} \right]^T \middle| \check{s}^{(1)}, \check{s}^{(2)}, \cdots, \check{s}^{(L)} \in \mathcal{M}_c \right\}, \tag{5.2}$$

where $\mathcal{M}_c$ denotes the set containing the 2^m number of legitimate complex constellation points associated with the specific modulation scheme employed. Explicitly, the number of metric evaluations required for detecting the optimum vector increases exponentially with the number of users L.

Furthermore, the optimum ML-based decision metric of Equation (5.1) may also be used in the GA-based MUD for the sake of detecting the estimated transmitted symbol vector $\hat{\mathbf{s}}_{\text{GA}}$. In the context of the SDMA-OFDM system employing P receiver antenna elements, the decision metric required for the p^{th} receiver antenna, namely the antenna-specific *objective function (OF)* [40] can be derived from Equation (5.1), yielding:

$$\Omega_p(\check{\mathbf{s}}) = |x_p - \mathbf{H}_p\check{\mathbf{s}}|^2, \tag{5.3}$$

where x_p is the received symbol at the input of the p^{th} receiver at a specific OFDM subcarrier, while $\mathbf{H}_p$ is the p^{th} row of the channel transfer function matrix $\mathbf{H}$. Therefore the decision rule for the optimum multiuser detector associated with the p^{th} antenna is to choose the specific L-symbol vector $\check{\mathbf{s}}$, which minimizes the metric given in Equation (5.3). Thus, the estimated transmitted symbol vector of the L users based on the knowledge of the received signal at the p^{th} receiver antenna and a specific subcarrier is given by:

$$\hat{\mathbf{s}}_{\text{GA}_p} = \arg\left\{ \min_{\check{\mathbf{s}}} \left[\Omega_p(\check{\mathbf{s}}) \right] \right\}. \tag{5.4}$$

However, it transpires from above derivation that we will have P metrics in total for the P receiver antennas. Since the channel impulse responses of each of the P antennas are statistically independent, the L-symbol vector that is considered optimum at antenna 1 may not be considered optimum at antenna 2, etc. In other words, this implies that a decision conflict is encountered, which may be expressed as:

$$\arg\left\{ \min_{\check{\mathbf{s}}} \left[\Omega_i(\check{\mathbf{s}}) \right] \right\} = \hat{\mathbf{s}}_{\text{GA}_i} \neq \hat{\mathbf{s}}_{\text{GA}_j} = \arg\left\{ \min_{\check{\mathbf{s}}} \left[\Omega_j(\check{\mathbf{s}}) \right] \right\}, \tag{5.5}$$

where $\forall\, i, j \in \{1, \cdots, P\}$, $i \neq j$. This decision conflict therefore leads to a so-called multi-objective optimization problem, since the optimization of the P metrics may result in more than one possible L-symbol solutions. A similar decision conflict resolution problem was studied in [467] in an attempt to reconcile the decision conflicts of multiple

antennas resulting in a decision dilemma. In order to resolve this problem we may adopt a similar approach and may amalgamate the P number of antenna-specific L-symbol metrics into a joint metric as follows:

$$\Omega\left(\check{\mathbf{s}}\right) \quad = \quad \sum_{p=1}^{P} \Omega_p\left(\check{\mathbf{s}}\right). \tag{5.6}$$

Hence, the decision rule of the GA MUD is to find the specific estimated transmitted L-symbol vector $\hat{\mathbf{s}}_{\text{GA}}$ that minimizes $\Omega\left(\mathbf{s}\right)$ in Equation (5.6) for every OFDM subcarrier considered.

5.2.2.2 Concatenated MMSE-GA Multi-User Detection

The BER performance of the MMSE MUD is somewhat limited, since it is the total mean-square estimation error imposed by the different simultaneous users that is minimized, rather than directly optimizing the BER performance. Therefore, the MMSE-SDMA-OFDM system's BER performance may be potentially further improved with the aid of a concatenated GA-aided MUD, which is capable of exploiting the output provided by the MMSE MUD of Section 4.2.2.1 in its initial population. For the sake of brevity, we will portray the philosophy of the proposed system in as simple terms as possible. However, the readers who are unfamiliar with GAs might like to consult Appendix A.1 for a rudimentary introduction to GA-based optimization in the context of multi-user SDMA-OFDM systems.

The GA invoked in the SDMA-OFDM system commences its search for the optimum L-symbol solution at the initial *generation* with the aid of the MMSE combiner. In other words, using GA parlance, the so-called *individuals* of the $y = 1^{st}$ generation having a *population* size of X are created from the estimated length-L transmitted symbol vector provided by the MMSE combiner, where the x^{th} $(x = 1, \cdots, X)$ individual is expressed as $\tilde{\mathbf{s}}_{(y,x)} = [\ \tilde{s}^{(1)}_{(y,x)},\ \tilde{s}^{(2)}_{(y,x)},\ \cdots,\ \tilde{s}^{(L)}_{(y,x)}\ ]$, and we have $\tilde{s}^{(l)}_{(y,x)} \in \mathcal{M}_c$ $(l = 1, \cdots, L)$. Note that here a complex symbol representation of the individuals is employed, which is derived from the classic *binary encoding* technique [40], where a binary vector constituted by binary zeros and ones is used to represent an individual. Then the GA-based optimization selects some of the L-symbol candidates from a total of X legitimate individuals in order to create a so-called *mating pool* of T number of L-symbol *parent* vectors [40]. Two L-symbol parent vectors are then combined using specific GA operations for the sake of creating two L-symbol *offspring* [40] and this 'genetic evolution-like' process of generating new L-symbol offspring continues over Y number of consecutive generations, so that the optimum L-symbol solution may be found.

The selection of the L-symbol individuals for creating the mating pool containing T number of L-symbol parents is vital in determining the GA's achievable quality of optimization [468]. In our research the individual-selection strategy based on the concept of the so-called *Pareto Optimality* [457] was employed. This strategy favours the so-called *non-dominated* individuals and ignores the so-called *dominated* individuals [40]. More specifically, the u^{th} L-symbol individual is considered to be dominated by the v^{th} individual, if we have [469]:

$$\begin{aligned} &\forall i \in \{1, \cdots, P\}:\ \Omega_i\left(\tilde{\mathbf{s}}_{(y,v)}\right) \leq \Omega_i\left(\tilde{\mathbf{s}}_{(y,u)}\right) \\ \wedge\ &\exists j \in \{1, \cdots, P\}:\ \Omega_j\left(\tilde{\mathbf{s}}_{(y,v)}\right) < \Omega_j\left(\tilde{\mathbf{s}}_{(y,u)}\right). \end{aligned} \tag{5.7}$$

If an individual is not dominated in the sense of Equation (5.7) by any other individuals in the population, then it is considered to be non-dominated. All the non-dominated individuals are then selected and placed in the mating pool, which will have a size of $2 < T \leq X$ [40]. Two of the T number of L-symbol individuals in the mating pool are then selected as parents based on their corresponding diversity-based *fitness* values calculated with the aid of Equation (5.6) according to the so-called *fitness-proportionate* selection scheme [40], which is described as follows. First the so-called *windowing-mapping* [462] technique is invoked in order to get the fitness value $f_{(y,x)}$ associated with the x^{th} individual, which is given by:

$$f_{(y,x)} \quad = \quad \Omega_{y,T} - \Omega\left(\tilde{\mathbf{s}}_{(y,x)}\right) + c, \tag{5.8}$$

where

$$\Omega_{y,T} = \max_{t \in \{1, \cdots, T\}} \left\{ \Omega\left(\tilde{\mathbf{s}}_{(y,t)}\right) \right\} \tag{5.9}$$

is the maximum *Objective Score (OS)*[1] achieved by evaluating the T number of individuals in the mating pool at the y^{th} generation, and c is a small positive constant, which is used for the sake of ensuring the positiveness of $f_{(y,x)}$.

[1] Note that the individual having the maximum OS out of the pool of the T candidates is considered as the worst solution in the context of the current mating pool, since the GA searches for the optimum solution which minimizes Equation (5.6).

Then the fitness-proportionate selection probability p_x of the x^{th} individual can be formulated as:

$$p_x = \frac{f_{(y,x)}}{\sum_{t=1}^{T} f_{(y,t)}}. \tag{5.10}$$

When two L-symbol parents are selected, the so-called *uniform cross-over*, *mutation* and *elitism* operations [40] are invoked for offering a chance of evolving the parents' one or more element symbols to other symbols of the set $\mathcal{M}_c$, resulting in two offspring. The above operation is repeated, until a new population consisting of X offspring is created. Furthermore, the so-called *incest prevention* [40] technique was invoked during the selection process, which only allows different individuals to be selected for the cross-over operation. Finally, the GA terminates after Y number of generations and thus the L-symbol individual having the highest diversity-based fitness value will be considered as the detected L-user transmitted symbol vector corresponding to the specific OFDM subcarrier considered.

From the above arguments, we note that in the GA MUD the different users' signals are jointly detected. This mechanism is different from that of the SIC or PIC MUDs, where each user's estimated transmitted signal is inferred by removing the interference imposed by the others. Therefore, there is no error propagation between the different users' signal detections in the GA MUD.

5.2.3 Simulation Results

In this section, we characterize the performance of the proposed TTCM-assisted SDMA-OFDM system using the concatenated MMSE-GA MUD. The channel is assumed to be 'OFDM-symbol-invariant', implying that the taps of the impulse response are assumed to be constant for the duration of one OFDM symbol, but they are faded at the beginning of each OFDM symbol [5]. The simulation results were obtained using a 4QAM scheme communicating over the SWATM CIR of Figure 3.32, assuming that the channels' transfer functions are perfectly known. Each of the paths experiences independent Rayleigh fading having the same normalized Doppler frequencies of $f'_d = 1.235 \times 10^{-5}$. The OFDM modem employed $K = 512$ subcarriers and a cyclic prefix of 64 samples, which is longer than the maximum channel delay spread. For the iterative TTCM scheme [359] employed, the code memory ν is fixed to 3, while the number of iterations is set to 4. Hence the total number of trellis states is $2^3 \cdot 4 \cdot 2 = 64$, since there are two 8-state decoders which are invoked in four iterations. The generator polynomial expressed in octal format for the TTCM scheme considered is $[13 \quad 6]$, while the codeword length and channel interleaver depth are fixed to 1024 symbols. The various techniques and parameters used in our simulations discussed in this section are summarized in Table 5.1.

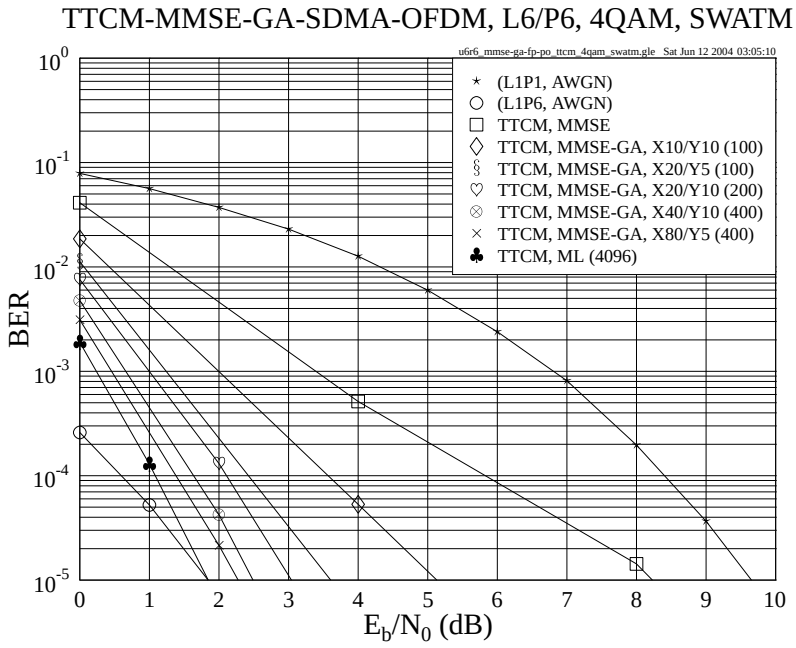

Figure 5.2: BER versus E_b/N_0 performance of the **TTCM-assisted MMSE-GA-SDMA-OFDM** system employing a 4QAM scheme for transmission over the SWATM channel, where **L=6** users are supported with the aid of **P=6** receiver antenna elements. The basic simulation parameters are given in Table 5.1.

TTCM	Modem	4QAM
	Code rate	0.5
	Code memory ν	3
	Octal generator polynomial	$[13 \quad 6]$
	Codeword length	1024 symbols
	Channel interleaver depth	1024 symbols
	Number of turbo iterations	4
GA	Population initialization method	MMSE
	Mating pool creation strategy	Pareto-Optimality
	Selection method	Fitness-Proportionate
	Cross-over	Uniform cross-over
	Mutation	M-ary mutation
	Mutation probability p_m	0.1
	Elitism	Enabled
	Incest prevention	Enabled
	Population size X	Varied
	Generations Y	Varied
Channel	CIRs	SWATM [5]
	Paths	3
	Maximum path delay	48.9 ns
	Normalized Doppler frequency f_d	1.235×10^{-5}
	Subcarriers K	512
	Cyclic prefix	64

Table 5.1: The various techniques and parameters used in the simulations of Section 5.2.3.

The BER performance of the TTCM-assisted MMSE-GA-SDMA-OFDM system employing a 4QAM scheme for transmission over the SWATM channel, where six users are supported with the aid of six receiver antenna elements, is portrayed in Figure 5.2. The performance of the TTCM-assisted MMSE-detected SDMA-OFDM system, the TTCM-aided optimum ML-detected system, and the uncoded single-user scheme employing either a single receiver or invoking Maximum Ratio Combining (MRC) when communicating over an AWGN channel are also provided for reference, respectively. The numbers in the round brackets seen in the legends of Figure 5.2 represent the total GA or ML complexity[2]. It is observed from Figure 5.2 that the BER performance of the TTCM-assisted MMSE-SDMA-OFDM system was significantly improved with the aid of the GA having a sufficiently large population size X and/or a larger number of generations Y. This improvement was achieved, since a larger population may contain a higher variety of L-symbol individuals, and similarly, a larger number of generations implies that again, a more diverse set of individuals may be evaluated, thus extending the GA's search space, which may be expected to increase the chance of finding a lower-BER solution. On the other hand, it may be observed that when we have the same total number of $(X \times Y)$ correlation metric evaluations according to Equation (5.3), the performance improvement achieved by increasing the population size X was more substantial than that upon increasing the Y number of generations. For example, when we have $X \times Y = 100$, the GA-assisted scheme employing a population size $X = 20$ and $Y = 5$ number of generations achieved about 1.5dB E_b/N_0 gain over its corresponding counterpart that has $X = 10$ and $Y = 10$, as evidenced by Figure 5.2. This may suggest that in the TTCM-assisted MMSE-SDMA-OFDM system investigated, the GA's convergence speed tends to be faster, when we have a larger population size X instead of a higher number of generations Y. However, when the affordable complexity increases, the improvement achieved by a larger-population GA at a certain value of $(X \times Y)$ becomes modest. For instance, given the maximum affordable complexity of $X \times Y = 400$, the system associated with $X = 80$ and $Y = 5$ brought about a modest E_b/N_0 improvement of 0.25dB over the system

[2]The quantification of the GA or ML complexity will be given in Section 5.2.4.

associated with $X = 40$ and $Y = 10$, as shown in Figure 5.2. This is because most of the achievable performance gain of the system is likely to have been attained.

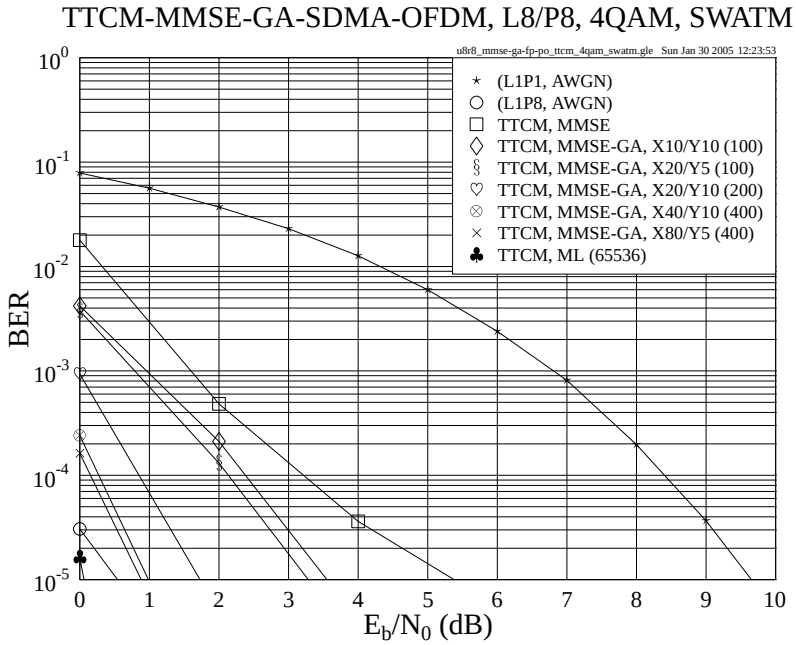

Figure 5.3: BER versus E_b/N_0 performance of the **TTCM-assisted MMSE-GA-SDMA-OFDM** system employing a 4QAM scheme for transmission over the SWATM channel, where **L=8** users are supported with the aid of **P=8** receiver antenna elements. The basic simulation parameters are given in Table 5.1.

Figure 5.3 shows the performance achieved by the proposed TTCM-MMSE-GA-SDMA-OFDM system in the scenario, where the number of supported users and receiver antenna elements was increased to eight. As shown in Figure 5.3, again, the TTCM-aided MMSE-SDMA-OFDM system's performance was significantly improved by employing the GA. We may also note that at a specific computational complexity, the E_b/N_0 gain achieved by the GA MUD was decreased, when compared to that attained in the six-user-six-receiver scenario of Figure 5.2. For example, when we have $X = Y = 10$ and $L = P = 6$, the E_b/N_0 gain achieved by the TTCM-MMSE-GA-SDMA-OFDM system over the TTCM-MMSE-SDMA-OFDM system was about 3dB, as seen in Figure 5.2. By contrast, Figure 5.3 shows that this gain decreased to about 1.8dB, when we used the same GA and $L = P = 8$. This phenomenon may be explained as follows. On one hand, when the number of users increases, the separation of the different users' signal becomes more challenging, since the interference imposed by the undesired users becomes stronger. Therefore, a higher-complexity GA MUD has to be employed, if we aim for maintaining the same E_b/N_0 gain achieved by the system having a lower user load. On the other hand, when we have more receiver antenna elements installed at the BS, namely when using a 'higher-order' SDMA system, a higher spatial diversity gain may be achieved. Hence, in a 'higher-order' SDMA system, a higher probability of achieving the total attainable gain may be expected than in a 'lower-order' SDMA system, potentially approaching the best possible AWGN performance. Hence, this trend also results in a less significant GA-induced performance gain.

Furthermore, it can be seen in Figures 5.2 and 5.3 that the MMSE-GA-detected TTCM-SDMA-OFDM system was slightly outperformed by its optimum ML-detected counterpart, since the GAs are unable to guarantee that the optimum ML solution would be found [40]. However, the near-optimum performance of the GA-aided TTCM-SDMA-OFDM system was achieved at a significantly lower computational complexity than that imposed by the ML-aided system, as it will be demonstrated in Section 5.2.4.

5.2.4 Complexity Analysis

In this section, an analysis of the associated computational complexity imposed by the optimum ML MUD aided SDMA-OFDM system and the GA-aided MMSE-SDMA-OFDM system will be presented. For the sake of simplicity, we only compare the optimum ML MUD's complexity to that of the GA MUD, since the simple MMSE MUD is used for providing a single initial solution for the GA's initial population and imposes a significantly lower complexity than that of its concatenated GA-aided counterpart. More specifically, since the proposed GA-aided MUD optimizes the

metric of Equation (5.3)[3], we will quantify the complexity imposed in terms of the number of metric computations required by the optimization process.

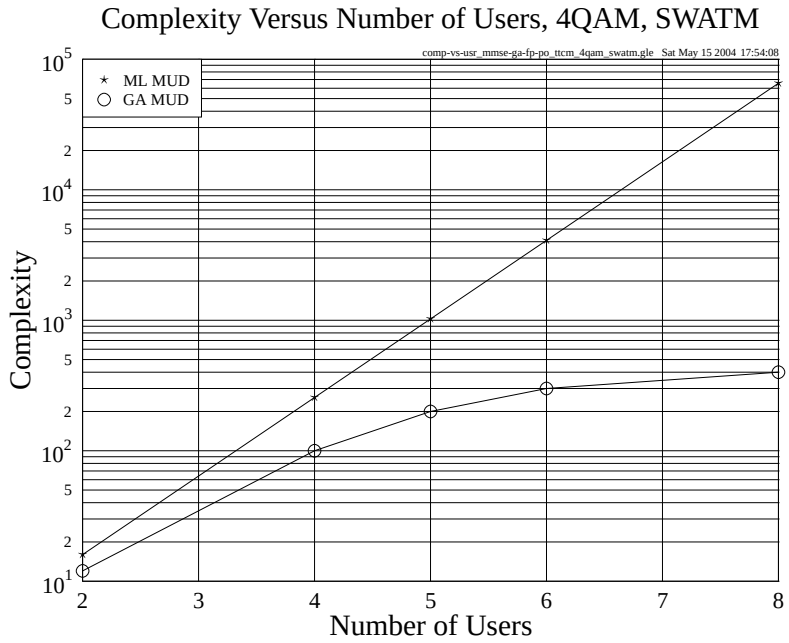

Figure 5.4: Comparison of the MUD complexity in terms of the number of metric evaluations, versus the number of users performance of the 4QAM TTCM-MMSE-GA-SDMA-OFDM and TTCM-ML-SDMA-OFDM systems. The number of receiver antenna elements employed is equivalent to the number of users supported, i.e. $L = P$.

As mentioned in Section 5.2.2.1, for the ML MUD, 2^{mL} number of metric computations have to be carried out for finding the optimum solution [5], namely the most likely transmitted L-user vector, where m denotes the number of bits per symbol. By contrast, our proposed GA MUD requires a maximum of $(X \times Y)$ metric evaluations, since X number of L-symbol vectors are evaluated during each of the Y number of generations, as shown in round brackets in the legends of Figures 5.2 and 5.3. Furthermore, the number of such metric evaluations may readily be reduced by avoiding repeated evaluations of identical individuals, either within the same generation or across the entire iterative process, provided that the receiver has the necessary memory for storing the corresponding evaluation history. In Figure 5.4, we compare both the ML- and the GA-aided schemes in terms of their complexity, i.e. the number of metric computations. At a specific user load, we always select an appropriate GA-aided scheme for comparison, which suffers from less than 1dB E_b/N_0 loss at the BER of 10^{-5} compared to the ML-aided system. As shown in Figure 5.4, the ML-aided system imposes an exponentially increasing complexity on the order of $O(2^{mL})$, when the number of users increases, while the complexity of the GA-aided system required for maintaining a near-optimum performance increases only slowly.

5.2.5 Conclusions

From the investigations conducted, we conclude that the GA-assisted TTCM-aided MMSE-SDMA-OFDM system is capable of achieving a similar performance to that of the optimum ML-assisted TTCM-SDMA-OFDM system. Furthermore, this is attained at a significantly lower computational complexity than that imposed by the ML-assisted system, especially when the number of users is high. For example, a complexity reduction in excess of a factor of 100 can be achieved by the proposed system for $L = P = 8$, as evidenced by Figure 5.4.

5.3 Enhanced GA-based Multi-User Detection

In Section 5.2, we have presented a detailed characterization of the concatenated MMSE-GA MUD designed for the TTCM-assisted multi-user SDMA-OFDM system. In this section, an enhanced GA-based multi-user detector will be introduced, which is capable of further improving the proposed system's performance.

[3]Similarly, the ML-aided MUD optimizes the metric of Equation (5.1), from which Equation (5.3) is derived.

As discussed in Section 5.2, the proposed MMSE-GA-assisted TTCM-SDMA-OFDM system achieves a close-to-optimum performance at a significantly lower computational complexity than its optimum ML-assisted counterpart. Moreover, the GA-aided system can be further improved in each or both of the following two aspects:

- By optimizing the component(s) of the GA MUD for the sake of finding a better configuration that may improve the GA's performance in the context of the SDMA-OFDM system;
- By invoking an iterative detection framework so that the system's performance may be improved iteration by iteration.

In the following sections we will discuss the techniques that may be applied in terms of the above-mentioned two aspects for achieving an improved system performance.

5.3.1 Improved Mutation Scheme

In the context of GA-based detection techniques, the efficiency of the mutation scheme employed is important for the success of the entire evolution procedure, since it provides a chance for the individuals of the current population to influence the forthcoming ones, so that new areas of the total search space may be explored and thus the chance of finding the optimum solution increases [470]. An efficient mutation scheme is expected to be capable of guiding the search process in the correct direction for the sake of finding the global optimum, rather than the local ones. In the context of the GA-assisted multi-user SDMA-OFDM system, when the number of users L increases or a high-throughput modulation scheme is used, the total search space consisting of 2^{mL} number of L-user symbol vectors would become excessive. In such cases, the role of mutation may become vital for the success of the overall system, since the GA may get trapped in local optima without appropriate assistance of the mutation scheme.

In Section 5.3.1.1, we will first discuss a widely-used conventional mutation scheme as well as its drawbacks, which is followed by the introduction of an improved new mutation mechanism in Section 5.3.1.2.

5.3.1.1 Conventional Uniform Mutation

In Section 5.2.3, M-ary mutation was employed by the GA MUD. More specifically, each *gene* $\hat{s}^{(l)}$ $(l = 1, \cdots, L)$ of a length-L GA individual $\hat{\mathbf{s}}$ in the X-element population is represented by a specific symbol in $\mathcal{M}_c$, where $\mathcal{M}_c$ is the set containing the 2^m number of legitimate constellation points. In other words, the l^{th} gene denotes the l^{th} user's estimated transmitted symbol - which is a hard-decoded version of the complex signal - at the subcarrier considered. During the genetic evolution, when a gene is subjected to mutation, it will be substituted by a different symbol in $\mathcal{M}_c$ based on a uniform *mutation-induced transition probability* $p_{mt}^{(ij)}$ [4], which quantifies the probability of the i^{th} legitimate symbol becoming the j^{th}. For the sake of brevity, from now on we refer to this probability as the *transition probability*. Furthermore, we shall refer to the mutation scheme employing uniformly distributed $p_{mt}^{(ij)}$ values as *Uniform Mutation (UM)*, which is a widely-used conventional mutation scheme known in the literature and was also employed by the GAs invoked in [40].

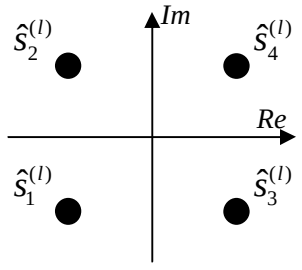

Figure 5.5: A 4QAM constellation.

More specifically, UM mutates to all the candidate symbols in $\mathcal{M}_c$ with the same probability. For example, let us consider the 4QAM modem constellation shown in Figure 5.5, where $\hat{s}_i^{(l)} \in \mathcal{M}_c$ $(i = 1, \cdots, 4)$ are the constellation

[4] Note that the mutation probability p_m of Table 5.1 is different from the probability $p_{mt}^{(ij)}$ of mutating to a specific symbol in $\mathcal{M}_c$. The former denotes the probability of how likely it is that a gene will mutate, while the latter specifies, how likely it is that a specific symbol in $\mathcal{M}_c$ becomes the mutated gene.

points as well as possible gene candidates for the l^{th} user at a specific subcarrier. When $\hat{s}_i^{(l)}$ is subjected to mutation, we have:

$$\hat{s}_j^{(l)} \quad = \quad MUTATION\left(\hat{s}_i^{(l)} \mid p_{mt}^{(ij)}\right), \quad i,j \in \{1,\cdots,4\},\ i \neq j. \tag{5.11}$$

For the UM scheme, the transition probability $p_{mt}^{(ij)} = 1/(2^m - 1)$ is equal for all $i,j \in \{1,\cdots,4\},\ i \neq j$.

Based on the mechanism of UM, the GA has a chance of successfully identifying the actually transmitted symbol of the l^{th} user at the subcarrier considered. However, UM has a drawback that may prevent the GA from rapid convergence under certain conditions. To explain this further, again, let us consider the example of Figure 5.5. Without loss of generality, let us make the following assumptions:

a) $\hat{s}_1^{(l)}$ is the received symbol, which is the original gene to be mutated, and

b) $\hat{s}_1^{(l)}$ is *not* the transmitted symbol.

Hence, the task of mutation is to find the actually transmitted symbol from the set of three candidates, namely $\hat{s}_i^{(l)}$ $(i = 2,\cdots,4)$. According to UM, the probability that $\hat{s}_1^{(l)}$ hops to $\hat{s}_2^{(l)}$, $\hat{s}_3^{(l)}$ or $\hat{s}_4^{(l)}$ is equal. In other words, in this case the chance of finding the true transmitted symbol of the specific user during a single UM operation is $1/3$. However, this fixed uniform transition probability fails to reflect the realistic channel condition that the system is subjected to. More precisely, at different Signal-to-Noise Ratio (SNR) levels, some symbols in $\mathcal{M}_c$ should not constitute high-probability mutation targets. For example, at high SNRs, the chances are that $\hat{s}_2^{(l)}$ or $\hat{s}_3^{(l)}$ is more likely to be the transmitted symbol, rather than $\hat{s}_4^{(l)}$, since the noise effects are insignificant and thus the signal corruption from the most distant symbol $\hat{s}_4^{(l)}$ to the received symbol $\hat{s}_1^{(l)}$ is rare. Hence, it may be more reasonable to consider $\hat{s}_2^{(l)}$ and $\hat{s}_3^{(l)}$ only as the potential mutation candidates, and assign a modified transition probability $p_{mt}^{(1j)} = 0.5$ $(j \in \{2,3\})$. This fact implies that at different SNR levels we may restrict the *effective* GA search space with the aid of a biased mutation, which ignores the constellation points that are far from the received symbol. This is especially beneficial for the system employing high-throughput modulation schemes such as 16QAM, where the total search space is exponentially expanded as a function of the number of BPS compared to lower-throughput modems. In such a system, the UM-aided GA which allows mutation to all legitimate symbols may suffer from a slow convergence speed and might result in a high residual error floor, since a considerable portion of the GA's searching power may be wasted on mutating to highly unlikely gene candidates, especially in high-SNR scenarios. By contrast, the above-mentioned biased mutation guided GA is expected to achieve a better performance, since it searches for the optimum solution in a more efficient way, as it will be demonstrated in Section 5.3.1.2.

5.3.1.2 Biased Q-function Based Mutation

The conventional UM and its drawbacks have been discussed in Section 5.3.1.1. In this section, an improved novel mutation scheme will be presented, which we shall refer to as *Biased Q-function Based Mutation (BQM)*.

5.3.1.2.1 Theoretical Foundations

As discussed in Section 5.3.1.1, for an original gene to be mutated, a SNR-related *biased* transition probability $p_{mt}^{(ij)}$ has to be assigned to each of the target candidate symbols in $\mathcal{M}_c$. The calculation of $p_{mt}^{(ij)}$ may be carried out with the aid of the widely-known Q-function [471]:

$$Q(x) \quad = \quad \frac{1}{\sqrt{2\pi}} \int_x^\infty e^{-t^2/2} dt, \quad x \geq 0. \tag{5.12}$$

For the sake of easy explanation, let us first consider a simple one-dimensional (1D) scenario. In Figure 5.6 we plotted the 1D real component of the constellation symbols $\hat{s}_i^{(l)}$ in the context of the 4QAM modem constellation seen in Figure 5.5. The horizontal axis is then divided into two zones, each of which represents one specific 1D constellation symbol s_{Ri} $(i = 1,\cdots,2)$, as separated by the vertical dashed line of Figure 5.6. If s_{R1} is the original gene to be mutated, the Gaussian distribution $N(0,\sigma)$ may be centered at the position of s_{R1}, where σ is the noise variance at a

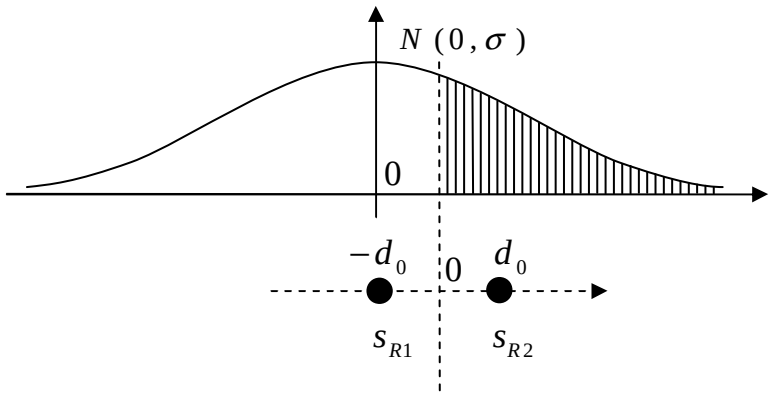

Figure 5.6: Illustration of the 1D transition probability $p_{mt}^{(ij)}$ for 4QAM.

given SNR level. In this specific example, s_{R2} is the only mutation target and the 1D transition probability of mutating from s_{R1} to s_{R2}, i.e. $p_{mt}^{(12)}$, is characterized by the shadow area shown in Figure 5.6, which is given by:

$$p_{mt}^{(12)} = Q(\frac{d_0}{\sigma}), \tag{5.13}$$

where d_0 is half of the distance between the neighbouring constellation symbols. Similarly, we have:

$$p_{mt}^{(21)} = Q(\frac{d_0}{\sigma}). \tag{5.14}$$

Furthermore, we also have a certain probability for the original gene to remain unchanged, which can also be expressed in terms of the Gaussian distribution as:

$$p_{mt}^{(11)} = p_{mt}^{(22)} = 1 - Q(\frac{d_0}{\sigma}). \tag{5.15}$$

$\{ij\}$	$p_{mt}^{(ij)}$
$\{12\},\{21\}$	$Q(\frac{d_0}{\sigma})$
$\{11\},\{22\}$	$1-Q(\frac{d_0}{\sigma})$

Table 5.2: The 1D transition probabilities for 4QAM.

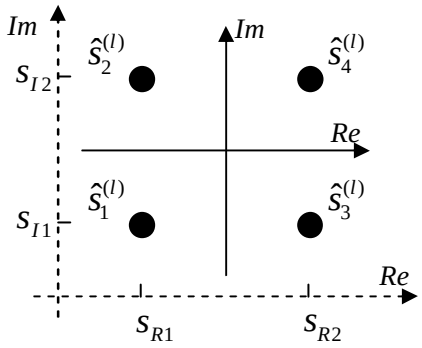

Figure 5.7: Illustration of the 2D transition probability $p_{mt}^{(ij)}$ for 4QAM, which is the product of the relevant 1D transition probabilities. s_{Ri} and s_{Ii} $(i \in \{1,2\})$ denote the 1D constellation symbols in the context of the real and imaginary components of the 4QAM constellation symbols, respectively.

The above-mentioned 1D transition probabilities are summarized in Table 5.2. The corresponding two-dimensional (2D) symbol transition probability $p_{mt}^{(ij)}$ can be derived by combining the 1D real and imaginary transition probabil-

ities[5]. Let us again consider the 4QAM modem of Figure 5.5 as an example, which is replotted in Figure 5.7. In Figure 5.7, for instance, the 2D transition probability of mutating from the constellation symbol $\hat{s}_1^{(l)}$ to $\hat{s}_2^{(l)}$, namely $p_{mt}^{(12)}$, can be calculated by multiplying the two relevant 1D transition probabilities according to[6]:

$$p_{mt}^{(12)} = p_{mt}^{(\underline{1}\underline{1})} \cdot p_{mt}^{(\underline{1}\underline{2})} = \left[1 - Q(\frac{d_0}{\sigma})\right] \cdot Q(\frac{d_0}{\sigma}), \tag{5.16}$$

while the associated 2D probability of remaining in the current state is:

$$p_{mt}^{(11)} = p_{mt}^{(\underline{1}\underline{1})} \cdot p_{mt}^{(\underline{1}\underline{1})} = \left[1 - Q(\frac{d_0}{\sigma})\right]^2. \tag{5.17}$$

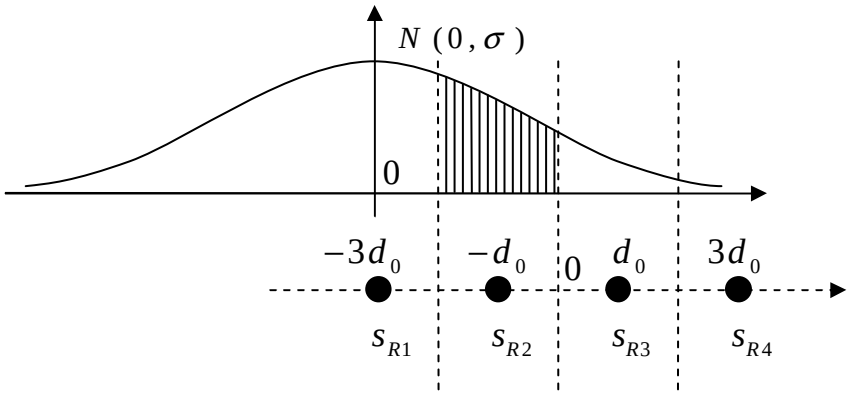

Figure 5.8: Illustration of the 1D transition probability $p_{mt}^{(\underline{ij})}$ for 16QAM.

For higher-throughput modems, for example for 16QAM and 64QAM, the same algorithm can be invoked for calculating the corresponding 1D and 2D transition probabilities. In Figure 5.8 an example associated with 16QAM is provided. According to Figure 5.8, assuming that s_{R1} is the original gene to be mutated, while s_{R2} is the mutation target, we have the following 1D transition probability of:

$$p_{mt}^{(\underline{1}\underline{2})} = Q(\frac{d_0}{\sigma}) - Q(\frac{3d_0}{\sigma}). \tag{5.18}$$

Similarly, we can derive the remaining 1D transition probabilities for 16QAM, which are summarized in Table 5.3. For the sake of brevity, here we omit the derivation of the corresponding 2D transition probabilities. Note that the proposed BQM scheme can be readily extended to M-dimensional (MD) constellations, since the MD transition probability associated with a specific MD symbol can be readily derived upon multiplying the M number of corresponding 1D transition probabilities.

However, when a mutation takes place during the evolution, the mutating gene or constellation symbol should not be allowed to be mutated to itself. Hence, the effect of the probability of mutating a symbol to itself should be removed. This can be achieved by normalizing the 2D transition probability $p_{mt}^{(ij)}$ $(i \neq j)$ with the aid of the original gene's probability of remaining unchanged, namely $p_{mt}^{(ii)}$, following the principles of conditional probability theory [472]. For more details concerning the normalization process, the interested reader is referred to Appendix A.2.

5.3.1.2.2 Simplified BQM

In Section 5.3.1.2.1 we have provided a detailed explanation of the mechanism of BQM. Furthermore, the proposed BQM scheme can be effectively simplified, when only a subset of all the theoretically-possible mutation target symbols are considered. More precisely, for the original gene subjected to mutation, we may only consider its adjacent neighbouring constellation symbols as mutation target candidates, since the original transmitted symbol is less unlikely to be corrupted to a relatively distant constellation symbol.

[5]Note that the 1D transition probability $p_{mt}^{(\underline{ij})}$ is different from the transition probability $p_{mt}^{(ij)}$, which is based on the 2D constellation symbols.

[6]Note that the superscripts i and j of the 2D transition probability $p_{mt}^{(ij)}$ denote the 2D constellation symbols $\hat{s}_i^{(l)}$ and $\hat{s}_j^{(l)}$, while the underlined superscripts i and j of the 1D transition probability $p_{mt}^{(\underline{ij})}$ represent the 1D constellation symbols s_{Ri} and s_{Rj}, respectively.

$\{ij\}$	$p_{mt}^{(ij)}$
$\{34\},\{21\}$	$Q(\frac{d_0}{\sigma})$
$\{24\},\{31\}$	$Q(\frac{3d_0}{\sigma})$
$\{14\},\{41\}$	$Q(\frac{5d_0}{\sigma})$
$\{11\},\{44\}$	$1-Q(\frac{d_0}{\sigma})$
$\{22\},\{33\}$	$1-2Q(\frac{d_0}{\sigma})$
$\{12\},\{23\},\{32\},\{43\}$	$Q(\frac{d_0}{\sigma})-Q(\frac{3d_0}{\sigma})$
$\{13\},\{42\}$	$Q(\frac{3d_0}{\sigma})-Q(\frac{5d_0}{\sigma})$

Table 5.3: The 1D transition probabilities for 16QAM.

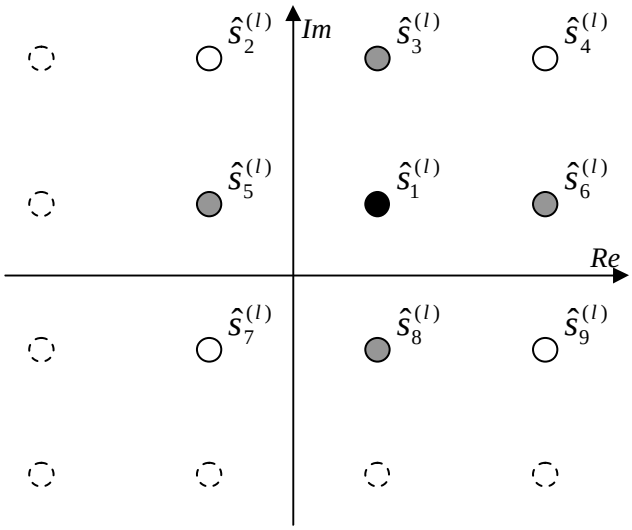

Figure 5.9: An example of the simplified BQM for 16QAM.

An example of the simplified BQM designed for 16QAM is provided in Figure 5.9. As shown in Figure 5.9, for example, we assume that $\hat{s}_1^{(l)}$ is the original gene subjected to mutation, and $\hat{s}_i^{(l)}$ $(i = 2, \cdots, 9)$ represents the adjacent neighbours of $\hat{s}_1^{(l)}$, while the symbols represented by the dashed-line circles are ignored. Therefore, the GA's entire search space is reduced. Moreover, the search space can be further compressed, when we only consider the nearest neighbours of $\hat{s}_1^{(l)}$. In this case, only the symbols $\hat{s}_i^{(l)}$ $(i = 3,5,6,8)$ printed in grey in Figure 5.9 will be regarded as the legitimate mutation candidates, each of which is assigned an equal 2D transition probability $p_{mt}^{(1j)} = 1/4$ $(j = 3,5,6,8)$, while all other constellation symbols printed in white are neglected. Since the transition probability for each selected mutation candidate is equally fixed, the BQM scheme is simplified to a scheme similar to UM, which we may refer to as the *Closest-Neighbour Uniform Mutation (CNUM)* scheme. Note that similar to the scenario of BQM, in CNUM the corresponding transition probability value is also dependent on the location of the original gene. For instance, if the original gene is located in one of the four corners of the constellation map plotted in Figure 5.9, the relevant transition probability $p_{mt}^{(ij)}$ becomes 1/2, since in this case only two nearest-neighbour symbols exist. The CNUM-related transition probability values of the different modems are summarized in Table 5.4. Hence, by introducing the simplified BQM scheme or the CNUM arrangement, the computational complexity of BQM can be reduced. This issue will be discussed in Section 5.3.3.

5.3.1.3 Simulation Results

In this section, we provide our simulation results characterizing the achievable performance of the TTCM-assisted MMSE-GA-SDMA-OFDM system employing UM or BQM. For the BQM-based schemes, all the parameters used, including the TTCM-, GA- and channel-related ones, are the same as those specified in Table 5.1, except that the UM

Modem	Transition probability value set
4QAM	1/2
16QAM	1/2, 1/3, 1/4
64QAM	1/2, 1/3, 1/4

Table 5.4: Possible transition probability values for the CNUM scheme.

component was substituted by the BQM in the GA MUD.

5.3.1.3.1 BQM Versus UM

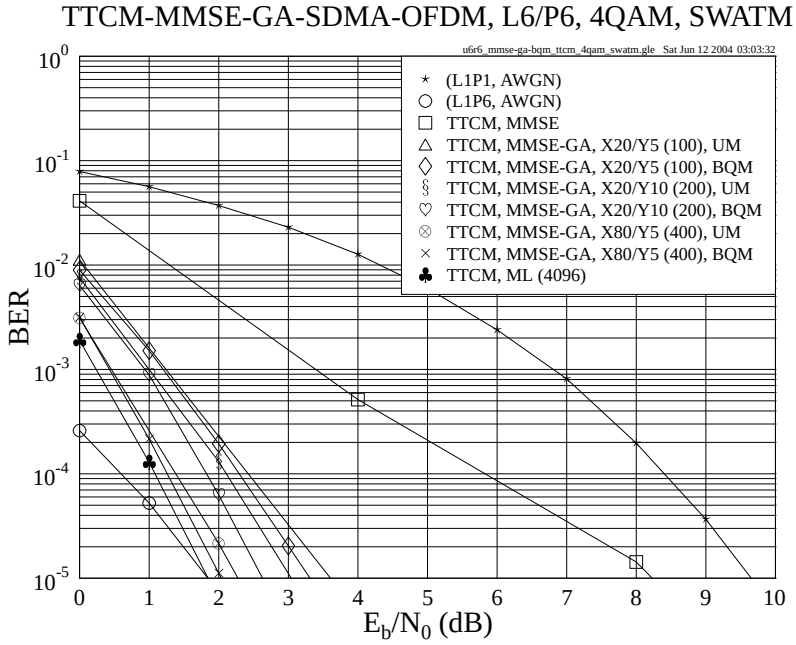

Figure 5.10: BER versus E_b/N_0 performance comparison of the **TTCM-assisted MMSE-GA-SDMA-OFDM** system using **UM** or **BQM**, while employing a **4QAM** scheme for transmission over the SWATM channel, where **L=6** users are supported with the aid of **P=6** receiver antenna elements. The basic simulation parameters are given in Table 5.1.

In Figure 5.10, the BER performance of the UM- and BQM-aided GA-assisted TTCM-MMSE-SDMA-OFDM systems employing a 4QAM scheme for transmission over the SWATM channel of Table 3.10 are compared, where six users are supported with the aid of six receiver antenna elements. Again, the performance of the TTCM-assisted MMSE-SDMA-OFDM system, the TTCM-aided optimum ML-detected system and the uncoded single-user scheme employing either a single receiver or invoking MRC when communicating over an AWGN channel are also provided for reference, respectively. As expected, we can see from Figure 5.10 that the BER performance of the TTCM-assisted MMSE-SDMA-OFDM system was further improved at relatively higher SNRs, when BQM rather than UM was used.

Furthermore, a higher performance improvement can be achieved by the BQM-aided scheme, when we have a higher user load or higher throughput, as seen in Figure 5.11. More specifically, the left hand side of Figure 5.11 shows the simulation results attained in the scenario, where a higher number of $L = 10$ users is supported. In this case, an E_b/N_0 gain of about 1dB was attained by the employment of BQM for a GA having a size of $X = 20$ and $Y = 5$ at the BER of 10^{-5}. This E_b/N_0 gain was achieved, since a higher user load results in a larger search space and hence the conventional UM suffers more from its inefficient mutation mechanism, while BQM may more readily be able to guide the mutation in the desirable directions even at low SNRs, especially in the scenarios having higher user loads. On the other hand, when a high-throughput modem such as for example 16QAM is employed, BQM may significantly outperform UM, as evidenced at the right hand side of Figure 5.11. As seen in the figure, the UM-aided scheme yielded a high residual error floor, since the GA apparently settled in local minima during its search due to the less efficient mutation strategy. By contrast, BQM significantly improved the GA's performance by lowering the error

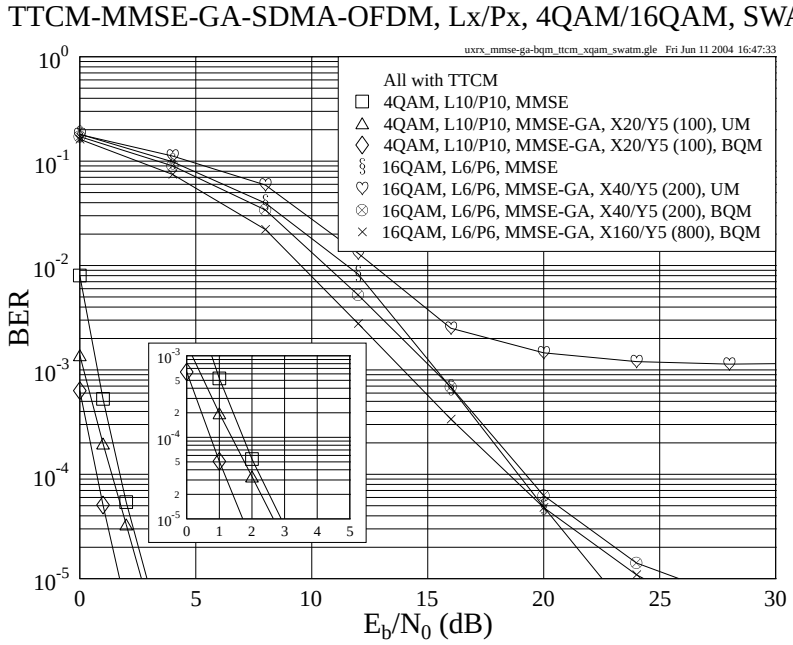

Figure 5.11: BER versus E_b/N_0 performance comparison of the **TTCM-assisted MMSE-GA-SDMA-OFDM** system using **UM** or **BQM**, while employing a **4QAM** or **16QAM** scheme for transmission over the SWATM channel, where **L=6** or **L=10** users are supported with the aid of **P=6** or **P=10** receiver antenna elements, respectively. The basic simulation parameters are given in Table 5.1.

floor by about two magnitudes to the BER of 10^{-5}. Note that at SNRs higher than 20dB, however, a cross-over point appeared on the curves, where a GA having $X = 160$ and $Y = 5$ could no longer improve the MMSE-aided system's performance, when the SNR was increased. The reason for encountering this phenomenon at a high SNR level is that it becomes more difficult for a moderate-complexity GA to mitigate the associated symbol errors, amongst the increased number of the 16QAM constellation symbols in comparison to the 4QAM constellation symbols. Hence, for the sake of improving the attainable performance of systems employing high-throughput modems, we may either use a more complex GA, which is less attractive for complexity-sensitive systems, or invoke an improved MUD framework, as it will be discussed in Section 5.3.2.

5.3.1.3.2 BQM Versus CNUM

As discussed in Section 5.3.1.2.2, the BQM scheme may be simplified to the CNUM arrangement, which mutates to only one of the closest neighbours of the original gene, thus incurring a lower complexity in comparison to BQM. However, CNUM does not necessarily degrade the system's performance dramatically. Figure 5.12 provides a comparison of CNUM and BQM for both low- and high-throughput systems. As observed in Figure 5.12, the BQM-GA-assisted system achieved a slightly better performance than its CNUM-GA-assisted counterpart. This may suggest that in such scenarios the CNUM scheme may become an attractive alternative to the BQM scheme for the sake of further decreasing the complexity imposed.

5.3.2 Iterative MUD Framework

In Section 5.3.1, we have presented an enhanced mutation scheme, namely BQM, which is capable of improving the GA MUD's performance, especially in systems having high user loads and/or employing high-throughput modems. This may be regarded as GA-related improvement in the context of the GA MUD. In this section, we will focus our attention on an enhanced iterative MUD framework, so that the system's performance may be further improved in all the scenarios considered so far.

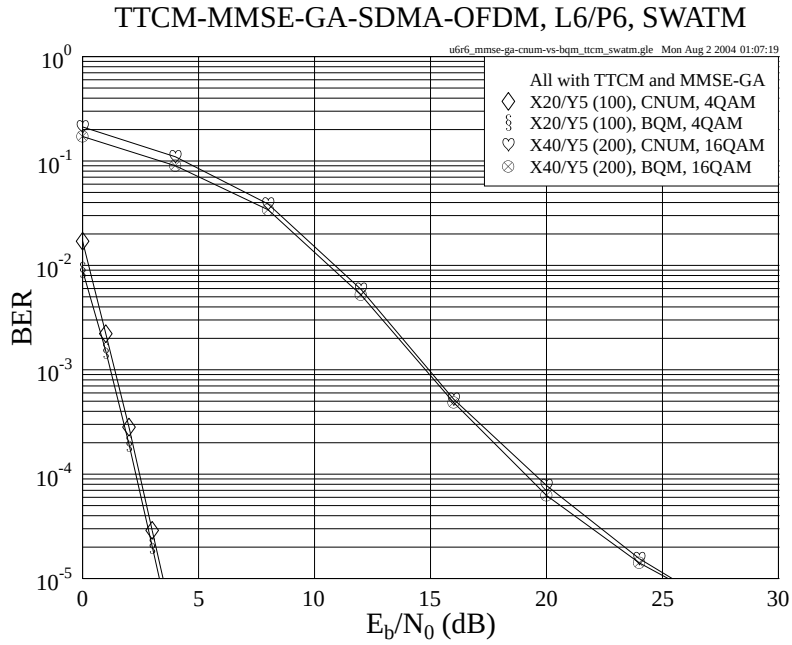

Figure 5.12: BER versus E_b/N_0 performance comparison of the **TTCM-assisted MMSE-GA-SDMA-OFDM** system using **CNUM** or **BQM**, while employing a **4QAM** or **16QAM** scheme for transmission over the SWATM channel, where **L=6** users are supported with the aid of **P=6** receiver antenna elements, respectively. The basic simulation parameters are given in Table 5.1.

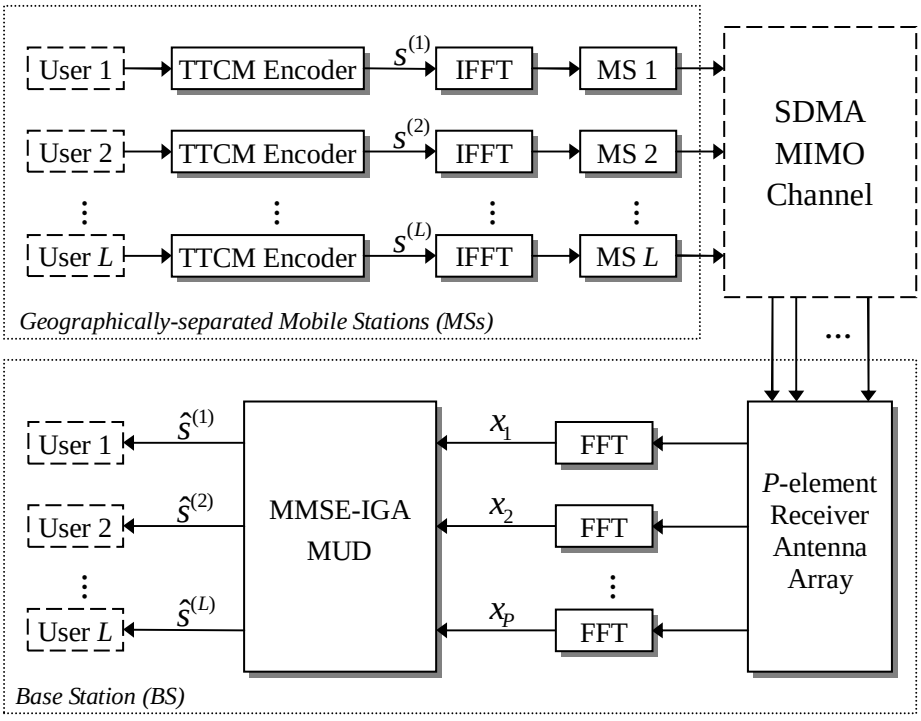

Figure 5.13: Schematic of the IGA MUD assisted multi-user SDMA-OFDM uplink system.

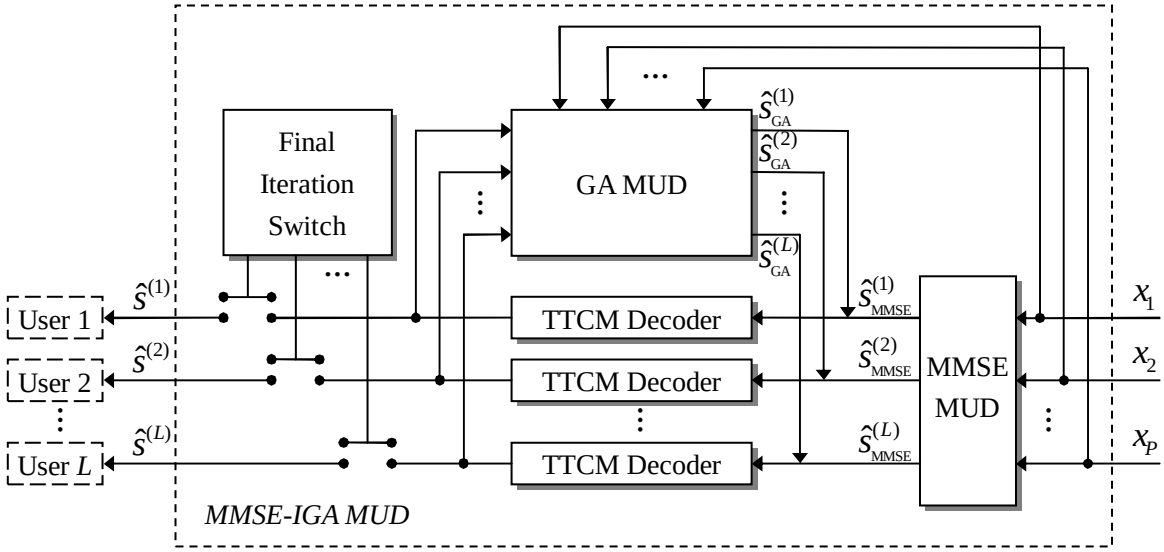

Figure 5.14: Structure of the MMSE-initialized iterative GA MUD used at the BS.

5.3.2.1 MMSE-initialized Iterative GA MUD

In the literature, iterative techniques such as Successive Interference Cancellation (SIC) [198, 442–444] and Parallel Interference Cancellation (PIC) [442, 444, 445], have been designed for multi-user OFDM systems. Following the philosophy of iterative detections, we propose a MMSE-initialized iterative GA (IGA) MUD for multi-user SDMA-OFDM systems. Figure 5.13 shows the proposed IGA MUD assisted multi-user SDMA-OFDM uplink system. Upon comparing Figure 5.1 and Figure 5.13, we can observe that the concatenated MMSE-GA MUD used in the BS of Figure 5.1 is replaced by the MMSE-assisted IGA MUD seen in the middle-bottom part of Figure 5.13, while the detailed structure of the IGA MUD is outlined in Figure 5.14. More specifically, the received length-P symbol vector $\mathbf{x}$ of Equation (4.2) is first detected by the MMSE MUD, which outputs the L MMSE-detected symbols $\hat{s}^{(l)}_{\text{MMSE}}$ $(l = 1, \cdots, L)$ of the L users, and forwards them to L number of independent TTCM decoders. The TTCM-decoded L-symbol vector, which is more reliable than the MMSE MUD's output, is then fed into the concatenated GA MUD for assisting the creation of the initial population. Then the genetically enhanced output symbol vector $\hat{\mathbf{s}}_{\text{GA}}$, which may be expected to become more reliable, will be fed back to the TTCM decoders in order to further improve the signal's quality, invoking a number of iterations. Following the last iteration, the final GA solution will be decoded by the TTCM decoders, and the hard-decision version of the estimated information bits of the L independent users is forwarded to the output, which is only enabled at the final iteration by the switch seen in Figure 5.14.

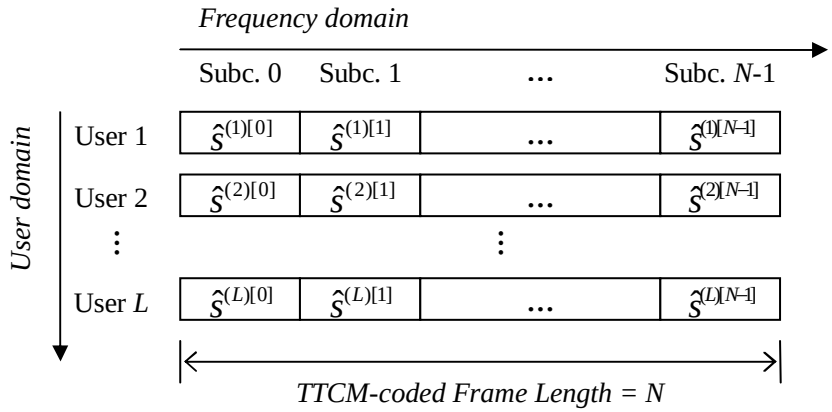

Figure 5.15: The 2D optimization provided by the MMSE-IGA MUD of Figure 5.14. The square brackets $[\cdot]$ denote the subcarrier indices in the TTCM-coded frame of length N.

Therefore, two improvements have been achieved by the MMSE-IGA MUD. Firstly, a more accurate initial knowledge of the transmitted signals, namely the output of the TTCM decoders rather than that of the MMSE MUD, is

supplied for the GA MUD. This reliable improvement therefore offers a better starting point for the GA's search. Secondly, the iterative processing ensures that the detected L-user symbol vector can be optimized in two dimensions, as demonstrated in Figure 5.15. During every iteration, on one hand, each L-symbol vector at a specified subcarrier slot is optimized by the GA in the context of the *user domain*. On the other hand, the entire TTCM-coded frame of each user is optimized by the TTCM decoder in the context of the TTCM-related *codeword domain*, or more specifically the *frequency domain*. Hence, as the iterative processing continues, an information exchange takes place between the two domains, resulting in a 2D optimization which may be expected to improve the system's performance.

5.3.2.2 Simulation Results

In this section, we combine the IGA MUD with BQM, which has been presented in Section 5.3.1.2, and compare the associated simulation results with our previous results. Note that for the sake of fairness, we halved the number of TTCM decoding iterations for the IGA-aided scheme, so that the total TTCM-related complexity remains approximately the same as in the non-iterative system. For the convenience of the reader, in Table 5.5 we summarize the basic simulation parameters used for generating the results provided in this section.

TTCM	Modem	4QAM
	Code rate	0.5
	Code memory ν	3
	Octal generator polynomial	$[13 \quad 6]$
	Codeword length	1024 symbols
	Channel interleaver depth	1024 symbols
	Number of turbo iterations	2
GA	Population initialization method	MMSE
	Mating pool creation strategy	Pareto-Optimality
	Selection method	Fitness-Proportionate
	Cross-over	Uniform cross-over
	Mutation	UM or BQM
	Mutation probability p_m	0.1
	Elitism	Enabled
	Incest prevention	Enabled
	Population size X	Varied
	Generations Y	Varied
	Number of IGA iterations	Varied
Channel	CIRs	SWATM [5]
	Paths	3
	Maximum path delay	48.9 ns
	Normalized Doppler frequency f_d	1.235×10^{-5}
	Subcarriers K	512
	Cyclic prefix	64

Table 5.5: The various techniques and parameters used in the simulations of Section 5.3.2.2.

5.3.2.2.1 Performance in Underloaded and Fully-loaded Scenarios

In this section, we will investigate the system's achievable performance generated in the so-called underloaded and fully-loaded scenarios, respectively, where the number of users L is less than or is equal to the number of receiver antennas P.

5.3.2.2.1.1 BQM-IGA Performance

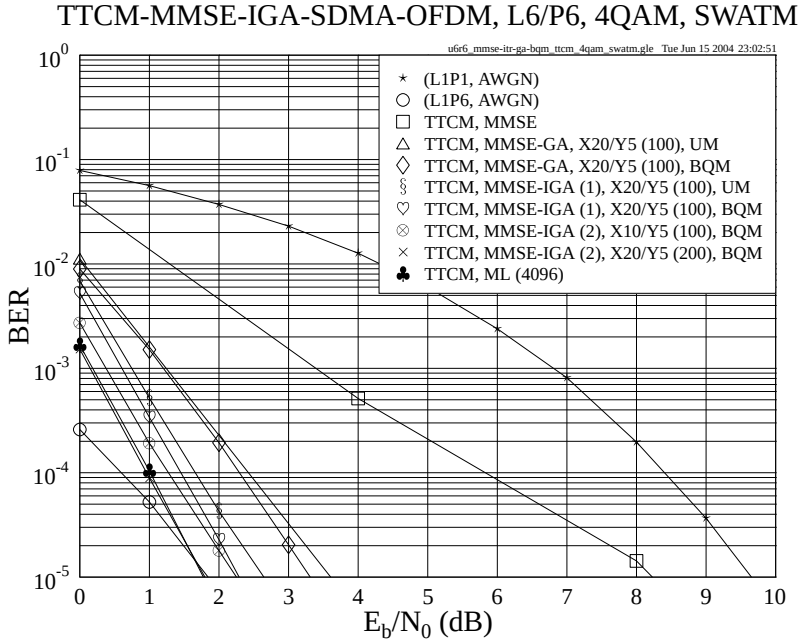

Figure 5.16: BER versus E_b/N_0 performance comparison of the **iterative** or **non-iterative TTCM-assisted MMSE-GA-SDMA-OFDM** system using **UM** or **BQM**, while employing a **4QAM** scheme for transmission over the SWATM channel, where **L=6** users are supported with the aid of **P=6** receiver antenna elements, respectively. The basic simulation parameters are given in Table 5.5.

Figure 5.16 shows the BER performance achieved by the various schemes considered. The numbers in the round brackets seen in the legends of Figure 5.16 denote the associated number of IGA MUD iterations and the total GA or ML complexity, respectively. From the results of Figure 5.16 two conclusions may be arrived at. Firstly, an improved performance can be achieved, when the GA commences its operation from a better initial population, regardless of the different mutation schemes used. For example, at the same GA complexity, the single-iteration IGA MUD assisted systems outperformed their non-iterative GA aided counterparts, since the initial GA population of the former systems were created based on the first-iteration outputs of the TTCM decoders, rather than on the less reliable MMSE MUD regardless, whether UM or BQM was employed.

Secondly, the system employing the BQM-aided two-iteration IGA MUD was capable of achieving the same performance as the optimum ML-aided system at an even lower complexity compared to the UM- or BQM-aided non-iterative GA MUD, which was characterized in Figure 5.10. For instance, Figure 5.16 shows that the two-iteration BQM-IGA MUD having a complexity of 200 achieved virtually undistinguishable performance in comparison to its ML-aided counterpart, while the non-iterative UM/BQM-GA MUD having a complexity of 400 attained a slightly inferior performance in comparison to the ML-aided arrangement, as observed in Figure 5.10.

Having investigated the system using the 4QAM modem, let us now consider various high-throughput scenarios. As mentioned in Section 5.3.1.3, the non-iterative GA MUD may result in a high residual error floor in high-throughput scenarios, even if BQM is employed. However, with the aid of the IGA MUD, the error floor can be effectively reduced, as seen in Figure 5.17. 16QAM modem was employed by all the schemes[7] characterized in Figure 5.17, except for the uncoded single-user benchmark scheme communicating over the AWGN channel, which used 8PSK for the sake of maintaining the same effective throughput of 3BPS as the other TTCM-coded schemes. Similarly to the 4QAM scenario of Figure 5.16, it can be seen in Figure 5.17 that a better initial population resulted in an improved performance in both the UM- and BQM-aided systems. However, we may notice that even when assisted by a reliable initial knowledge of the transmitted symbols, the UM-aided single-iteration IGA MUD was unable to substantially decrease the error floor. Even when we increased the number of UM-IGA MUD iterations, the situation remained the same, except for the modest improvements achieved at SNRs lower than 16dB. By contrast, the BQM-aided scheme is capable of substantially exploiting the benefits arising from both a better initial GA population and from an increased number of IGA MUD iterations. More specifically, on one hand, the improved initial population provides a

[7] Note that in this case the associated complexity of the ML-aided scheme is as high as on the order of $O(2^{mL}) = O(2^{4\cdot 6}) = O(16,777,216)$, which imposes an excessive complexity and hence cannot be simulated.

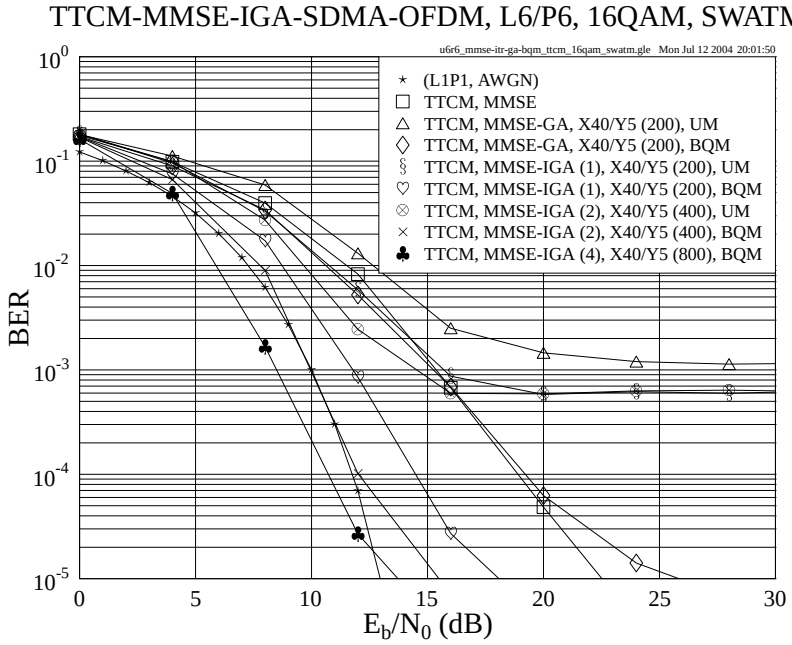

Figure 5.17: BER versus E_b/N_0 performance comparison of the **iterative** or **non-iterative TTCM-assisted MMSE-GA-SDMA-OFDM** system using **UM** or **BQM**, while employing a **16QAM** scheme for transmission over the SWATM channel, where **L=6** users are supported with the aid of **P=6** receiver antenna elements, respectively. The basic simulation parameters are given in Table 5.5.

good starting point for the GA, thus assisting the BQM, which in turn benefits the entire detection process, resulting in a substantial performance improvement. On the other hand, the iterative processing invoked by the IGA MUD further enhances the system's performance with the aid of the 2D optimization, as discussed in Section 5.3.2.1, since the beneficial information exchange between the user domain and the frequency domain assists both the GA MUD and the TTCM decoder in eliminating more and more errors found in the received signal, as the iterative procedure continues.

5.3.2.2.1.2 Effects of the Number of IGA MUD Iterations

Figure 5.18 shows the E_b/N_0 gain achieved by the BQM-IGA assisted TTCM-MMSE-SDMA-OFDM systems employing 16QAM at the BER of 10^{-5}, while using different number of IGA MUD iterations. The E_b/N_0 gain is defined here as the E_b/N_0 difference measured at the BER of 10^{-5} between the systems employing the BQM-IGA MUD or the MMSE MUD. As expected, when we had a higher number of IGA MUD iterations, a higher E_b/N_0 gain was attained. It is also found in Figure 5.18 that most of the achievable gain may be attained, when the number of IGA MUD iterations reaches 8. Furthermore, when the complexity of the GA MUD increases, because for example a higher population size is employed, a higher gain can be achieved, as seen in Figure 5.18. Moreover, we may also notice that when the number of IGA MUD iterations was increased, the difference between the E_b/N_0 gains achieved by the higher-complexity and the lower-complexity IGAs tends to be larger. For example, as observed in Figure 5.18, when we had only one IGA MUD iteration, the E_b/N_0 gain difference between the two curves was about 1dB, while this value increased to about 3dB, when the number of iterations was increased to 8. This suggests that a high-complexity IGA may benefit more from a higher number of IGA MUD iterations than its lower-complexity counterpart.

5.3.2.2.1.3 Effects of the User Load

Figure 5.19 exhibits the corresponding E_b/N_0 gains achieved by the SDMA-OFDM system exploiting $P = 6$ receiver antenna elements at the BER of 10^{-5} in the scenarios, where the user load varies. The user load of SDMA-OFDM systems was defined by Equation (4.14) in Section 4.3.2.1.1. As observed in Figure 5.19, firstly, it is shown that when the user load becomes higher, a higher gain can be attained. For example, for the single-iteration IGA-aided system, a further gain of about 3.5dB is achieved, when the number of users increases from four to six. This is because when more users were accommodated by the SDMA-OFDM system, the reference MMSE MUD suffered a higher

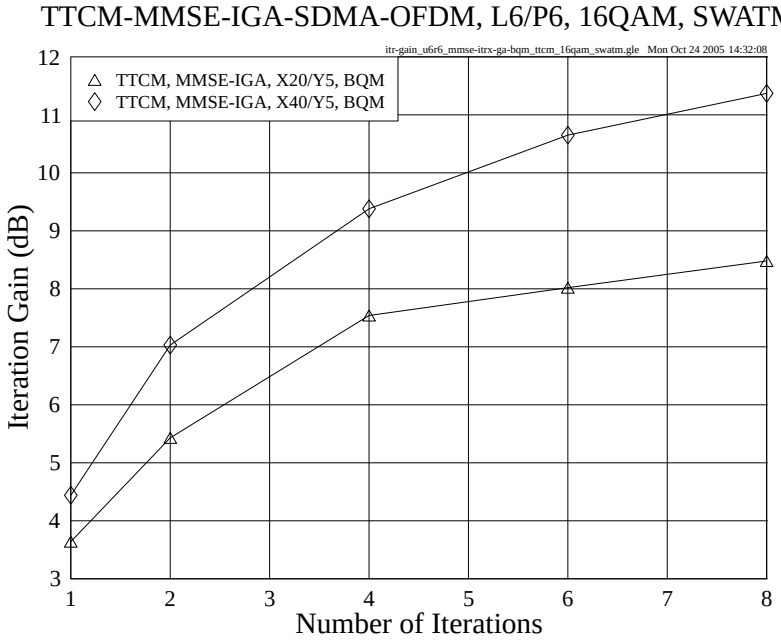

Figure 5.18: Iteration gain at the BER of 10^{-5} versus number of IGA MUD iterations performance of the **TTCM-assisted MMSE-IGA-SDMA-OFDM** system using **BQM**, while employing a **16QAM** scheme for transmission over the SWATM channel, where **L=6** users are supported with the aid of **P=6** receiver antenna elements. The basic simulation parameters are given in Table 5.5.

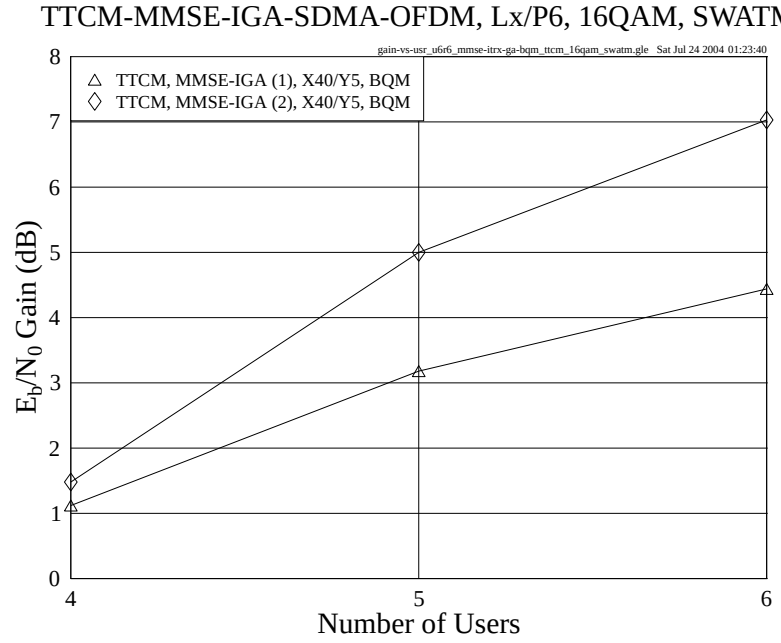

Figure 5.19: E_b/N_0 gain at the BER of 10^{-5} versus number of users performance of the **TTCM-assisted MMSE-IGA-SDMA-OFDM** system using **BQM**, while employing a **16QAM** scheme for transmission over the SWATM channel, where **L=4, 5, 6** users are supported with the aid of **P=6** receiver antenna elements, respectively. The basic simulation parameters are given in Table 5.5.

performance degradation than the IGA MUD, and thus a higher E_b/N_0 gain was attained by the IGA MUD. Secondly, a higher number of IGA MUD iterations provides a higher E_b/N_0 gain for the system. For instance, in the full-user-load scenario, namely for $L = P = 6$, the two-iteration IGA-aided system achieves a further gain of about 2.7dB over its single-iteration counterpart, providing an overall E_b/N_0 gain of 7dB over the base-line TTCM-MMSE-SDMA-OFDM benchmark system dispensing with the GA MUD.

5.3.2.2.2 Performance in Overloaded Scenarios

Recall that in Section 5.1 we pointed out that in practical applications the number of users L may be higher than that of the receiver antennas P, resulting in the overloaded scenario. However, most of the existing MUD techniques, such as for example the MMSE algorithm of [5,442] and the QRD-M algorithm of [173], suffer from a significant performance degradation in overloaded scenarios, owing to the insufficient degree of detection freedom at the receiver. By contrast, we will show in this section that the proposed IGA MUD is capable of adequately performing in overloaded scenarios.

5.3.2.2.2.1 Overloaded BQM-IGA

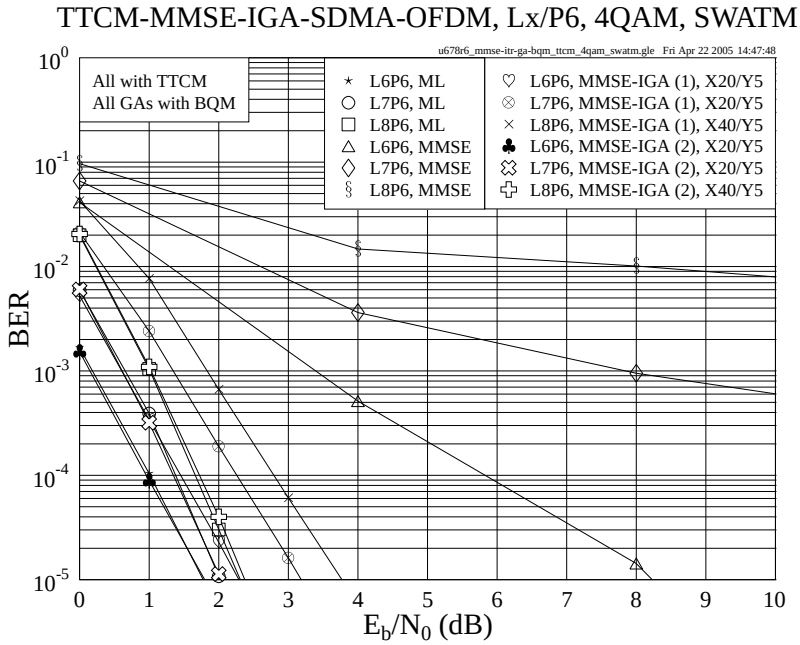

Figure 5.20: BER versus E_b/N_0 performance comparison of the **TTCM-assisted MMSE-IGA-SDMA-OFDM** system using **BQM**, while employing a **4QAM** scheme for transmission over the SWATM channel, where **L=6, 7, 8** users are supported with the aid of **P=6** receiver antenna elements, respectively. The basic simulation parameters are given in Table 5.5.

Figure 5.20 shows the performance achieved by the BQM-IGA aided TTCM-SDMA-OFDM system using 4QAM, when six, seven and eight users are supported by six receiver antenna elements, respectively. It is seen in Figure 5.20 that in the so-called overloaded scenarios, where the number of users exceeds the number of receiver antenna elements, the linear MMSE MUD suffered from an insufficient degree of freedom for separating the different users, since the high number of users incurred an excess Multi-User Interference (MUI). This results in a significant performance degradation in the context of the system using the MMSE MUD, when the number of users increased from six to eight, as observed in Figure 5.20. However, in such cases the system employing the proposed BQM-IGA MUD was still capable of maintaining a near-ML performance. For example, when we had $L = 8$, the two-iteration based BQM-IGA MUD reduced the BER measured at 3dB by four orders of magnitude in comparison to the MMSE-aided benchmark system, as evidenced by Figure 5.20. This result characterizes the robustness of the BQM-IGA MUD, which has successfully suppressed the high MUI experienced in overloaded scenarios.

Figure 5.21 shows the iteration gain achieved by the BQM-IGA assisted TTCM-MMSE-SDMA-OFDM system employing 4QAM at the BER of 10^{-5}, while using different number of IGA MUD iterations. The iteration gain is defined here as the E_b/N_0 difference of the systems employing different number of IGA MUD iterations measured

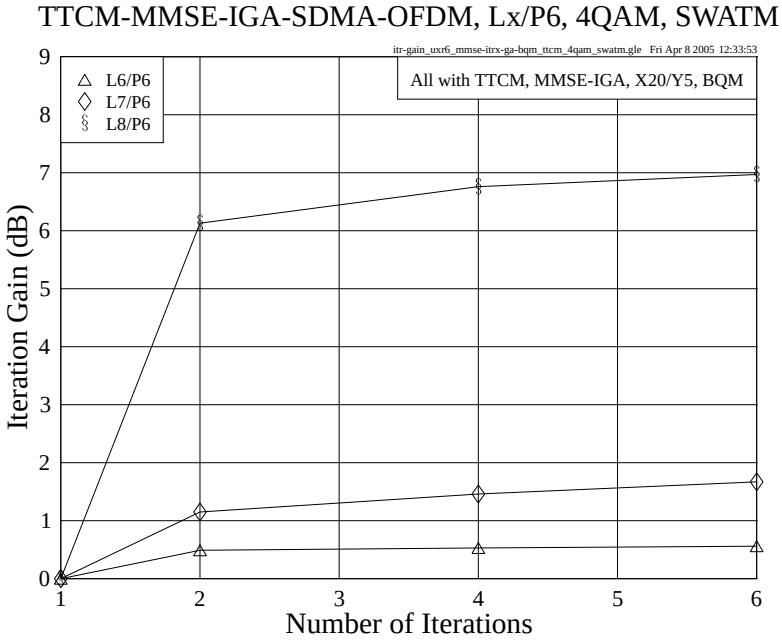

Figure 5.21: Iteration gain at the BER of 10^{-5} versus number of IGA MUD iterations performance of the **TTCM-assisted MMSE-IGA-SDMA-OFDM** system using **BQM**, while employing a **4QAM** scheme for transmission over the SWATM channel, where **L=6, 7, 8** users are supported with the aid of **P=6** receiver antenna elements, respectively. The basic simulation parameters are given in Table 5.5.

at the BER of 10^{-5} in comparison to the baseline system employing a single IGA MUD iteration. It is found in Figure 5.21 that when more users are supported, higher iteration gains may be obtained by iterative detection. For example, a gain of about 6dB was attained by the eight-user system at the second IGA MUD iteration, while that attained by the six-user system was only about 0.5dB. Furthermore, as the number of iterations was increased from two to six, the former scheme provided a further gain of about 1dB, while no explicit gain was achieved by the latter arrangement, as shown in Figure 5.21. It is also seen in Figure 5.21 that most of the achievable iteration gain has been attained at the second IGA MUD iteration for all the schemes.

5.3.2.2.2.2 BQM Versus CNUM

In Section 5.3.1.3.2, we have shown the performance of the CNUM arrangement discussed in Section 5.3.1.2.2 in a fully-loaded scenario. In Figure 5.22, we characterize the CNUM aided system's performance achieved in an overloaded scenario, where six receiver antennas were used. As seen in Figure 5.22, the BQM-IGA aided system slightly outperformed the CNUM-IGA aided system. This suggests that similar to the case of fully-loaded scenarios, the CNUM scheme may also be employed in overloaded scenarios for achieving a further complexity reduction over the BQM scheme without suffering from a significant performance loss.

5.3.2.2.3 Performance Under Imperfect Channel Estimation

As a further investigation, we provide the simulation results generated in the scenario, where the Channel State Information (CSI) was assumed to be imperfect. The estimated CIRs $\hat{h}_i$ were generated by adding random Gaussian noise to the true CIR taps h_i as:

$$\hat{h}_i[n] \quad = \quad h_i[n] + \sqrt{\frac{\sigma_n^2}{\varepsilon}} n_i[n], \quad i = 1, \cdots, \mathcal{L}, \tag{5.19}$$

where ε is the effective noise factor, σ_n^2 is the noise variance at the specific SNR level, n_i is an AWGN sample having zero-mean and a variance of unity, $\mathcal{L}$ is the number of CIR taps and $[n]$ denotes the n^{th} OFDM symbol. In the scenarios associated with imperfect CIRs, ε was set to 64 and $\mathcal{L}$ was set to 3 for the three-path SWATM channel used. In this case, the effective noise power added to the true CIR taps during each OFDM symbol for the sake of simulating imperfect channel estimation was $\sigma_n^2 \cdot \mathcal{L}/\varepsilon = \sigma_n^2 \times 4.69\%$. A snap shot of the SWATM channel is portrayed in

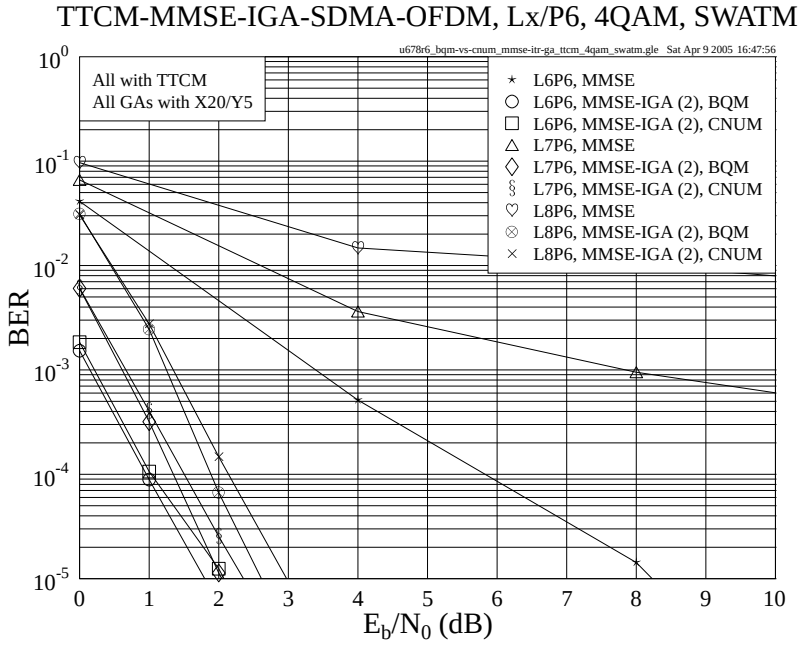

Figure 5.22: BER versus E_b/N_0 performance comparison of the **TTCM-assisted MMSE-IGA-SDMA-OFDM** system using **BQM** or **CNUM**, while employing a **4QAM** scheme for transmission over the SWATM channel, where **L=6, 7, 8** users are supported with the aid of **P=6** receiver antenna elements, respectively. The basic simulation parameters are given in Table 5.5.

Figure 5.23, which shows both the real and imaginary components of the FD-CHTFs associated with both perfect and imperfect CIRs.

Our performance comparison of the proposed BQM-IGA aided TTCM-MMSE-SDMA-OFDM system under the assumptions both of perfect and imperfect CSI is provided in Figure 5.24. As seen in Figure 5.24, the proposed system was capable of attaining an acceptable performance even without accurate channel knowledge. Moreover, it was found that when imperfect channel estimation was assumed, the BQM-IGA aided system outperformed its ML-aided counterpart, especially in the scenarios associated with higher user loads. This phenomenon may be explained as follows. When the CSI is imperfect, the ML-detected signal becomes less reliable than that detected in the scenario benefitting from perfect CSI. The relatively unreliable output of the ML MUD may readily mislead the TTCM decoder due to error propagation, resulting in a performance degradation. However, the detrimental effects of imperfect CSI may be mitigated by the proposed IGA MUD. More specifically, the IGA MUD optimizes the detected signal in two dimensions, namely in both the user domain as well as in the frequency domain, as discussed in Section 5.3.2.1. The beneficial information exchange offered by the IGA MUD between the two domains may effectively assist the concatenated detection-decoding procedure in counteracting the detrimental effects of imperfect channel estimation. This therefore results in a better system performance in comparison to that achieved by the ML-aided system. Furthermore, when a higher number of users had to be supported, the ML-aided system using imperfect CSI suffered more from the inaccurate multi-user detection, while a more robust behaviour was exhibited by the IGA-aided system, as shown in Figure 5.24.

5.3.3 Complexity Analysis

Compared to the conventional UM scheme, BQM is capable of significantly improving the GA's performance, especially in high-throughput or high-SNR scenarios, as discussed in Section 5.3.1.3.1. Furthermore, this performance improvement was achieved at the cost of a modest complexity increase and a modest memory requirement. More specifically, at different SNR levels, for each of the 2^m constellation symbols, a specific set containing $(2^m - 1)$ number of normalized 2D transition probabilities has to be created. However, this only imposes a modest "once-for-all" calculation, since we can derive the associated transition probabilities with the aid of off-line experiments for a number of typical SNR levels, where the calculated data can be stored in the base station's memory, hence incurring no further computational complexity. Furthermore, by introducing the simplified BQM scheme of Section 5.3.1.2.2, the associated complexity and memory cost may be dramatically reduced, especially for high-throughput modems such

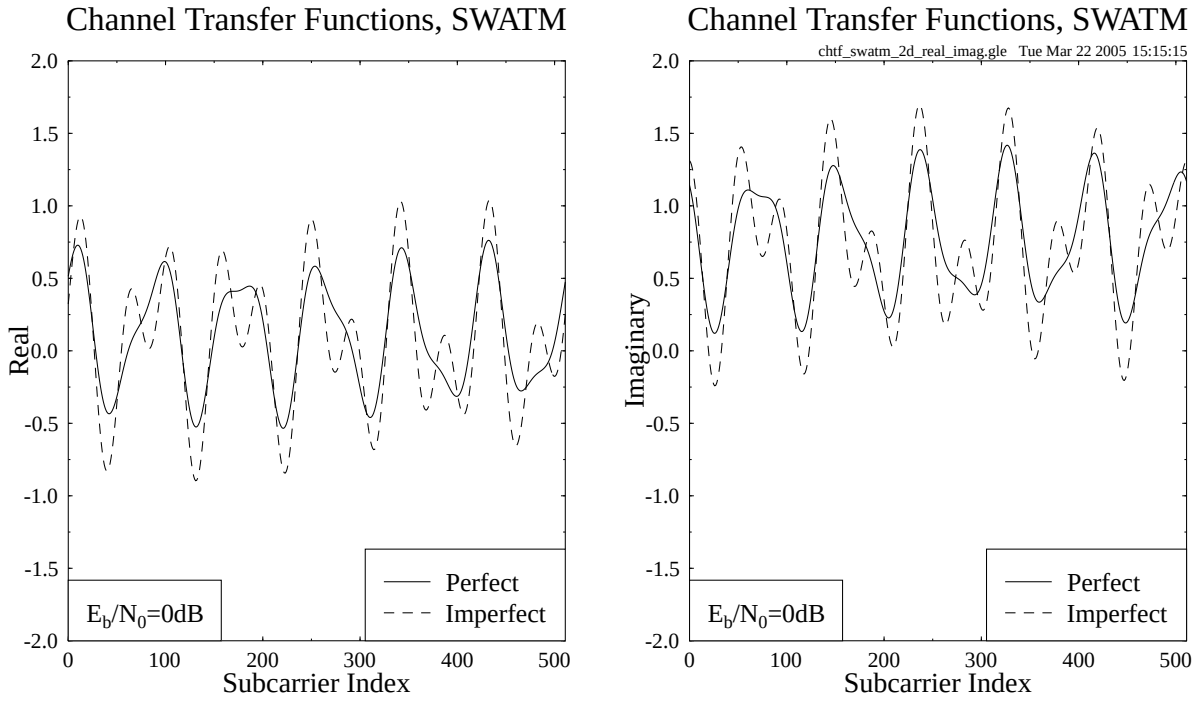

Figure 5.23: The real and imaginary components of the FD-CHTFs of the SWATM channel measured during one OFDM symbol at a E_b/N_0 value of 0dB in terms of both perfect and imperfect CIRs.

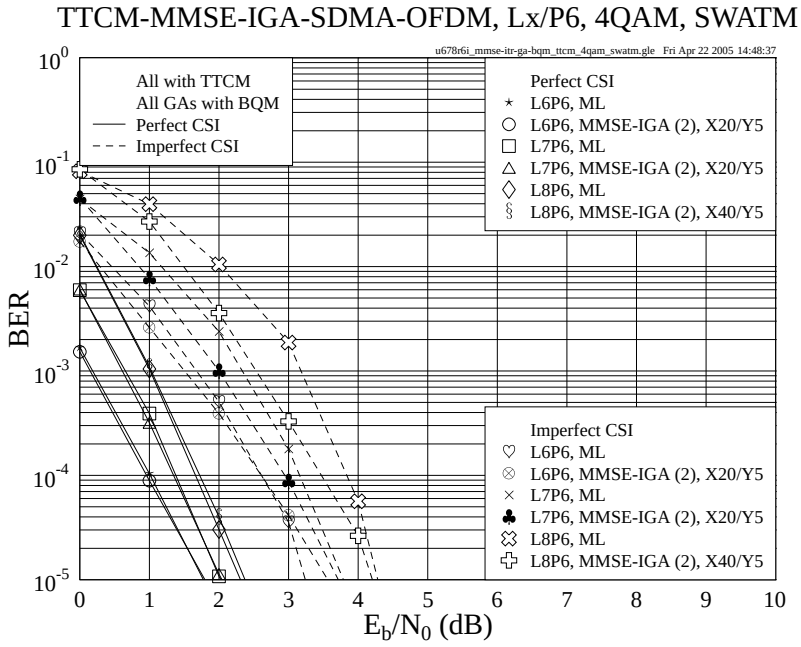

Figure 5.24: BER versus E_b/N_0 performance comparison of the **TTCM-assisted MMSE-IGA-SDMA-OFDM** system using **BQM** with perfect or imperfect CSI , while employing a **4QAM** scheme for transmission over the SWATM channel, where **L=6, 7, 8** users are supported with the aid of **P=6** receiver antenna elements, respectively. The basic simulation parameters are given in Table 5.5.

as 16QAM or 64QAM, since the number of mutation target candidates decreases and thus fewer transition probability calculations are required. Moreover, if the CNUM scheme is employed, the associated complexity can be further decreased, since in this case there is no need to calculate the transition probabilities, which are already available in Table 5.4. This may significantly reduce the associated complexity and memory requirement, while still maintaining a similar performance to that of the BQM scheme, as seen in Figures 5.12 and 5.22.

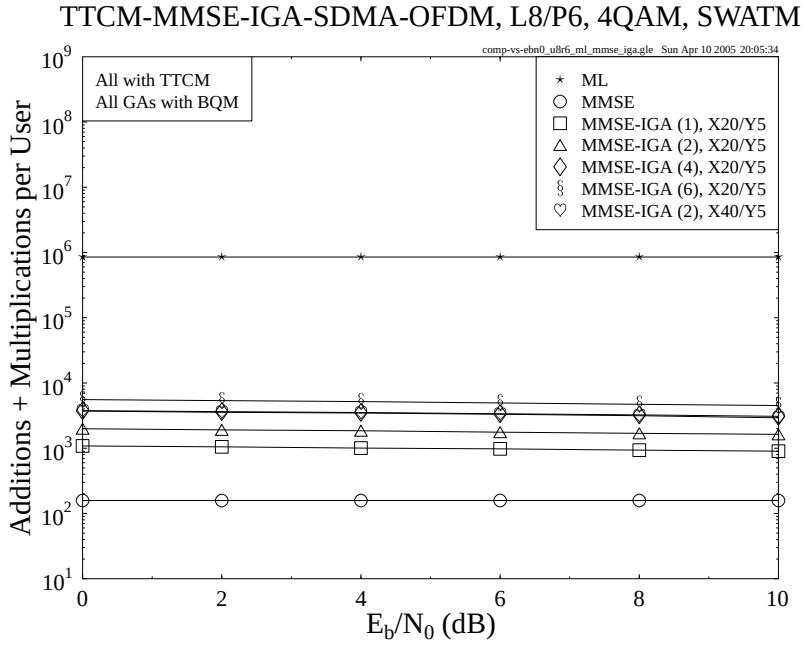

Figure 5.25: Complexity per user versus E_b/N_0 performance comparison of the **TTCM-assisted MMSE-SDMA-OFDM**, **ML-SDMA-OFDM**, and **MMSE-BQM-IGA-SDMA-OFDM** systems, while employing a **4QAM** scheme for transmission over the SWATM channel, where **L=8** users are supported with the aid of **P=6** receiver antenna elements. The basic simulation parameters are given in Table 5.5.

As shown in Figures 5.18 and 5.21, the system's performance can be further improved, when the number of IGA MUD iterations is increased. When the other parameters remain the same, using a higher number of IGA MUD iterations will result in a further increased complexity. However, this may still be significantly lower than that imposed by the ML-aided scheme. Figure 5.25 provides our comparison of the TTCM-assisted MMSE-SDMA-OFDM, ML-SDMA-OFDM and MMSE-BQM-IGA-SDMA-OFDM systems in the context of their MUD complexity, which was quantified in terms of the number of complex additions and multiplications imposed by the different MUDs on a per user basis. As illustrated in Figure 5.25, the complexity of the ML MUD is significantly higher than that of the MMSE MUD or the IGA MUD. Furthermore, the IGA MUD's complexity does not significantly vary at different E_b/N_0 values and depends on the number of IGA MUD iterations as well as on the GA's parameters, for example the population size. In Figure 5.26 the complexity of the various systems is compared in terms of different user loads at an E_b/N_0 value of 0dB. At a specific user load, we always select an appropriate GA-aided scheme for comparison, which achieved a similar performance compared to the ML-aided system at the BER of 10^{-5}. As seen in Figure 5.26, the ML-aided system imposes a linearly increasing complexity on a logarithmic scale, which corresponds to an exponential increase when the number of users increases. By contrast, the complexity of the IGA-aided system required for maintaining a near-optimum performance increases only moderately.

In order to characterize the advantage of the BQM-IGA scheme in terms of the performance-versus-complexity tradeoff, in Table 5.6 we summarize the computational complexity imposed by the different MUDs assuming an E_b/N_0 value of 3dB. As observed in Table 5.6, the complexity of the ML MUD is significantly higher than that of the MMSE MUD or the IGA MUD, especially in highly overloaded scenarios. By contrast, the IGA MUD reduced the BER by up to five orders of magnitude in comparison to the MMSE MUD at a moderate complexity.

5.3.4 Conclusions

In Sections 5.3.1 and 5.3.2 we proposed specific techniques designed for further enhancing the achievable performance of the TTCM-assisted MMSE-GA-SDMA-OFDM system. The novel BQM scheme is capable of improving the GA's

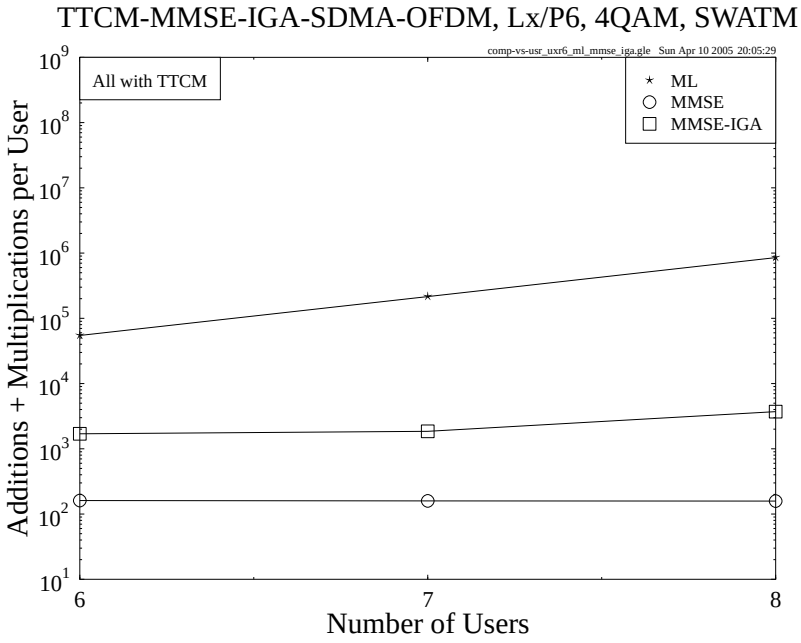

Figure 5.26: Complexity per user versus number of users performance comparison of the **TTCM-assisted MMSE-SDMA-OFDM**, **ML-SDMA-OFDM** and **MMSE-BQM-IGA-SDMA-OFDM** systems, while employing a **4QAM** scheme for transmission over the SWATM channel, where **L=6, 7, 8** users are supported with the aid of **P=6** receiver antenna elements. The basic simulation parameters are given in Table 5.5.

L	MUD	+	×	BER
6	ML	2.8×10^4	2.7×10^4	1.8×10^{-7}
	IGA	8.1×10^2	7.9×10^2	2.2×10^{-7}
	MMSE	7.1×10^1	9.0×10^1	1.5×10^{-3}
7	ML	1.1×10^5	1.1×10^5	5.1×10^{-7}
	IGA	8.7×10^2	8.5×10^2	6.2×10^{-7}
	MMSE	7.1×10^1	8.8×10^1	7.5×10^{-3}
8	ML	4.3×10^5	4.2×10^5	8.5×10^{-7}
	IGA	1.8×10^3	1.7×10^3	9.8×10^{-7}
	MMSE	7.1×10^1	8.7×10^1	2.2×10^{-2}

Table 5.6: Comparison of MUD complexity in terms of number of complex additions and multiplications measured at $E_b/N_0 = 3$dB on a per user basis in the 4QAM TTCM-SDMA-OFDM system.

search at a modest complexity increase, thus significantly increasing the chances of finding the optimum GA solution in high-SNR and/or high-throughput scenarios. On the other hand, the 2D optimization provided by the proposed IGA MUD has been shown to be beneficial for the SDMA-OFDM system in both the frequency and user domains. Finally, the scheme that combines BQM with the IGA MUD yields the best and near-optimum performance in all scenarios considered, including the so-called overloaded scenario, where the performance of most of the conventional detection techniques such as the classic linear MMSE MUD significantly degrades, owing to the insufficiently high degree of freedom. Furthermore, this superior performance of the proposed scheme is achieved at a significantly lower computational complexity than that imposed by the ML-assisted system, especially when the number of users is high. For example, a complexity reduction of three orders of magnitude can be achieved by the proposed BQM-IGA aided system in the overloaded scenario associated with $L = 8$, as evidenced by Figure 5.26. Moreover, we demonstrate that the proposed scheme is capable of providing a satisfactory performance even when the channel estimation is imperfect.

5.4 Chapter Summary

In this chapter, we proposed a TTCM-assisted MMSE-GA MUD designed for SDMA-OFDM systems. In Section 5.2.1 we provided a system overview of the proposed GA-assisted TTCM-MMSE-SDMA-OFDM system. The optimization metric designed for the proposed GA MUD was described in Section 5.2.2.1. Section 5.2.2.2 outlined the concatenated MMSE-GA MUD, while its performance was evaluated in Section 5.2.3, where the GA-based schemes were shown to be capable of achieving a near-optimum performance. Furthermore, a complexity comparison between the proposed GA MUD and the optimum ML MUD was provided in Section 5.2.4, where we showed that the complexity of the GA MUD was significantly lower than that of the ML MUD.

For the sake of further improving the performance of the TTCM-assisted MMSE-GA-SDMA-OFDM system, an enhanced GA MUD was proposed in Section 5.3. This was described in two steps. Firstly, the novel BQM scheme was proposed in Section 5.3.1, including a review of the conventional UM scheme, followed by the detailed explanation of the BQM mechanism, which were the subjects of Sections 5.3.1.1 and 5.3.1.2, respectively. The BQM-aided GA MUD exploits an effective mutation strategy and thus it is capable of achieving a better performance in comparison to its UM-aided counterpart, especially at high SNRs or high user loads, as evidenced by the simulation results given in Section 5.3.1.3. Moreover, this was achieved at a modest complexity increase. Secondly, a MMSE-initialized IGA MUD was introduced in Section 5.3.2. The theoretical foundations of the IGA MUD were presented in Section 5.3.2.1, where the IGA framework as well as its optimization capability were characterized. Our related simulation results were provided in Section 5.3.2.2, where the combined BQM-IGA assisted system was found to give the best performance in all scenarios considered, while maintaining a modest computational complexity. In low-throughput scenarios, for example a six-user system employing a 4QAM modem, a two-iteration BQM-IGA MUD associated with $X = 20$ and $Y = 5$ was capable of achieving the same performance as the optimum ML-aided system at a complexity of 200, which is only about 50% and 5% of the MUD-related complexity imposed by the conventional UM-aided single-iteration IGA MUD and the optimum ML MUD, respectively. On the other hand, in high-throughput six-user systems employing for example a 16QAM modem, a two-iteration BQM-IGA MUD associated with $X = 40$ and $Y = 5$ achieved an E_b/N_0 gain of about 7dB over the MMSE MUD benchmarker at the BER of 10^{-5}, while the UM-aided GA or IGA MUDs suffered from a high residual error floor even when the iterative framework was employed. Furthermore, the associated E_b/N_0 gain was attained at a modest complexity of 400, which is only 0.00238% of the excessive complexity imposed by the ML MUD that cannot be simulated in this case.

Moreover, the proposed BQM-IGA MUD is capable of providing a near-optimum performance even in the so-called overloaded scenarios, where the number of users is higher than the number of receiver antenna elements, while many conventional detection techniques suffer from an excessively high error floor. For example, when we had $L = 8$ users and $P = 6$ receivers, the two-iteration based BQM-IGA MUD reduced the BER recorded at an E_b/N_0 value of 3dB by four orders of magnitude in comparison to the classic MMSE MUD aided benchmarker system, as shown in Figure 5.20. This result characterizes the robustness of the BQM-IGA MUD, which has successfully suppressed the high MUI experienced in overloaded scenarios. As a further investigation, we demonstrated in Section 5.3.2.2.3 that the proposed system is capable of achieving a satisfactory performance even in the case of imperfect channel estimation. Furthermore, the complexity of the proposed detection scheme is only moderately higher than that imposed by the linear MMSE MUD, and is substantially lower than that imposed by the optimum ML MUD, as discussed in Section 5.3.3. We also showed that in both the fully-loaded scenario of Section 5.3.1.3.2 and in the overloaded scenario of Section 5.3.2.2.2.2 the complexity of the BQM approach can be further reduced by employing its simplified version, namely the CNUM scheme of Section 5.3.1.2.2, at the cost of a slightly degraded system performance.

Note that the system parameters of the IGA framework, such as the number of TTCM iterations, the number of IGA MUD iterations and the GA-related parameter settings, are all readily configurable, enabling us to strike an attractive

tradeoff between the achievable performance and the complexity imposed. For specific scenarios, the TTCM scheme used in the system can also be conveniently substituted by other FEC schemes, for example the TC codes. Therefore, the facility provided by the proposed IGA MUD may make it possible to applications in multi-mode terminals, where good performance, low complexity and easy flexibility are all important criterions. It is also worth pointing out that the proposed BQM-aided IGA MUD can be readily incorporated into the multi-user CDMA systems, for example those of [40]. In this case, the initial detected signal supplied to the GA MUD for creating the first GA population is provided by the bank of matched filters installed at the CDMA BS, rather than by the MMSE MUD. However, the BQM scheme may remain unchanged.

In the next chapter, our attention will be focused on a TTCM-assisted MMSE-IGA multi-user detected SDMA-OFDM system employing a new type of Frequency-Hopping (FH) technique for the sake of achieving further performance enhancements.

Chapter 6

Direct-Sequence Spreading and Slow Subcarrier-Hopping Aided Multi-User SDMA-OFDM Systems

6.1 Conventional SDMA-OFDM Systems

In Chapters 4 and 5, Coded Modulation (CM) [359] assisted SDMA-OFDM systems invoking both Minimum Mean-Square Error (MMSE) and Genetic Algorithm (GA) based Multi-User Detection (MUD) have been investigated, respectively. Specifically, in terms of the bandwidth sharing strategy the SDMA-OFDM systems discussed in these chapters are referred to here as the *conventional* SDMA-OFDM systems [5, 194], where all the users exploit the entire system bandwidth for their communications. However, this bandwidth sharing strategy exhibits a few drawbacks.

On one hand, the conventional SDMA-OFDM systems can exploit little frequency diversity, since each user activates all available subcarriers. This limitation can be mitigated by combining both Frequency-Hopping (FH) and SDMA-OFDM techniques, resulting in the FH/SDMA-OFDM systems. In FH/SDMA-OFDM systems the total system bandwidth is divided into several sub-bands, each of which hosts a number of consecutive subcarriers, and a so-called FH pattern is used for controlling the sub-band allocation for the different users. Since each user activates different sub-bands from time to time, the achievable frequency diversity improves, as the width of the sub-bands is reduced.

On the other hand, when the number of users becomes higher in conventional SDMA-OFDM systems, a higher Multi-User Interference (MUI) is expected across the entire bandwidth and hence all users will suffer from a performance degradation. Unfortunately, the same phenomenon is encountered also in FH/SDMA-OFDM systems at those sub-bands that are shared by excessive number of users. Undoubtedly, the best solution to eliminate the MUI is to avoid sub-band collisions between the different users by assigning each sub-band exclusively to a single user. This "one-subband-for-one-user" scheme will inevitably reduce the system's overall throughput. The attainable system throughput can be increased with the aid of higher-order modems, which are more vulnerable to transmission errors as well as impose an increased MUD complexity at the receivers, which is undesirable. Therefore, subcarrier-reuse based SDMA-OFDM using efficient frequency-hopping techniques is preferable, since it is capable of maintaining a sufficiently high overall system throughput even with the employment of a relatively low-order, low-complexity modem, while effectively suppressing the associated high MUI.

In this chapter, we will introduce a new bandwidth-efficient approach for employment in SDMA-OFDM systems designed for solving the two problems mentioned above.

6.2 Introduction to Hybrid SDMA-OFDM

During last decades, a range of Time Division Multiple Access (TDMA) [38], Frequency Division Multiple Access (FDMA) [38] and Code Division Multiple Access (CDMA) [39–43] schemes have found employment in the first-,